

UNIVERSITAT POLITÈCNICA DE VALÈNCIA

DEPARTMENT OF APPLIED THERMODYNAMICS



Empa

Materials Science and Technology

departamento de **TERMODINÀMICA**
de APLICADA

**Multi-sector thermophysiological head simulator
for headgear research**

A thesis
submitted to the Universitat Politècnica de
València for the degree of Doctor of
Philosophy

Natividad Martínez Guillamón

Directors:

Prof. José Miguel Corberán Salvador

Dr. René Michel Rossi

Dr. Agnes Psikuta

Dr. Simon Annaheim

Valencia (Spain), January 2016

Todas las culturas forman parte del patrimonio común de la humanidad. La identidad cultural de un pueblo se renueva y enriquece en contacto con las tradiciones y valores de los demás. La cultura es diálogo, intercambio de ideas y experiencias, apreciación de otros valores y tradiciones, se agota y muere en el aislamiento.

DECLARACIÓN DE MÉXICO SOBRE LAS POLÍTICAS CULTURALES
Conferencia mundial sobre las políticas culturales México D.F., 26 de julio - 6 de agosto de 1982

Acknowledgement

Firstly, I would like to express my deep gratitude to my supervisor Prof. José Miguel Corberán, because this thesis has been possible thanks to his encouragement and support throughout all these many years. I would really like to thank my supervisors at Empa, Dr. Agnes Psikuta, Dr. Simon Annaheim and Dr. René Rossi for their personal and technical support, I am glad of having had the opportunity of learning from them.

Special thanks to my colleagues in Empa for sharing moments of fun and making me feel at home, without the friendship and support of Gökçe, Emel, Hande and María it would have not been possible. I distinctively thank my colleague Matthew Morrissey for his altruistic and high-valuable contributions in experiments, discussion, programming and advice in English language and Rolf Stämpfli for making every technical trouble quickly disappear. I also thank Max Aeberhard and Barbara Koelblen for contributing to confirm my results with their measurements and Manuela Weibel for her interesting discussion about simulations. Thanks a lot to Maribel and Javi for their perfect translation of the summary into Valencian language.

I would like to acknowledge the State Secretariat for Education, Research and Innovation that under the COST Action TU1101: *Towards safer bicycling through optimization of bicycle helmets and usage* provided funding and a highly collaborative network to develop this PhD investigation. I specially thank partners in the working group 4 for their inestimable help and valuable discussion.

Multi-sector thermophysiological head simulator

Thank you to all colleagues in the Department of Physiology at the Faculty of Medicine and Odontology and the Department of Physical and Sport Education (Research Group in Sport Biomechanics (GIBD)) at the Faculty of Physical Activity and Sport Sciences in the University of Valencia for kindly hosting me during a short scientific mission.

I really appreciate the efficient and friendly delivery of literature from the Library for the Research Institutes within the ETH domain, especially thanks to Christine and Sandrine. I want to thank the logistic support and patience showed by Miguel Granell from the School of Doctorate and Ginesa and Adriana from the Secretary of the Department of Applied Thermodynamics at the Polytechnic University of Valencia. Thanks to all of them for being such great professionals.

I cannot forget to thank all my colleagues from the IBV in Valencia, where my career and my PhD studies started and my interest for the research was woken up some years ago.

Deeply thanks to my family and friends for their continuous support and affection in every situation. I specially thank to my parents and Óscar, Esmeralda and Pilar always encouraging me in the distance. They are my self-improvement and eagerness models. I really feel lucky.

Thank you to Claudio for always showing the sunny side.

Natividad Martínez

St. Gallen, January 2016

ABSTRACT

Predicting thermal comfort perceived during wearing protective clothing is important especially for the head. The head has been reported to be one of the most sensitive body parts to heat. Since helmets typically induce an additional thermal insulation that impairs the heat dissipation from the head, a special attention should be drawn to a heat strain leading to a decrease of the cognitive performance and to adverse health effects.

Thermal manikins allow systematic analysis of the heat and mass transfer properties of protective clothing. Typically, they operate in steady-state mode following the set point values of a constant heat flux or surface temperature defined by the researcher. Specialized body parts manikins are an increasing trend as an alternative to full-body manikins. Due to a finer segmentation, they allow determining local thermal properties of garments or protective equipment with a great detail. Although this methodology enables a reproducible comparison between protective clothing and gear, which is highly valuable for clothing industry, it does not provide sufficient information about the local and the whole body human physiological response in different cases of use.

The prediction of the physiological state of the body is provided by a mathematical model of human thermal physiology and comfort. Although models are powerful tools to predict human thermal response, they are not capable of accounting for complex heat and mass exchange processes at the skin surface when the clothing is worn and in complex environments. Instead, the thermal devices could measure the overall effect of these processes when wearing the given actual gear and being exposed to the surrounding environment. Several attempts to couple thermal manikins (full-body manikins and cylinders) with physiological models have been undertaken. They have proved to accurately evaluate the effect of clothing and environmental factors on the human thermal response. Nevertheless, the partial coupling of a body part manikin with a physiological model has not been addressed so far. Hence, the aim of this work was to develop a novel thermophysiological human head simulator for headgear evaluation based on the coupling of a thermal head manikin with a thermophysiological model. This method would be able to realistically reproduce the effect of clothing on the heat and mass transfer from the head's skin to the environment and its impact on the wearer's thermal response.

A thermal nine-zone head manikin with a dedicated segmentation for headgear testing was evaluated for the thermophysiological human head simulator. The initial analysis of the precision of the heat flux measurements revealed the need of applying some technical adjustments to the manikin. This nine-zone head manikin showed consistent data in convection and combined convection and radiation tests when compared to previously published data of a less segmented head manikin with some exceptions due to differences in head geometry. The more detailed investigation of the local heat transfer at head brought additional information

regarding the contribution of the local design characteristics of the headgear to the overall heat exchange.

The thermal head manikin was evaluated in the most demanding scenarios according to the human physiology to determine opportunities and possible constraints when simulating the human head thermal response. It was possible to consistently define four head parts independently controlled in the coupled system, namely, forehead, cranial, face and neck parts with similar surface areas and combined heat transfer coefficients. When heterogeneous surface temperature distribution was applied on the head manikin, the gradients between head parts resulted in uncontrolled lateral heat exchange that could compromise the precision of skin temperature prediction at forehead and face. The passive heating and cooling responsiveness of the head manikin did not present any limitation for simulating sudden temperature step changes observed in the human response. However, when the manikin heating and cooling processes were modulated by the PI control with default settings, the time needed to reach the temperature set point was larger than the time required by the human physiology.

The physiological model foreseen for the coupled system was validated for prediction of global and local skin temperatures by comparing simulations against human experimental data in scenarios representing a wide range of conditions. The physiological model showed a good precision in general when predicting core and mean skin temperature. A reduced precision was observed for forehead skin temperature most probably due to lack of information about measurement circumstances and for thigh during exercising exposures probably due to an overestimation of the sweat evaporative cooling.

Multi-sector thermophysiological head simulator

Finally, the thermal head manikin and the physiological model were coupled to build up the thermophysiological head simulator. Hence, the head parts were dressed with actual gear and exposed to the actual environment, whereas the rest of the body was virtually simulated. The coupling principle consisted of a real-time feedback loop in which the physiological model provided the skin temperatures and sweat rates for the different head parts of the manikin and received the heat fluxes as an integral feedback from the environment. The comparison of the prediction of the coupled system with human experimental data in several scenarios combining different environmental temperatures and activity levels showed a good agreement in predictions of rectal and mean skin temperatures. However, some greater discrepancy was observed for forehead temperature predictions that differed from pure virtual simulations for exposures in which participants were exercising in moderate and warm environments. In these activity exposures, the cooling of the skin had to be reached mainly by the evaporation of the sweat. The skin temperature in the coupled simulations was always above the skin temperature predicted in the pure virtual simulations in moderate and warm exposures, however, the agreement with the experimental data depended on the particular exposure. The representation of the human sweat evaporation could be affected by a reduced evaporation efficiency and the wetting and drying transients processes at the head manikin surface and its skin fabric. This work has introduced an advanced methodology for headgear testing based on the prediction of the human thermophysiological response of the wearer. The industry will benefit from this thermophysiological human head simulator, which will lead to the development of helmet designs with enhanced thermal comfort, and therefore, with higher acceptance by users.

RESUMEN

Poder predecir el confort térmico durante el uso de indumentaria de protección es muy relevante especialmente en el caso de la cabeza, ya que es una de las partes más sensibles del cuerpo al calor. Los elementos de protección frente a impactos (cascos entre otros) incorporan un aislamiento adicional que dificulta la disipación de calor en la cabeza. Este hecho tiene especial importancia cuando el estrés térmico afecta negativamente a la función cognitiva y a la salud.

Los maniqués térmicos permiten analizar de manera sistemática las propiedades de transferencia de calor y humedad de la indumentaria de protección. Habitualmente funcionan en modo estacionario siguiendo los valores de consigna para flujo de calor o temperatura superficial definidos por el usuario. Los maniqués que representan partes del cuerpo de manera separada suponen una alternativa al alza frente a los maniqués de cuerpo completo ya que debido a su mayor división en zonas independientes, permiten determinar con mayor nivel de detalle las propiedades térmicas de la ropa e indumentaria de protección. Sin embargo, aunque esta metodología permite realizar estudios comparativos entre diferentes

productos y proporciona información de alto valor para la industria, no permite inferir la respuesta fisiológica del usuario cuando utiliza la prenda.

En la actualidad existen modelos matemáticos que permiten predecir el estado fisiológico del cuerpo humano y el confort percibido. No obstante, a pesar de que estos modelos son capaces de predecir la respuesta fisiológica humana en detalle, presentan algunas limitaciones cuando se trata de simular los complejos procesos de transferencia de calor y humedad que ocurren al nivel de la superficie de la piel cuando está cubierta con ropa. En este caso, un maniquí térmico podría cuantificar el intercambio real de calor que se produce con el ambiente térmico cuando se viste una determinada prenda y el ambiente térmico es complejo. Algunas experiencias previas en las que un maniquí de cuerpo completo o un cilindro que lo representa han sido acoplados con una modelo de la fisiología humana han demostrado que estos sistemas pueden evaluar de manera precisa el impacto de la ropa y de otros factores ambientales en la respuesta fisiológica humana. Sin embargo, el acoplamiento de un maniquí que representa únicamente una parte del cuerpo con un modelo de la fisiología humana no ha sido llevado a cabo hasta ahora. Por lo tanto, el objetivo de este trabajo ha sido desarrollar una nueva metodología para evaluar cascos y equipos de protección para la cabeza basándose en el acoplamiento de un maniquí térmico de cabeza con un modelo fisiológico. Esta metodología permitiría representar el efecto real de la ropa en la transferencia de calor y humedad en la cabeza entre la superficie de la piel y el ambiente y su impacto en la respuesta térmica del usuario.

Un maniquí térmico de cabeza con una división en nueve zonas independientes especialmente diseñado para un detallado análisis térmico de cascos y equipos de protección para la cabeza ha sido evaluado para ser acoplado con un modelo de la

fisiología humana. Un análisis inicial de la precisión en la medida del flujo de calor mostró la necesidad de reajustar el maniquí para un correcto funcionamiento en el sistema acoplado. Una vez ajustado, las medidas de este maniquí fueron consistentes con resultados anteriormente publicados realizados con un maniquí en menos seccionado con algunas excepciones atribuidas a diferencias en la geometría en situaciones de convección pura y combinada con radiación. El mayor nivel de detalle en la investigación de la transferencia de calor en las diferentes zonas de la cabeza introdujo información adicional sobre la contribución en particular de las distintas características de diseño del casco al intercambio de calor global.

El maniquí térmico de cabeza fue evaluado en los escenarios más extremos identificados para la fisiología humana para determinar las posibles limitaciones durante la simulación de la respuesta térmica de la cabeza. Se pudo identificar cuatro partes independientemente controladas en el sistema acoplado, frente, cráneo, cara y cuello que presentaron áreas y coeficientes de transferencia de calor similares. En el caso de simular una distribución heterogénea de temperatura en la superficie del maniquí de cabeza, los gradientes generados entre las diferentes partes causaron un intercambio de calor lateral no controlado que podría comprometer potencialmente la precisión en la predicción de la temperatura de la piel en la frente y la cara. La capacidad pasiva de calentamiento y enfriamiento del maniquí de cabeza no supuso ninguna limitación para simular los cambios súbitos de temperatura de la piel observados en la fisiología humana. Sin embargo, cuando el control PI del maniquí moduló los procesos de calentamiento y enfriamiento con los parámetros definidos por el fabricante, el tiempo necesario para alcanzar la temperatura de consigna fue mayor que el tiempo de reacción observado en la fisiología humana.

Multi-sector thermophysiological head simulator

Las predicciones de temperatura obtenidas con el modelo de la fisiología humana previsto para formar parte del sistema acoplado fueron validadas a nivel global y local mediante la comparación con datos humanos experimentales recogidos en escenarios representando un amplio rango de condiciones térmicas. En general, el modelo mostró buena precisión para la predicción de la temperatura interna y la temperatura media de la piel. Sin embargo, la precisión observada fue menor para la predicción de la temperatura de la frente y del muslo, probablemente debido a una descripción incompleta de las circunstancias de la medida o debido a una sobrestimación del enfriamiento debido a la evaporación del sudor.

Finalmente, el maniquí térmico de cabeza y el modelo de la fisiología humana fueron acoplados y por tanto, la partes del cuerpo correspondientes a la cabeza fueron vestidas y expuesta al ambiente térmico en la realidad mientras que el resto del cuerpo fue simulado de manera virtual. El principio para el acoplamiento consistió en un lazo de realimentación en tiempo real en el cual el modelo proporcionaba las temperaturas de la piel y las tasas de sudoración para cada parte de la cabeza representada en el maniquí y éste reaccionaba proporcionando los flujos de calor correspondientes. La comparación de las predicciones del sistema acoplado con datos humanos experimentales en escenarios representando diferentes combinaciones de temperatura ambiente y actividad física mostraron concordancia en el caso de la temperatura rectal y media de la piel de manera similar a las predicciones que el modelo mostró por sí solo. No obstante, se observó una mayor discrepancia en la predicción de la temperatura de la frente si se comparaba las simulaciones obtenidas con el modelo por sí solo y con el sistema acoplado en escenarios en los que los participantes realizaban actividad física ambientes moderados o cálidos. En estos casos, el principal mecanismo de enfriamiento de la piel sería la evaporación del sudor. Se observó que la

temperatura de la piel simulada con el sistema acoplado solía estar por encima de la temperatura simulada con el modelo solamente en ambientes moderados y cálidos pero su concordancia con los datos humanos experimentales dependía del caso específico que era simulado. La representación de la evaporación del sudor humano en el sistema acoplado podría estar condicionada por una menor eficiencia en la evaporación y los procesos de mojado y secado que tienen lugar en la superficie del maniquí de cabeza y en la tela que lo cubre para distribuir el sudor. Este trabajo ha generado una avanzada metodología para evaluar cascos y otros elementos de protección para la cabeza mediante la predicción de la respuesta termofisiológica del usuario. La industria se podrá beneficiar de este sistema para avanzar en el desarrollo de nuevos productos que proporcionen mayor confort térmico y que por lo tanto sean mejor aceptados por los usuarios.

RESUM

Poder predir el confort tèrmic durant l'ús d'indumentària de protecció es especialment rellevant en el cas del cap, ja que és una de les parts més sensibles del cos a la calor. Els elements de protecció contra impactes (cascs entre altres) incorporen un aïllament adicional que dificulta la dissipació de la calor al cap. Aquest fet és particularment dramàtic quan l'estrès tèrmic afecta negativament a la funció cognitiva i té efectes negatius sobre la salut.

Els maniquins tèrmics permeten analitzar de manera sistemàtica les propietats tèrmiques de la indumentària de protecció. Habitualment funcionen en mode estacionari seguint els valors de flux de calor o temperatura superficial definits per l'usuari. Els maniquins que representen parts del cos de manera separada suposen una alternativa a l'alça front als maniquins de cos complet ja que degut a la seua major divisió en zones independents, permeten determinar en més nivell de detall les propietats tèrmiques de la roba i indumentària de protecció. No obstant, encara que aquesta metodologia permet realitzar estudis comparatius entre diferents

Multi-sector thermophysiological head simulator

productes i proporciona informació d'alt valor per a la indústria, no permet inferir la resposta fisiològica de l'usuari quan utilitza la indumentària.

En l'actualitat existixen models matemàtics que permeten predir l'estat fisiològic del cos humà i el confort recaptat. No obstant, tot i que aquestos models son capaços de predir la resposta fisiològica humana en detall, presenten algunes limitacions quan es tracta de simular els complexos processos de transferència de calor i humitat que ocorren al nivell de la superfície de la pell quan està coberta amb roba. En aquest cas, un maniquí tèrmic podria quantificar l'intercanvi real de calor que es produïx en l'ambient tèrmic quan es porta una determinada indumentària. Algunes experiències prèvies en les que un maniquí de cos complet o un cilindre que ho representa han sigut acoblats en un model de la fisiologia humana han demostrat que aquestos sistemes poden evaluar de manera precisa l'impacte de la roba i d'altres factors ambientals en la resposta fisiològica humana. No obstant, l'acoblament d'un maniquí que representa únicament una part del cos en un model de la fisiologia humana no ha sigut dut a terme fins ara. Per tant, l'objectiu d'aquest treball es desenvolupar una nova metodologia per a evaluar cascs i indumentària de protecció per al cap basada en l'acoblament d'un maniquí tèrmic de cap amb un model fisiològic. Aquesta metodologia permetria representar l'efecte real de la roba a la transferència de calor i humitat al cap entre la superfície de la pell i l'ambient, i el seu impacte a la resposta tèrmica de l'usuari.

Un maniquí tèrmic de cap, en una divisió de zones independents especialment dissenyat pera un detallat anàlisi tèrmic de cascs i equips de protecció per al cap ha sigut valorat per a ser acoplat en un model de la fisiologia humana. Un anàlisi inicial de la precisió en la mesura del flux de calor va a mostrar la necessitat de reajustar el maniquí per a un correcte funcionament en el sistema acoblat. Una

volta ajustades les mesures del maniquí, van ser consistents amb els resultats publicats anteriorment i que es van realitzar en maniquís menys seccionats amb algunes excepcions atribuïdes a diferències en la geometria en situacions de convecció pura i combinada amb radiació. El major nivell de detall en l'investigació de la transferència de calor en les diferents zones del cap introdueix informació adicional sobre la contribució particular de les diferents característiques del disseny dels cascs a l'intercanvi de calor global.

El maniquí tèrmic de cap ha sigut valorat en els escenaris més extrems identificats per la fisiologia humana per determinar les possibles limitacions en la simulació de la resposta tèrmica del cap. Es van poder identificar quatre parts independentment controlades al sistema acoblat, front, crani, cara i coll que presentaren àrees i coeficients de transferència de calor similars. En el cas de simular una distribució heterogènia de temperatura en la superfície del maniquí de cap, els gradients generats entre les diferents parts causaren un intercanvi de calor lateral no controlat que podria comprometre potencialment la precisió en la predicció de la temperatura de la pell en el front i la cara. La capacitat passiva de calfament i refredament del maniquí de cap no va suposar ninguna limitació per simular els canvis sobtats de temperatura de la pell observats en la fisiologia humana. No obstant, quant el control PI del maniquí modulà els processos de calfament i refredament en els paràmetres definits pel fabricant, el temps necessari per aconseguir la temperatura de consigna va ser major que el temps de reacció observat en la fisiologia humana.

Les prediccions de temperatura obtingudes en el model de la fisiologia humana previst per formar part del sistema acoblat van ser validades a nivell global i local mitjançant la comparació amb dades humanes experimentals recollides en

Multi-sector thermophysiological head simulator

escenaris representant una ampla varietat de condicions tèrmiques. En general, el model va mostrar una bona precisió en la predicció de la temperatura interna i la temperatura mitjana de la pell. No obstant, la precisió va ser menor en la predicció de la temperatura del front i de la cuixa, probablement degut a una descripció no completa de l'exposició o per causa d'una sobreestimació del refredament per l'evaporament de la suor.

Finalment, el maniquí tèrmic de cap i el model de la fisiologia humana van ser acoblats i per tant, les parts del cos corresponents al cap van ser vestides i exposades a l'ambient tèrmic en la realitat mentre que la resta del cos va ser simulat de manera virtual. El principi per l'acoblament va consistir en, un llaç de realimentació en temps real en el qual el model proporcionava les temperatures de la pell i les taxes de suor per a cada part del cap representat en el maniquí i aquest reaccionava proporcionant els fluxos de calor corresponents. La comparació de les prediccions del sistema acoblat amb dades humanes experimentals, en escenaris representant diferents combinacions de temperatura ambient i activitat física mostraren concordança en el cas de la temperatura rectal i mitjana de la pell de manera similar a les prediccions que el model mostrà per sí mateix. No obstant, s'observà una major discrepància en la predicció de la temperatura del front quant es comparaven les simulacions obtingudes en el model per sí mateix i el sistema acoblat en escenaris en els quals els participants realitzaven activitat física en ambients moderats o càlids. En aquestos casos, el principal mecanisme de refredament de la pell seria l'evaporament del suor. S'observà que la temperatura de la pell simulada en el sistema acoblat solia estar per damunt de la temperatura simulada en el model per sí mateix en ambients moderats i càlids però la seua aproximació amb les dades humanes experimentals depenia del cas específic que era simulat. La representació de l'evaporament del suor humà en el sistema acoblat

podria estar condicionada per una menor eficiència en l'evaporament i els processos de banyat i secat que tenen lloc en la superfície del maniquí de cap i a la tela utilitzada per a distribuir la suor. Aquest treball ha generat una avançada metodologia per a evaluar cascs i altres elements de protecció per al cap mitjançant la predicció de la resposta termofisiològica de l'usuari. La indústria es podra beneficiar d'aquest sistema per a avançar en el desenvolupament de nous productes que proporcionen un major confort tèrmic i per tant més acceptats per els usuaris.

Contents

Abstract	v
Resumen	ix
Resum	xv
List of figures.....	xxix
List of tables	xxxvii
List of abbreviations.....	xli
1 Motivation of the work	45
1.1 Background	45
1.2 Introduction	46

Contents

1.3	Aim and objectives.....	53
2	Evaluation of the nine-zone thermal head manikin.....	57
2.1	Introduction.....	57
2.2	Aim and objectives.....	59
2.3	Selection and characterization of the elements constituting the testing setup	59
2.3.1	The nine-zone sweating head manikin.....	59
2.3.2	Climatic chamber and wind tunnel.....	62
2.3.3	In-depth analysis of the precision of the heat fluxes provided by the thermal head manikin.....	63
2.3.4	Temperature calibration of the head manikin.....	72
2.3.5	Fluid calibration of the head manikin.....	75
2.4	Analysis of the performance of the nine-zone thermal head manikin for headgear testing.....	75
2.4.1	Introduction.....	75
2.4.2	Methods.....	76
2.4.3	Results.....	84
2.4.4	Discussion.....	93

Multi-sector thermophysiological head simulator

2.5	Conclusion	98
3	Specific requirements for the head manikin under physiological control mode	101
3.1	Introduction	101
3.2	Aim and objectives.....	106
3.3	Definition of head parts in the coupled system	107
3.3.1	Introduction	107
3.3.2	Methods	108
3.3.3	Results.....	108
3.3.4	Discussion	109
3.4	Heat transfer coefficients at head parts.....	110
3.4.1	Introduction	110
3.4.2	Methods	112
3.4.3	Results.....	113
3.4.4	Discussion	114
3.5	Uncontrolled lateral heat exchange between head parts.....	115
3.5.1	Introduction	115

Contents

3.5.2	Methods	116
3.5.3	Results	119
3.5.4	Discussion	122
3.6	Thermal passive responsiveness of the head manikin	123
3.6.1	Introduction	123
3.6.2	Methods	124
3.6.3	Results	125
3.6.4	Discussion	127
3.7	Thermal controlled responsiveness of the head manikin	128
3.7.1	Introduction	128
3.7.2	Methods	129
3.7.3	Results	130
3.7.4	Discussion	130
3.8	Adjustment of the thermal controlled responsiveness of the head manikin 132	
3.8.1	Introduction	132
3.8.2	Methods	132

Multi-sector thermophysiological head simulator

3.8.3	Results	133
3.8.4	Discussion	137
3.9	Characterization of the evaporation efficiency and evaporation responsiveness of the head manikin	138
3.9.1	Introduction	138
3.9.2	Methods	140
3.9.3	Results	144
3.9.4	Discussion	147
3.10	Conclusions	150
4	Validation of a thermophysiological model against a dedicated database of human experiments.....	155
4.1	Introduction	155
4.2	Aim and objectives.....	162
4.3	Development of a human experiments database.....	163
4.4	Investigation of local skin temperatures during cycling in a moderate environment.....	168
4.4.1	Introduction	168
4.4.2	Methods	169

4.4.3	Results	172
4.4.4	Discussion	175
4.5	Verification of temperature sensors attaching method	176
4.5.1	Introduction	176
4.5.2	Methods	177
4.5.3	Results	179
4.5.4	Discussion	180
4.6	Validation of the physiological model by Fiala for prediction of global and local skin temperatures.....	181
4.6.1	Introduction	181
4.6.2	Methods	182
4.6.3	Results	187
4.6.4	Discussion	193
4.7	Conclusion	208
5	Development and validation of the coupled system.....	211
5.1	Introduction	211
5.2	Aim and objectives.....	216

Multi-sector thermophysiological head simulator

5.3	Coupling method.....	217
5.3.1	Coupling principle.....	217
5.3.2	Operation of the coupled system.....	219
5.3.3	Description of the coupling interface.....	220
5.4	Consistency of predictions for different types of boundary conditions.....	224
5.4.1	Introduction.....	224
5.4.2	Method.....	226
5.4.3	Results.....	227
5.4.4	Discussion.....	233
5.5	Analysis of the convergence of the coupled system towards pure simulations.....	236
5.5.1	Introduction.....	236
5.5.2	Methods.....	236
5.5.3	Results.....	238
5.5.4	Discussion.....	241
5.6	Validation against human data.....	248
5.6.1	Introduction.....	248

Contents

5.6.2	Methods	249
5.6.3	Results	252
5.6.4	Discussion	255
5.7	Conclusions	261
6	Conclusions and future work.....	265
6.1	Conclusions	265
6.2	Future work	275
7	References.....	279
8	Appendix	301
8.1	Appendix 1: Local skin temperatures upon the 14 body-sites (ISO 9886) 302	
8.2.	Appendix 2: Local skin temperatures at head-site	306

List of figures

Figure 1.1. Anatomical head parts (adapted from (Netter, 2014))	49
Figure 2.1. Nine-zone thermal head manikin segmentation.....	60
Figure 2.2. Standard setup for thermal testing of headgear including wind effect.	63
Figure 2.3. Heat fluxes of nine-zone head manikin for surface temperature set constant at 35°C at ambient 25°C / 50%RH / 3.1m·s ⁻¹ wind (test duration of 11 hours).	64
Figure 2.4. Surface temperature of the nine-zone head manikin for heat flux set constant at 200 W·m ⁻² and ambient of 5°C / not controlled RH / Still air (v _a < 0.1 m·s ⁻¹) (test duration of 6 hours).	65
Figure 2.5. Heat flux for the temperature set point of 35°C. First six hours shows left temple heated alone and the following six hours shows left temple and lower head back heated at the same time at the temperature set point of 35°C. The rest of the zones stayed disabled (guard and enclosure included) (22°C / 50%RH / Still air (v _a < 0.1 m·s ⁻¹)).	69
Figure 2.6. Laboratory setup for head manikin temperature calibration.	72

Multi-sector thermophysiological head simulator

Figure 2.7. Surface temperature of the manikin measured at the calibration point at 25°C/50%RH/Still air ($v_a < 0.15 \text{ m}\cdot\text{s}^{-1}$) using head manikin and Pt100 sensors.74

Figure 2.8. Nine-zone thermal head manikin (9zM, a) and two-zone thermal head manikin (2zM, b).78

Figure 2.9. Convection tests setup (a) and radiation tests setup (b).83

Figure 2.10. Correlation for heat loss at facial (a) and cranial (b) sections between 2-zone manikin (2zM) and 9-zone manikin (9zM). Graphs include the line of identity.86

Figure 2.11. Correlation for radiant heat gain (RHG) at facial and cranial sections between 2-zone manikin (2zM) and 9-zone manikin (9z M). The graph includes the line of identity.88

Figure 2.12. Comparison of convective cooling performance (CCP) provided by each helmet for each headform at the different testing conditions. Helmets are presented in ascending order according to CCP for 2zM.89

Figure 2.13. Comparison of radiant shielding (RS) provided for facial and cranial section for each helmet without visor (NV) and with visor (VI). Helmets are presented in ascending order according to RS for 2zM.90

Figure 2.14. CCP at cranial section and at individual zones of 9zM (Crown, Upper Head Back, Lower Head Back and Occipital) in low wind and tilted head test condition for some illustrative helmets.92

Figure 2.15. RS at facial and cranial section and at corresponding individual zones of 9zM (Forehead and Face within Facial Section and Crown and Upper Head Back within Cranial Section) for some illustrative helmets at test condition with visor (VI).....93

Figure 3.1. Heterogeneous surface temperature set points set at the head manikin for testing heat exchanged by lateral conduction and internal convection and radiation for scenario 1 and 2.....117

Figure 3.2. Comparison of the maximal temperature increase at the skin predicted by the physiological model and the maximal temperature increase measured by the head manikin for each defined head part during heating up at maximal nominal power ($800 \text{ W}\cdot\text{m}^{-2}$).126

- Figure 3.3. Comparison of surface temperature drop measured on the head manikin and the skin temperature drop predicted by the physiological model at ambient temperature of 5°C and 25°C respectively for each defined head part.127
- Figure 3.4. Average time needed to achieve the target temperature changes of 3, 2, 1 and 0.5°C positive and negative calculated with $\pm 0.2^\circ\text{C}$ tolerance when the thermal reaction is modulated by the manikin PI controller in two ambient temperatures 5 and 25°C. The error bars show standard deviation of the four head parts foreseen in the coupled system. It should be noticed that time for a step change of -3°C in temperature ambient of 25°C is constrained by maximal passive cooling responsiveness of the head manikin.130
- Figure 3.5. Comparison of the average manikin thermal responsiveness for PI default settings and PI fast response settings manually adjusted when a negative and a positive step change of 3°C was programmed for a high heat flux case (at ambient temperature of 5°C). Comparison of surface temperature for cooling, comparison of surface temperature for heating, comparison of heat flux for cooling and comparison of heat flux for heating are shown.134
- Figure 3.6. Average time needed to achieve the target temperature changes of 3, 2, 1 and 0.5°C positive and negative calculated with $\pm 0.2^\circ\text{C}$ tolerance when the thermal reaction is modulated with the PI default settings ($K_p = 0.18$ and $K_i = 0.002$) and the PI fast response settings ($K_p = 0.48$ and $K_i = 0.015$). Results separated by ambient temperatures 25 and 5°C. The error bars account with standard deviation of the four head parts foreseen in the coupled system. It should be noticed that maximum passive cooling was 0.7 and $1.9^\circ\text{C}\cdot\text{min}^{-1}$ at 25°C and 5°C.136
- Figure 3.7. a) Evaporative cooling over the head parts and b) evaporation efficiency calculated as a ratio of the measured evaporative heat loss to the evaporative potential calculated based on the mass loss. Notice that evaporative efficiency for individual zones were not corrected for water migration effect and evaporative efficiency of the entire head at $1000 \text{ ml}\cdot\text{m}^{-2}\cdot\text{h}^{-1}$ was not corrected for water that dripped off. Values are presented as average and standard deviation.145

Multi-sector thermophysiological head simulator

Figure 3.8. Wetting time measured between the onset of the sweating and the development of 75% of the maximal steady-state evaporative heat loss for each sweat rate. Values are presented as average and standard deviation.146

Figure 3.9. Drying time measured between the stop of the sweating and the reduction of the maximal steady-state evaporative heat loss to be just 25% above the dry heat loss for each sweat rate. Values are presented as average and standard deviation.147

Figure 3.10. Initial development of the sweat at the head manikin showing lack of hydrophilicity.....149

Figure 4.1. Distribution of exposures in data base regarding to air temperature, wind speed and physical activity.....165

Figure 4.2. Test protocol indicating measuring periods.....171

Figure 4.3. Mean skin temperature based on 14 measurement points throughout the test. Data are presented separated by workload: Main test 50% Pmax (n=14) and Main test 35% Pmax (n=14). Error bars for standard deviation are presented only positive or negative for better readability.....173

Figure 4.4. Mean skin temperature at head based on equally-weighted 6 measurement points throughout the test. Data are presented separated by workload: Main test 50% Pmax (n=14) and Main test 35% Pmax (n=14). Error bars for standard deviation are presented only positive or negative for better readability.174

Figure 4.5. Core temperature throughout the test. Data are presented separated by workload: Main test 50% Pmax (n=13) and Main test 35% Pmax (n=14). Error bars for standard deviation are presented only positive or negative for better readability...175

Figure 4.6. Experimental setup for measuring attached sensors effect on dry and wet heat transfer experiments.....178

Figure 4.7. Comparison of temperature measurements by different instruments on the surface of the cotton fabric placed on top of hot plate.179

Figure 4.8. Overall values for precision (rmsd), accuracy (bias) and experimental inter-participant standard deviation (SD_{exp}) for a total of 41 simulations carried out with FPCm5.3.188

Figure 4.9. Core temperature measured in experiments and predicted using FPCm5.3 model. a) Exposure 1: Standard person walking on a treadmill at 3.3 and 4.4 met, $T_a = 40^\circ\text{C}$, RH = 30%, protective clothing worn. Rest period between minutes 20 and 40, $T_a = 25^\circ\text{C}$, RH = 30%. b) Exposure 4: Well-trained athletes cycling at 7.3 met, $T_a = 20^\circ\text{C}$, RH = 50%, short cycling clothing.194

Figure 4.10. Forehead skin temperature in exposure 13: Standard person standing in a cold environment (one hour at 5°C , half an hour at $T_a = -10^\circ\text{C}$, still air), cold protective clothing. Experimental data are presented together with simulations that considered dressed and undressed forehead.196

Figure 4.11. Forehead skin temperature in exposure 1 and 24. Exemplary results showing effect of possibly cumulated sweat on forehead surface due to previous exercising conditions. a) Exposure 1: Standard person walking on a treadmill at 3.3 and 4.4 met, $T_a = 40^\circ\text{C}$, RH = 30%, protective clothing worn. Resting period between minutes 20 and 40, $T_a = 25^\circ\text{C}$, RH = 30%. b) Exposure 24: Well-trained athletes cycling at 4 met, $T_a = 21.8^\circ\text{C}$, RH = 39.4%, short cycling clothing. Resting period after 68 min.197

Figure 4.12. Experimental and predicted chest temperature in exposure 1 and 34. a) Exposure 1: Standard person walking on a treadmill at 3.3 and 4.4 met, $T_a = 40^\circ\text{C}$, RH = 30%, protective clothing worn. Resting period between minutes 20 and 40, $T_a = 25^\circ\text{C}$, RH = 30%. b) Exposure 34: Standard person exposed in a cold environment at $T_a = -12^\circ\text{C}$, sedentary, protective clothing.198

Figure 4.13. Chest temperature and evaporation rate measured in the experiment and predicted by FPCm5.3 in exposure 17 and 25 representing cycling scenario in warm environment. a) Exposure 17: Well-trained athletes cycling at 7.12 met, $T_a = 29^\circ\text{C}$, RH = 80%. b) Exposure 25: Well-trained athletes cycling at 5.3 met, $T_a = 21.2^\circ\text{C}$, RH = 39%RH (exercise period between minutes 21 and 68).201

Figure 4.14. Prediction of thigh and calf temperature in exposure 12. Exposure 12: Standard person standing in the cold wearing cold protective clothing (pre-exposure: 60 minutes at $T_a = 20^\circ\text{C}$, still air / main exposure 30 minutes at $T_a = -10^\circ\text{C}$, $5\text{ m}\cdot\text{s}^{-1}$ frontal wind applied).204

Multi-sector thermophysiological head simulator

Figure 4.15. Prediction of thigh and calf temperatures in exposure 25. Exposure 25: Well-trained athletes cycling at 5.3 met, $T_a = 21.2^{\circ}\text{C}$, $\text{RH} = 39\%\text{RH}$ (exercise period between minutes 21 and 68).206

Figure 5.1. Principle of the partial coupling between the head manikin and the physiological model.....219

Figure 5.2. Flow chart for a coupled simulation.....221

Figure 5.3. Comparison of prediction of overall thermal response between the three model applications in the cold scenario, a) rectal temperature and b) mean skin temperature. BC1 (boundary conditions type 1 entire body), BC2 (boundary conditions type 2 entire body) and BC1/BC2 (combined boundary conditions as in the coupled head system).228

Figure 5.4. Comparison of local skin temperature at forehead between the three model applications in the cold scenario. BC1 (boundary conditions type 1 entire body), BC2 (boundary conditions type 2 entire body) and BC1/BC2 (combined boundary conditions as in the coupled head system).228

Figure 5.5. Comparison of prediction of overall thermal response between the three model applications in a warm scenario, a) rectal temperature, b) mean skin temperature and c) total sweat rate. BC1 (boundary conditions type 1 entire body), BC2 (boundary conditions type 2 entire body) and BC1/BC2 (combined boundary conditions as in the coupled head system).231

Figure 5.6. Comparison of prediction of local thermal response at forehead between the three model applications in a warm scenario, a) local skin temperature at forehead and b) local sweat rate at forehead. BC1 (boundary conditions type 1 entire body), BC2 (boundary conditions type 2 entire body) and BC1/BC2 (combined boundary conditions as in the coupled head system).232

Figure 5.7. Evolution of the forehead skin temperature and skin heat loss in the cold exposure for pure virtual and coupled simulations. Pure virtual simulation is presented calculated for different types of boundary conditions for a better estimation of the size of the discrepancy just due to having head physically

represented. BC1 (boundary conditions type 1 entire body), BC2 (boundary conditions type 2 entire body) and BC1/BC2 (combined boundary conditions as in the coupled head system).243

Figure 5.8. Evolution of the skin temperature, skin heat loss and local sweat rate for cranial and neck parts in the warm exposure for pure virtual and coupled simulations. Pure virtual simulation is presented calculated for different types of boundary conditions for a better estimation of the size of the discrepancy just due to having head physically represented. BC1 (boundary conditions type 1 entire body), BC2 (boundary conditions type 2 entire body) and BC1/BC2 (combined boundary conditions as in the coupled head system).245

Figure 5.9. Overview of the air temperature and activity level of ten exposures selected for the validation.251

Figure 5.10. Box-plot diagram of the overall bias and rmsd values calculated for ten validation exposures for the pure virtual simulations (model alone) and the coupled system simulations. Box divisions corresponds to data quartiles, upper whisker to the upper quartile plus 1.5 times the interquartile range and lower whisker to the lower quartile minus 1.5 times the interquartile range.253

Figure 5.11. Differences in rmsd values [°C] between pure virtual and coupled simulations for core, mean skin and forehead temperature predictions. Average results are presented separately for sedentary, activity and all exposures.255

Figure 5.12. Prediction of skin temperature (Tsk) and sweat rate (msw) at forehead for exposure 25. Well-trained athletes cycling at 5.3 met in a moderate environment at Ta = 21.2°C.258

Figure 5.13. Prediction of skin temperature (Tsk) and sweat rate (msw) at forehead for exposure 22. Well-trained athletes walking at 4.9 met in a warm environment at Ta = 30°C.258

Figure 5.14. Prediction of skin temperature (Tsk) and sweat rate (msw) at forehead for exposure 21. Well-trained athletes walking at 5.9 met in a cold environment at Ta = 10°C.260

List of tables

Table 2.1. Head manikin zones areas.	61
Table 2.2. Maximum differences in surface temperatures [°C] found in test with heat flux set point of 200 W·m ⁻² after 120 minutes elapsed.	66
Table 2.3. Average value and variation of the surface temperature and heat flux for forehead, left temple and lower head back when individually heated at temperature set point of 35°C (environmental conditions 22°C / 50%RH / Still air ($v_a < 0.1 \text{ m}\cdot\text{s}^{-1}$). Absolute variation is represented by standard deviation (SD) and relative variation by coefficient of variation (%).	67
Table 2.4. Variation of other zones when left temple was heated with at a temperature set point of 35°C (environmental conditions 22°C / 50%RH / Still air ($v_a < 0.1 \text{ m}\cdot\text{s}^{-1}$)).	68
Table 2.5. Geometry description of 9zM and 2zM headforms.	78
Table 2.6. Reliability analysis for facial and cranial sections heat losses (W·m ⁻²) for 2-zone manikin (2zM) and 9-zone manikin (9zM) in convection tests (data for 6 helmets and nude head at 4 test conditions). ICC (intra-class correlation index), CV (coefficient of variation) and SD (standard deviation).	85

Multi-sector thermophysiological head simulator

Table 2.7. Reliability analysis of heat fluxes for light off (HFLight OFF) and light on (HFLight ON) conditions as well as radiant heat gain (RHG) calculations for facial and cranial sections for 2-zone manikin (2zM) and 9-zone manikin (9zM) in radiation tests (data for 5 helmets in 2 test conditions, without and with visor and nude head). ICC (intra-class correlation index), CV (coefficient of variation) and SD (standard deviation).87

Table 3.1. Head part surface areas and their assignment for physiological model and thermal head manikin.109

Table 3.2. Comparison of the heat transfer coefficients between those assumed by the physiological model and those measured at head manikin in the same scenario at 20°C / 50%RH / Still air ($v_a < 0.1 \text{ m}\cdot\text{s}^{-1}$).113

Table 3.3. Relative deviations in heat exchange (%) with regard to a theoretical uniform temperature distribution due to extreme and moderate non-uniform surface temperature distributions. Heat flux has been compared between heterogeneous and homogeneous temperature distributions.119

Table 3.4. Differences in local skin temperatures at head-site caused by deviations in the manikin heat flux measurements with a heterogeneous temperature distribution. 121

Table 3.5. Summary of manikin thermal response for PI default settings and PI fast response settings.136

Table 4.1. Maximum and minimum values of parameters of the database164

Table 4.2. General description of human data base166

Table 4.3. Individual characteristics for trained athletes profile in exposures 4-9, 17 and 21-25.186

Table 4.4. Statistical parameters for measured variables in each exposure. Cases marked with * provided core temperature at intestinal-site and are not included in statistical calculations.....190

Table 5.1. Description of the boundary conditions type 1 (BC1) or virtual environment for the cold and the warm scenario.....226

List of tables

Table 5.2. Bias and rmsd for the comparison of physiological model predictions in the cold scenario calculated between cases BC1 (boundary conditions type 1 entire body) and BC2 (boundary conditions type 2 entire body).229

Table 5.3. Bias and rmsd for the comparison of physiological model predictions for the warm scenario calculated between cases BC1 (boundary conditions type 1 entire body) and BC2 (boundary conditions type 2 entire body).233

Table 5.4. Bias and rmsd for the comparison of physiological model predictions for the warm scenario calculated between cases BC1 (boundary conditions type 1 entire body) and BC1/BC2 (combined boundary conditions as in the coupled head system).233

Table 5.5. Description of boundary conditions in the exposures selected for the virtual and coupled simulations.237

Table 5.6. Bias and rmsd for the comparison of predictions of pure virtual model and the coupled system simulations for body temperatures and skin heat loss in the cold exposure.....239

Table 5.7. Bias and rmsd for the comparison of predictions of the pure virtual model and the coupled system simulations for body temperatures and skin heat loss in the thermoneutral exposure.240

Table 5.8. Bias and rmsd for the comparison of predictions of the pure virtual model and the coupled system simulations for body temperatures, skin heat loss and sweat rates in the warm exposure.241

Table 5.9. Description of the human exposures included in the validation study of the coupled system.250

Table 5.10. Statistical parameters for measured variables in each exposure when simulated by the model alone and when simulated by the coupled system with human subject experimental data as a reference.....254

List of abbreviations

Abbreviation	Units	Definition
<i>2zM</i>	--	Two-zone head manikin
<i>9zM</i>	--	Nine-zone thermal head manikin
<i>A_i</i>	m ²	Head manikin zone surface area
<i>BC</i>	--	Indicate boundary condition
<i>BC1</i>	--	Indicate boundary condition type 1 or virtual environment
<i>BC2</i>	--	Indicate boundary condition type 2 or skin heat loss
<i>CCP</i>	%	Convective cooling performance
<i>CV</i>	%	Coefficient of variation
<i>Eff_{evap}</i>	%	Evaporative efficiency
<i>FPCm5.3</i>	--	Software implementing the physiological model by Fiala
<i>h_{combined}</i>	W·m ⁻² ·K ⁻¹	Combined heat transfer coefficient

Multi-sector thermophysiological head simulator

$h_{convective}$	$W \cdot m^{-2} \cdot K^{-1}$	Convective heat transfer coefficient
$HF_{Cranial\ section\ Helmet\ i}$	$W \cdot m^{-2}$	Heat loss observed at cranial section while wearing a specific helmet
$HF_{Cranial\ section\ Nude\ head}$	$W \cdot m^{-2}$	Heat loss observed at cranial section for the nude head manikin
$HF_{Light\ OFF}$	$W \cdot m^{-2}$	Heat loss corresponding either to facial or cranial section if light source off
$HF_{Light\ ON}$	$W \cdot m^{-2}$	Heat loss corresponding either to facial or cranial section if light source on
HF_i	$W \cdot m^{-2}$	Head manikin zone heat flux
HF_{part}	$W \cdot m^{-2}$	Heat flux for each head part
$h_{radiative}$	$W \cdot m^{-2} \cdot K^{-1}$	Radiative heat transfer coefficient
ICC	--	Intra-class correlation index
IRT	--	Infrared thermography
Ki	--	PID integral parameter
Kp	--	PID proportional parameter
L_{air}	$K \cdot Pa^{-1}$	Lewis constant
$mskEv$	$g \cdot min^{-1}$	Local evaporated skin moisture rate
msw	$g \cdot min^{-1}$	Local skin moisture secretion
$mTsk$	$^{\circ}C$	Mean skin temperature
NV	--	Indicate helmets without visor
Pearson's r	--	Pearson's correlation coefficient
PI	--	Proportional-Integral control
PID	--	Proportional-Integral-Derivative control
$Pmax$	W	Maximum cycling power at 90 rpm
qsk	$W \cdot m^{-2}$	Skin heat loss
R	$m^2 \cdot ^{\circ}C \cdot W^{-1}$	Thermal insulation in the head manikin
REL	n.d	Relative evaporative locus

List of abbreviations

<i>RHG</i>	$W \cdot m^{-2}$	Radiant heat gain
<i>RHG</i> <i>Helmet i</i>	$W \cdot m^{-2}$	Radiant heat gain for manikin covered with a specific helmet
<i>RHG</i> <i>Nude head</i>	$W \cdot m^{-2}$	Radiant heat gain for the nude head
<i>rmsd</i>	$^{\circ}C$	Root-mean square deviation
<i>Rnude</i>	$m^2 \cdot ^{\circ}C \cdot W^{-1}$	Thermal resistance of the adjacent air layer
<i>RS</i>	%	Radiant shielding
<i>Rt tight fabric</i>	$m^2 \cdot ^{\circ}C \cdot W^{-1}$	Total thermal resistance of the tight-fitting fabric and the adjacent air layer together
<i>SD</i>	--	Standard deviation
<i>sMsw</i>	$g \cdot min^{-1}$	Total skin moisture secretion
<i>Tabdomen</i>	$^{\circ}C$	Local skin temperature at abdomen
<i>Tair</i>	$^{\circ}C$	Air temperature
<i>Tcalf</i>	$^{\circ}C$	Local skin temperature at calf
<i>Tchest</i>	$^{\circ}C$	Local skin temperature at chest
<i>Tforehead</i>	$^{\circ}C$	Local skin temperature at forehead
<i>Tmanikin</i>	$^{\circ}C$	Manikin surface temperature
<i>Tpart</i>	$^{\circ}C$	Surface temperature at the corresponding head part
<i>Tre</i>	$^{\circ}C$	Rectal temperature
<i>Tscapula</i>	$^{\circ}C$	Local skin temperature at scapula
<i>Tsk</i>	$^{\circ}C$	Local skin temperature
<i>Tthigh</i>	$^{\circ}C$	Local skin temperature at thigh
<i>Va</i>	$m \cdot s^{-1}$	Air velocity
<i>VI</i>	--	Indicate helmets equipped with visor
α	$^{\circ}$	Knee extension angle
λ_{H2O}	$J \cdot g^{-1}$	Latent heat of water

1 MOTIVATION OF THE WORK

1.1 BACKGROUND

This PhD work was performed at Empa in the frame of the project "Prediction of wearing comfort of bicycle helmets" that was supported by the State Secretariat for Education, Research and Innovation (grant SBFI C11.0137) under the COST Action TU1101: Towards safer bicycling through optimization of bicycle helmets and usage (<http://www.bicycle-helmets.eu/>).

The project aimed at encouraging the use of bicycle helmets among cyclists by increasing the wearing comfort. The working group 4 focused its activity on thermal aspects of helmets. To understand the effect of environmental conditions and helmets on the perception of local thermal discomfort it was proposed to develop a multi-segmented thermal head manikin. The thermal head manikin was conceived for a more detailed investigation of local heat and mass transport

phenomena through headgear. Moreover, the thermal head manikin was foreseen to be coupled with a physiological model for predicting the human thermal response when wearing different kinds of headgear. Industry will benefit from this knowledge and it will lead to helmet designs with enhanced thermal comfort and that will increase, therefore, the acceptance by cyclists.

1.2 INTRODUCTION

Although core body temperature can reach up to 42°C, the brain could not stand with temperatures beyond 40.6°C without falling into a heat stroke situation (Gisolfi and Mora, 2000). Therefore, the head holds a crucial role in the body thermoregulation and exhibits a high heat-sensitivity in order to control the brain and whole body temperature. The human head is intended to act as a heat sink although the existence of a selective brain cooling mechanism similar to mammals has not been universally accepted (Cabanac, 1993).

Despite head and face surface represents just 7% of the total body surface (Hardy and DuBois, 1938; ISO9920, 2007), the head can provide relatively high heat loss when compared with other body parts (Froese and Burton, 1957; Rasch et al., 1991). The ratio between its area and its mass is relatively high. Besides, the head's natural thermal insulation is very low as vasoconstriction ability is reduced and there is almost no muscle and fat tissue between brain and environment (Fiala et al., 1999; Fox et al., 1962). Additionally, the human head presents one of the highest sweating rates among body regions (Machado-Moreira et al., 2008b; Smith and Havenith, 2011). It is the most sensitive body part for warm stimulus for both men and women, during rest and exercise (Gerrett et al., 2014; Nakamura et al., 2008) and furthermore, its local thermal sensation is the highest related to the overall

thermal sensation in different situations (Arens et al., 2006a; Boutcher et al., 1995). Particularly high is the thermal sensitivity and the effect on sweating regulation of the face for cold and warm stimulus being at least three times higher than at chest, abdomen or thigh (Cotter and Taylor, 2005; Nadel et al., 1973). Due to the observed high thermal sensitivity and high sudomotor responsiveness, head and face have been suggested for an effective application of cooling methods to alleviate perceptive and physiological heat strain (Cheung, 2007; Desruelle and Candas, 2000; Nunneley et al., 1971).

Head and whole body thermal regulation could be affected by wearing protective headgear as it usually imposes additional insulation that highly impairs heat dissipation and moisture evaporation from head to the environment (Rasch and Cabanac, 1993). The use of helmets is more and more promoted for different kinds of working and leisure time activities because of their important protective role. However, low wearing rates for helmets are observed in European countries mainly if their use is not mandatory, as it is shown for cycling (Amoros et al., 2012; Uibel et al., 2012). Thermal discomfort is referred to as one of the main factors limiting helmets use acceptance (Finnoff et al., 2001; Rezendes, 2006; Wardle and Iqbal, 1998).

Thermoregulation and thermal perception may be affected when wearing different types of headgear. Even differences in heat loss as small as 1 W can be felt by helmet wearers in the facial and cranial regions (Brühwiler et al., 2004; Buyan et al., 2006). To increase wearer's comfort, which most probably contributes to cyclists' willingness to wear a helmet, several modifications to standard helmet designs have been proposed. Inserting vents, changing properties of the outer shell part and increasing clearance between the head and helmet have been demonstrated to

Multi-sector thermophysiological head simulator

increase dry and wet heat transfer through different kinds of helmets using heated headforms (Brühwiler et al., 2006; Fonseca, 1976; Liu and Holmér, 1997; Reischl, 1986). The characterization of twenty-four different bicycle helmets showed convective cooling ranging from 65 to 93% compared to nude head condition (Brühwiler et al., 2006). Radiation was shielded by different helmets from 50 up to 85% (Brühwiler, 2008). In case of human participants trials, design modifications on helmets provided lower temperatures and humidity levels under the helmet (Guan et al., 2007; Holland et al., 2002) and reduced hotness perception (Abeysekera and Shahnava, 1988; Davis et al., 2001; Dullah et al., 2011).

Numerous studies have substantiated the complexity of the head thermal response. Research on local differences in skin and air temperature, regional variation of sweat rates in the cranial region (De Bruyne et al., 2010, 2008; Machado-Moreira et al., 2008b), as well as moisture accumulation under a helmet (De Bruyne et al., 2008; Dullah et al., 2011), have provided some basis for head heat transfer mapping. Dependency of local thermal perception on local temperatures and humidity under a helmet also indicates the importance of knowing spatial differences in microclimates at the head (Bogerd et al., 2010; Dullah et al., 2011). Based on this knowledge, local cooling could be optimised in helmets taking into account spatial differences in thermal sensitivity at head. Observations regarding thermal sensitivity at the scalp revealed site-wise variations in warmth perception thresholds (i.e. 5°C between the most sensitive location at the temporal region and the least sensitive at parietal region) (Mehrabyan et al., 2011) and significant variations in thermal thresholds, both cool and warmth sensitivities, in the face as well (Essick et al., 2004). Figure 1.1 shows the head division based on the main bones forming the skull.

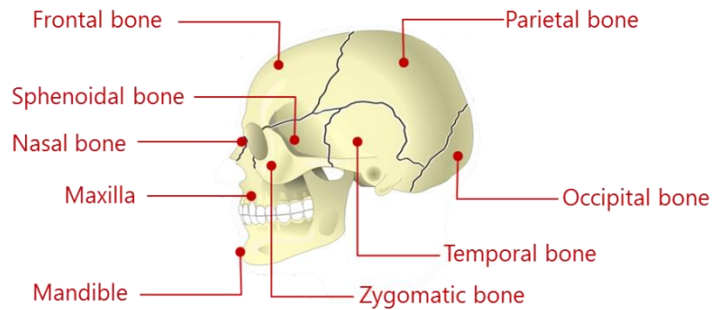


Figure 1.1. Anatomical head parts (adapted from (Netter, 2014))

According to the local differences in thermal sensitivities at the human head, research providing a higher spatial resolution in local heat transfer of helmets has become crucial for fully understanding heat losses mechanism of the head. De Bruyne et al. and Van Brecht et al. evidenced regional differences in ventilation efficiency of bicycle helmets by applying an adapted tracer gas measurement technique distributed on thirteen and nine sampling locations, respectively (De Bruyne et al., 2012; Van Brecht et al., 2008). An eight-thermocouple lay-out placed on a thermal headform surface allowed detecting higher temperature increases in the lower parietal region ($1.7 \pm 0.1^{\circ}\text{C}$) than in the region just above the ear ($0.5 \pm 0.1^{\circ}\text{C}$) when wearing different cricket helmets (Pang et al., 2013).

Thermal manikins representing human body anatomy either fully or partially are an extended methodology to systematically analyse heat and mass transfer in clothing research. Their application enables a reproducible comparison between protective equipment and gear that provides highly valuable information for the industry (ISO15831, 2004; ISO9920, 2007). Specialized body parts thermal manikins are an increasing trend as an alternative to full-body manikins for investigating heat transfer properties of human wear goods. Beside lower cost, their operation control

Multi-sector thermophysiological head simulator

is clearer for separate body parts as thermal interaction between parts is reduced and due to smaller size, environmental heterogeneities are expected to be less. Due to a finer segmentation, they allow investigation of local thermal properties of garments or protective equipment with great detail.

Likewise full-body manikins, the surface temperature of a body part manikin (i.e. head manikin) is typically controlled by means of a feedback loop at a fixed set point similar to human skin temperature at thermoneutral state (e.g. between 34°C and 36°C) (Brühwiler, 2003; Fonseca, 1974; Liu and Holmér, 1995; Pang et al., 2011; Reischl, 1986). The heating power needed to maintain this temperature on the manikin surface during a steady-state period quantifies the combined net heat loss through convection, conduction, radiation and eventually evaporation. Current thermal head manikins can actively heat but cooling can be only passively achieved by not heating and evaporating water from its surface. Some of the thermal headforms described in the literature are equipped with a limited number of water-releasing outlets to simulate sweating, and hence, to quantify evaporative heat losses (Brühwiler, 2003; Fonseca, 1974; Liu and Holmér, 1995).

Apart from a temperature control mode, other operation modes aimed at approaching the human thermal physiology have been also reported. In the constant heat flux mode, constant heating power is delivered to every manikin part with the aim of simulating different metabolic rates. Nevertheless, depending on the environmental conditions, it can result in unrealistic temperature distribution due to the absence of the thermoregulatory actions. Another approach dealing exclusively with neutral condition is provided by the comfort mode. In this mode, the mean surface temperature is dynamically regulated according to the heat exchanged with the environment according to a linear relationship derived from

Fanger's comfort equation and necessary assumptions accounting for limitation of the manikin measurement system (Bogdan and Zwolinska, 2012; Foda and Sirén, 2012; Tanabe et al., 1994). Additionally, in a multiple-parts manikin it is possible to set different temperature set-points for each independent zone, for mimicking one static human body temperature distribution (McCullough et al., 1985). However, irrespectively of the operation mode, the ability of thermal manikins to replicate the underlying thermophysiological adaptive reactions that exist in human-beings especially in cold or hot environments is very constrained.

The prediction of the physiological state of the body is provided by mathematical models of human thermal physiology and comfort. Mathematical models of the human physiology use spatially-divided body anatomy for the simulation to increase accuracy of the results. Although models are powerful tools to predict human thermal response, they are not capable of accounting for complex heat and mass exchange processes occurring in human skin-clothing-environment system when the clothing is worn as they mostly simplify clothing description in few static parameters mainly thermal insulation and evaporative resistance. The dynamic nature of the thermal exchange occurring within the clothing might significantly affect the complex coupled heat and mass transfer phenomena, such as moisture absorption-desorption cycles, condensation-evaporation cycles or perspiration migration across clothing layers that can share substantial heat loss depending on fabric properties and location (Fan and Cheng, 2005a; Havenith et al., 2013, 2008; Wissler and Havenith, 2009; Wu and Fan, 2008). Instead, the thermal devices could experimentally quantify the real heat and mass exchange due to the given actual gear and surrounding environment. Therefore, the possibility of incorporating the exact heat loss at skin into the physiological model calculations is a high reliable alternative to the virtual modelling of the transient response and can potentially

Multi-sector thermophysiological head simulator

lead to a more precise prediction of human thermal response (Jones, 2002). For this reason, several attempts to couple thermal manikins (full-body manikins and cylinders) with thermophysiological models have been undertaken. They have proved to accurately evaluate effect of clothing and environmental factors on human thermal response (Burke et al., 2009; Foda and Sirén, 2012; Psikuta et al., 2008; Rugh et al., 2004). Nevertheless, the partial coupling of a body part manikin with a mathematical model of the thermal physiology has not been addressed so far.

The aim of this PhD work is to couple a multi-segmental body part manikin - a nine-zone thermal head manikin (Sweating Thermal Head, *Thermetrics*, Seattle WA, USA) with one of the most advanced thermophysiological models currently existing (Fiala and Havenith, 2015; Fiala et al., 2001, 1999; Psikuta et al., 2012a). Hence, the availability of detailed and realistic spatial data about heat and mass transfer process through the clothing provided by a high-segmented instrument will be combined with an advanced thermophysiological model, constituting a promising tool able to predict global and local human physiological response when using headgear in different environmental situations and activities. Industry will benefit from a reduction in human testing costs, and thus, this novel advanced method for headgear evaluation, so-called thermophysiological human head simulator, will contribute to speed up the development and optimization of thermal and comfort aspects in new headgear concepts.

1.3 AIM AND OBJECTIVES

The aim of this PhD work was to develop a novel advanced method for headgear evaluation based on the coupling of a nine-zone thermal head manikin with a thermophysiological model. This aim was realized in the following stages:

1. Commission and evaluation of a commercially available nine-zone thermal head manikin for headgear testing. To complete this stage, four objectives were carried out:
 - Definition of the additional equipment for representing realistic conditions for headgear testing.
 - Analysis of the precision of the nine-zone thermal head manikin heat flux measurements.
 - Analysis of the consistency of the nine-zone thermal head manikin data with data of a two-zone thermal head manikin previously published.
 - Evaluation of additional findings for the local investigation of heat transfer provided by the novel head segmentation into nine independent zones.

2. Determination of opportunities and constraints of the thermal head manikin when simulating human head thermal regulation. To complete this stage, six objectives were carried out:
 - Definition of the independently controlled head parts in the coupled system.
 - Analysis of the effect of heterogeneous temperature distribution on lateral heat exchange in the head manikin.
 - Analysis of the passive thermal responsiveness of the head manikin.

Multi-sector thermophysiological head simulator

- Analysis of the thermal responsiveness of the head manikin if operated using a dedicated active control (PI) during sudden surface temperature change.
 - Adjustment of the dedicated active control (PI) values to provide a more adequate response of the head manikin.
 - Characterization of the evaporation efficiency and evaporation responsiveness of the head manikin sweating system.
3. Validation of the physiological model for prediction of global and local skin temperatures against a dedicated database of human experiments. To complete this stage, four objectives were carried out:
- Development of a comprehensive database of experimental data including detailed information on local physiological parameters to be used for the validation of any advanced model of human thermoregulation.
 - Completion of the human data base by collecting human physiological data for cycling activity in a moderate environment.
 - Verification of the effect of the sensors attaching method on surface temperature measurements.
 - Validation of the physiological model running alone for prediction of global and local body temperatures in a wide range of scenarios including relevant human and environmental factors, such as cold, moderate and warm environmental temperature, different levels of relative humidity, high wind speed, presence of solar radiation, moderate and high activity levels and protective clothing.

4. Coupling the nine-zone thermal head manikin with the mathematical model of the human physiology to achieve a dynamic manikin control according to the real-time predicted human thermal response and validation of the coupled system. To complete this stage, four objectives were carried out:
 - Development of an algorithm implemented in Matlab R2013a to allow the communication between the thermal head manikin and the physiological model in a real-time feedback loop.
 - Analysis of the consistency of pure virtual simulations calculated by the physiological model under different types of boundary conditions.
 - Analysis of the convergence of the coupled simulations towards the pure virtual simulations.
 - Validation of the coupled system by comparing predicted global and local thermal responses against human data in ten different exposures representing different environmental temperatures and activity levels as preliminary study before its application for clothing evaluation.

The work is presented in five chapters apart from this introductory chapter 1. The chapter 2 shows the commissioning of the thermal head manikin and the corresponding experimental set-up for a detailed investigation of local heat loss through headgear. The chapter 3 aims at analysing the opportunities that allow the performance of the thermal head manikin when simulating the human head physiology. The chapter 4 describes the development of an experiment database containing human physiological data needed for validation of the physiological simulations and an extensive validation of the physiological model foreseen for the coupling when running alone. The chapter 5 explains the coupling method considered for operating the thermal head manikin in a physiological mode and

Multi-sector thermophysiological head simulator

some examples of validation of the newly developed methodology. Finally, the chapter 6 provides the general conclusions and the recommendations for future work.

2 EVALUATION OF THE NINE-ZONE THERMAL HEAD MANIKIN

2.1 INTRODUCTION

One of the most extended techniques for evaluating thermal properties of headgear is thermal manikins. Thermal head manikins have been developed enabling reproducible and systematic analysis of heat transfer properties of headgear. The use of different thermal headforms, mainly to study ventilation and radiant shielding properties of helmets, has been reported for many different applications such as bicycle (Alam et al., 2010; Brühwiler, 2009, 2008; Brühwiler et al., 2006, 2004; Reid and Wang, 2000), motorcycle (Bogerd and Brühwiler, 2008; Bogerd et al., 2010), rowing (Bogerd et al., 2008), cricket (Pang et al., 2013, 2011), firefighting (Reischl, 1986), industrial safety (Abeysekera et al., 1991; Hsu et al., 2000; Liu and Holmér, 1997) and military headgear (Fonseca, 1974; Oscewski,

Multi-sector thermophysiological head simulator

1996). Thermal head manikins provide an anatomical representation of the human head geometry and size with a typical simplification of the face region, where ears and hair are usually not present. The surface of thermal headforms is divided into a diverse number of independent heated zones (Brühwiler, 2003; Liu and Holmér, 1995; Oszcewski, 1996; Reid and Wang, 2000; Reischl, 1986). Several heating methods have been applied in different manikins with heating resistance wires being most common (Brühwiler, 2003), a light bulb inserted into the head or filling the head with warm water (Hsu et al., 2000; Pang et al., 2011; Reischl, 1986). The surface temperature of the manikin is typically measured using a resistance wire evenly wounded on the independent zones and controlled at a fixed set-point temperature corresponding to human skin temperature at thermoneutral state (e.g. between 34 °C and 36 °C (Brühwiler, 2003; Fonseca, 1974; Liu and Holmér, 1995; Pang et al., 2011; Reischl, 1986)). The power needed to maintain this temperature at stable environmental conditions (air and radiant temperature, relative humidity and wind speed) refers to the net combined heat loss through convection, conduction and radiation.

Despite the high reliability and reproducibility achieved by thermal head manikins, head segmentations described so far are not detailed enough to provide valuable assessment of local heat losses over the entire head surface. Therefore, a finer and dedicated segmentation might allow investigating thermal properties of headgear with adequate spatial resolution to be related to local physiology. Combining the reproducibility of thermal head manikins with high spatial resolution in the study of local heat loss might yield to a better understanding of the mechanisms underlying thermal effects in headgear.

2.2 AIM AND OBJECTIVES

This chapter 2 aimed at defining the operation conditions of a novel nine-zone thermal head manikin for headgear testing. For this purpose, four main objectives have been undertaken and described in this chapter:

- Selection and characterization of the elements constituting the testing setup.
- In-depth analysis of the precision of the heat fluxes measurements by the nine-zone thermal head manikin.
- Analysis of the consistency of the nine-zone thermal head manikin data with data of a two-zone thermal head manikin previously published.
- Evaluation of additional findings for the local investigation of heat transfer provided by the novel head segmentation into nine independent zones.

2.3 SELECTION AND CHARACTERIZATION OF THE ELEMENTS CONSTITUTING THE TESTING SETUP

2.3.1 The nine-zone sweating head manikin

The measuring system is a Sweating Thermal Head (*Thermetrics*, Seattle WA, USA, 2012). The thermal head manikin's surface is divided into 9 independent heated zones able to measure individual heat loss and surface temperature (Figure 2.1) and to control sweating rates. Head circumference measured above eyebrow-site is 59 cm. The headform is made of carbon fibre-epoxy with thermally conductive reinforcement. Distributed heating wires and wire temperature sensors are wounded on the inner and outer surface for each zone, respectively. The thermal head manikin presents a dedicated segmentation designed according to Empa's

Multi-sector thermophysiological head simulator

previous experience in headgear testing. The cranial region of the nine-zone manikin was finely segmented into six independent zones typically covered by headgear. The zones included right and left temple as well as a serial fragmentation of the area in-between for more detailed investigation of heat transfer from anterior to posterior parts. Face, forehead and neck were the remaining independent zones. A thermal guard is placed at the base of the neck to prevent lateral conductive heat loss downwards to the enclosure box. Zone surface areas are given in Table 2.1.

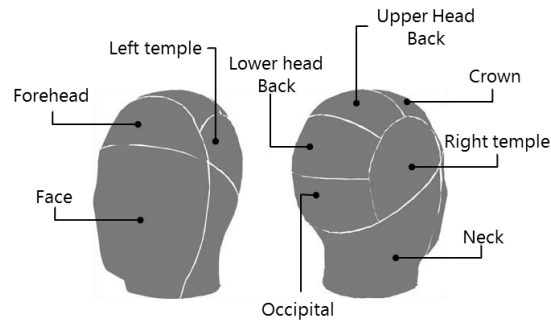


Figure 2.1. Nine-zone thermal head manikin segmentation.

Table 2.1 shows the surface area size for each zone of the head manikin.

Table 2.1. Head manikin zones areas.

Head manikin geometry	
Zone	Area [m²]
Forehead	0.0094
Face	0.0357
Left temple	0.0094
Right temple	0.0094
Crown	0.0095
Upper head back	0.0095
Lower head back	0.0095
Occipital	0.0095
Neck	0.0366
Total area	0.1385

The system includes with two environmental temperature and one relative humidity sensors (Temperature: Betatherm, *Thermetrics*, Seattle WA, USA and RH: *Vaisala Oyj*, Helsinki, Finland).

The sweating system of the head manikin consists of a general pump and each zone flow is controlled by a micro-controller acting on a single valve. The time for which the valve has to be open to release a given amount of sweat has to be regularly calibrated to account for potential partial clogging due to water bacteria activity (see manufacturer procedure described in the system manual). For multi-outlets zones, a number of capillary tubes placed downstream the valve is equally distributing the sweat to the outlets. The head manikin was pre-equipped with a

tight elastic fabric that had to be placed on the manikin to evenly distribute the sweat all over the head surface.

2.3.2 Climatic chamber and wind tunnel

For an accurate evaluation of the headgear, thermal testing of headgear has to be done under controlled environmental conditions. Therefore, the thermal head manikin was placed in a climatic chamber (Temperature range [-5, +35; $\pm 1^\circ\text{C}$], Relative humidity range [20, 70; $\pm 3\%$], dimensions 680 x 300 x 202 cm, *York International*).

To simulate different realistic situations of use some headgear could be tested applying wind. The thermal head manikin was placed downstream at the exit of a small wind tunnel with 50 x 50 cm cross-section (see Figure 2.2). Previous characterization of the wind speed applied by the wind tunnel indicated a maximum deviation of $0.2 \text{ m}\cdot\text{s}^{-1}$ for wind speeds in the range of 0 and $7 \text{ m}\cdot\text{s}^{-1}$ (Brühwiler, 2003). Wind speed was set according to measurements of a multi-directional anemometer (Sensoanemo 5100CL, *Sensors Electronic*, Gliwice, Poland) placed 25 cm before the exit of the tunnel. Additionally, the head manikin system can be placed on a scale (ICS425, accuracy $\pm 0.1 \text{ g}$, *Mettler-Toledo*, Switzerland) to monitor the changes in the clothing weight due to water absorption and evaporation during wet tests.



Figure 2.2. Standard setup for thermal testing of headgear including wind effect.

2.3.3 In-depth analysis of the precision of the heat fluxes provided by the thermal head manikin

2.3.3.1 Characterization of measurements stability

To evaluate the precision of heat fluxes measured by the head manikin, measurements at different environmental temperatures (25, 22, 20, 18, 15, 10 and 5°C, no wind applied) and different wind speeds (0, 3.1, 6.2 m·s⁻¹, ambient temperature 25°C) to screen several combinations of environmental conditions were done. Relative humidity was kept at 50% in all tests. Two kinds of tests were carried out: temperature control mode test and heat flux control mode test.

Temperature control mode test

The protocol consisted of measuring heat fluxes given at each zone of the head manikin when surface temperature was controlled at a set point of 35°C during time periods between 4 and 12 hours.

These long-term measurements revealed a recurring variation in all cases. However, the amplitude of the variation strongly depended on environmental conditions.

Multi-sector thermophysiological head simulator

Generally, the higher the heat flux demanded to keep the manikin surface at 35°C, the higher of variation was observed. In the case presented in Figure 2.3, a maximum heat flux variation up to 70 W·m⁻² representing 21% of the average heat flux was observed for forehead in steady-state environmental conditions. This large instability demonstrated the unreliability in heat flux measurements and resulted in a high inter-test variability.

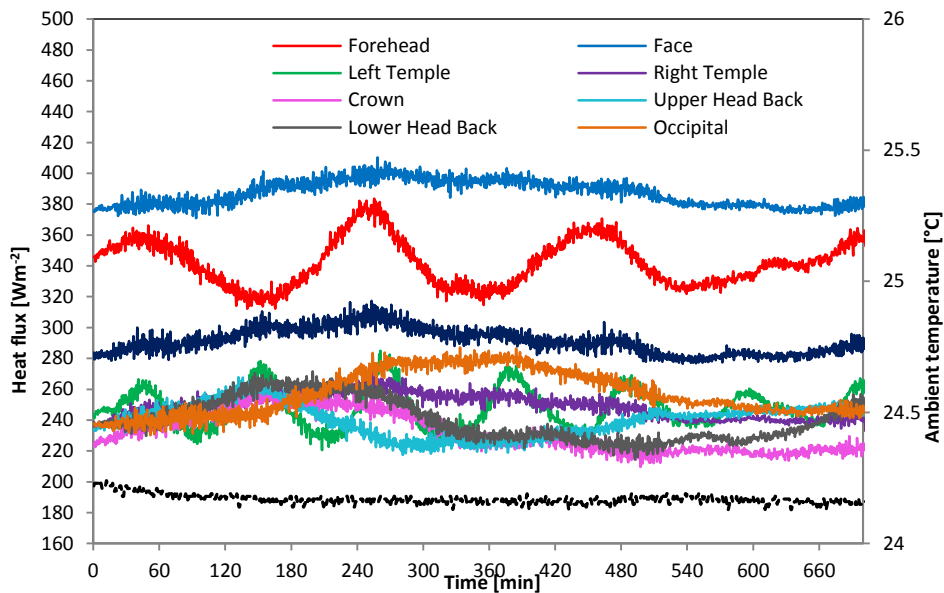


Figure 2.3. Heat fluxes of nine-zone head manikin for surface temperature set constant at 35°C at ambient 25°C / 50%RH / 3.1m·s⁻¹ wind (test duration of 11 hours).

Heat flux control mode test

The protocol consisted of measuring surface temperature at each zone when every head manikin zone was controlled by a constant heat flux set point of 200 W·m⁻² in

Evaluation of the nine-zone thermal head manikin

an environment of 5°C/ not controlled RH/ Still air ($v_a < 0.1 \text{ m}\cdot\text{s}^{-1}$). Guard and enclosure were not controlled by a constant heat flux set point but with a temperature set point of 34°C.

The head manikin surface temperature at each zone together with environmental temperature is presented in Figure 2.4 throughout the whole test duration of 6 hours. Maximum differences in surface temperature over time for individual zones during the steady-state period reached up to 1.5°C in some zones such forehead and left temple.

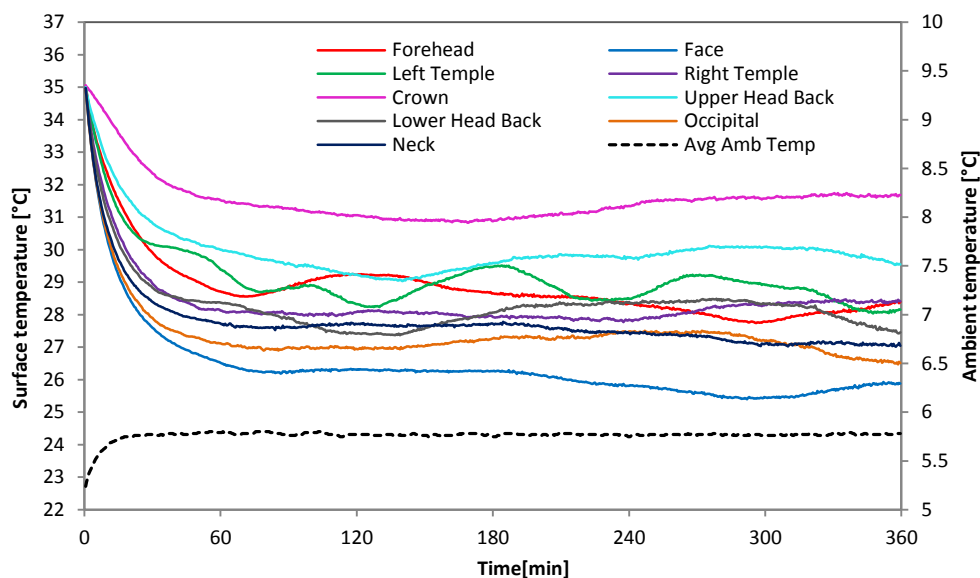


Figure 2.4. Surface temperature of the nine-zone head manikin for heat flux set constant at 200 $\text{W}\cdot\text{m}^{-2}$ and ambient of 5°C / not controlled RH / Still air ($v_a < 0.1 \text{ m}\cdot\text{s}^{-1}$) (test duration of 6 hours).

Maximum differences observed after a stabilization period of two hours for each zone are gathered in Table 2.2. Although ambient temperature was very stable ($5.8 \pm 0.01^\circ\text{C}$ with a maximum variation of 0.04°C), the average maximum variation on

Multi-sector thermophysiological head simulator

head zones was $1.06 \pm 0.28^\circ\text{C}$. However, a long-term surface temperature measurement with all heaters switched off showed an average maximum temperature difference on head zones of just $0.033 \pm 0.005^\circ\text{C}$ (steady-state over 9 hours in an environment 18°C / 50%RH / Still air ($v_a < 0.1 \text{ m}\cdot\text{s}^{-1}$). Average standard deviation for head zones was $0.31 \pm 0.07^\circ\text{C}$ in the test with constant heat flux at $200 \text{ W}\cdot\text{m}^{-2}$, whereas it was just $0.01 \pm 0.00^\circ\text{C}$ for the test in which none of the head zones were heating.

Table 2.2. Maximum differences in surface temperatures [$^\circ\text{C}$] found in test with heat flux set point of $200 \text{ W}\cdot\text{m}^{-2}$ after 120 minutes elapsed.

Maximum differences in surface temperature [$^\circ\text{C}$]								
Forehead	Face	Left Temple	Right Temple	Crown	Upper Head Back	Lower Head Back	Occipital	Neck
1.51	0.92	1.47	0.71	0.92	1.09	1.12	1.04	0.77

2.3.3.2 Detection of source of variation: one active zone

According to results in section 2.3.3.1., every head zone was presenting increased variation in both heat flux and surface temperature once the steady-state was reached in different environmental conditions. To further investigate the possible source of this variation, it was necessary to check if the variation observed at each head zone was related to variation of other head zones. Therefore, temperature control mode tests were carried out having just one individual heated zone controlled at a surface temperature set point of 35°C . Heated zones were randomly selected to be forehead, left temple and lower head back, consecutively. The climatic chamber was set at 22°C / 50%RH / Still air ($v_a < 0.1 \text{ m}\cdot\text{s}^{-1}$). The variation at

Evaluation of the nine-zone thermal head manikin

the heated and non-heated zones was analyzed for each of the three heated zones tested.

Table 2.3 shows variation of the surface temperature and heat flux for steady-state periods over 6 hours of each heated zone during the corresponding test. It can be observed that coefficient of variation stayed below 0.02% and corresponding heat flux variation was below 0.4% in the three presented cases of individually heated manikin zones.

Table 2.3. Average value and variation of the surface temperature and heat flux for forehead, left temple and lower head back when individually heated at temperature set point of 35°C (environmental conditions 22°C / 50%RH / Still air ($v_a < 0.1 \text{ m}\cdot\text{s}^{-1}$). Absolute variation is represented by standard deviation (SD) and relative variation by coefficient of variation (%).

Heated zone	Avg Temperature [°C]	SD Temperature [°C]	CV Temperature [%]	Avg Heat flux [W·m ⁻²]	SD Heat flux [W·m ⁻²]	CV Heat flux [%]
Forehead	35.000	0.007	0.019	337.055	1.326	0.393
Left Temple	35.000	0.0017	0.005	310.042	0.541	0.175
Lower Head Back	35.000	0.0031	0.009	303.112	0.753	0.248

Although variation of surface temperature of the individually heated zone remained below 0.02%, some other non-heated zones showed higher deviation values. Table 2.4 illustrates the case in which just the left temple was heated. Generally, a variation eight times higher than the variation observed for the left temple was observed in surface temperature measurements of other non-heated zones (i.e. coefficient of variation of 0.054% and 0.066% were observed for forehead and crown, respectively).

Multi-sector thermophysiological head simulator

Table 2.4. Variation of other zones when left temple was heated with at a temperature set point of 35°C (environmental conditions 22°C / 50%RH / Still air ($v_a < 0.1 \text{ m}\cdot\text{s}^{-1}$)).

	Avg Temperature [°C]	SD Temperature [°C]	CV Temperature [%]
Forehead	22.788	0.012	0.05
Face	21.64	0.012	0.05
Left Temple	35.00	0.002	0.01
Right Temple	22.319	0.012	0.05
Crown	23.634	0.016	0.07
Upper Head Back	23.887	0.012	0.05
Lower Head Back	22.946	0.012	0.05
Occipital	22.565	0.011	0.05
Neck	21.821	0.016	0.07

These findings showed that the heated zone can potentially induce some variation to the surface temperature of another non-heated zone. Moreover, these results suggest that the variation observed for either all zones heated or not might be related or connected between individual zones.

2.3.3.3 Detection of the source of variation: two or more active zones

To clarify the relationship between the variations observed at each of the head zones, they were investigated in the test in which two head zones were heated simultaneously. Temperature control mode tests with a temperature set point of 35°C were carried out with zones heated in pairs in random combinations at 22°C / 50%RH / Still air ($v_a < 0.1 \text{ m}\cdot\text{s}^{-1}$) environmental conditions. Figure 2.5 presents a first phase of measurements in which left temple was heated alone followed by a second phase in which the lower head back was heated at the same time. It was

revealed that variation in the heat flux at left temple increased as soon as lower head back zone started heating as well showing recurring peaks occurring almost regularly every 1.5 hours. In this particular case, coefficient of variation in the steady-state heat flux for the left temple increased from 0.17% up to 0.66% when the lower head back was heated at the same time.

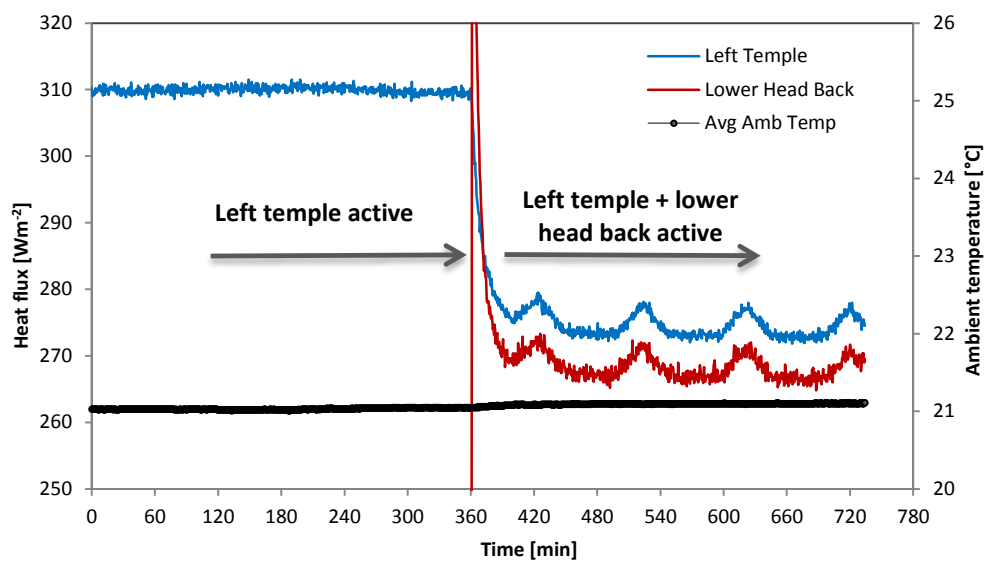


Figure 2.5. Heat flux for the temperature set point of 35°C. First six hours shows left temple heated alone and the following six hours shows left temple and lower head back heated at the same time at the temperature set point of 35°C. The rest of the zones stayed disabled (guard and enclosure included) (22°C / 50%RH / Still air ($v_a < 0.1 \text{ m}\cdot\text{s}^{-1}$)).

Several temperature control mode tests for other different zone combinations were investigated and different levels of interaction between the heat flux variations were observed depending on the particular zones being active. The recurring peaks occurring almost regularly at different time intervals depending on the zones combination were detected in most cases. For this reason and due to the high stability of the environmental conditions, this variation was attributed to a possible

electrical interaction between zones. Even though the coefficient of variation of heat flux observed for every zone remained below 1% in this particular test configuration (two zones active and 22°C / 50%RH / Still air ($v_a < 0.1 \text{ m}\cdot\text{s}^{-1}$), the recurring peaks responsible for the increased variation, resembled the variation observed in heat flux when all the head zones were heated controlled at the set point of 35°C (Figure 2.3).

2.3.3.4 Effect of enclosure activation and wind

The tests described in this section aimed at determining the effect of enclosure and wind on zone heat flux variations. In ambient conditions of 22°C / 50%RH, different tests were carried out to separate the effect of both factors. Similarly to section 0, one individual zone was heated at a temperature set point of 35°C for six hours combining presence of wind or not and having the enclosure active or not as well. Individual heated zones were randomly selected to be forehead, face, left and right temples. Results confirmed that when just one zone was heated, variation on measured heat flux were similar both when wind (i.e. $3.1 \text{ m}\cdot\text{s}^{-1}$) or no wind was applied. Nevertheless, an increase in heat flux variation similar to the one observed for head zones interaction was observed when enclosure heater was active, both in presence and absence of wind. For example, heat flux variation at left temple was found to be 0.17% if the zone was heated alone. If enclosure heater was on, coefficient of variation increased up to 1.1%. If left temple was heated alone at $3.1 \text{ m}\cdot\text{s}^{-1}$ wind, the coefficient of variation increased up to 0.3%.

2.3.3.5 Discussion

When all the heaters were switched off or just one zone was heated (section 0), heat flux signals remained stable throughout long periods of time but slightly

increased variation was observed at surface temperature of non-heated zones. When two or more zones were heated to follow the temperature set point of 35°C, heat flux measurements showed recurring peaks that were causing an increased variation in heat flux (Figure 2.3 and Figure 2.5). Likewise, when two or more zones were heated at a constant heating power set point of 200 W·m⁻², the corresponding surface temperature signals showed as well increased long-term variation (Figure 2.4). The magnitude of this variation depended on the demanded heat flux required to maintain the surface temperature at 35°C and on the number of zones simultaneously heated and the specific heated zones at the same time.

It was concluded that when more than one zone was heated, some electrical cross-interaction between the zone heating and temperature sensing circuits could provide some instabilities in the measured temperature, and hence, in the heating power supply reacting to these instabilities at the different zones. All these results were communicated to the equipment manufacturer that after realizing the problem proceeded to readjust the system.

After repair, absolute heat fluxes average intra-test variation reduced from 4% down to 1.4%. More noticeable was the improvement in the inter-test variation for more precise calculated variables, such as radiant heat gain (section 2.4.2.3), for which an improvement from 23 to 13% for facial section and from 17 to 5% for cranial section of the thermal head manikin was observed. Therefore, this improvement in the electrical control was considered acceptable to proceed with the planned further investigations.

2.3.4 Temperature calibration of the head manikin

The head manikin temperature sensors were calibrated against external surface temperature sensors (Kelvimat type 4342-V600 with sensor Pt100 with accuracy $\pm 0.015^{\circ}\text{C}$, *Minco*, Minneapolis, USA) at three environmental conditions: 15, 25 and 35°C and 50% relative humidity in still air conditions ($v_{\text{air}} < 0.15 \text{ m}\cdot\text{s}^{-1}$). The Pt100 sensors were attached to each of the head zones by using a small piece of aluminum foil which was proved to be a reliable method for measuring surface temperature (Psikuta et al., 2013a). For large zones (face and neck) and temples, two Pt100 sensors were attached and just one for the rest of the zones each time. Seven Pt100 sensors were available and previously calibrated using Optical integrated humidity calibrator system (*Michell Instruments*, Ely, UK).

The head manikin was placed centered in the climatic chamber and outside of the wind tunnel. The environmental conditions were externally monitored with a thermal conditions monitoring system (ThermCondSys 5500, *Sensors Electronic*, Gliwice, Poland) that was placed next to head manikin (Figure 2.6).



Figure 2.6. Laboratory setup for head manikin temperature calibration.

Evaluation of the nine-zone thermal head manikin

Head manikin heaters remained switched off and recording was started after the whole system reached thermal balance with the environment. Head manikin surface temperature sensors and Pt100 sensors measurements were compared during a two-hours steady-state (surface temperature variation below 0.05°C).

Figure 2.7 shows results of temperature calibration at 25°C / 50%. Some differences between head manikin zones and Pt100 sensors could be observed depending on the zone. It was also observed that differences among head manikin zones reached $0.21 \pm 0.03^\circ\text{C}$, whereas it only reached $0.13 \pm 0.05^\circ\text{C}$ for Pt100. Similar observations were made at 15°C (0.18°C for head zones and 0.08°C for Pt100) but not at 35°C when differences between Pt100 were apparent as well (0.23°C for head zones and 0.17°C for Pt100). Interestingly, the mentioned maximum differences observed in surface temperature values were observed between left and right temples at the three ambient temperatures. Differences in temperature values showed by the head sensors and Pt100 sensors remained within $0.02 \pm 0.02^\circ\text{C}$ for right temple, whereas they rose up to $0.21 \pm 0.02^\circ\text{C}$ for left temple. Face, upper head back, occipital and neck consistently showed differences between temperature values measured by the head sensors and Pt100 sensors of above 0.1°C as well.

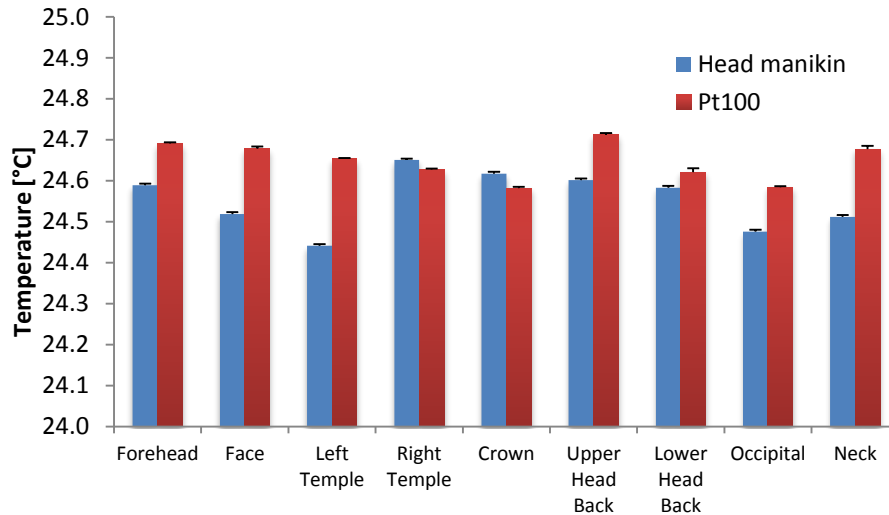


Figure 2.7. Surface temperature of the manikin measured at the calibration point at 25°C/50%RH/Still air ($v_a < 0.15 \text{ m}\cdot\text{s}^{-1}$) using head manikin and Pt100 sensors.

These results suggested slight differences in the calibration done of the surface temperature sensors at the manufacturer for the head zones. Some of the head zones showed a good agreement with the Pt100 measurement, such as right temple, crown and lower head back (differences below 0.02°C). It seemed that mainly the left temple was calibrated below the reference temperature since its average difference to Pt100 sensors was $0.21 \pm 0.02^\circ\text{C}$. The differences found for the face, upper head back, occipital and neck showed by the head sensors and Pt100 sensors were between $0.1\text{-}0.2^\circ\text{C}$ and might suggest calibration values at the manufacturer slightly below those obtained with the Pt100. Nevertheless, this deviation remained within variability found among Pt100 sensors attached to head ($0.13 \pm 0.05^\circ\text{C}$). Despite a consistent difference between the surface temperature values measured by some of the head sensors and the temperature values measured by the reference sensors Pt100, no adjustment was done on the head

zones as these differences were within the variation observed among Pt100 plus the corresponding standard deviation.

2.3.5 Fluid calibration of the head manikin

According to the manikin manufacturer, fluid can be accurately delivered for sweat rates between 30 and 3000 ml·m⁻²·h⁻¹. Hence, the volumetric fluid calibration according to manufacturer procedure should be carried out regularly to keep the flow conductance values updated. The accuracy of the fluid calibration has been increased by applying a gravimetric procedure instead of volumetric.

2.4 ANALYSIS OF THE PERFORMANCE OF THE NINE-ZONE THERMAL HEAD MANIKIN FOR HEADGEAR TESTING

2.4.1 Introduction

In this section, the performance of the novel nine-zone thermal head manikin in comparison to two previously published data obtained with a two-zone thermal head manikin was analysed (Brühwiler, 2003). This manikin was intensively used for investigating heat transfer properties of different kind of headgear at Empa (Brühwiler, 2008, 2003; Brühwiler et al., 2006, 2004; Buyan et al., 2006).

The first part of this work in this section aimed at determining the consistency of the nine-zone thermal head manikin data with previously published data of the two-zone thermal head manikin for bicycle helmets testing in two cases of measurements highly related to cycling scenarios: i) Convective heat transfer (Brühwiler et al., 2006) and ii) Combined convective and radiative heat transfer (Brühwiler, 2008). The second part of the work aimed at determining the additional benefits of the novel head segmentation of nine independent zones such as

detailed investigation of the local heat transfer. It should be noticed that convective and radiative heat transfer mechanisms are always present even though no specific source of radiation is added. However, the combined convective and radiative heat transfer has been lumped under the prevailing convection phenomena using the term convective unless a specific radiation source was added for a better readability.

2.4.2 Methods

2.4.2.1 Strategy for thermal head manikins comparison

Heat transfer data for various bicycle helmets published by Brühwiler (Brühwiler, 2008; Brühwiler et al., 2006) was used for the evaluation of the nine-zone manikin (hereafter 9zM) (Figure 2.8 (a)). One study investigated convective heat losses (Brühwiler et al., 2006), while in the other study they measured combined convective and radiative heat transfer for various bicycle helmets (Brühwiler, 2008). In these studies, heat transfer was investigated for the facial and cranial sections using the two-zone thermal head manikin (hereafter 2zM) (Figure 2.8 (b); (Brühwiler, 2003)). Part of these studies were replicated with the 9zM to assess consistency of the measurements and to provide a detailed analysis based on the local information obtained from the more finely segmented thermal head.

A two-zone thermal head manikin (2zM) (Brühwiler, 2003) has been intensively used for investigating heat transfer properties of different kind of headgear (Brühwiler, 2008, 2003; Brühwiler et al., 2006, 2004; Buyan et al., 2006). This headform was adapted from a polyester shop window manikin (see Figure 2.8 (b)). It was divided into two measuring sections: cranial section (the upper and rear part of the head) and the facial section (comprising also forehead, ears and a small part

of the neck). A third zone below called neck had the function of thermal guard. The heating system was divided in three different circuits. Heating foils were attached to the inner surface of the cranial and neck sections, whereas face was heated by means of a heating wire densely placed inside. The average surface temperature of each head section was independently measured with a resistance wire wounded in the outer surface and covered by a thin layer of varnish. Head circumference was 58 cm (Brühwiler, 2003).

To compare data from 9zM with 2zM, outputs from the 9 zones were merged (area-weighted average) to obtain equivalent sections to the 2zM (facial and cranial sections; Table 2.5). Heat fluxes obtained for manikins at facial and cranial sections were expressed relative to surface area ($W \cdot m^{-2}$) to correct for the slight differences in surface area. Although differences in sections size could be negligible, the borders separating the head in two sections were not exactly in the same position and in case of 9zM part of the forehead would belong to cranial section if separation line from 2zM would be applied.

Multi-sector thermophysiological head simulator

Table 2.5. Geometry description of 9zM and 2zM headforms.

9zM		2zM		Difference
Zones	Areas [cm ²]	Sections	Areas [cm ²]	9zM-2zM [%]
Forehead	94.2	Facial section	813.6	0.5
Face	817.6			
Neck	366.4			
Left temple	94.1	Cranial section	554.7	2.3
Right temple	94.1			
Crown	94.6			
Upper head back	567.5			
Lower head back	94.7			
Occipital	95.0			
Entire head	1385.1		1368.3	1.2

Figure 2.8 provides additional information on qualitative differences between manikins:

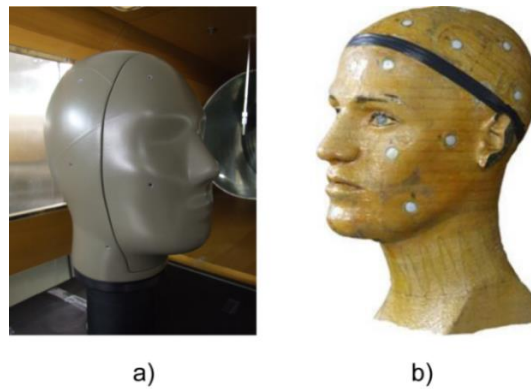


Figure 2.8. Nine-zone thermal head manikin (9zM, a) and two-zone thermal head manikin (2zM, b).

2.4.2.2 Convection tests

Helmets were tested applying four different conditions as described by Brühwiler et al. (Brühwiler et al., 2006) to provide an overview on the manikin performance comparison. Environmental temperature and relative humidity were 25°C and 60% for all the cases. Wind speed (Low: 1.6 m·s⁻¹; High: 6.1 m·s⁻¹) and tilt angle of head (Upright: 0°; Tilted: 30°) were combined as follows: low wind and upright head, high wind and upright head, low wind and tilted head and high wind and tilted head.

The same wind tunnel used for the 2zM was used for the experiments with 9zM. The thermal manikin was centred at the exit of the tunnel. The headform height was adjusted to maintain the centring as the forward tilt angle of the manikin basement was varied. The wind speeds were adjusted to the proposed values for low and high speeds using an omnidirectional anemometer (Sensoanemo 5100CL, *Sensors Electronic*, Gliwice, Poland) placed in the same location as for the 2zM experimental setup. Figure 2.9 (a) presents detailed setup for the convection tests.

Six out of twenty-four helmets investigated in the previous study (Brühwiler et al., 2006) were selected. The helmets were chosen based on observed heat losses (low, medium or high) and steadiness of results (low variation). The helmets were tested in the proposed configuration (including visor or soft pads if necessary) as they were sold and they were placed on the 9zM keeping the front brim 3.5 cm above the bridge of the nose. Same helmet coding as in the previous study was used.

The 9zM was heated to a constant temperature of 35°C and the heating power was recorded for each zone (see Table 2.5). Heating power was averaged over a 30-minute steady-state period (heating power variation within ± 3%). This state was reached 30 minutes after the start of each experiment at latest. The 9zM was

covered with an elastic tight-fitting fabric similarly to the 2zM. The main function of the fabric is to support the even dispersion of the moisture during perspiration tests. Even though such tests were not conducted in this study the fabric was applied. These fabrics induce an additional insulation, and thus, heat transfer is reduced compared to the configuration without fabric. To check the effect of these fabrics, some tests with and without fabric were done for high wind and upright head condition. Reductions of 55% and 29% for facial and cranial sections of the 2zM, respectively, and 30% and 14% for the 9zM were observed due to different materials of the fabrics and air gap size. For both manikins, helmets were added on the top of the fabric. The head manikin covered with the fabric was treated as the reference configuration for comparison and named nude head.

Convective cooling performance (CCP) at the cranial section was calculated for each bicycle helmet and condition as the average value of three repetitions. This parameter relates the heat loss observed while wearing a specific helmet ($HF_{Cranial\ section\ Helmet\ i}$) to the heat loss of the nude head manikin ($HF_{Cranial\ section\ Nude\ head}$) in the same condition (Equation 2.1). However, it should be noticed that the so-calculated CCP lumped the convective and radiative heat loss to the environment under the term convective. The consideration of relative values allows the comparison of helmet data obtained from different thermal head manikins. A value of 100% corresponds to a convective cooling performance equal to the nude head manikin.

$$CCP(\%) = \frac{HF_{Cranial\ section\ Helmet\ i} (W \cdot m^{-2})}{HF_{Cranial\ section\ Nude\ head} (W \cdot m^{-2})} \cdot 100\% \quad [2.1]$$

2.4.2.3 Radiation tests

The procedure described by Brühwiler et al. (Brühwiler, 2008) was applied for testing protection against radiation of bicycle helmets with the 9zM. Thermal head manikins are not able to detect radiant heat gain (RHG) directly because heat loss is determined based on heating power needed to maintain surface temperature. Therefore, a special experimental setting was built including the assessment of convective heat loss with and without radiation. Brühwiler et al. (Brühwiler, 2008) proposed ambient conditions of 25°C / 65% RH / 3.1 m·s⁻¹ wind speed with and without applying an infrared heat light of 150 W (T228, Osram, München, Germany). The temperature of the manikin surface was maintained at 35°C. Measurements with and without radiant heat load applied from the front were conducted subsequently to ensure the placement of the helmet on the headform remained the same for both configurations.

A pre-test for nude head with and without radiant load in the former study condition was carried out. However, in case of the configuration with light, local radiant heat gain exceeded heat loss, leading to uncontrollable surface temperature for some zones of the 9zM (particularly for the most exposed zones, forehead and crown). Therefore, ambient conditions of the original procedure had to be modified to obtain heat losses substantially higher than heat gain. Ambient temperature was reduced from 25 to 20°C and the radiant light was dimmed from 150 W to 130 W. Geometry of the 9zM ensemble did not allow keeping the same distances from the lamp if the manikin was centred in the wind tunnel. Position of the 9zM ensured to have the same incidence angle of the light of 53°. Five out of twenty-six helmets tested in the study (Brühwiler, 2008) were selected. The selection was done representing low, medium and high levels of radiant heat gain

Multi-sector thermophysiological head simulator

detected with the 2zM. Same helmet coding as in the previous study was used. Figure 2.9 (b) presents detailed setup for the radiation tests.

In the procedure with the 9zM, the role of the visor in the protection against radiation was also assessed by testing helmets without and with visor. In the same way as described for convection tests, the 9zM zones were heated up to 35°C and the heating powers were individually recorded for each independent zone (see Table 2.1). Unlike Brühwiler (Brühwiler, 2008) and due to the high sensitivity of individual zones, median value throughout 75 minutes of steady-state period (average heating power variation over the entire head surface within $\pm 3\%$) was calculated. Separately for facial and cranial sections, difference in heat losses for consecutive tests without (*HF Light OFF*) and with light (*HF Light ON*) source was defined to be the **radiant heat gain RHG** (Equation 2.2.). Similarly to convection tests, the heat loss referenced in the calculation lumped the convective and radiative heat loss to the environment in both situations, having an additional source of radiation when the infrared light was applied.

$$RHG (W \cdot m^{-2}) = HF_{Light\ OFF} - HF_{Light\ ON} \quad [2.2]$$

Based on RHG data, **radiant shielding (RS)** corresponding either to facial or cranial section was calculated for each bicycle helmet with and without visor as the average value of three repetitions. This parameter includes RHG for the nude manikin (*RHG Nude head*) as well as for the manikin covered with a specific helmet (*RHG Helmet i*) (Equation 2.3). This calculation allows comparing helmet data obtained from different thermal head manikins. A value of 100% indicates complete radiant shielding (no radiation reaches the head) whereas a value of 0% indicates no shielding effects.

$$RS(\%) = \frac{RHG_{Nude\ head}(W \cdot m^{-2}) - RHG_{Helmet\ i}(W \cdot m^{-2})}{RHG_{Nude\ head}(W \cdot m^{-2})} \cdot 100\% \quad [2.3]$$

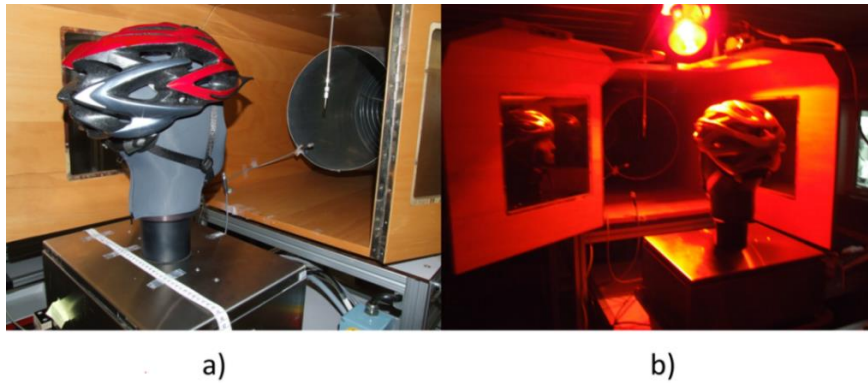


Figure 2.9. Convection tests setup (a) and radiation tests setup (b).

2.4.2.4 Statistical analysis

Statistical analysis was carried out with statistical software (IBM, SPSS Statistics 22) separately for convection and the radiation study. For manikin-performance-comparison, reliability tests were conducted and inter-manikin reproducibility was calculated. Differences in CCP and RS were analysed separately for manikins.

Reliability for experiments conducted with 2zM and 9zM was assessed based on intra-class correlation coefficient (ICC, average measures coefficient), standard deviation (SD) and coefficient of variation (CV). ICC represented the intra-manikin repeatability (ideal ICC value for consistency of measurements is 1), SD represented the absolute variation and CV represented the relative variation of heat loss and radiant heat gain for all helmets and test conditions (convection and radiation tests). Inter-manikin reproducibility was evaluated by calculating Pearson's correlation coefficient (Pearson's r) for heat flux and radiant heat gain separately. In

Multi-sector thermophysiological head simulator

this analysis, helmet data for all test configurations (convection and radiation tests) were included. Data of the nude head manikins have been compared separately from helmet data.

Helmets were classified according to their CCP and RS for each manikin. A one-factor analysis of variance with Tukey post-hoc analysis was conducted to reveal statistical differences. The level of significance was set at $P < 0.05$.

Statistical comparison between helmets based on local data of the nine zones of 9zM was carried out by the same one-factor analysis of variance. For convection tests, differences for CCP of the cranial section were contrasted with differences for CCP obtained at each individual zone of the 9zM, partially or totally covered by the helmet. Face and neck zones were not included in the analysis of CCP as they were not covered by the helmet. Likewise, differences for RS of each individual zone of the 9zM were contrasted with the corresponding RS of the facial and cranial sections in case of radiation tests.

2.4.3 Results

2.4.3.1 Reliability and inter-manikin reproducibility analysis

Convection tests

Heat loss for the nude headform was higher for the 9zM with regards to the 2zM (average values of four testing conditions were 42% and 1% higher for facial and cranial sections, respectively). Both devices showed high reliability with lower variation of data for 9zM compared to 2zM (see Table 2.6). Inter-manikin reproducibility analysis revealed that for similar test configurations, the 9zM required higher heat fluxes at facial section to maintain the manikin surface

Evaluation of the nine-zone thermal head manikin

temperature at 35°C. A significant and high correlation was found for heat losses at facial and cranial sections ($P < 0.01$, Pearson's $r > 0.98$). Figure 2.10 shows the correlation observed between heat loss measured with both head manikins at facial and cranial section. Despite the high correlation observed for both facial and cranial section, Figure 2.10 shows that the heat loss measured at facial section was systematically lower for the 2zM than for the 9zM whereas heat loss at cranial section seemed to be close to the line of identity.

Table 2.6. Reliability analysis for facial and cranial sections heat losses ($W \cdot m^{-2}$) for 2-zone manikin (2zM) and 9-zone manikin (9zM) in convection tests (data for 6 helmets and nude head at 4 test conditions). ICC (intra-class correlation index), CV (coefficient of variation) and SD (standard deviation).

		2zM	9zM
Facial section	ICC	0.94	0.99
	CV [%]	1.96	0.71
	SD [$W \cdot m^{-2}$]	3.07	1.66
Cranial section	ICC	0.99	1.00
	CV [%]	1.76	0.69
	SD [$W \cdot m^{-2}$]	2.78	1.03

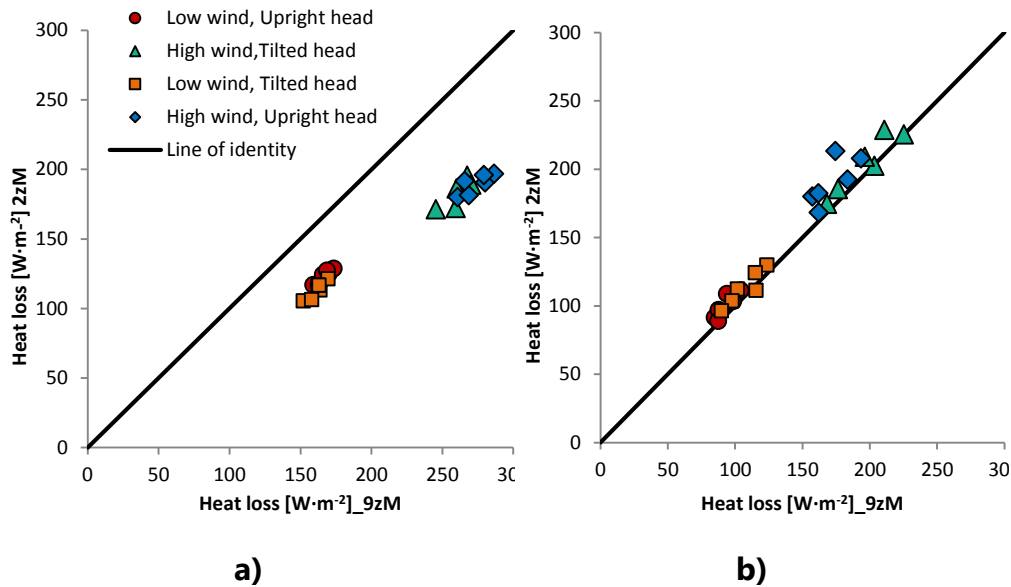


Figure 2.10. Correlation for heat loss at facial (a) and cranial (b) sections between 2-zone manikin (2zM) and 9-zone manikin (9zM). Graphs include the line of identity.

Radiation tests

In nude head conditions, due to ambient temperature was reduced by 5°C if compared with the original setup, 9zM had to provide 37% and 32% higher heat flux than 2zM when the light was turned off at facial and cranial sections respectively. Total radiant heat gained by the entire head was 9.30 W and 8.86 W for 2zM and 9zM respectively. However, it was differently distributed between facial and cranial sections (44% and 56% for 2zM and 67% and 33% for 9zM). Table 2.7 shows the reliability analysis for heat fluxes (HF Light OFF and HF Light ON) and RHG at facial and cranial sections of both headforms for radiation tests conditions. Reliability was high (ICC > 0.8) for both manikins in all cases except for HFLight ON

Evaluation of the nine-zone thermal head manikin

at facial section of the 2zM. The 9zM showed lower deviations for single HFLight OFF and HFLight ON measurements than 2zM. Deviation was the same for RHG at cranial section and it was reduced for RHG at facial section for 2zM. Inter-manikin reproducibility analysis showed significant and high Pearson's correlation ($P < 0.05$, Pearson's $r > 0.90$) for RHG only at the cranial section. Figure 2.11 shows the correlation observed between radiant heat gain measured with both head manikins at facial and cranial section. Generally, higher RHG was observed for the 2zM than for the 9zM at the facial section whereas the opposite trend occurred at the cranial section.

Table 2.7. Reliability analysis of heat fluxes for light off (HFLight OFF) and light on (HFLight ON) conditions as well as radiant heat gain (RHG) calculations for facial and cranial sections for 2-zone manikin (2zM) and 9-zone manikin (9zM) in radiation tests (data for 5 helmets in 2 test conditions, without and with visor and nude head). ICC (intra-class correlation index), CV (coefficient of variation) and SD (standard deviation).

Facial section						
	2zM			9zM		
	HFLight OFF	HFLight ON	RHG	HFLight OFF	HFLight ON	RHG
ICC	0.84	0.58	1.00	0.96	0.97	0.99
CV [%]	3.54	3.74	5.70	0.98	0.86	13.23
SD [W·m⁻²]	9.68	9.72	0.76	4.00	3.27	3.00

Cranial section						
	2zM			9zM		
	HFLight OFF	HFLight ON	RHG	HFLight OFF	HFLight ON	RHG
ICC	0.99	0.93	0.99	1.00	1.00	0.99
CV [%]	2.33	2.77	4.86	0.91	1.17	4.85
SD [W·m⁻²]	4.25	4.07	2.14	1.97	2.27	1.17

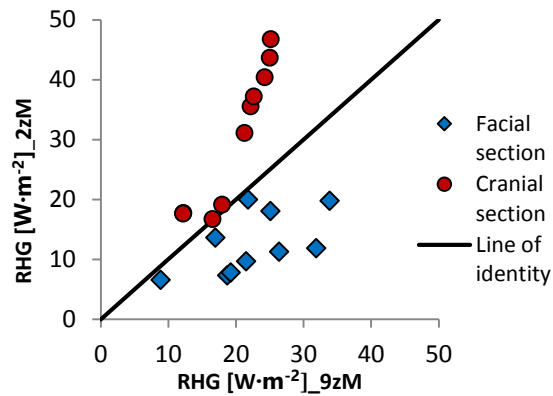
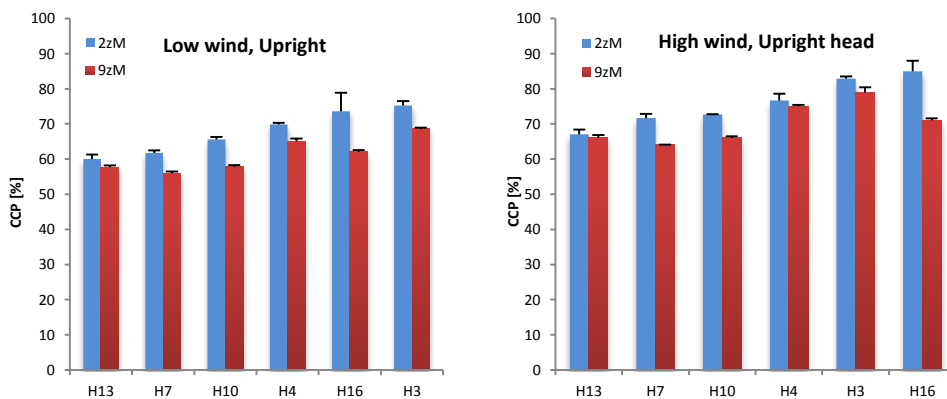


Figure 2.11. Correlation for radiant heat gain (RHG) at facial and cranial sections between 2-zone manikin (2zM) and 9-zone manikin (9z M). The graph includes the line of identity.

2.4.3.2 Statistical comparison between helmets according to 2zM and 9zM

Convection tests

Figure 2.12 shows CCP for cranial section for each helmet and for both head manikins separately for each testing condition. Helmets are ordered according to classification obtained by 2zM (Brühwiler et al., 2006).



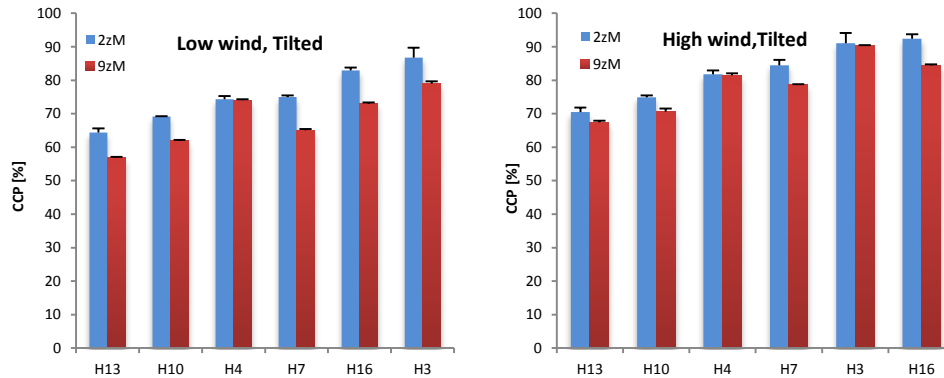


Figure 2.12. Comparison of convective cooling performance (CCP) provided by each helmet for each headform at the different testing conditions. Helmets are presented in ascending order according to CCP for 2zM.

In general, CCP was reduced on average 6 percentage point for 9zM compared to 2zM (significant differences ($P < 0.05$) for all conditions except for high wind and tilted head). Similarities and differences analysis between helmets according to each device showed some significant differences ($P < 0.05$) and some helmets were differently rated. For example, in low wind and upright head condition, helmet 3 provided the same CCP than helmets 4 and 16 when using 2zM, whereas CCP of helmet 3 was significantly higher for test with 9zM. Similarly, the opposite case was observed for high wind and upright head condition for helmets 10 and 13 as they were significantly different according to 2zM and the same according to 9zM. For the low wind and tilted head, CCP of helmets 4 and 16 was different according to 2zM but the same according to 9zM. In case of high wind and tilted head condition, the 2zM did not detect significant differences between helmets 4 and 7 and between 3 and 16, whereas differences were found with 9zM.

Radiation tests

RS for the facial and cranial sections for each device and helmet are shown in Figure 2.13. Helmets are ordered according to classification obtained by 2zM (Brühwiler, 2008).

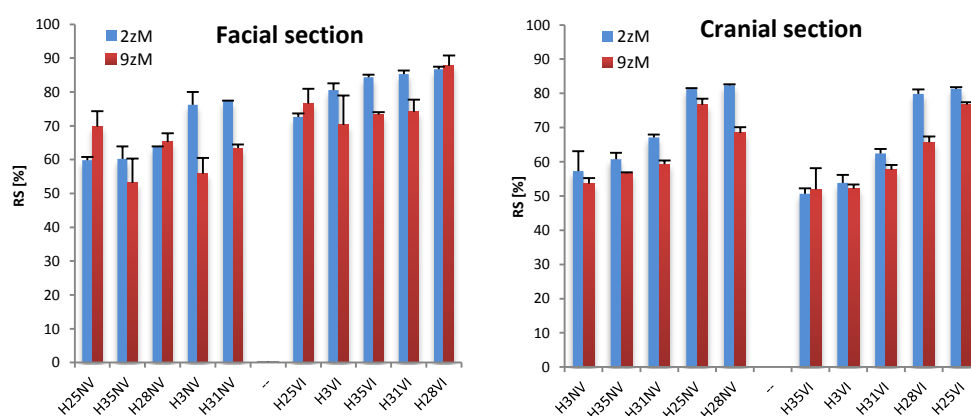


Figure 2.13. Comparison of radiant shielding (RS) provided for facial and cranial section for each helmet without visor (NV) and with visor (VI). Helmets are presented in ascending order according to RS for 2zM.

For facial section, the 2zM distinguished two significantly different helmets groups based on RS data without visor such as helmets presenting low radiant shielding (helmets 25, 35 and 28) and high shielding (helmets 3 and 31). In contrast, the 9zM showed a different order for helmets according RS at facial section. Interestingly, helmet 25 and 28 were pointed as the least protective according to the 2zM and they were rated as the most protective according to 9zM. Similarly, in cases with visor, both manikins detected statistically significant differences between helmets for protection of the facial section. Nevertheless, when provided with a visor, helmet 25 was significantly ($P < 0.05$) the least protective according to 2zM and

one of the most protective according to 9zM. In case with visor, both manikins agreed for helmet 28 as the one offering the highest radiant shielding at the facial section ($P < 0.05$).

For RS at the cranial section, in both cases with and without a visor, both manikins showed the same classification except for helmets 25 and 28. These helmets were not different when using 2zM. However, helmet 25 provided significantly higher shielding at cranial section than helmet 28 when using 9zM.

2.4.3.3 Statistical comparison between helmets based on local data of 9zM

Convection tests

Three selected helmets were analysed based on individual zones exposed to the same conditions for CCP assessment to illustrate additional local data of the 9zM. Figure 2.14 shows the CCP values for low wind and tilted head condition. For the cranial section, helmet 3 showed the highest heat loss for all testing conditions ($P < 0.05$) (Figure 2.12). The analysis of the individual zones disclosed that the CCP of helmet 3 was not the highest at the rear part of the head (upper and lower head back zones). Helmet 16 had significantly higher cooling rates than helmet 3 in these two zones ($P < 0.05$). Differences in CCP for individual zones became apparent for the upper and lower head back as well as for the occipital zone, where helmet 4 presented the highest CCP among these selected helmets ($P < 0.05$).

Multi-sector thermophysiological head simulator

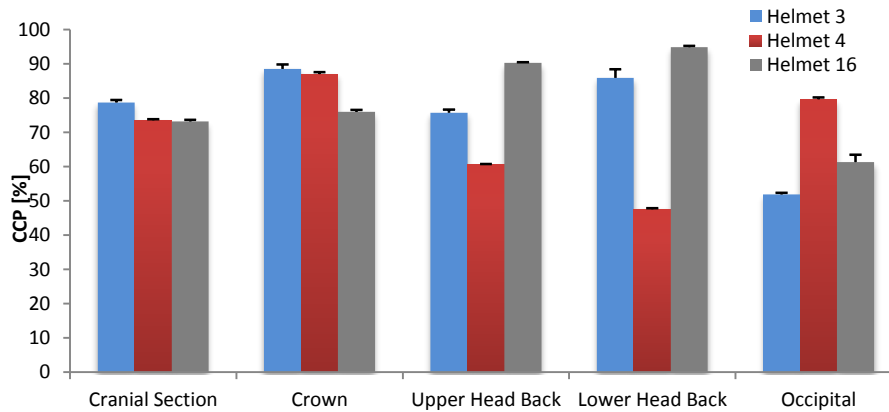


Figure 2.14. CCP at cranial section and at individual zones of 9zM (Crown, Upper Head Back, Lower Head Back and Occipital) in low wind and tilted head test condition for some illustrative helmets.

Radiation tests

Local data for helmets 25 and 31 for facial section and for helmets 3 and 35 for cranial section with visor are presented in Figure 2.15 to illustrate additional local information provided by the 9zM. Averaged RS for facial and cranial section agreed with the most exposed individual zones to the radiation source included in the corresponding section. Nevertheless, some additional local effects on radiant shielding due to helmet design could be detected by the 9zM.

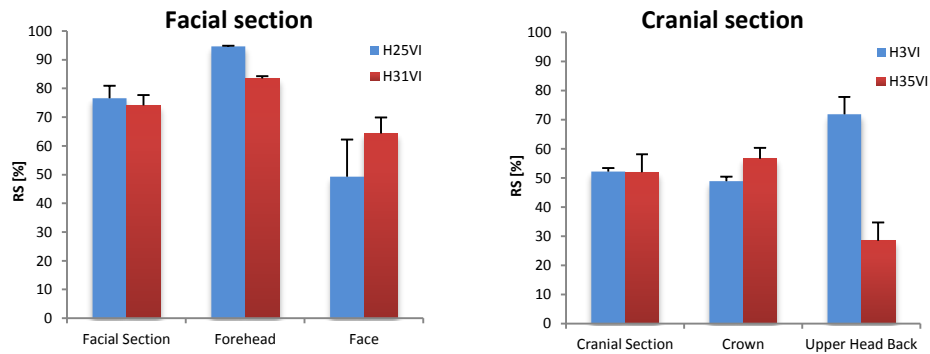


Figure 2.15. RS at facial and cranial section and at corresponding individual zones of 9zM (Forehead and Face within Facial Section and Crown and Upper Head Back within Cranial Section) for some illustrative helmets at test condition with visor (VI).

When equipped with visor, no significant differences between ($P > 0.05$) were found for RS in the facial section between helmets 25 and 31. However, helmet 25 was shielding radiation significantly higher at the forehead ($P < 0.05$). Helmet 3 and 35 provided the same radiant shielding at cranial section when equipped with visor. Nevertheless, it was possible to detect that helmet 35 protected the crown zone significantly higher than helmet 3 ($P < 0.05$). Contrarily, for upper head back zone, helmets 3 shielded radiation more effectively ($P < 0.05$) than helmet 35. Protection added by the visor played a significant role in face shielding for all the helmets except helmet 3 ($P < 0.05$). Significance of the effect was similar at facial section and locally at face zone.

2.4.4 Discussion

2.4.4.1 Reliability and inter-manikin reproducibility

Inter-test reliability for heat flux measurements in convection tests was very high as shown by the ICC values close to 1 for both manikins and for both facial and cranial

Multi-sector thermophysiological head simulator

sections (Table 2.6). The 9zM showed high ICC-values for heat flux when applying the experimental setup for radiation tests while corresponding ICC-values for the 2zM were noticeably reduced in case of facial section (Table 2.7). Standard deviation and CV of heat fluxes from the 9zM were lower than those from 2zM for convection and radiation tests (see Table 2.6 and Table 2.7). In literature, different reference values for heat flux variation have been reported such as 4% of variation was proposed in international standards (ISO15831, 2004), a CV of 5% is stated as a good reproducibility in thermal insulation and moisture-vapour resistance (Fan and Qian, 2004) and a CV of 3% was reported for walking conditions or low wind speeds (Holmér and Nilsson, 1995). An inter-laboratory comparison on thermal insulation of whole body manikins (eight European research institutions) provided a common value for intra-laboratory coefficient of variation of 3% (Anttonen et al., 2004).

The resulting RHG out of radiation tests showed a high reliability for both manikins at facial as well as at cranial section (ICC > 0.9). Standard deviation for the RHG was lower with 9zM only for cranial section. CV of RHG achieved by 9zM was higher for facial section but the same values were observed at cranial section (Table 2.7). This fact resulted in a lower resolution for RHG assessment in case of 9zM at facial section. Different factors may have contributed to this increased variability. Some long-term instability at heat fluxes on different head zones has been observed, especially in case of face and forehead zones. Due to the radiation setup, forehead, face and neck are the zones showing the higher heat loss as they are directly facing the wind, whereas radiant heat gain values at facial section for helmets ranged between 9 and 34 W·m⁻² (area-weighted averaged values). Due to this circumstance, they could be the most critical to exhibit the effect of any small instability in the power supply. Besides, the modifications in the experimental setup

for radiation tests with the 9zM (see section 2.4.2.3) and the non-uniformly distributed irradiation on head zones could be responsible of data variation as well.

Pearson's correlation analysis for convection tests indicated highly significant agreement of heat fluxes at facial and cranial sections for 2zM and 9zM. For the cranial section, thermal head manikins provided nearly identical values. Lower heat fluxes were observed for 2zM at facial section than for 9zM (Figure 2.10, section 2.4.3.1). This could be due to the application of a fabric in these experiments. Both manikins were fully covered with their corresponding elastic tight-fitting fabrics providing different additional insulation. This fact, together with more prominent anatomy of the facial section of the 2zM (see Figure 2.8), could contribute to higher heat loss at facial section for the 9zM than 2zM due to reduced air gaps (30% reduction in heat loss for 9zM vs. 55% for 2zM with regards to the uncovered headform) (see section 2.4.2.2). In case of radiation tests, correlations between RHG of both manikins were found to be high and significant only for cranial section (Pearson's $r > 0.9$, see Figure 2.11, section 2.4.3.1). Due to the local application of radiation in the top front part of the head manikin, differences in the relative position of the facial and cranial sections as defined could be responsible for differences in the distribution of the radiant heat gain reaching each section between manikins. In the radiation tests, the absolute heat loss values provided by 9zM head manikin were 37% and 32% higher respectively at facial and cranial sections due to ambient temperature was reduced by 5°C when the infrared light was off if compared with the original setup (section 2.4.2.3).

2.4.4.2 Statistical comparison between helmets according to 2zM and 9zM

CCP and RS were calculated to classify helmets irrespective of the inherent differences between manikins. In general, the 9zM provided systematically lower

CCP at cranial section for all helmets in all test conditions. Nevertheless, these differences depended on specific test conditions and helmets, yielding some significant differences in helmets classification when comparing results between manikins. This could be based on the differences between manikins geometries. Differences in head circumferences (58 cm and 59 cm measured just above the eyebrows line for 2zM and 9zM) hinted bigger clearances between the headform and the inner surface of the helmets when using the 2zM. Moreover, apparent anatomical differences between headforms could be responsible for air gaps distributing differently at head parts (see Figure 2.8).

In case of RS at the facial section, the 2zM and the 9zM provided different classification. Differences are remarkable in case of helmet 25 without visor, as it was rated as the least protective according to 2zM and the most protective according to 9zM. Reasons for this disagreement could be based on the extremely high radiant shielding that this particular helmet is providing locally on the forehead. In case of the 9zM part of the forehead is placed at the hypothetical crown position if head division of the 2zM was applied. This might result in an overall higher protection of the facial section for this helmet. In case of cranial section, both manikins mostly agreed in the same helmet classification. Differences in RS between helmets 25 and 28 were just detected by the 9zM ($P < 0.05$).

2.4.4.3 Statistical comparison between helmets based on local data of 9zM

To investigate local impacts of bicycle helmets on heat exchange at the head, CCP and RS were analysed at the individual zones of the 9zM. The main finding is that helmets classification according to overall CCP and RS does not always correspond to classifications according to local CCP and RS determined at each zone.

For selected helmets, different order in the helmet classification according to local CCP ($P < 0.05$) was found if considering the front or the rear part of the cranial section. Based on the local heat losses, effects of the helmet design on the local ventilation can be investigated. For example in low wind and tilted head condition, helmet 3 was rated with the highest CCP at cranial section but after the analysis of local CCP, it was possible to determine that it actually provided the highest ventilation in the front part, however at the rear part, helmet 16 showed 15 percentage points higher CCP values (see Figure 2.14). Therefore, observing these two helmets could provide some guidelines about how to improve the helmet design for the optimization of overall ventilation performance at cranial section. Helmet 4 and 16 presented similar CCP at cranial section. Nevertheless, the heat transfer was not equally distributed in the cranial section since helmet 16 allowed 30 and 47 percentage points more cooling power at upper and lower head back zones respectively than helmet 4, whereas high cooling areas of helmet 4 were concentrated in crown and occipital zones (11 and 18 percentage points more cooling than helmet 16).

For radiation tests, overall RS for facial and cranial section usually agreed with the most exposed individual zones probably due to local application of the radiant load. Nevertheless, local assessment of RS by 9zM provided additional information for helmets evaluation. For example, in case of helmets equipped with visor, helmet 25 and 31 were rated with the same RS in the facial section (including forehead, face and neck zones). However, helmet 25 shielded 11 percentage points more radiation than helmet 31 at the forehead ($P < 0.05$) (Figure 2.15). According to RS at cranial section, helmets 3 and 35 presented similar radiant protection (no significant differences between them) but helmet 35 provided 8 percentage point

more shielding at the crown ($P < 0.05$) and helmet 3 shielded radiation at upper head back more efficiently than helmet 35 (Figure 2.15).

Consequently, the quantification of the local heat transfer separately exhibits the relevance and contribution of each single helmet part to the overall heat loss of the entire head. This improvement on helmet classification provides helmets industry with information for developing more specialised products according to physiological demands of each situation of use such as short-term use in urban spaces, sport scenarios, where heat and moisture should be dissipated at high rates or cycling downhill, where paths of wind inside the helmet are the main responsible for thermal comfort.

2.5 CONCLUSION

The nine-zone thermal head manikin provides high spatial resolution when investigating heat transfer at head-site. Local heat transfer through headgear can be accurately quantified in several realistic situations accounting with different environmental conditions and air speeds for occupational, traffic or sport headgear applications.

Initially, an in-depth analysis of the stability of heat fluxes provided by the head manikin revealed some some electrical cross-interaction between the zone heating and temperature sensing circuits resulting in lack of reliability in heat flux measurements and excessive high inter-test variability. After repair, the absolute heat fluxes average intra-test variation reduced from 4% down to 1.4% and the inter-test variation for more precise calculated variables, such as radiant heat gain (see section 2.4.2.3), reduced from 23 to 13% for facial section and from 17 to 5%

for cranial section. The calibration of the surface temperature sensors pointed to a maximum temperature differences of up to 0.21°C in the extreme case of the left temple. No adjustment was applied on the head zones as these differences were within the variation observed among Pt100 plus the corresponding standard deviation. Additionally, the fluid calibration procedure was slightly improved for better accuracy as compared to the protocol recommended by the manikin manufacturer by applying a gravimetric procedure.

The analysis of the performance carried out for cycling scenarios showed the additional benefits of a more detailed investigation of headgear properties. Results of the reliability analysis for convection and radiation tests showed that the 9zM provided heat loss measurements with high consistency with already published data from a less segmented manikin (2zM) under the described test conditions. Variation of measured heat fluxes are within the values reported in the literature. Results from convection tests indicate a comparable overall thermal behaviour of the 9zM compared to a former 2zM. In case of radiation tests, some limitations have been detected when tests were performed according to the previously described setup. For radiant heat gain measurements, the finer segmentation of the headform limited the amount of radiation that the manikin can accept while maintaining a reliable measurement of the heat fluxes. The reduction of the effect provided might affect to the accuracy in the measurements. Based on the existence of nine independent zones, local differences in heat transfer are detectable, whereas it was not possible to exactly allocate them with a less segmented headform. Therefore, the 9zM provides a precise quantification of local heat losses in steady-state and thus, a reliable assessment of the contribution of design characteristics to the overall heat exchange that will support the conception of new helmet designs for optimised heat exchange.

Multi-sector thermophysiological head simulator

Although precise heat flux quantification in steady-state provides highly valuable comparison between headgears for clothing industry, an adaptive response of the manikin heat flux to environmental conditions and headgear could potentially simulate the human physiological response and enhance the thermal analysis for various helmets applications. For this reason, the coupling of the head manikin with a physiological model was undertaken and the manikin characteristics that could allow the coupled system to precisely mimic the human physiology are discussed in the next chapter 3.

3 SPECIFIC REQUIREMENTS FOR THE HEAD MANIKIN UNDER PHYSIOLOGICAL CONTROL MODE

3.1 INTRODUCTION

Thermal manikins are mainly conceived for testing heat and mass transfer properties in protective clothing and equipment. The combined net heat loss through convection, conduction, radiation and eventually evaporation can be investigated using a standard operating procedure which is mainly based on the temperature controlled regulation. In case of the evaporative heat loss measurements through garments, standard measurements usually require the entire manikin surface available for evaporation, meaning fully-wet surface during the entire test period and suggest even pre-wetting the fabric by externally sprayed

Multi-sector thermophysiological head simulator

water (ASTM F2370-10, 2010). Therefore, the surface temperature of a thermal manikin is typically controlled at a fixed set point temperature similar to human skin temperature at thermoneutral state (e.g. between 34°C and 36°C). The power needed to maintain this temperature over a steady-state period is recorded and allows the quantification of combined net heat loss.

Adding a physiological control to the thermal manikin implies different requirements for the manikin operation than those generally required by the manikin standards (ASTM F2370-10, 2010; ISO15831, 2004; ISO9920, 2007). Human head physiology usually presents heterogeneous temperature distributions on head surface. In addition, temperatures at head can undergo frequent and fast changes and the sweat secretion and its evaporation from the human skin occur dynamically. Thus, it was necessary to determine if there were any limitations of the thermal head manikin to fulfill the requirements of mimicking the course of the human physiological response. To calculate thermal requirements posed to the thermal head manikin, we used the physiological model foreseen in the coupled system to determine the typical and extreme boundary conditions in a series of simulations.

The strategy adopted in this project for adding a physiological control to the head manikin considered the head manikin reproducing local skin temperatures and sweat rates values provided by the physiological model in a real-time. The corresponding local heat exchange measured by the manikin represented skin heat loss towards the environment and was used for setting the local boundary conditions at head-site for the next time step (Psikuta et al., 2008). When coupled with the head manikin, the physiological model calculated the resulting local skin temperatures and sweat rates based on the measured resultant heat exchange.

Specific requirements for the head manikin under physiological control mode

Therefore, the accuracy in the measurement of the heat flux exchanged with the environment was crucial for the reliability of the coupled system. To ensure reliable heat flux measurements, the following requirements were addressed:

- **Definition of head geometry.** The physiological model calculates the heat loss from human head individually according to a certain head division. Physiology of the head elements, namely cranial part, face and neck, is very heterogeneous in terms of thermal capacity, vasomotion or sweating response (Fiala et al., 1999). In physiological modelling, each of the head elements accounts with a dedicated description of its thermal properties and they might react differently for the same environmental conditions. For example, heat conductivity of head is $0.04 \text{ W}\cdot\text{K}^{-1}$, whereas it is just $0.02 \text{ W}\cdot\text{K}^{-1}$ or $0.01 \text{ W}\cdot\text{K}^{-1}$ for face and neck, respectively (Fiala et al., 1999). In spite of differences in local heat transfer coefficient, forehead sweats at least six times more profusely than cheeks or twice as much as the neck (Smith and Havenith, 2011). Differences in head part definition between the physiological model and the manikin might be especially relevant in scenarios accounting for heterogeneous clothing insulation or heterogeneous local environmental conditions due to a mismatching physiology. For example, if neck is defined as a bigger zone in the manikin than in the physiological model, it might be partially covered by the headgear, whereas for smaller surface such in the model, it might remain uncovered and show a different thermal response. Hence, the head manikin geometry had to match the size and segmentation of the virtual head in the physiological model to ensure consistent heat loss data.
- **Comparison of heat transfer coefficients.** Head anatomy is very detailed and presents many peculiarities. Approximation to the anatomical head shape and corresponding head segmentation is not enough for ensuring consistent heat

loss with human head physiology. Due to several factors as head manikin materials and their thickness, simplified features such as ears or lack of thermal interaction with a full-body shape, heat fluxes measured by the head manikin for a certain surface temperature could be different than heat fluxes observed when the human skin is regulated at the same temperature. This might produce unrealistic calculation on the side of the physiological model. Therefore, actual and simulated heat transfer coefficients in a reference state had to be similar for each head part to ensure realistic calculations according to the model.

- **Quantification of uncontrolled lateral heat loss in the head manikin.** Heterogeneous temperature distribution over the head surface is often the case in a physiological scenario. Most thermal manikins are firstly conceived for operating at homogeneous surface temperature and representing temperature gradients between head parts could result in some uncontrolled heat transfer by conduction or internal convection and radiation and subsequent inaccuracies in the measured heat fluxes. These inaccuracies in measured heat flux could produce deviations in the thermophysiological response once the head manikin is controlled by the physiological model. Therefore, the extent to which there is an effect on the physiological response due to the uncontrolled lateral heat loss had to be within the deviation observed in human data (Psikuta et al., 2012a).
- **Quantification of thermal responsiveness of the head manikin.** The human head skin temperature changes dynamically as an adaptive physiological response to environmental heat exchange to keep the brain in the prescriptive thermal zone. The surface temperature increase and decrease can occur at different rates and different frequency. When coupled with the physiological

Specific requirements for the head manikin under physiological control mode

model, the thermal responsiveness of the head manikin could impair a close follow-up of the dynamic changes in the surface temperature, and effectively, misled the course of the simulated physiological response. Thus, the head manikin had to be able to reproduce the changes in surface temperature and to react as fast as the human physiology does.

- **Assessment of the evaporative resistance and responsiveness of the sweating function.** The sweat secretion usually corresponds to the dynamic changes in environmental and activity level conditions and its evaporation is an effective mechanism to remove heat from the body. According to the physiological model, the sweat evaporates from human body with 100% efficiency, meaning that the evaporation of each gram of sweat would remove the heat equal to the latent heat of vaporization at the corresponding temperature. However, due to the characteristics of the head manikin sweating system, the water evaporates not directly from the head manikin surface but from a tight-fitting fabric and its secretion is limited to 21 sweating outlets. This fact could be responsible for a reduction in the evaporative efficiency, and thus, the predicted evaporative heat loss could be less than the expected one for a given amount of sweat. Additionally, the evaporation could be affected by the responsiveness of the sweat delivery system and skin fabric wicking properties. The evaporation responsiveness of the system could induce some delay between the onset of the flow and the moment that the evaporative cooling becomes effective as opposed to the immediate evaporation assumed in the physiological model. Therefore, the evaporation efficiency and the evaporation responsiveness had to be characterized to estimate to what extent they could affect the evaporative heat loss from the head manikin as compared to the human skin.

3.2 AIM AND OBJECTIVES

This chapter 3 aimed at determining the most demanding thermal scenarios by simulations with the physiological model and evaluating if the head manikin characteristics could allow the coupled system to precisely mimic the human physiology in those cases. For this purpose, seven main objectives have been undertaken and described in this chapter, namely:

- Definition of the independently controlled head parts in the coupled system by comparison of head segmentation described in the physiological model and in the head manikin.
- Comparison of heat transfer coefficients assumed by the physiological model and the measured combined coefficients for head manikin at each head part.
- Analysis of the effect of heterogeneous temperature distribution on lateral heat exchange in the head manikin for extreme and moderate heterogeneous surface temperature distribution.
- Analysis of the passive thermal responsiveness of the head manikin.
- Analysis of the thermal responsiveness of the head manikin if operated using a dedicated active control (PI) during sudden surface temperature change.
- Adjustment of the dedicated active control (PI) values to provide a more adequate response of the head manikin.
- Characterization of the evaporation efficiency and the evaporation responsiveness of the head manikin sweating system.

3.3 DEFINITION OF HEAD PARTS IN THE COUPLED SYSTEM

3.3.1 Introduction

The physiological model foreseen for the coupled system was the mathematical model of the human physiology developed by Fiala (Fiala and Havenith, 2015; Fiala et al., 2012, 2001, 1999) in its more recent version released in 2015 (FPCm5.3, *Ergosim*, Germany). It represents the human geometry divided in 20 elements (head, face, neck, thorax, abdomen, hip, shoulders, upper arms, lower arms, hands, upper legs, lower legs and feet). Only three out of the 20 elements described in the physiological model were represented by a body part manikin, namely, head, face and neck. The body elements in the physiological model are further divided into 63 sectors for which thermal response is calculated independently. The head element consists of forehead and cranial sectors, face has anterior and two superior sectors and neck consists of anterior, posterior and two superior sectors. The physiological model provides a symmetrical version and a left/right non-symmetrical version. In the last case, superior sector is unfolded in left and right as well.

The head manikin segmentation was specifically chosen to investigate heat transfer mechanisms on headgear. Therefore, the cranial region of the head manikin is segmented into six independent zones typically covered by headgear. These zones included right and left temple as well as a serial fragmentation of the area in-between. Face, forehead and neck were the remaining independent zones with the forehead being a zone partially covered by the headgear (see full-description in Figure 2.1 in chapter 2).

Since the head manikin segmentation did not correspond to the physiological model segmentation, some sectors in the model and zones in the head manikin were grouped to represent possibly similar body areas by both size and physiology. The aim of this section was to define the head parts that could be independently controlled in the coupled system.

3.3.2 Methods





The head segmentation of both physiological model and head manikin in the finest level was compared according to segments position and area. The six independent zones in the cranial region of the head manikin were allocated to the cranial sector of the physiological model. Every sector included in the face and neck elements according to the physiological model corresponded to a one single face and one single neck zone in the head manikin respectively. Forehead remained a single segment since it corresponded directly to a zone in the head manikin and element in the physiological model.

3.3.3 Results

The physiological control of the head manikin was based on four independent head parts, such as forehead, cranial part, face and neck. Table 3.1 summarizes the assignment and the total surface areas for each head part.

Specific requirements for the head manikin under physiological control mode

Table 3.1. Head part surface areas and their assignment for physiological model and thermal head manikin.

Coupled system	Physiological model		Thermal head manikin		
	Parts	Sectors	Area (m ²)	Zones	Area (m ²)
Forehead		Forehead (Head, Anterior sector)	0.0060	Forehead	0.0094
Cranial		Head (Head, Posterior sector)	0.0630	Cranial region*	0.0568
Face		Anterior Superior (Left&Right)	0.0380	Face	0.0357
Neck		Anterior Posterior Superior (Left&Right)	0.0360	Neck	0.0366
Total head			0.1430		0.1385

*Cranial region in the head manikin includes left and right temples, crown, upper and lower head back and occipital zones areas.

The comparison of head geometry of the head manikin and the model revealed a slightly bigger surface area of the entire head in the physiological model than in the head manikin. The head manikin was 3% smaller than the head defined in the model. When grouping the corresponding areas of the head manikin and the physiological model for the different head parts in the coupled system, the cranial and face parts were smaller in the head manikin by 10% and 6%, respectively, with regard to the physiological model. Oppositely, the neck and forehead parts were bigger in the head manikin with respect to the model by 2% and 57%, respectively.

3.3.4 Discussion

The chosen allocation of the zones and sectors in head manikin and physiological model, respectively, allowed the definition of four head parts that could be

independently controlled in the coupled system. Due to the disagreement in the segmentation of both systems, representing separately left and right sides of the head was not possible, although the physiological model could calculate in an asymmetrical mode. The total surface area of each head part considerably agreed except for the forehead. Some differences in heat loss could be expected between simulations carried out with the model alone and simulations once the head manikin is coupled in cases in which covered area of head is not consistent. Henceforth, the analysis will be based on these four head parts as the maximal number of controlled units.

3.4 HEAT TRANSFER COEFFICIENTS AT HEAD PARTS

3.4.1 Introduction

In the coupled system, the physiological model calculates the resulting local skin temperatures and sweat rates at head-site exclusively based on the heat exchange measured by the head manikin. Therefore, the measured heat fluxes by the head manikin have to approximate skin heat fluxes for a certain surface/skin temperature in order to obtain realistic physiological model calculations.

When a solid body is placed in a fluid field, its heat loss is primary determined by the convective heat transfer coefficients. Factors depicting convective heat transfer coefficient for free convection are temperature gradient, gravitational constant, dimensions of the body and density, dynamic viscosity and thermal expansion properties of the fluid. For forced convection, mainly fluid velocity, density, dynamic viscosity account for heat transfer coefficient values (Gagge and Nishi, 2011).

Specific requirements for the head manikin under physiological control mode

In the physiological model, the convective heat transfer coefficients found its basis on the work of Wang (Wang, 1990a, 1990b, 1990c) who measured local convective heat losses in a heated whole-body manikin with realistic temperature distribution for natural and forced convection. The adapted convective heat exchange model was in agreement compared with other works by Fiala (Fiala et al., 1999).

For calculating the heat exchanged by long-wave radiation, the physiological model applies the concept of a mean surface temperature at the radiant envelope enclosing each body sector. The local view factors between each sector and the surroundings were calculated individually for each cylindrical and spherical body elements. The calculations distinguished sectors facing directly the environment or sectors facing any other body element for both reclining and standing/seating body postures (Fiala et al., 1999).

Despite of its anatomical form, the head manikin assumes simplification of some features such as the presence of ears or hair. This head manikin is made out of carbon fiber-epoxy with thermally conductive reinforcement and distributed heating wires and wire sensors are wounded on the inner and outer surface for each zone respectively. As it is a body part manikin, instead of the whole human body shape below the head, a thermal guard is placed at the base of the neck to prevent lateral conductive heat loss downwards to the enclosure box. The enclosure box is a rectangular stain-steel box with an upper surface of 30 x 40 cm. These construction characteristics of the head manikin might deviate the measured heat flux from predicted skin heat loss when both manikin and human skin are regulated at the same temperature due to the absence of the thermal plume created by the rest of the body.

Consequently, the aim of this study was to compare the heat transfer coefficients computed by the physiological model with those measured at the head manikin surface in the climatic chamber for each head part to quantify the potential deviation in the heat flux measured by the head manikin with regard to the human skin losses due to its constructive characteristics. This is necessary when comparing pure virtual and coupled simulation for a better understanding of the comparison of the heat transfer processes in each system.

3.4.2 Methods

The natural convective and radiative heat transfer coefficients assumed by the physiological model were taken from a scenario in which a sedentary nude person in upright position was exposed during one hour to an ambient of 20°C / 50%RH / Still air ($v_a=0.1 \text{ m}\cdot\text{s}^{-1}$). The values were averaged during the last 30-minutes of the exposure. The head manikin was placed in the middle of the climatic chamber covered with the tight-fitting fabric for sweat distribution as in the coupled system configuration. The same scenario was reproduced in the climatic chamber (actual environment $19.7 \pm 0.0^\circ\text{C}$ / $52.9 \pm 0.3 \text{ \%RH}$ / Still air ($v_a=0.09 \pm 0.01 \text{ m}\cdot\text{s}^{-1}$) and the heating power needed to keep the whole head surface temperature at 35°C was measured and averaged over a 30-minute steady-state (heating power variation within $\pm 3\%$). The combined heat transfer coefficient for each head part was calculated according to equation 3.1.

$$h_{combined,part} = \frac{HF_{part}}{T_{part} - T_{air}} \quad [3.1]$$

where HF_{part} is the heat flux for each head part in $\text{W}\cdot\text{m}^{-2}$ obtained by calculation of the area-weighted average heat flux of head zones included in the head part as described in equation 3.2.

Specific requirements for the head manikin under physiological control mode

$$HF_{part} = \frac{\sum^{part} HF_{zone} \cdot Area_{zone}}{\sum^{part} Area_{zone}} \quad [3.2]$$

Similarly, T_{part} is the the area-weighted average surface temperature at the corresponding head part and T_{air} is the actual air temperature in the climatic chamber, both in °C.

3.4.3 Results

Table 3.2 shows the comparison of the combined heat transfer coefficients between the physiological model and the head manikin.

Table 3.2. Comparison of the heat transfer coefficients between those assumed by the physiological model and those measured at head manikin in the same scenario at 20°C / 50%RH / Still air ($v_a < 0.1 \text{ m}\cdot\text{s}^{-1}$).

	$h_{convective}$ (model) [W·m ⁻² ·K ⁻¹]	$h_{radiative}$ (model) [W·m ⁻² ·K ⁻¹]	$h_{combined}$ (model) [W·m ⁻² ·K ⁻¹]	$h_{combined}$ (manikin) [W·m ⁻² ·K ⁻¹]	$h_{combined}$ (model) – $h_{combined}$ (manikin) [W·m ⁻² ·K ⁻¹]	$h_{combined}$ (model) – $h_{combined}$ (manikin) [%]
Forehead	4.05	5.54	9.60	9.74	-0.14	-1.5
Cranial	4.07	4.39	8.46	8.59	-0.13	-1.5
Face	3.95	4.83	8.77	9.71	-0.94	-10.7
Neck	3.44	4.8	8.24	9.66	-1.42	-17.2
Entire head	3.88	4.66	8.53	9.24	-0.71	-8.3

In the aforementioned conditions, the combined heat transfer coefficients for natural convection and radiation measured at the head manikin were higher than those calculated by the model. The coefficients at the head manikin were by 1.5% bigger for the forehead and cranial parts than in the model, whereas for the face and neck, the discrepancies increased up to 10.7% and 17.2%, respectively.

3.4.4 Discussion

The combined heat transfer coefficient measured for the whole head manikin was $9.24 \text{ W}\cdot\text{m}^{-2}\cdot\text{K}^{-1}$. This observed value was consistent with the mean value $8.9 \pm 2.5 \text{ W}\cdot\text{m}^{-2}\cdot\text{K}^{-1}$ measured at head-site for four different full-body thermal manikin by Psikuta et al. (Psikuta et al., 2015a). In that case, the studied manikins presented a large variability in their characteristics at head-site, namely detailed or more prominent facial features, presence of hair or electrical connectors at this body part. The Newton manikin (Newton, *Thermetrics*, USA from Loughborough University) included in the study was constructed with the same technology than the head manikin and accounted for the thermal effect of the rest of the body on head-site. Interestingly, it presented a heat transfer coefficient of $8.6 \text{ W}\cdot\text{m}^{-2}\cdot\text{K}^{-1}$ at head, being very similar to the combined heat transfer coefficient calculated by the physiological model ($8.53 \text{ W}\cdot\text{m}^{-2}\cdot\text{K}^{-1}$) for the entire head.

In the study from Psikuta et al. (Psikuta et al., 2015a), there was no information separately for convective and radiative coefficients. For a female thermal manikin (Monika), De Dear et al. (de Dear et al., 1997) determined a natural convective ($v < 0.1 \text{ m}\cdot\text{s}^{-1}$) and radiative heat transfer coefficients of 3.6 and $4.1 \text{ W}\cdot\text{m}^{-2}\cdot\text{K}^{-1}$, respectively, in standing position that were not much different as well from the values included in the physiological model. However, this manikin had shoulder-length hair that could have added some additional insulation.

The comparison between the combined heat transfer coefficient measured for the entire head manikin and measured for a full-body manikin constructed with the same technology (Newton, *Thermetrics*, USA from Loughborough University, (Psikuta et al., 2015a)), namely 9.24 and $8.6 \text{ W}\cdot\text{m}^{-2}\cdot\text{K}^{-1}$, respectively, could quantify the effect of the head manikin construction. The physiological model based its

Specific requirements for the head manikin under physiological control mode

convective heat exchange model on local convective heat transfer coefficients measured over a full-body manikin as well (Wang, 1990a, 1990b, 1990c). The thermal plume of a whole-body manikin might have affected the forehead, head, face and neck parts differently than the thermal plume due to the heated enclosure box underneath the head manikin (see Figure 2.1 in chapter 2). Regarding the radiative heat exchange, the view factors that the physiological model considers were obtained for simplified geometries of the body elements (cylinders and spheres). As the head manikin represents the human head anatomy, the actual view factors could be different from those calculated for those simplified geometries. The heated enclosure box might provide slightly different radiative area than represented by the shoulders in the human body.

Hence, the heat transfer coefficients observed at head-site were certainly affected by the absence of the rest of the body underneath the head. Therefore, some slight deviations between heat flux measured by the head manikin and the human skin heat loss predicted by the physiological model can occur especially in high heat loss exposures at the face and neck parts.

3.5 UNCONTROLLED LATERAL HEAT EXCHANGE BETWEEN HEAD PARTS

3.5.1 Introduction

Human physiological response accounts for heterogeneous temperature distribution over the head surface. As most thermal manikins are firstly conceived for operating at homogeneous surface temperature, temperature gradients between head parts might result in some uncontrolled heat transfer by conduction

Multi-sector thermophysiological head simulator

or internal convection and radiation between head parts and subsequent inaccuracies in the measured heat fluxes for each part.

When the head manikin is coupled with the physiological model, the head physiological state will be exclusively calculated according to the net heat exchange measured by the head manikin. Hence, inaccuracies in the local heat exchange measured by the head manikin with heterogeneous temperature could produce unacceptable deviations in the physiological response.

The aim of this study was twofold. Firstly, the uncontrolled lateral heat exchange between head parts was quantified in steady-state for an extreme and a moderate heterogeneous temperature distribution. Secondly, the extent to which the physiological response could be misled due to a heterogeneous temperature distribution was evaluated based on skin temperature at head parts.

3.5.2 Methods

3.5.2.1 Quantification of uncontrolled lateral heat exchange at head manikin

The skin temperatures for each head part were simulated with the physiological model for a high heat loss scenario with extreme heterogeneous temperature (scenario 1) and a low heat loss scenario with moderate heterogeneous temperature (scenario 2). Scenario 1 consisted of a nude person exercising with moderate activity (3 met) in an ambient of 35°C that was suddenly moved into an ambient temperature of 5°C, whereas in scenario 2 the aforementioned person moved to an ambient temperature of 25°C during a two-hour exposure. The obtained skin temperature distributions at the end of the exposure were then used

Specific requirements for the head manikin under physiological control mode

to calculate temperature of head parts and lateral temperature gradients between them.

A heterogeneous surface temperature distribution was set in the head manikin parts with temperature set points representing the maximal differences between head parts observed in scenario 1 and 2, respectively, that occurred at the end of the exposure. Additionally, a series of pertinent homogeneous surface temperature distribution tests corresponding to the individual temperature set points in scenario 1 and 2 were carried out. Each homogeneous surface temperature test was considered as the reference heat flux measurement for the head part at the corresponding temperature set point. For both, heterogeneous and homogeneous surface temperature distribution tests, the heat flux from each head part was measured over a 30-minute steady-state (heat flux variation within $\pm 3\%$). Figure 3.1 shows surface temperature set points considered in each heterogeneous scenario.

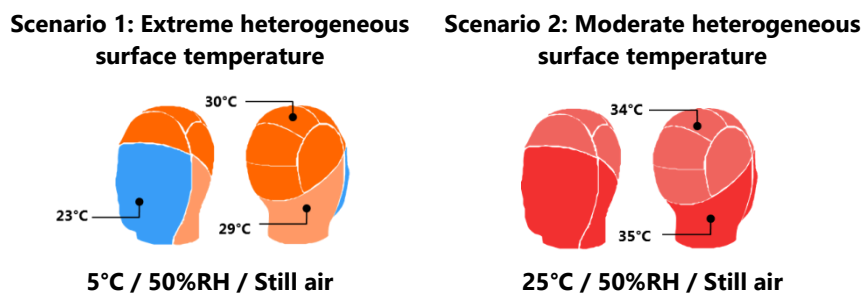


Figure 3.1. Heterogeneous surface temperature set points set at the head manikin for testing heat exchanged by lateral conduction and internal convection and radiation for scenario 1 and 2.

The measured heat flux for the defined head parts in steady-state was compared between the heterogeneous and the corresponding homogeneous temperature distribution test for each head part. The relative difference expressed in percentage of the corresponding homogeneous heat flux was considered as the uncontrolled

lateral heat exchange exclusively due to a heterogeneous temperature distribution for each of the four head parts foreseen in the coupled system.

3.5.2.2 Effect of uncontrolled lateral heat exchange on head physiological response

Scenarios 1 and 2 described in section 3.5.2.1 were simulated in the physiological model for determining local skin temperature at head-site. In the coupled system, the human head thermal response was calculated exclusively based on the skin heat loss measured by the head manikin. The impact of the uncontrolled lateral heat exchange on the local skin temperatures at head-site had to be assessed. Therefore, the local skin temperatures were calculated by the model in cases without and with accounting for the uncontrolled lateral heat exchange for each scenario and differences for each head part skin temperature were quantified.

In the first simulation case, the exact local skin heat losses for forehead, cranial, face and neck parts were input as boundary conditions. The exact skin heat loss for each scenario was obtained from the previous simulation described in section 3.5.2.1, in which the boundary conditions were introduced as environmental conditions, clothing and activity level. In the second simulation case, the aforementioned exact local skin heat losses were applied accounting for the uncontrolled lateral heat exchange measured individually at each head part. In both simulation cases, the boundary conditions for the rest of the body were introduced as skin heat loss and corresponded to mean skin heat loss for all body parts.

The maximal differences in local skin temperature between both simulation cases were reported for representing the maximum deviation expected in the physiological response produced by the uncontrolled lateral heat exchange.

3.5.3 Results

3.5.3.1 Quantification of uncontrolled lateral heat exchange at head manikin

Table 3.3 depicts the relative heat exchange deviation (%) for each head part in scenario 1 and 2.

Table 3.3. Relative deviations in heat exchange (%) with regard to a theoretical uniform temperature distribution due to extreme and moderate non-uniform surface temperature distributions. Heat flux has been compared between heterogeneous and homogeneous temperature distributions.

	Forehead	Face	Cranial	Neck
Scenario 1: Extreme non-uniform surface temperature	19%	-24%	5%	6%
Scenario 2: Moderate non-uniform surface temperature	-10%	2%	-7%	3%

In case of scenario 1 with extremely heterogeneous surface temperatures, the heat exchange at forehead was higher by 19% ($45.9 \text{ W}\cdot\text{m}^{-2}$) when compared to the homogeneous situation. Consequently, the heat exchange at face was diminished by 24% ($41.2 \text{ W}\cdot\text{m}^{-2}$) with regard to the corresponding homogeneous temperature distribution due to having neighboring zones at higher temperature, such as the forehead and neck. The heat exchange at the neck was higher by 6% ($12.9 \text{ W}\cdot\text{m}^{-2}$) with regard to the homogeneous test as a result of the heat drifted to the face set at lower temperature and the heat received from a warmer section. In homogeneous temperature distribution, the cranial part provided $206 \text{ W}\cdot\text{m}^{-2}$. When the head manikin temperatures were heterogeneous according to this scenario, the

Multi-sector thermophysiological head simulator

cranial part had to provide 5% ($10.8 \text{ W}\cdot\text{m}^{-2}$) more heat to compensate additional heat exchange drifted to other head parts such as face and neck.

In case of scenario 2 with moderate heterogeneous surface temperatures, a lower amount of heat was exchanged between neighboring zones in absolute terms. When the head manikin temperatures were set according to heterogeneous distribution proposed in scenario 2, face and neck parts had to increase their heat flux by 2 and 3% (2.6 and $3.2 \text{ W}\cdot\text{m}^{-2}$), respectively, compared to the homogeneous temperature situation. These deviations appeared to compensate for lateral heat flux to the forehead and cranial part set at a lower temperature. As a result, the forehead and the cranial part provided less heat flux by 10% and 7% (9.4 and $5.0 \text{ W}\cdot\text{m}^{-2}$) in the heterogeneous distribution, respectively, due to the additional heat gains from the face and neck parts.

3.5.3.2 Effect of uncontrolled lateral heat exchange on head physiological response

Table 3.4 shows the maximum differences in simulated local skin temperatures obtained with the physiological model between the simulation case using exact heat loss at each head part and the case using heat loss deviated by the measured uncontrolled lateral heat exchange as quantified in Table 3.3.

Specific requirements for the head manikin under physiological control mode

Table 3.4. Differences in local skin temperatures at head-site caused by deviations in the manikin heat flux measurements with a heterogeneous temperature distribution.

	Deviation in local skin temperature [°C]			
	Forehead	Face	Cranial	Neck
Scenario 1: Extreme non-uniform surface temperature	-1.4	2.0	-0.3	-0.5
Scenario 2: Moderate non-uniform surface temperature	0.30	0.0	0.20	-0.1

In scenario 1, the comparison of the skin temperatures at head parts between both simulations highlighted that a decreased skin heat loss rate at face part by 24% due to warmer neighboring parts (forehead, cranial and neck) produced a maximal increase of 2°C in skin temperature at this part. Oppositely, the heat loss at the forehead, cranial and neck parts was 19, 5 and 6% higher, respectively, to mainly compensate for a colder face, resulting in corresponding skin temperature reductions of 1.4, 0.3 and 0.5°C, respectively.

In scenario 2, the comparison of the skin temperatures at head parts between both simulations highlighted that decreasing heat loss in forehead and cranial part by 10 and 7% produced higher skin temperature by 0.3 and 0.2°C at these parts, respectively. The additional heat loss observed in face and neck (2 and 3%, respectively) caused due to cooler forehead and head produced small temperature reductions by 0.1°C in neck and almost no noticeable deviation in face temperature.

3.5.4 Discussion

The maximum differences in simulated surface temperature between forehead and face parts corresponded to 7 and 1°C for extreme and moderate heterogeneous temperature distributions, respectively. The cranial part provided 10.8 W·m⁻² more and 5.0 W·m⁻² less heat loss for the extreme and the moderate scenarios, respectively, when compared with a corresponding homogeneous temperature distribution. In case of face part, differences of 41.2 W·m⁻² less and 2.6 W·m⁻² more heat loss were observed for scenario 1 and 2, respectively, whereas heat exchange at neck was 12.9 and 3.2 W·m⁻² more in both scenarios.

The maximal deviation in the measured heat flux at cranial and neck parts due to uncontrolled lateral heat exchange caused a maximum skin temperature deviation of 0.3°C and 0.5°C, respectively, for the scenario with extreme heterogeneous surface temperature. This maximum deviation observed was within the accepted standard deviation observed for skin temperature measurements in human subjects tests of 1°C and thus, no noticeable deviation in physiological response is expected for any skin temperatures distribution accounting with differences below the extreme case proposed in scenario 1 (Haslam and Parsons, 1994; Psikuta et al., 2012a). However, due to the deviations observed for heat flux measured at the forehead and face in scenario 1, differences of up to 1.4°C and 2°C, respectively, appeared at these head parts. As a consequence, the precision of the coupled system for the skin temperature prediction at forehead and face may be compromised in case of large temperature gradients.

3.6 THERMAL PASSIVE RESPONSIVENESS OF THE HEAD MANIKIN

3.6.1 Introduction

The human head skin temperature drops or increases dynamically as an adaptive response to the heat exchanged with the environment. The heating or cooling processes can occur at different rates with dynamic target temperatures as well. Thus, when coupled with the physiological model, the head manikin should be able to reproduce the changes and to react as fast as required by the human physiological responses.

The ability of the head manikin to represent the human physiology is constrained by its maximal thermal capacity or passive responsiveness. The thermal head manikin is not equipped with an active cooling system, and therefore, the fastest cooling rate that can be achieved corresponds to passive cooling rate at each ambient temperature when heating power is minimized or switched off. Similarly, the fastest heating rate possible is limited by the maximal nominal heating power.

Therefore, it was important to evaluate if the thermal passive responsiveness and the nominal heating power of the system would limit the coupled system from closely following the physiological temperature values in the different scenarios. The aim of this work was to assess the passive responsiveness of the head manikin for sudden ambient temperature transient and to compare it with required physiological transient in head skin temperature obtained from the physiological model.

3.6.2 Methods

The coupled system required the highest level of responsiveness of the head manikin for the most sudden transient cooling and heating scenarios. To determine the maximal changes in head skin temperature for extreme transient conditions, a systematic batch of simulations has been carried out for such conditions using the physiological model. Cooling rates for each head part have been determined in five different scenarios in which a nude person in thermoneutral conditions with no activity for one hour (activity level of 1 met) was suddenly moved to environments at 5, 10, 15, 20 and 25°C and 50% relative humidity, still air ($v_a = 0.05 \text{ m}\cdot\text{s}^{-1}$) conditions for two hours. Heating rates for each head part have been determined in a total of 35 scenarios. Scenarios consisted of a nude person pre-cooled in an ambient temperature of 10°C with sedentary activity (activity level of 1 met) during two hours that was suddenly moved to environments of 15, 20, 25, 30, 35, 40 and 45°C and 50% relative humidity respectively in combination with activity level of 1, 3, 5, 7 and 10 met in still air conditions ($v_a = 0.05 \text{ m}\cdot\text{s}^{-1}$) for two hours.

To characterize the transient response of the head manikin, the maximal increase and decrease in surface temperature were tested during its passive response. The head manikin was placed in the middle of the climatic chamber and outside of the wind tunnel enclosure. It was covered with the tight-fitting fabric aimed at spreading the sweat since it was the expected configuration in the coupled system. Two kinds of tests were carried out:

- **Heating response test.** The head manikin firstly cooled down to an ambient temperature of 5°C, and then the heaters of all zones were set at constant maximum nominal power of $800 \text{ W}\cdot\text{m}^{-2}$ according to manufacturer's specifications and surface temperatures were recorded till

Specific requirements for the head manikin under physiological control mode

any of the zones reached 38°C. The maximal rate of increase of the surface temperature at each head part was evaluated.

- **Cooling response test.** The head manikin including the guard and enclosure box with an initial surface temperature of 35°C was left to cool down in the climatic chamber down to the ambient temperature. Heaters remained switched off by setting the surface temperature set point 2°C below the ambient temperature. This characterization for cooling was done at five different ambient temperatures of 5, 10, 15, 20 and 25°C. The relative surface temperature change at each head part was recorded throughout the cooling process.

3.6.3 Results

The maximal temperature increase rate possible at the human head skin was predicted by the physiological model to occur when a nude person pre-cooled in an ambient condition of 10°C with no activity (sedentary posture, activity level of 1 met) for two hours was suddenly moved to an environment at 45°C, regardless the activity level. Figure 3.2 shows the comparison between maximal physiological changes and maximal temperature increase rate for different head parts achieved by the head manikin when the maximal nominal power was constantly delivered.

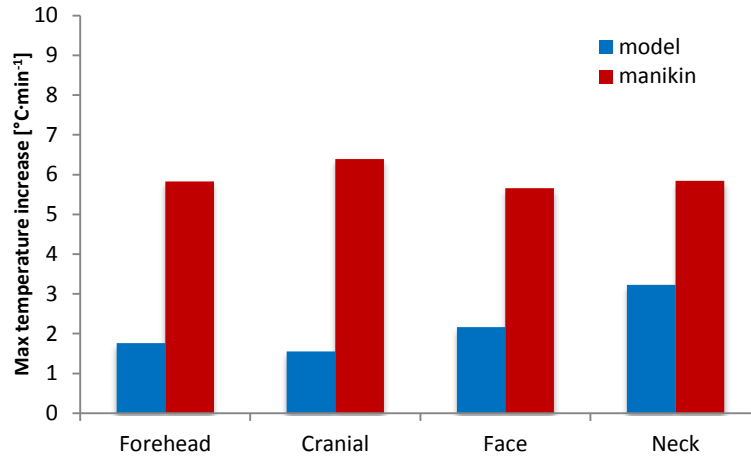


Figure 3.2. Comparison of the maximal temperature increase at the skin predicted by the physiological model and the maximal temperature increase measured by the head manikin for each defined head part during heating up at maximal nominal power ($800 \text{ W}\cdot\text{m}^{-2}$).

Figure 3.3 presents the comparison of the time evolution of surface temperature drop measured in the head manikin passively cooled in the climatic chamber and the skin temperature drop predicted by the physiological model for a thermoneutral person moving into an ambient of 5 and 25°C respectively. Similar results were observed at 10, 15 and 20°C.

Specific requirements for the head manikin under physiological control mode

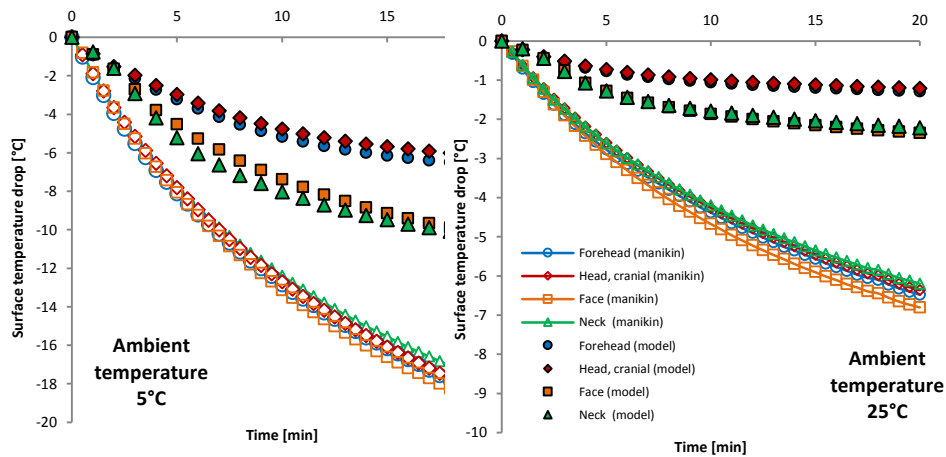


Figure 3.3. Comparison of surface temperature drop measured on the head manikin and the skin temperature drop predicted by the physiological model at ambient temperature of 5°C and 25°C respectively for each defined head part.

3.6.4 Discussion

The maximal passive responsiveness of the system either for heating or cooling has been shown to be above the maximum temperature increments demanded by the physiological model. Therefore, the manikin would be able to increase surface temperature at least at the double speed than the maximum possible increase predicted for the human physiology by delivering the maximal nominal heating power. In case of representing skin temperature drops, the manikin could be able to cool at least twice faster than the human skin for every head part. Therefore, no restriction for the coupled system would be expected to represent human physiology during sudden transient exposures.

3.7 THERMAL CONTROLLED RESPONSIVENESS OF THE HEAD MANIKIN

3.7.1 Introduction

Thermal manikins are usually built up to maintain a constant surface temperature for measuring clothing thermal insulation and evaporative resistance (ISO15831, 2004; ISO9920, 2007; McCullough, 2005). The heating power needed for maintaining the manikin surface temperature at a fixed set-point temperature corresponding to human skin temperature at thermoneutral state (e.g. between 34°C and 36°C) in stable environmental conditions refers to the net combined heat loss. The manikin heating control system is predominantly designed to maintain this surface temperature as stable as possible with a minimal fluctuation of the heating power.

The control of the heating system is commonly achieved with a proportional-integral-derivative (PID) controller. The implemented feedback loop control system calculates the error between actual temperature value and target temperature set point and it accordingly adjusts the heating power. As thermal manikins are mainly dedicated to standardized measurements over steady-state periods, the parameters of the PID controller are optimized for preventing over- and under-shooting in the surface temperatures and early and slow adjustment of heating power to maximize the power output stability. For this thermal head manikin, the regulation of the heating power is implemented by a PI control. Generally, a PI control is defined by two parameters K_p being the gain proportional to the error and K_i accounting for cumulated error and responsible for the oscillations developed in the system.

Specific requirements for the head manikin under physiological control mode

When coupled with the physiological model the PI default settings might slow down and limit the head manikin from closely following the dynamic changes in the surface temperature set points, and effectively, misled the course of the simulated physiological response. The aim of this work was to assess the responsiveness of the head manikin for sudden ambient temperature transient when controlled by the default PI settings proposed by the manufacturer.

3.7.2 Methods

To characterize the manikin responsiveness when modulated by the default PI settings, a stepwise cycle consisting of step changes in surface temperature set points of 3, 2, 1 and 0.5°C from a 35°C reference temperature, representing moderate and extreme physiological one-minute transients was carried out. According to the physiological model simulations, one extreme heating transient resulting in an increase of 2.15°C (~2°C) for the skin temperature of the whole head was detected for a person pre-cooled for 2 hours in an ambient of 10°C that moved to an ambient of 45°C. Similarly, one extreme cooling transient resulting in a temperature decrease of 0.8°C (~1°C) for the whole head was predicted when a nude sedentary person suddenly changed from thermoneutral condition to an ambient temperature of 5°C.

The same test was run at two different environmental conditions to represent situations with low and high heat fluxes, namely, 25°C / 50%RH / Still air ($v_a < 0.1 \text{ m}\cdot\text{s}^{-1}$) and 5°C / 50%RH / Still air ($v_a < 0.1 \text{ m}\cdot\text{s}^{-1}$). The head manikin was placed in the middle of the climatic chamber and outside of the wind tunnel enclosure. It was covered with the tight-fitting fabric aimed at spreading the sweat as it was the intended configuration for the coupled system. The surface temperature signals were recorded for each head zone. The time needed to accomplish the

temperature change to the required set point temperature was determined with $\pm 0.2^\circ\text{C}$ tolerance.

3.7.3 Results

Figure 3.4 presents the average time needed for the head manikin to achieve the target surface temperature set points calculated with a tolerance of $\pm 0.2^\circ\text{C}$.

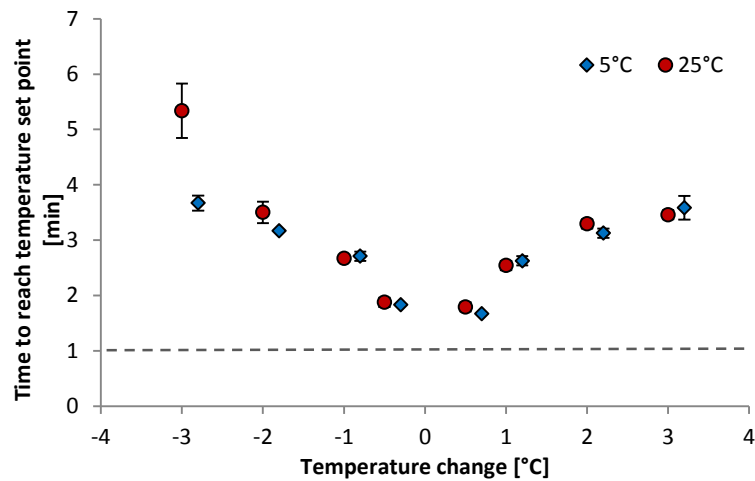


Figure 3.4. Average time needed to achieve the target temperature changes of 3, 2, 1 and 0.5°C positive and negative calculated with $\pm 0.2^\circ\text{C}$ tolerance when the thermal reaction is modulated by the manikin PI controller in two ambient temperatures 5 and 25°C . The error bars show standard deviation of the four head parts foreseen in the coupled system. It should be noticed that time for a step change of -3°C in temperature ambient of 25°C is constrained by maximal passive cooling responsiveness of the head manikin.

3.7.4 Discussion

When the manikin thermal response was modulated by the PI controller with default settings, the step changes in surface temperature expected within one minute always took longer for every head part. The maximum skin temperature increase at head within one minute was predicted by the physiological model to be

Specific requirements for the head manikin under physiological control mode

2.15°C. It corresponded to the temperature increase on the entire head for a person moving from an ambient of 10°C to 45°C, regardless the intensity of activity. When delivering the maximum nominal power (800 W·m⁻²), the thermal head manikin was able to heat up at 6°C·min⁻¹ for the first minute (without controlling activities). However, when controlled by the PI default settings, thermal head manikin needed 3.2 minutes on average for achieving an increase of 2°C in surface temperature.

The maximum skin temperature decrease within one minute was predicted by the physiological model to be 0.8°C. It corresponded to the temperature decrease on the entire head for a nude sedentary person suddenly changing from thermoneutral condition to an ambient temperature of 5°C. For the head manikin, the maximal uncontrolled reduction in surface temperature within one minute was found to be -1.9°C·min⁻¹ when cooling from a surface temperature of 35°C to 5°C ambient temperature. However, when cooling rate was modulated by the PI controller with default settings, it took 3.3 minutes on average to reduce surface temperature by 2°C.

The parameters of the PI were by default regulated to maintain the surface temperature as stable as possible with minimal fluctuation of the heating power, and thus, the regulation of the heating power needed to change surface temperature occurred slowly rather than immediately. Therefore, these PI parameters should be adjusted for a faster response. Otherwise, they can prevent the head manikin to precisely represent the skin temperature at head during sudden transients.

3.8 ADJUSTMENT OF THE THERMAL CONTROLLED RESPONSIVENESS OF THE HEAD MANIKIN

3.8.1 Introduction

The K_p and K_i parameters are editable in the manikin software and they can be manually tuned to modify the thermal controlled responsiveness of the head manikin. This work aimed at determining new regulation parameters for the head manikin PI controller to achieve faster cooling and heating rates as demanded by the physiological model in one-minute time if necessary.

3.8.2 Methods

For the manual tuning process, the head manikin was set under the environmental conditions of 20°C / 50%RH / Still air ($v_a < 0.1 \text{ m}\cdot\text{s}^{-1}$) as described in section 3.7.2. The test protocol included a temperature step increase from 32°C to 35°C simultaneously for every manikin zone. The protocol was repeated with different K_p and K_i values till the time to reach the temperature set point was within a minute. Initial restriction for modification of K_p and K_i values was keeping the over- and undershooting values within $\pm 0.2^\circ\text{C}$. This value corresponded to the accuracy required for surface temperature measurements on thermal manikins standards (ISO15831, 2004). Unless there was any constraint from the passive cooling, it should be noticed that the PI control acted symmetrically for heating and cooling processes (see Figure 3.4). The manual tuning was therefore, focused mainly in the heating process as cooling might depends on other factors, i.e. maximum cooling capacity.

Once the PI parameters were adjusted to obtain appropriate heating and cooling rates, the same stepwise test as described in section 3.7.2 was repeated under the

Specific requirements for the head manikin under physiological control mode

same conditions at ambient temperatures of 5 and 25°C. The time required to reach the targeted surface temperature for each increase and decrease in the temperature set point with a tolerance of $\pm 0.2^\circ\text{C}$ was compared when the head manikin operated with PI default settings and PI adjusted settings. As regulation of PI control settings might influence the stability of the thermal response, some additional parameters were defined to assess the overall performance of the system.

- **Overshoot [$^\circ\text{C}$].** Average overshoot calculated for the largest temperature step change as it was expected to be the most critical. This calculation considered surface temperature of all the head zones when a new temperature set-point of 35°C is set for all the zones stabilized at 32°C. The maximum acceptable overshoot was 0.2°C.
- **Undershoot [$^\circ\text{C}$].** Average undershoot calculated for the largest temperature step change as it was expected to be the most critical. This calculation considered surface temperature of the head zones when a new temperature set point of 32°C is set for all the zones stabilized at 35°C. The maximum acceptable undershoot was 0.2°C.
- **Coefficient of variation in steady-state heat flux CV [%].** Average coefficient of variation of heat flux measurements of all head zones calculated during a 30-min steady-state for each temperature set point. A reference value of 4% for inter-test heat flux variation have been reported in international standards (ISO15831, 2004).

3.8.3 Results

Figure 3.5 shows curves of the thermal manikin responsiveness for a programmed negative and positive step change in surface temperature of 3°C in an ambient of

Multi-sector thermophysiological head simulator

5°C when controlled by PI defined by default settings optimized for steady-state ($K_p = 0.18$ and $K_i = 0.002$) and for PI defined by new settings adjusted for a faster response ($K_p = 0.48$ and $K_i = 0.015$). Surface temperature and heat fluxes corresponded to area-weighted averaged values of the entire head.

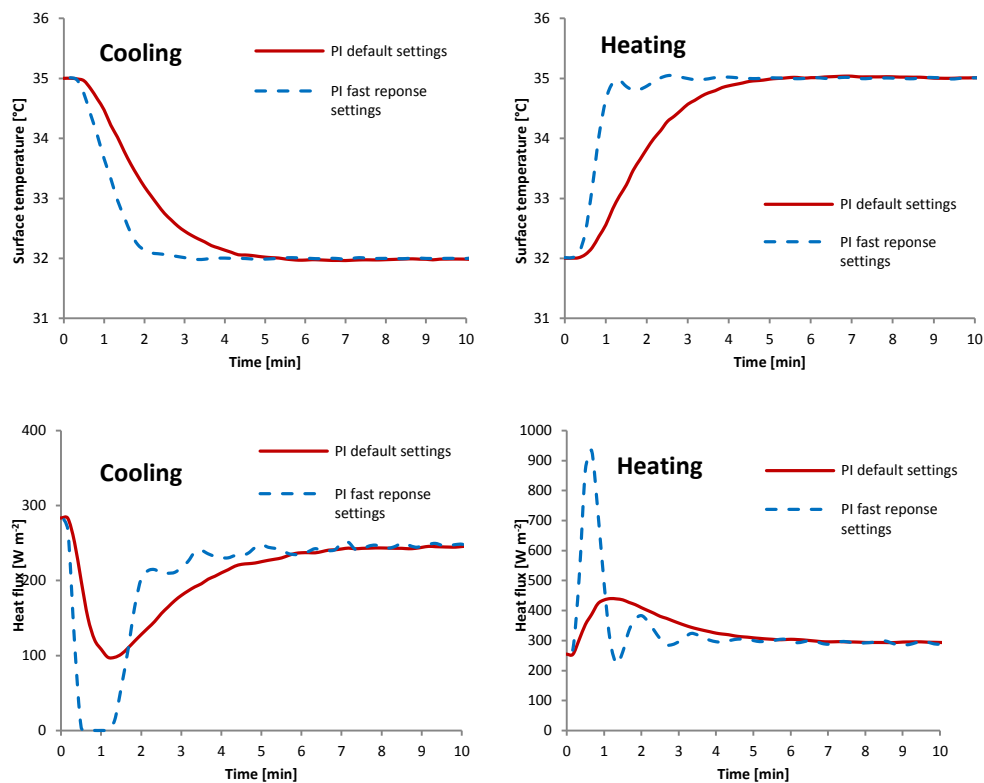


Figure 3.5. Comparison of the average manikin thermal responsiveness for PI default settings and PI fast response settings manually adjusted when a negative and a positive step change of 3°C was programmed for a high heat flux case (at ambient temperature of 5°C). Comparison of surface temperature for cooling, comparison of surface temperature for heating, comparison of heat flux for cooling and comparison of heat flux for heating are shown.

The surface temperature for heating shows that after modifying the PI control parameters, the temperature set point with a $\pm 0.2^\circ\text{C}$ tolerance was reached within one-minute for heating, whereas it took 3.6 minutes in case of the manikin

Specific requirements for the head manikin under physiological control mode

operating with PI default settings. In case of cooling, the time needed to decrease the surface temperature by 3°C with $\pm 0.2^\circ\text{C}$ tolerance was still above one minute because the maximum passive cooling at ambient temperature of 5°C was limited to $1.9^\circ\text{C}\cdot\text{min}^{-1}$. Nevertheless, the cooling time was reduced from 3.7 minutes in case of PI default settings to 1.8 minutes. Although the controlled reaction with the adjusted PI settings was faster, it led to some additional over- and undershooting that were moderate in surface temperature but more noticeable in heat flux. The modification of both K_p and K_i parameters produced bigger instabilities in the heat flux curves. However, oscillations seemed to be more sensitive to the increase in K_i than in K_p in this specific case aiming at adjusting the PI for a large and constant temperature step change. Moreover, in this extreme cooling transient, the thermal capacity of the head manikin was exceeded and the heating power stayed at zero for a certain time, causing the heat flux to be zero during this period. Figure 3.6 summarizes the reduction in the time needed to reach the corresponding temperature set point when the PI was adjusted. The thermal manikin could achieve all step changes in surface temperature within one minute in heating. The adjustment of the PI yielded to response times within one minute as well for cooling unless the thermal response of the head manikin was limited by the maximum passive cooling. Therefore, for the temperature decrease larger than 0.7°C in ambient of 25°C and larger than 1.9°C in ambient of 5°C , the time needed for decreasing surface temperature was considerably reduced but still above one minute.

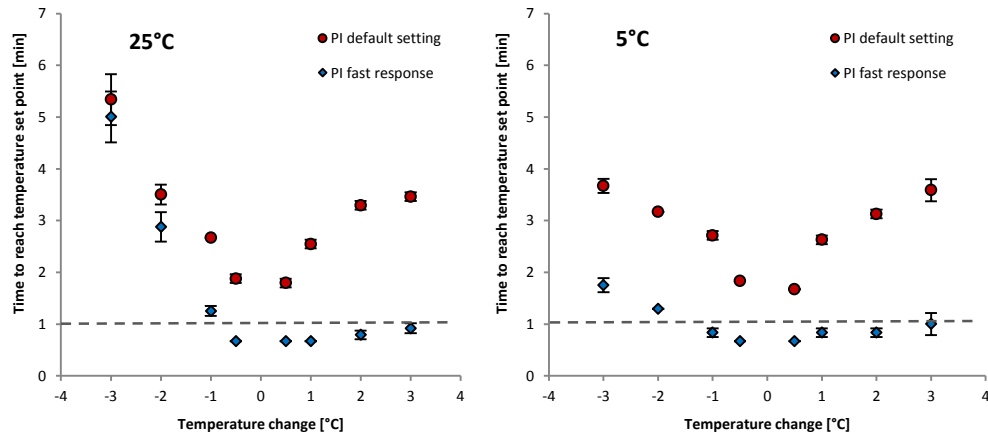


Figure 3.6. Average time needed to achieve the target temperature changes of 3, 2, 1 and 0.5°C positive and negative calculated with $\pm 0.2^\circ\text{C}$ tolerance when the thermal reaction is modulated with the PI default settings ($K_p = 0.18$ and $K_i = 0.002$) and the PI fast response settings ($K_p = 0.48$ and $K_i = 0.015$). Results separated by ambient temperatures 25 and 5°C. The error bars account with standard deviation of the four head parts foreseen in the coupled system. It should be noticed that maximum passive cooling was 0.7 and $1.9^\circ\text{C}\cdot\text{min}^{-1}$ at 25°C and 5°C.

Table 3.5 shows the values of the additional parameters defined to assess the performance of the manikin thermal response when operating with PI defined by default settings and for PI defined by settings adjusted for a faster response.

Table 3.5. Summary of manikin thermal response for PI default settings and PI fast response settings.

	25°C		5°C	
	PI default settings	PI fast response settings	PI default settings	PI fast response settings
Overshoot [°C]	0.03	0.11	0.04	0.06
Undershoot [°C]	0.02	0.02	0.04	0.03
CV steady-state heat flux [%]	1	5	1	3

Specific requirements for the head manikin under physiological control mode

The adjustment in the PI settings for a faster response increased the average surface temperature overshoot in both ambient temperatures 25 and 5°C, however, the values were still within 0.2°C which is the accuracy required in thermal manikins standards (ISO15831, 2004). Similarly, the PI settings adjustment had little effect in the surface temperature undershoot. Due to the new PI settings, the average variation observed in the steady-state heat flux noticeably increased.

3.8.4 Discussion

In general, the time needed to reach a new surface temperature set point was reduced after adjusting the PI settings for a faster response. For all heating steps, it was possible to achieve the step change within one minute. For cooling steps, the adjustment of the PI yielded in the response times within one minute unless the thermal response of the head manikin was limited by the maximum passive cooling capacity. The surface temperature over- and undershoot were kept within 0.2°C corresponding to the accuracy required for surface temperature measurements in thermal manikins (ISO15831, 2004). However, the variation of the heat flux in steady-state increased from 1% to 5 and 3% in ambient 25 and 5°C, respectively. This variation for steady-state heat flux is in the upper limit of acceptance according to international standards (ISO15831, 2004).

In the extreme cooling transient, the heating power stayed at zero for a certain time. The head manikin precisely estimated heat loss just before the thermal capacity of the head manikin was exceeded. The case in which the heating power is zero provided the highest error in the heat loss measurement. This lack of reliability in heat flux data may compromise the precision of the coupled system when predicting physiological response during this period or introduce an offset in the physiological response afterwards.

3.9 CHARACTERIZATION OF THE EVAPORATION EFFICIENCY AND EVAPORATION RESPONSIVENESS OF THE HEAD MANIKIN

3.9.1 Introduction

The skin evaporation model in the physiological model assumed that the potential evaporation of the sweat when clothing is worn is given by the difference between the saturated partial vapour pressure at skin temperature and the partial vapour pressure in the ambient air and modulated by an evaporative coefficient depending on the thermal insulation and moisture permeability from skin to clothing of individual clothing layers, the clothing area factor of the outer layer, convective heat transfer and Lewis constant for air ($L_{\text{air}}=0.0165 \text{ K}\cdot\text{Pa}^{-1}$) (Fiala et al., 1999). The evaporative heat loss corresponds to the latent heat of vaporization of water in the produced sweat at the skin temperature that is removed from the body ($\lambda_{\text{H}_2\text{O}}=2430 \text{ J}\cdot\text{g}^{-1}$ at 30°C (Havenith et al., 2013)). In case there is no sweat production the evaporative heat loss accounts solely for the insensible skin perspiration in basal state described in the model as a basic property of the human skin (Fiala et al., 1999).

When a thermal manikin is simulating the evaporative heat exchange at human skin, there are some factors that might potentially decrease the theoretical evaporation rate assumed by the model. The most advanced thermal manikins are equipped with a limited number of water-releasing outlets to simulate sweating. However, the distribution of these outlets is outweighed by far by the number of human sweat glands on skin allowing surface rather than punctual sweating. To minimize the problem of punctual sweating in manikins they usually include a tight-fitting elastic fabric skin that aims at evenly spreading the water on the

Specific requirements for the head manikin under physiological control mode

thermal manikin surface and increasing the evaporation surface. Havenith et al. (Havenith et al., 2013) showed that the further from the skin the sweat evaporates, the less evaporative heat is actually removed from the skin. In their study, they considered the tight-fitting elastic cotton fabric as the skin and calculated the evaporation efficiency in the ratio between the evaporative heat loss observed on the manikin for this fabric skin and the maximum potential evaporation achievable defined by the latent heat of the mass lost (see equation 3.2 in section 3.9.2.1). Havenith et al. showed that heat loss due to evaporative cooling of the dressed manikin did not correspond to the equivalent mass loss. They pointed to a microclimate heat-pipe effect when the ambient temperature dropped below the skin temperature and to the fact that some latent heat can be drawn from environment as plausible reasons of this discrepancy (Havenith et al., 2008). Wang et al. quantified the latent heat taken from the environment to be between 10.9 and 23.8% for different types of clothing in isothermal condition (34°C) concluding that the higher the thermal insulation of the clothing ensemble, the less evaporative energy was taken from the environment (Wang et al., 2011). They studied this effect further for several one-layer tight sportswear fabrics (thickness less than 1.2mm) and found that in warm environments (35°C) about 17-49% of the heat needed for evaporation could be drawn from the surrounding air instead from the manikin surface (Wang et al., 2013).

Secondly, during transient periods the evaporation might be affected by the structure and operating principle of the sweat delivery system. It was observed that although a new sweat flow set point was immediately set in the head manikin software, some delay occurred between the setting of the flow and the moment that the evaporative cooling became effective. Physical distance between the water meniscus in the sweating duct and the manikin surface might require some time for

the water droplet moving to head surface especially if the flow rate is very small. Typically, the sweating system of the head manikin was rinsed before measurements to remove any air from the sweating ducts. However, the water meniscus in the sweating duct was constantly dropping due to the evaporation during the stabilization period before the measurement and during actual measurement time without sweating. The wettability and wicking properties of the tight-fitting fabric skin could finally also imply some delay in the moisture spreading to reach the nearest surface temperature sensor at the head manikin outer shell.

The aim of this work was to analyse in-depth the evaporative heat exchange at the head manikin surface for a more comprehensive interpretation of the coupled system predictions when the sweating was present. For this purpose, two aspects have been analysed, such as:

- Analysis of the evaporative efficiency of the head manikin tight-fitting fabric at different sweat rates.
- Analysis of the evaporation responsiveness on the head manikin surface at different sweat rates.

3.9.2 Methods

3.9.2.1 Analysis of the evaporative efficiency of the head manikin tight-fitting fabric skin

The evaporative efficiency of the tight-fitting fabric has been determined according to the experimental method reported by Burton (Burton, 1944; Havenith et al., 2013) and calculated according to equation 3.3.

Specific requirements for the head manikin under physiological control mode

$$Eff_{evap} = \frac{Evaporative\ heat\ loss}{Mass\ loss \cdot \lambda_{H_2O}} \quad [3.3]$$

Where the *Evaporative heat loss* is the increase in heat loss with regards to the dry heat loss (i.e. total wet manikin heat loss – dry manikin heat loss) expressed in $W \cdot m^{-2}$, *Mass loss* corresponds to the mass of the sweat liquid released on the manikin expressed in g, λ_{H_2O} is the latent heat of vaporization of water at 30°C expressed in $J \cdot g^{-1}$. To relate the evaporative efficiency obtained in this study to other studies and skin types and to confirm the Burton's relationship (Burton, 1944) the location of the evaporation, the so-called relative evaporative locus (REL), was determined. In the single-layer fabric case, the REL corresponded to the ratio of the adjacent-air-layer thermal insulation and the total thermal insulation (fabric and adjacent air layer) as calculated in equation 3.4.

$$REL = \frac{R_{nude}}{R_{t\ tight\ fabric}} \quad [3.4]$$

Where *R_{nude}* is the thermal resistance of the adjacent air layer and *R_{t tight fabric}* is the total thermal resistance of the tight-fitting fabric and the adjacent air layer together, both expressed in $m^2 \cdot ^\circ C \cdot W^{-1}$. The thermal insulation of the adjacent air layer and the total thermal insulation of the tight-fitting fabric were determined in environmental conditions of 20°C / 50% RH and still air ($v_a < 0.1\ m \cdot s^{-1}$) when the head manikin was controlled at 35°C constant and homogeneous surface temperature for one hour. The adjacent-air-layer and total thermal insulation was calculated according to equation 3.5:

$$R = \frac{T_{manikin} - T_{air}}{\frac{\sum A_i \cdot HF_i}{A_i}} \quad [3.5]$$

Multi-sector thermophysiological head simulator

Where R is the measured thermal insulation in $\text{m}^2 \cdot ^\circ\text{C} \cdot \text{W}^{-1}$, T_{manikin} is the surface temperature of the head manikin in $^\circ\text{C}$, T_{air} is the actual temperature in the climatic chamber in $^\circ\text{C}$ and A_i and HF_i are the surface areas and the corresponding heat fluxes of each head zone averaged for a 30-minute steady-state expressed in m^2 and $\text{W} \cdot \text{m}^{-2}$, respectively. Due to the tight fit of the fabric, the clothing area factor was assumed to be one for a very tight fabric skin.

The evaporative cooling and efficiency were measured for different sweat rates. The head manikin was placed in the centre of the climatic chamber set at $25^\circ\text{C} / 50\% /$ Still air ($v_a < 0.1 \text{m} \cdot \text{s}^{-1}$) and was covered with the tight-fitting elastic fabric used to evenly distribute the sweat. All head zones heaters were controlled in constant temperature mode at 35°C and a work cycle with different one-hour phases of uniform sweating rates (10, 30, 50, 100, 300, 500 and $1000 \text{ml} \cdot \text{m}^{-2} \cdot \text{h}^{-1}$) was programmed. The phases with sweat rates were separated by drying phases to ensure that the measured heat flux at the beginning of each sweating phase was as the one in the initial dry phase ($\pm 3\%$). Average heat flux for a steady-state of 15 minutes of each sweating period was calculated for each head zone (average heat flux variation for all head zones was less than 5%). Individual zone heat fluxes were area-weighted averaged for the entire head and compared with entire head dry heat flux. Additional heat fluxes due to moisture evaporation at each sweat rate were obtained after subtracting the dry heat flux. These heat fluxes were not corrected by the change in the thermal insulation of the tight-fitting fabric when wet. Consequently, it should be noticed that the so-calculated and so-referred evaporative heat loss in this section included not only strictly pure evaporative heat loss but some marginal heat loss due to wet conduction and other changes in heat loss due to wet skin. It could be referred as apparent as Havenith et al. did but no correction of the surface temperature of the outer wet skin was applied (Havenith

Specific requirements for the head manikin under physiological control mode

et al., 2013). The measurements were repeated three times. Finally, a theoretical efficiency of the evaporation (Eff_{evap}) at the head manikin surface has been calculated by comparing the evaporative heat loss with the corresponding theoretical evaporative heat loss calculated based on mass loss if all secreted sweat would evaporate taking heat from the manikin surface being at 30°C ($\lambda_{\text{H}_2\text{O}} = 2430 \text{ J}\cdot\text{g}^{-1}$ at 30°C, (Havenith et al., 2013)). To calculate the evaporative heat loss, the steady-state evaporative heat loss was assumed to occur between the wetting and drying times described in the upcoming section 3.9.2.2. To calculate the theoretical evaporative heat loss based on the mass loss, the evaporated mass accounted for the sweat rate over the one-hour step. Due to the difficulty of measuring water migration that existed between zones, the evaporative efficiency values reported for head parts could not fulfill the assumption of mass loss solely due to evaporation for equation 3.3 for individual head parts. Moreover, Koelblen (unpublished data) determined the maximum moisture content for this tight-fitting fabric and water drip-off for $1000 \text{ ml}\cdot\text{m}^{-2}\cdot\text{h}^{-1}$ for the entire head was confirmed. However, the exact amount of water drip-off could not be precisely measured and evaporative efficiency calculation for the entire head was not corrected by subtracting the water mass that dripped off.

3.9.2.2 Evaporation responsiveness of the sweating system

The responsiveness of the complete water delivery system to reach a certain evaporative cooling was analyzed. Particularly, the time needed for developing the steady-state heat flux at each sweat rate and for returning to the dry steady-state heat flux was determined based on the measurements described in section 3.9.2.1. Therefore, the wetting and the drying time for each sweating period were defined as follows and were calculated as the average value of three repetitions:

- **Wetting time.** - Time elapsed from the sweat rate set point introduction till the 75% of the maximal steady-state evaporative heat loss was reached.
- **Drying time.** - Time elapsed from the sweat rate setting to zero till the evaporative heat loss was reduced to be just 25% above of the steady-state dry heat loss.

These percentages of the evaporative heat loss were chosen to generally approach the steady-state and allowing for any punctual variation of the system.

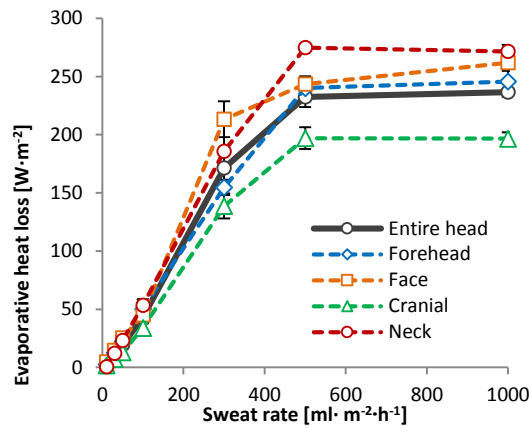
3.9.3 Results

3.9.3.1 Analysis of the evaporation efficiency of the head manikin tight-fitting fabric skin

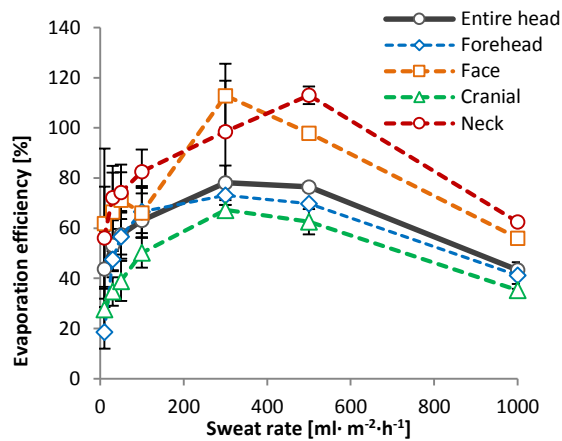
In the REL experiment, the actual values of the environmental parameters measured in the climatic chamber were $19.70 \pm 0.00^{\circ}\text{C}$, $52.94 \pm 0.26\%$ and $0.09 \pm 0.01 \text{ m}\cdot\text{s}^{-1}$ and the total thermal insulation calculated for the adjacent air layer and for the tight-fitting fabric were 0.1013 and $0.1106 \text{ m}^2\cdot^{\circ}\text{C}\cdot\text{W}^{-1}$, respectively, which yielded to the REL of 0.92. Figure 3.7 shows the average evaporative heat loss and the evaporation efficiency for each head part and the entire head at each sweat rate. In general, the evaporation efficiency tended to increase with the sweat rate till a maximum of 78% and 76% observed for the entire head at 300 and 500 $\text{ml}\cdot\text{m}^{-2}\cdot\text{h}^{-1}$ and it dramatically decreased for the highest sweat rate of 1000 $\text{ml}\cdot\text{m}^{-2}\cdot\text{h}^{-1}$ as the calculation was not corrected for the water mass that dripped off. For all sweat rates, the lowest efficiency was observed at the cranial part, whereas the highest was usually at face and neck. Interestingly, evaporation efficiency for the face and neck parts reached values above 100% for sweat rates of 300 and 500 $\text{ml}\cdot\text{m}^{-2}\cdot\text{h}^{-1}$. As mentioned, the evaporative efficiency values reported for head parts could not fulfill the assumption of mass loss solely due to evaporation for equation 3.2 for

Specific requirements for the head manikin under physiological control mode

individual head parts due to the difficulty of quantifying the water migration that existed between parts.



a)



b)

Figure 3.7. a) Evaporative cooling over the head parts and b) evaporation efficiency calculated as a ratio of the measured evaporative heat loss to the evaporative potential calculated based on the mass loss. Notice that evaporative efficiency for individual zones were not corrected for water migration effect and evaporative efficiency of the entire head at $1000 \text{ ml} \cdot \text{m}^{-2} \cdot \text{h}^{-1}$ was not corrected for water that dripped off. Values are presented as average and standard deviation.

3.9.3.2 Evaporation responsiveness of the sweating system

Figure 3.8 shows the wetting times corresponding to each sweat rate for the different head parts and the average of the entire head. The average wetting times for entire head varied between 3 and 10 minutes and tended to be slightly higher when sweat was set at 300 and 500 $\text{ml}\cdot\text{m}^{-2}\cdot\text{h}^{-1}$. The lowest wetting times were observed for the minimum and maximum sweat rates, respectively.

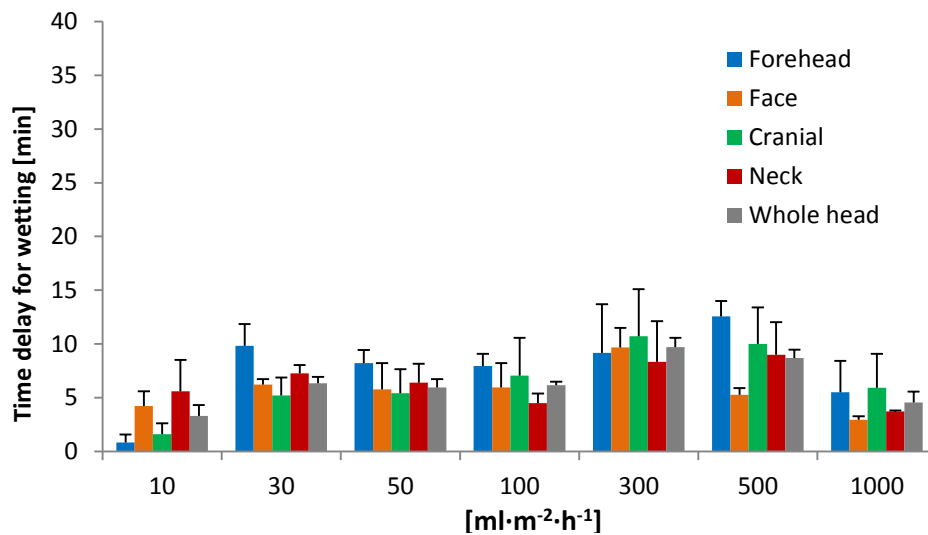


Figure 3.8. Wetting time measured between the onset of the sweating and the development of 75% of the maximal steady-state evaporative heat loss for each sweat rate. Values are presented as average and standard deviation.

Figure 3.9 shows drying times after each sweat rates for the different head parts and the average of the entire head. The drying time increased as long as the sweat rate did, almost linearly for the entire head till 500 $\text{ml}\cdot\text{m}^{-2}\cdot\text{h}^{-1}$. For sweat rates of 500 $\text{ml}\cdot\text{m}^{-2}\cdot\text{h}^{-1}$ and 1000 $\text{ml}\cdot\text{m}^{-2}\cdot\text{h}^{-1}$, the increase in the drying time was more apparent for face and neck than for forehead and cranial parts.

Specific requirements for the head manikin under physiological control mode

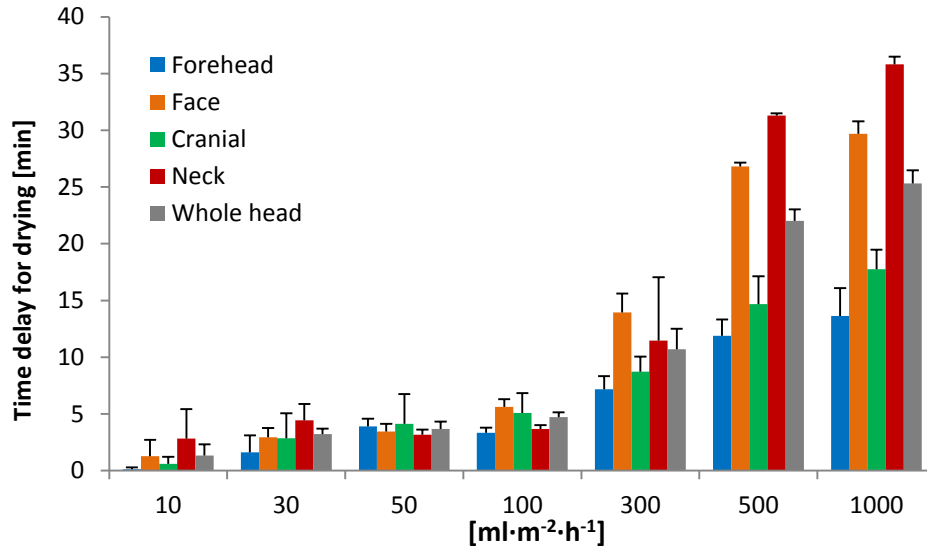


Figure 3.9. Drying time measured between the stop of the sweating and the reduction of the maximal steady-state evaporative heat loss to be just 25% above the dry heat loss for each sweat rate. Values are presented as average and standard deviation.

3.9.4 Discussion

Due to the characteristics of the sweating system, the water evaporated not directly from the head manikin surface but from the tight-fitting fabric. This fact might be responsible for a reduction in the evaporation efficiency. The efficiency of the evaporation was studied at different sweat rates. A general increasing trend was observed according to increasing the sweat rate from an average value for the entire head of 44% at 10 ml·m⁻²·h⁻¹ till a maximum value of 78% and 76% at 300 and 500 ml·m⁻²·h⁻¹, respectively. Previous experience on this type of testing have shown that the water absorption and spreading characteristics of the fabric became better as soon as it was wetted, and thus, evaporation could have been facilitated. When the sweat rate increased beyond a sweat rate of 500 ml·m⁻²·h⁻¹, the efficiency of the evaporation dramatically decreased due to water dripping off as evaporation

efficiency calculation could not be corrected (i.e. about 43% at a sweat rate of 1000 ml·m⁻²·h⁻¹). In this analysis, the change of the thermal insulation of the fabric due to partial wettedness was not considered. Additional thermal insulation measurements carried out by Koelblen (unpublished) on a similar type of fabric on a TORSO thermal device (Psikuta, 2009) showed that the thermal resistance was decreased by 20% in a fully wet state in comparison to dry state. This simplification could induce a marginal error in the calculation of the evaporative heat loss as it was expected to be slightly lower due to higher sensible heat loss when the tight-fitting fabric was partially or fully wet. Among the different head parts, the face and neck consistently showed the highest evaporative efficiency at every sweat rate with some peaks beyond 100%, whereas the cranial part showed the lowest. The fact that the face and neck parts are located in the lower part of the head suggested a possible water migration from top to the bottom of the head. This factor could not be controlled, and therefore, the calculation of the evaporative efficiency for individual part did not strictly agree with the equation 3.2 in section 3.9.2.1 and results should be carefully interpreted. The maximum evaporation efficiency of 78% and 76% was observed for a sweat rate of 300 and 500 ml·m⁻²·h⁻¹. Burton's relationship (Burton, 1944) assumed that evaporation heat is entirely taken from the skin if REL=1 (evaporative efficiency equal to 100%) and is entirely taken from the environment if REL =0 (evaporative efficiency is 0). According to this model, an evaporation efficiency of 92% for a measured REL of 0.92 was predicted. Later on, Havenith et al. (Havenith et al., 2013) performed similar tests and they calculated the relationship between REL and the evaporative efficiency for a permeable two-layer ensemble and for a combination of permeable and semipermeable layers. These model predicted lower evaporative efficiency for the same REL, i.e. 83% for a REL of 0.92 and it was explained by some wicking effect during the tests. However,

Specific requirements for the head manikin under physiological control mode

in their studies, they considered the tight-fitting fabric as the skin and all evaporative efficiency calculation were referenced to the maximum evaporation observed on it.

The observed wetting time for the entire head could reach up to 10 minutes at the different sweat rates. This delay could be due to the time needed by the sweating valves to deliver the water and the wetting time needed by the tight-fitting fabric till it is detected by the head manikin temperature sensors. Some delay in the evaporative cooling, and thus, some increased surface temperature during initial periods of exposures combining warm environments and activity could be expected during the coupled simulations rather than in pure virtual simulations. At this respect, Koelblen (unpublished) quantified the hydrophilicity of several fabrics by measuring the contact angle of a water droplet left on their surface. She showed much better hydrophilicity for other fabric samples such as cotton and polyester than for the pre-equipped tight-fitting fabric of the head manikin even after washing it with a surfactant solution. Figure 3.10 shows the initial development of the sweat at the head manikin surface where a lack of hydrophilicity for this fabric could be recognized.

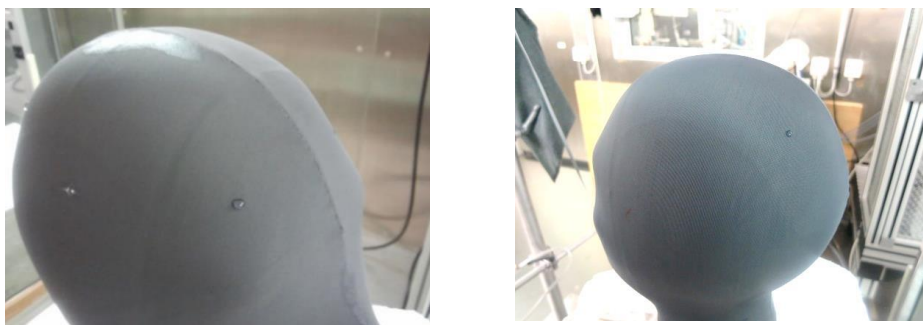


Figure 3.10. Initial development of the sweat at the head manikin showing lack of hydrophilicity.

When the sweating stopped, some water remained absorbed in the tight-fitting fabric and some further evaporative cooling seemed to occur for a certain time afterwards. The observed drying time tended to slightly increase with the sweat rate almost linearly for the entire head up to a rate of $500 \text{ ml}\cdot\text{m}^{-2}\cdot\text{h}^{-1}$. It showed values about 10 minutes when the sweat rate was $300 \text{ ml}\cdot\text{m}^{-2}\cdot\text{h}^{-1}$ and reached times above 20 minutes on average for the entire head for $500 \text{ ml}\cdot\text{m}^{-2}\cdot\text{h}^{-1}$ and upwards. This effect could physically represent the accumulation of liquid sweat on the human skin differently as it is considered in the pure simulations by the physiological model which assumes the difference between the excreted and the evaporated sweat up to a maximum of $35 \text{ g}\cdot\text{m}^{-2}$ (Fiala et al., 1999; Jones and Ogawa, 1992).

3.10 CONCLUSIONS

This chapter 3 has highlighted the potential constraints of the head manikin for precisely representing the human head physiology as described by the physiological model foreseen for the coupled system.

By combining the head segmentation as in the physiological model and the one provided by the head manikin, it was possible to consistently define four head parts independently controlled in the coupled system, namely, forehead, cranial, face and neck parts. The total area of each head part considerably agreed when merging the head manikin zones and the head sectors proposed by the physiological model, except for forehead. When the combined heat transfer coefficients accounting for convective and radiative heat exchange were compared in still air conditions for these four head parts, differences below 2% were observed for the forehead and cranial parts, whereas they were bigger for the face and neck. Therefore, similar dry

Specific requirements for the head manikin under physiological control mode

heat exchange rates could be expected for forehead and cranial parts. As the head manikin does not account for the thermal influence of the thermal plume resulting from lower body parts, some discrepancies between the dry heat loss predicted by the physiological model alone and the coupled system could be expected.

When heterogeneous surface temperature distribution occurred in the head manikin, the gradients between head parts resulted in uncontrolled lateral heat exchange. The analysis of the effect of the deviations in heat flux at each head part for an extreme heterogeneous distribution, revealed acceptable local skin temperature deviation at cranial and neck parts within 1°C. However, the skin temperature at the forehead and face was too low and high by 1.4 and 2°C respectively. Thus, no noticeable deviation in the physiological response of cranial and neck parts is expected for any skin temperatures distribution accounting with differences below those in this extreme scenario, whereas precision of the coupled system would be compromised in case of forehead and face in case of large temperature gradients (Haslam and Parsons, 1994; Psikuta et al., 2012a). Moreover, these local extreme deviations could have a physiological impact on other body parts and mislead the overall thermal response.

The passive heating and cooling responsiveness of the head manikin did not present any limitation for simulation of sudden temperature step changes observed in the human physiology. Nevertheless, when the manikin heating and cooling processes were modulated by the PI control with default settings, the time needed to reach the temperature set point was larger than the time required by the human physiology for both extreme and moderate one-minute transients. To achieve a faster response, the PI control settings K_p and K_i were manually tuned. The time needed to achieve a temperature increase or decrease was reduced after adjusting

the PI settings for a faster response for all heating step changes. For cooling step changes, the time needed to reach the temperature set point was within one minute unless the thermal response of the head manikin was limited by the maximum passive cooling capacity. However, the variation in the steady-state heat flux increased from 1% up to 5 and 3% at 25 and 5°C respectively.

The evaporation efficiency of the sweating at the head manikin has been studied for steady-state and transient periods. The evaporation efficiency in the head manikin was reduced to evaporation taking place in the fabric and not directly on the head manikin surface (Burton, 1944) due to some latent heat taken from the environment in warm conditions instead of the manikin surface (Havenith et al., 2013; Wang et al., 2013). The efficiency of the evaporation studied at different sweat rates tended to increase from an average value for the entire head of 44% at $10 \text{ ml}\cdot\text{m}^{-2}\cdot\text{h}^{-1}$ till a maximum value of 78% and 76% at 300 and 500 $\text{ml}\cdot\text{m}^{-2}\cdot\text{h}^{-1}$ but it strongly decreased till 43% at a sweat rate of 1000 $\text{ml}\cdot\text{m}^{-2}\cdot\text{h}^{-1}$ because water drip-off was not considered. Time needed for wetting raised up to 10 minutes till at least 75% of the steady-state evaporative heat loss was reached at the different sweat rates and thus, reduced evaporative heat loss might occur at the early stages of the sweating onset.

Similarly, some time elapsed between the sweat function stopped and the evaporative heat loss decreased to be just 25% above the dry heat loss. This drying time could be above 20 min for sweat rates from 500 $\text{ml}\cdot\text{m}^{-2}\cdot\text{h}^{-1}$ and upwards. This effect could physically represent the accumulation of liquid sweat on the human head skin and its evaporative further cooling differently as represented in the physiological model. However, till which extend these time resemble the actual drying times on the human skin has to be further studied.

Specific requirements for the head manikin under physiological control mode

The potential constraints for the head manikin to represent the head physiology as described in the physiological model were determined. However, models are by definition simplifications of the reality that they intend to represent and thus, the precision of the physiological model itself for simulating the real human thermal response must be assessed as well. Hence, the next chapter 4 aims at validating the prediction of the physiological model by comparing the predicted physiological response in several simulated scenarios with human experimental data obtained for a wide range of environmental conditions, clothing and activity levels.

4 VALIDATION OF A THERMOPHYSIOLOGICAL MODEL AGAINST A DEDICATED DATABASE OF HUMAN EXPERIMENTS

4.1 INTRODUCTION

Human experiments are valuable to observe human thermophysiological response to specific conditions in a systematic and controlled way. This observation provides important inputs to enhance human health, performance and comfort. The experimental quantification of thermal strain and comfort is of special interest in fields such as sport physiology (Formenti et al., 2013; Gerrett et al., 2014; Gunga et al., 2008; Merla et al., 2010; Teunissen et al., 2012), clinical research (Lahiri et al., 2012), protective clothing design (Bogerd et al., 2010; Chou et al., 2008; De Bruyne

Multi-sector thermophysiological head simulator

et al., 2008), automotive industry (Tanaka et al., 1992) or building environmental ergonomics (Arens et al., 2006a, 2006b; Zhang et al., 2010a). Although the examination of people directly exposed to the environment of interest provide comprehensive information about physiological changes and how they are perceived, not all scenarios can be addressed due to ethical reasons. Furthermore, large sample sizes are needed to come into a reliable conclusion due to high inter- and intra-subject variability observed among human beings, and, thus, time-consuming and high cost testing are associated.

Mathematical models of the human physiology are very useful instruments for advancing ergonomics research as they are able to predict human thermal response in a wide range of environmental conditions. Consequently, they allow reducing the amount of human experiments to do research in the field of thermal ergonomics. Several models with different levels of complexity are referenced in the scientific literature, for which the acceptance of their reliability might depend on the specific purpose of the model. For example, models available in environmental ergonomics standards strongly simplify human physiology and rely their assessment mostly on heat balance equations. They aimed either at determining a potentially hazardous situation (i.e. PHS model (Malchaire et al., 2001) in ISO 7933(2004) or IREQ model in ISO 11079(2007)) or assessing thermal comfort in human occupancy spaces such as PMV index based on Fanger's comfort equation (Fanger, 1970) in ISO 7730(2005) or Effective Temperature (ET) developed by Houghton and Yaglou (Houghton and Yaglou, 1923) standardized by ASHRAE. Gagge (1971) proposed a further modification of this ET comfort model by applying a human body model with two compartments consisting of core and shell (skin). Furthermore, a model of the body thermoregulatory actions validated for

moderate activities in uniform environments was added (Gagge, 1971; Haslam and Parsons, 1994; Takada et al., 2011).

One of the first models approaching human thermal physiology simulation in detail was developed by Stolwijk (Stolwijk, 1971). This 25-node model considers a simplified human body geometry (i.e. cylinders or spheres) divided in six segments. Each segment was divided into four concentric layers (core, muscle, fat and skin) and a central blood pool representing main arteries and veins. It included an algorithm for the control of thermoregulation mechanisms. Most advanced models presented in the recent decades are based on this model (Fiala et al., 2001, 1999; Huizenga et al., 2001; Kobayashi and Tanabe, 2013; Salloum et al., 2007; Smith, 1991; Tanabe et al., 2002; Xu and Werner, 1997). Due to a highly detailed physiology, multi-node models are able to predict global and local human thermal response under steady-state, transient and asymmetrical exposure conditions. These models have shown higher agreement with experimental data than the more basic models (Psikuta et al., 2012a). Nevertheless, models usually predict thermal response for a standard person while the thermophysiological reactions are modelled based on statistical regression models rather than physiological principles. Moreover, physiological models include in general a simplified model for clothing considering a few static parameters which are mainly thermal and evaporative resistances. However, the dynamic nature of the thermal exchange occurring within the clothing might significantly affect complex coupled heat and mass transfer phenomena, such as moisture absorption-desorption cycles, condensation or perspiration migration across clothing layers. These transient processes can share substantial heat loss depending on the fabric thermal capacity and wetting properties, location within the layered ensemble and air gap distribution at each body region (Fan and Cheng, 2005a; Frackiewicz-Kaczmarek et

al., 2015; Havenith et al., 2013, 2008; Jones and Ogawa, 1993; Li et al., 2004; Lotens and Havenith, 1994; Lotens et al., 1995; McCullough, 1991; Psikuta et al., 2012b; Wissler and Havenith, 2009; Wu and Fan, 2008). Although these clothing models simulating transient processes in the human skin-clothing-environment system are available in the literature, they have still some simplification in the modelling of determining aspects, such as air gaps or contact area over the body surface (Fan and Cheng, 2005b; Li et al., 2004; Lotens and Havenith, 1994; Lotens et al., 1995). Additionally, they are scarcely combined with advance physiological models (Fiala et al., 1999; Tanabe et al., 2002; Wissler, 1985) or if combined, their performance has not been validated (Fan and Cheng, 2005a, 2005b; Li et al., 2004). Therefore, the precision of the predictions after these simplifications need to be validated against human subject data.

Validation of thermal physiology models against human experimental data is subjected to availability, accurate description and consistency of data and experimental procedures. Thermal responses depend on multiple parameters including the environment, clothing, physical activity and individual factors (Havenith and Middendorp, 1990; Havenith, 2001; Havenith et al., 1998; van Marken Lichtenbelt et al., 2004). Thus, the comprehensive validation procedure addressing these factors becomes complex. The prediction precision of a model is limited by the accuracy of the inputs to it (Jones, 2002). Therefore, the accuracy of the parameters defining the scenario and reliability and consistency of the physiological measurements used as reference become as important as the model algorithms themselves. Collection of experimental data such as local sweat rates is really delicate as the methodologies are not standardized (De Bruyne et al., 2010; Machado-Moreira et al., 2008a; Smith and Havenith, 2011). The most common physiological variables available are core and local skin temperatures. Several

methods and body sites are reported for core temperature measurements (i.e. rectal and esophageal probes, ingestible pills aimed at intestine-site, or infra-red thermometers for tympanic membrane). The differences in reaction time, maximum peak and rate of change have been recognized and controversially discussed for either slow or acute changes in core temperature attributed to pill ingestion timing or posture-related blood perfusion rates during exercise (Easton et al., 2007; Kelly, 2006; Kolka et al., 1997; Lee et al., 2000; Teunissen et al., 2012). Measurements methods can provide also some artifacts in temperature readings, especially for the skin temperature measurement due to sensor shape and attachment method (Buono and Ulrich, 1998; Psikuta et al., 2013a; Tyler, 2011) or due to differences in application of infra-red thermography (James et al., 2014; Zaproudina et al., 2008). Besides, there is a lack of data for important body parts such as head. The presence of hair usually limits the measurement area to the forehead as the only single point available for placing the sensor. Furthermore, insufficient information about pre-exposure conditions can bias the accuracy of the model predictions as initial sweating, vasoconstriction or vasodilation states might induce different heat exchange at the beginning of the exposure (Haslam and Parsons, 1994).

Another important factor when modelling the human thermal responses is the clothing description and how the ensembles are worn by subjects. The standard methods to measure or estimate thermal insulation and clothing area factor are based on a standardized body size in standing straight posture, which may not reflect the exact experimental condition (ISO15831, 2004; ISO9920, 2007; McCullough et al., 1985). Some further inaccuracy might be introduced due to insufficient or lack of data for actual value of local clothing parameters at different body parts. In case of evaporative resistance, no international manikin standard is

available (only ASTM F2370-10, 2010) and bench test measurements are often used for estimation of this parameter.

Generally, validation studies for the human thermoregulation models are scarce in scientific literature. In many cases, the validation studies available have not addressed demanding situations such as exercise. The original 25-node Stolwijk model was initially presented with validation in four scenarios and has been further validated in several studies mainly based on global physiological data (Haslam and Parsons, 1994; Stolwijk, 1971). More recently, it has been re-evaluated by Munir et al. (2009) on the basis of local skin temperatures for different thermal-transient conditions and low activity levels presented in two datasets finding some discrepancies due to skin blood flow distribution (Munir et al., 2009). The Waseda University model (Kobayashi and Tanabe, 2013; Tanabe et al., 2002) has been validated at least in eight different scenarios representing steady-state and transient conditions with participants in sedentary conditions. An improved version of the thermoregulatory model by Werner (Werner and Webb, 1993) representing the human-clothing-environment heat exchange was presented and validated by Xu and Werner (Xu and Werner, 1997). After adding more complexity to the original multi-segmental model by supplementing the initial two-layer compartment (core and shell) with the thermal properties of muscle, fat and clothing layers, they contrasted the model calculations against six experimental data bases including heat, cold, exercise (cycling workload up to 60 W), clothing and transient phases. However, they presented a graphical evaluation only based on which no quantitative assessment of the precision can be done. The Berkeley model (Huizenga et al., 2001; Zhang et al., 2010a, 2010b) has been recently suggested as the most fitted model for predicting thermal sensation based on the thermophysiological response for human occupancy spaces (Croitoru et al., 2015).

Validation of a thermophysiological model against a dedicated database

Although it has been extensively validated with satisfactory results in steady-state, transient and non-uniform conditions for global and local thermal response, its applicability for exercise scenarios have not been addressed so far. Yokoyama et al. (Yokoyama et al., 2007) presented their model which aimed at implementing adjusted local characteristics of each segment. They validated the model predictions against data of seven human experiments, however, all of them represented steady-state scenarios.

One of the most extensively validated thermal physiological models is the mathematical model of the human thermal physiology by Fiala (Fiala and Havenith, 2015; Fiala et al., 2012, 2001, 1999; Psikuta et al., 2012a). It has been implemented in commercially available software which is constantly being improved. This model has been already validated in many different scenarios mainly for core and mean skin temperatures. The model by Fiala was presented together with 23 validation scenarios compiling a wide range of conditions. Moreover, Psikuta et al. (Psikuta et al., 2012a) did a further quantitative and qualitative validation study (58 exposures) and showed an acceptable agreement of the model, mainly for mean skin and core temperatures, in a wide range of environmental conditions, clothing and activity level for both steady-state and transient exposures. Nevertheless, other physiological parameters such as local skin temperatures or evaporative heat loss were not systematically analyzed, possibly due to lack of experimental data.

The study on the precision of predictions for local skin temperature using physiological models has been limited to sedentary activities in different climates (Foda et al., 2011; Werner and Webb, 1993). Hence, no human thermoregulation model has been widely validated for prediction of local skin temperatures so far, especially in exercising scenarios. The predictability of local skin temperatures has

been mostly studied within thermal comfort range, whereas in more demanding scenarios for the thermoregulatory system, the performance of thermophysiological models has been mostly assessed based on core and mean skin temperatures.

4.2 AIM AND OBJECTIVES

This chapter 4 aimed at validating the mathematical model of the human physiology by Fiala (FPCm5.3. model, *Ergosim*, Germany) for prediction of global and local skin temperatures in a wide range of scenarios collected in a dedicated database. This validation is of high relevance as the model is foreseen for developing the coupled system. After collecting data of different human experiments from the literature and unpublished results, it was decided to carry out some dedicated human experiments to complete the human data base with physiological data obtained during cycling activity in a moderate environment. The local effect of the attachment of the thermal contact sensors on the heat and mass exchange occurring at the human skin during rest, exercise and recovery phase was verified with measurement on a hot plate. The need of considering this aspect for a critical interpretation of simulation results was already shown by Psikuta et al. (Psikuta et al., 2012a). To achieve this aim, the work has included the four following objectives:

- Development of a comprehensive database of experimental data including detailed information on local physiological parameters to be used for validation of any advanced model of human thermoregulation in a wide range of scenarios.

Validation of a thermophysiological model against a dedicated database

- Completion of the human data base by collecting human physiological data for cycling activity in a moderate environment.
- Verification of the effect of the sensors attaching method on surface temperature measurements.
- Validation of the FPCm5.3. model for prediction of global and local skin temperature by comparing simulations against the developed data base in scenarios that included relevant human and environmental factors, such as cold, moderate and warm environmental temperature, different levels of relative humidity, high wind speed, presence of solar radiation, moderate and high activity levels and protective clothing.

4.3 DEVELOPMENT OF A HUMAN EXPERIMENTS DATABASE

Twelve different human studies have been selected from literature including relevant human and environmental factors, such as cold, moderate and warm environmental temperature, different levels of relative humidity, high wind speed, presence of solar radiation, moderate and high metabolic rate, and protective clothing. A total of 41 exposures accompanied by descriptions of experimental protocol, environmental conditions and clothing parameters have been included in this study. The ranges of the experimental parameters of all exposures are given in Table 4.1 in form of maximum and minimum values, whereas detailed description of each exposure can be found in Table 4.2.

Multi-sector thermophysiological head simulator

Table 4.1. Maximum and minimum values of parameters of the database

	Air temp [°C]	Radiant temp [°C]	Relative humidity [%]	Air speed [m·s ⁻¹]	Solar radiation [W·m ⁻²]	Activity [met]	Mean clothing thermal resistance [m ² K·W ⁻¹]	Mean clothing evaporative resistance [m ² Pa·W ⁻¹]
Max	40	96	80	18.0	109	7.3	0.64	96.77
Min	-25	-25	20	0.1	0	0.8	0.05	2.44

Three out of the 41 exposures took place outdoor and two in a temperature-controlled rooms, whereas the rest of the experiments were conducted in climatic chambers. Twenty-one out of the 41 exposures included a transient exposure to environmental temperatures when participants were transferred from a climatic chamber to an adjacent temperature-controlled room. In 19 exposures participants conducted exercise periods at different metabolic rates and in five out of these 19 exposures, participants experienced changes in the environmental temperature in addition to changes in the metabolic rate. In 23 out of 41 exposures, wind speed higher than 1m·s⁻¹ was applied from front either on the whole body or just locally at some body parts. The maximum radiant temperature exposure (exposure 23) corresponded to the equivalent radiant temperature of a frontal infrared panel providing 500 W·m⁻² at the participant's site. For the outdoor exposures including solar radiation (exposures 19 and 20), the radiant temperature was set equal to air temperature and solar radiation was considered as diffuse solar radiation. Figure 4.1 shows an overview of distribution of exposures according to the most relevant parameters. For the classification according to the activity level, the maximal activity level was chosen as qualifying parameter in case different levels of activity were used.

Validation of a thermophysiological model against a dedicated database

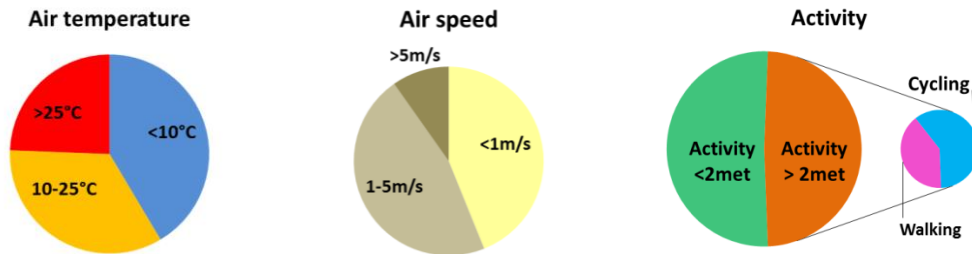


Figure 4.1. Distribution of exposures in data base regarding to air temperature, wind speed and physical activity.

The total number of tests included in the validation study was 301. A description of the essential experimental conditions and number of participants is provided in Table 4.2 for each exposure.

Multi-sector thermophysiological head simulator

Table 4.2. General description of human data base

Experiment	Exposure	Exposure description	Duration [min]	Air temperature [°C]	Radiant temperature [°C]	Relative humidity [%]	Air speed [m.s ⁻¹]	Solar radiation [W.m ⁻²]	Activity [met]	Mean clothing thermal resistance [m ² K.W ⁻¹]	Mean clothing evaporative resistance [m ² Pa.W ⁻¹]	Number of participants [male/female]	Reference
1	1	Hot exposure with protective clothing	86	40/25	40/25	30	0.5	0	3.3/4.4	0.42	77.29	10/0	Unpublished data from Annaheim, Empa, Switzerland
	0.38									77.30			
	0.14									26.09			
2	4	Cycling in moderate environments	95	20	20	50	3	0	3.4/7.3	0.06	3.67	9/0	(Jack, 2010)
	2.8/4.7								0.06	3.99	0/5		
	3.4/7.3								0.05	3.72	9/0		
	2.8/4.7								0.05	4.08	0/5		
	3.4/7.3								0.06	3.69	9/0		
2.8/4.7	0.06	4.01	0/5										
3	10	Standing in the cold	90	20/-10	20/-10	50	0.2/0.2	0	1/1.2	0.29/0.37	51.55/96.78	8/0	(Mäkinen et al., 2000) and unpublished data from H. Rintamäki, Finnish Institute of Occupational Health, Oulu, Finland
	0.2/1												
	0.2/5												
	0.2/0.2												
	0.2/1												
0.2/5													
0.37	96.78												
4	16	Sedentary activity in cold	120	10	10	40	0.05	0	0.8	0.12	5.38	10/0	(Wagner and Horvath, 1985)
5	17	Cycling in warm environment	30	29	29	80	0.2	0	5.1/7.1	0.06	3.39	8/0	(Bogerd et al., 2010a)
6	18	Guard duty in the cold	180	0	0	82	18	0	1.6	0.64	61.74	4/0	Unpublished from I. Mekjavic, Josef Stefan Institute in Ljubljana, Slovenia
7	19	Hiking in warm conditions	180	22	22	71	1.1	57	4.3	0.22	16.16	6/0	Unpublished from I. Mekjavic, Josef Stefan Institute in Ljubljana, Slovenia
	24											24	

Validation of a thermophysiological model against a dedicated database

Table 4.2. General description of human data base (continuation)

Experiment	Exposure	Exposure description	Duration [min]	Air temperature [°C]	Radiant temperature [°C]	Relative humidity [%]	Air speed [m·s ⁻¹]	Solar radiation _{total, 0-21}	Activity [met]	Mean clothing thermal resistance [m ² ·K·W ⁻¹]	Mean clothing evaporative resistance [m ² ·Pa·W ⁻¹]	Number of participants [male/female]	Reference
8	21	Walking in the cold	120	10	10	50	0.5	0	1.4/5.9	0.32	27.85	10/0	(Niedermann et al., 2014)
9	22 23	Walking in hot conditions	145	30/25.7	30/25.7 96/25.7	40/19.6	0.3 0.3	0	4.9/5.9/1	0.21	20.95	10/0	(Niedermann et al., 2014)
10	24 25	Cycling in moderate environment	81	21.8 21.2	21.8 21.2	39	0.2/ 0.4	0	2.5/4 2.5/5.3	0.05	2.47	14/0	(Priego Quesada et al., 2015) and unpublished data from Empa, Switzerland
11	26 27 28 29 30 31	Cycling in moderate and warm environment	120	20 30 30 30	20 30 30 30	50 80 20	0.3	0	1.3/5.3 1.3/1.8 1.3/1.7 1.3/4.6 1.3/1.7 1.3/4.8	0.16 0.06	17.42 6.63	1/1	(den Hartog, 2002)
12	32 33 34 35 36 37 38 39 40 41	Sedentary cold exposures	120	3/23 -12/23 -25/23	3/23 -12/23 -25/23	n.r.	4 8 1 2 4 6 8 1 2 4	0	1.5	0.54 0.58	48.04 56.62	8/0	Unpublished data from From Kuklane, National Institute for Working Life, Sweden. Test conditions and limb cooling are described in (Geng et al., 1998; Kuklane et al., 1998)

4.4 INVESTIGATION OF LOCAL SKIN TEMPERATURES DURING CYCLING IN A MODERATE ENVIRONMENT

4.4.1 Introduction

Specific human trials were carried out in collaboration with the University of Valencia with the aim of investigating the evolution of core and local skin temperatures at different body parts with special focus on the head-site during cycling in moderate environments. This work was carried out as a short-term scientific mission funded by COST Action TU1101 project.

The hosting groups were the Department of Physiology at the Faculty of Medicine and Odontology and the Department of Physical and Sport Education (Research Group in Sport Biomechanics (GIBD)) at the Faculty of Physical Activity and Sport Sciences. The collaboration has been performed in the frame of their project THERMOBIKE: *“Applying infra-red thermography to improve sport performance, to reduce injuries incidence and to increase thermal comfort at cycling activity”*.

The outcome of this work was the experiment 10 (exposures 24 and 25) in the validation database (Table 4.2). Additionally, this data was used for validation of absolute skin temperatures measurements examined by infra-red thermography (IRT) by the research group of the University of Valencia (Priego Quesada et al., 2015).

4.4.2 Methods

4.4.2.1 Experimental design

Fourteen healthy male cyclists participated in the study (age: 28.9 ± 8.3 years, body mass: 72.8 ± 10.6 kg, height: 175.8 ± 8 cm, average cycling training: 162 ± 77 km · week⁻¹, peak power output: 281.7 ± 38.3 W). All participants signed an informed consent term in agreement with the Committee of Ethics in Research with Humans at the University of Valencia (approval number H1384344515519), and in agreement with the Declaration of Helsinki. Each of them completed three examination days in the laboratory of Biomechanics of the Faculty of Physical Activity and Sport Sciences (University of Valencia) between 18th November and 27th December 2013 to perform the following tests:

- Pre-test:
 - Subject characterization by gathering anthropometrical data (height, weight, optimal saddle height to reach a maximum knee extension of $\alpha = 150\text{-}155^\circ$, asymmetry lower limbs and upper limbs) and by completing a brief injuries and medical anamnesis.
 - Incremental cycling test (initial work load: 50 W, step duration: 1 min, progressive workload increase: 25 W until exhaustion, pedaling frequency: 90 revolutions per minute [rpm])(Lucia et al., 2002). Exhaustion was defined as the moment when cyclists were no longer capable of maintaining the pedaling frequency of 90 rpm. Maximum cycling power output was defined as the workload of last stage completed. By this incremental test, maximum cycling power at 90 rpm and the corresponding heart rate were determined.
- Test 1: Main test at 50% of the maximum cycling power at 90 rpm.

Multi-sector thermophysiological head simulator

- Test 2: Main test at 35% of the maximum cycling power at 90 rpm.

Execution order of test 1 and 2 was randomized. Pre-test aimed at individualizing the cycling position and the workload for subsequent tests 1 and 2. Test 1 and 2 aimed at collecting core body temperature and local skin temperatures by thermoresistive sensors and by IRT imaging during cycling tests in laboratory. No naturally bald subjects participated in the tests and only two out of fourteen had a shaved head.

All tests were carried out in a moderate indoor environment. Environmental conditions during the tests were $21.2 \pm 0.8^{\circ}\text{C}$ and $39.0 \pm 4.9\%$ relative humidity for test 1 and $21.8 \pm 0.7^{\circ}\text{C}$ and $39.4 \pm 4.5\%$ for test 2. Participants were cycling on an ergometer (*Cardgirus Medical, Bikemarc, Sabadell, Spain*) and they were wearing cycling short pants while upper body was undressed.

4.4.2.2 Test protocol

Two experimental tests were carried out to collect body temperatures by thermoresistive sensors and by IRT imaging during cycling tests in laboratory (test 1 and 2). Test protocol consisted of the following four phases (Figure 4.2):

- Acclimatization phase (15 min): Standing in the laboratory. The investigator was attaching the skin temperature sensors within the first minutes of this phase.
- Warming-up phase: (3 min): Cycling at 50 W at 90 rpm.
- Main activity phase (45 min): Cycling either at 50 or 35% of the maximum cycling power at 90 rpm.
- Cooling-down phase (10 min): Standing in the laboratory.

4.4.2.3 Skin temperatures

Local skin temperatures were recorded at 18 locations by means of iButtons sensors (Type DS1922L, Maxim Integrated Products, San Jose, CA, USA) attached to the skin with Hypafix™ clinical tape (BSN Medical GmbH, Hamburg, Germany). Locations agreed with those proposed in ISO 9886:2004 for mean skin temperature calculation based on 14 measurement sites, such as forehead, back of the neck, right scapula, left upper chest, right arm in upper location, left arm in lower location, left hand, right abdomen, left paravertebral, right anterior thigh, left posterior thigh, right shin, left calf and right instep. Additionally, four more sensors were placed on head surface at left cheek, right side of the neck, left temple and upper head back. The sensors at the left temple and upper head back were attached to a thin bandage wound on the head. Measurements were taken every 10 seconds and averaged for each minute for following time periods:

- *Pre-activity period* consisting of the last 3 minutes of acclimatization phase.
- *Activity period* consisting of the complete warming-up phase (3 minutes) and the complete main activity phase (45 minutes).
- *Post-activity period* consisting of the complete cooling-down phase (10min).
- *Termination period* consisting of the initial 3 minutes after the end of the cooling-down phase.

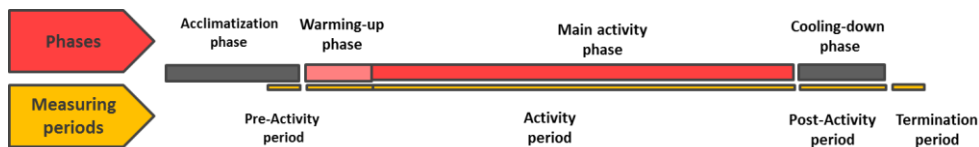


Figure 4.2. Test protocol indicating measuring periods

4.4.2.4 Core temperature

Core temperature was registered throughout the test by a telemetric system (*CorTemp™ Core Body Temperature Monitoring System, HQInc., Palmetto FL, USA*). Participants were asked to take the radio pills at least 7 hours before starting the test. Measurements were taken every 10 seconds and averaged for each minute for the time periods described in section 4.4.2.3.

4.4.3 Results

4.4.3.1 Skin temperatures

Figure 4.3 shows mean skin temperature based on 14-point measurements according to ISO 9886:2004 (ISO9886, 2004) throughout the test. Results showed that mean skin temperature decreased after starting the activity and reached the initial value of 31.5 and 31.8°C after 20 and 30 minutes of exercise in test 1 and 2 respectively. Individual local skin temperatures are shown in Appendix 1: Local skin temperatures upon the 14 body-sites (ISO 9886).

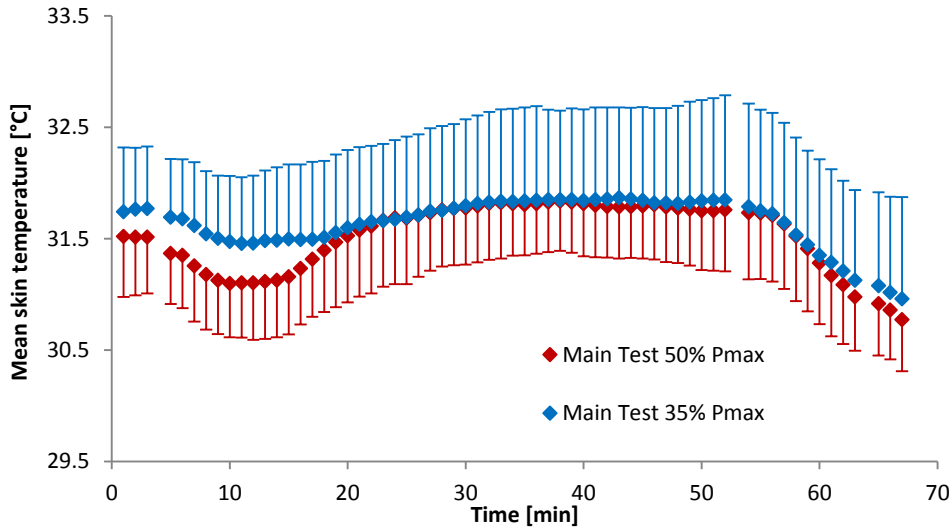


Figure 4.3. Mean skin temperature based on 14 measurement points throughout the test. Data are presented separated by workload: Main test 50% Pmax (n=14) and Main test 35% Pmax (n=14). Error bars for standard deviation are presented only positive or negative for better readability.

Figure 4.4 shows mean skin temperature of the head based on equally-weighted 6-point measurements (forehead, left cheek, right side of the neck, left temple, upper head back and back of the neck) throughout the test. At the beginning, average temperature at head was 32.5°C in both cases and it started to decrease after exercising for 15 minutes. At the end of the cooling-down phase, average head temperature observed for test 50%Pmax trended to be lower than the one corresponding to test 35%Pmax, but not significantly. Individual local skin temperatures at head-site are shown in Appendix 2: Local skin temperatures at head-site.

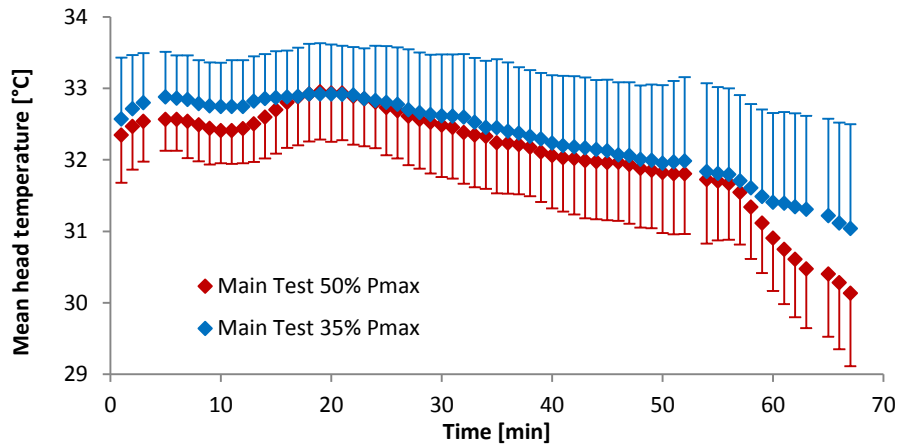


Figure 4.4. Mean skin temperature at head based on equally-weighted 6 measurement points throughout the test. Data are presented separated by workload: Main test 50% Pmax (n=14) and Main test 35% Pmax (n=14). Error bars for standard deviation are presented only positive or negative for better readability.

4.4.3.2 Core temperature

Figure 4.5 shows average value of the core temperature throughout the test. Core temperature reached 38.1°C at the end of the cycling phase for test 50%Pmax, whereas it rose up till 37.9°C in case of test at 35%Pmax. However, no significant differences were found between core temperature at both intensities throughout the test.

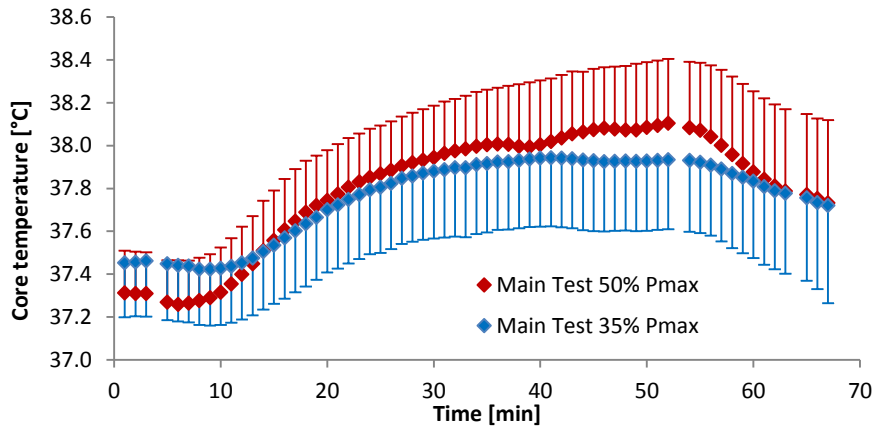


Figure 4.5. Core temperature throughout the test. Data are presented separated by workload: Main test 50% Pmax (n=13) and Main test 35% Pmax (n=14). Error bars for standard deviation are presented only positive or negative for better readability.

4.4.4 Discussion

These human trials provided highly valuable information about thermal physiology in cycling activity in a moderate environment. A moderate increase in core temperature measured at intestine-site was observed for both exposures in which participants cycled for 48 minutes at 50 or 35%Pmax. The mean skin temperature showed a very similar evolution in both tests. It was decreasing at the beginning but came back up to the initial value of 31.5 and 31.8°C after 20 and 30 minutes of activity in test 1 and test 2, respectively. The average temperature at head was 32.5°C in both cases and it started to decrease after exercising for 15 minutes, reaching a slightly lower value of 31.9°C at the end of the activity period. At the end of the cooling-down phase, average head temperature observed after cycling activity at 50%Pmax was lower than the one corresponding to test 35%Pmax, most likely due to a higher sweat production. The data obtained in this experimental study has been included in the database (experiment 10) for validation of any

physiological model representing cycling activity in moderate environments scenario.

4.5 VERIFICATION OF TEMPERATURE SENSORS ATTACHING METHOD

4.5.1 Introduction

Contact thermometry is a common methodology applied for determining skin surface temperature (Tyler, 2011). Application of sensors based on thermistor or thermocouples are frequently found in the scientific literature (Niedermann et al., 2014; Tyler, 2011). Although hard-wired sensors are widely used, wireless version are well-accepted because their applicability is more versatile and do not limit human participants activity during recording (van Marken Lichtenbelt et al., 2004). These sensors allow a continuous recording of the temperature in high-dynamic situations below or in-between clothing layers (Niedermann et al., 2014). To provide reliable measurements, a continuous contact with the skin even when it gets humid has to be ensured. Nevertheless, the sensors themselves and specially the attaching method (usually based on different types of clinical tapes) can potentially affect the local heat transfer, and hence, affect the accuracy of the measurement (Buono and Ulrich, 1998; Fernandes et al., 2014; Psikuta et al., 2013a; Tyler, 2011; van den Heuvel et al., 2003).

The objective of this section was to investigate the effect of the measuring configuration applied in the experiments described in section 4.4 by comparing surface temperature obtained with sensors (iButtons sensors attached to the skin with Hypafix™ clinical tape) with equivalent measurements determined by IRT

imaging. This investigation was carried out on a hot plate system that offered better controlled dry and wet heat transfer conditions.

4.5.2 Methods

A sweating guarded hot plate system according to ISO standards (ISO11092, 2014) (*Empa*, St. Gallen, Switzerland) was covered with a 40 x 40 cm piece of cotton fabric ($212.5 \text{ g}\cdot\text{m}^{-2}$). Six thermal sensors (iButtons sensors (Type DS1922L, Maxim Integrated Products, San Jose, CA, USA) were placed on the surface of the fabric (three covered with Hypafix™ clinical tape (*BSN Medical GmbH*, Hamburg, Germany), three uncovered). An IRT camera (*A40M*, *Flir Systems Inc.*, Portland, USA) with an infrared resolution of 320 x 240 pixels, thermal sensitivity of 0.08°C , and accuracy of $\pm 2^\circ\text{C}$ was placed 40 cm above the center of the plate (see Figure 4.6). Three areas of approximately the same size than those covered by the thermal sensors were defined between each pair of iButtons. Emissivity of the cotton fabric was 0.95, which was in agreement with previous studies (Carr et al., 1997; Fiala et al., 1999) for dry and wet conditions. Reflected temperature was measured according to ISO 18434-1:2008 (ISO18434-1, 2008). The air temperature, relative humidity and reflected temperature were recorded and provided to the camera software. The average temperature value of each defined region was extracted using commercial software (*Thermacam Researcher Pro 2.10 software*, *FLIR*, Wilsonville, Oregon, USA).

The hot plate surface temperature was set at $35.00 \pm 0.05^\circ\text{C}$. Two kinds of tests were carried out under this configuration: a 30-minutes dry test by applying the cotton fabric in dry state on the hot plate and a 60-minutes wet test in which the cotton fabric was homogeneously wetted with $507.7 \pm 45.3 \text{ g}\cdot\text{m}^{-2}$ of water using a domestic washing machine after spinning phase at 400 rpm. The wet test aimed at

Multi-sector thermophysiological head simulator

simulating evaporation from the hot plate surface avoiding the formation of any water layer on the surface. Each test was repeated three times and the iButton sensors were removed and placed again in the same locations before each test. Average value of a 20-minutes steady-state period (same period for all measurements sites and defined by a maximum temperature variation of 0.25°C) for each covered thermal contact sensor, for each non-covered thermal contact sensor, and for the areas defined for the IRT camera measurements were calculated.

Due to non-normally distributed hot plate data (Shapiro-Wilk test, $P < 0.05$), a non-parametric analysis of K-independent samples (Kruskal-Wallis test) test was applied to detect statistical differences in temperature measurements between methods in dry and wet conditions. Statistical significance was defined as $P < 0.05$.



Figure 4.6. Experimental setup for measuring attached sensors effect on dry and wet heat transfer experiments.

4.5.3 Results

Figure 4.7 shows average values for each group of temperature measurements instruments.

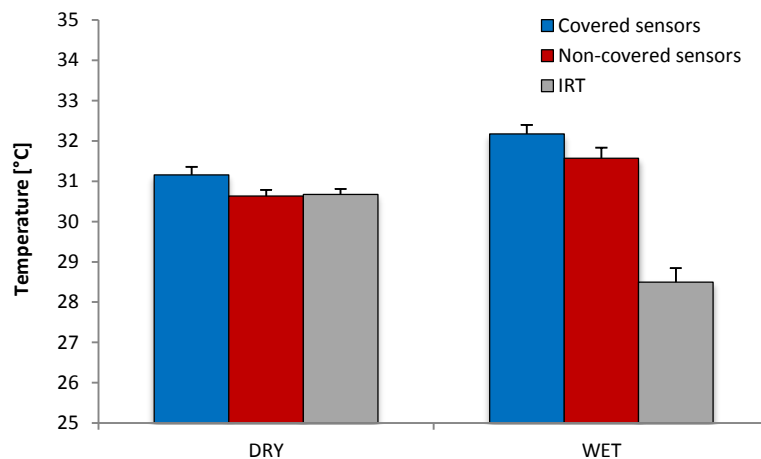


Figure 4.7. Comparison of temperature measurements by different instruments on the surface of the cotton fabric placed on top of hot plate.

Covered sensors measured a higher temperature than non-covered in dry ($P = 0.04$, 95%CI [0.4, 0.6°C]) and wet conditions ($P = 0.04$, 95%CI [0.05, 1.16°C]). The differences between covered sensors and IRT camera were 0.5°C for dry conditions ($P = 0.04$, 95%CI [0.4, 0.6°C]) and 3.7°C for wet conditions ($P = 0.04$, 95%CI [3.1, 4.2°C]). In the case of non-covered sensors, no differences between sensors and IRT camera were found for dry conditions ($P = 0.26$), but 3.0°C difference was observed for wet conditions ($P = 0.04$, 95%CI [2.5, 3.6°C]).

4.5.4 Discussion

No significant differences were observed when comparing non-covered thermal contact sensors and IRT camera measurements in dry conditions. Nevertheless, slightly increased temperature values were found in cases where the sensors were covered with clinical tape. Covered sensors recorded slightly but significantly higher temperature compared to the non-covered ones (0.5°C). This difference could be due to the thermal insulation induced by the Hypafix™ clinical tape (R_{ct} -value: $10.8 \cdot 10^{-3} \text{ m}^2 \cdot \text{K} \cdot \text{W}^{-1}$ obtained according to ISO 11092:1993 (Psikuta et al., 2013a)). In accordance to these findings, Buono and Ulrich (Buono and Ulrich, 1998) attributed differences due to tape from 0.4°C up to 1.3°C depending on environmental conditions when comparing skin temperature measurements using covered and non-covered probes. These results support the idea that thermal contact sensors attached to the skin might potentially interfere in the local dry heat exchange process at the measurement-site (Fernandes et al., 2014; Psikuta et al., 2013a; van den Heuvel et al., 2003).

In wet conditions, absolute differences between sensors and IRT rose up to 3°C and 3.7°C for non-covered and covered sensors, respectively. As the wet cotton fabric provided a fully-saturated water condition, maximum evaporation rates are presumably achieved in the free surface, whereas local evaporation might be reduced at the sensor-site due to the covered surface by the sensor itself and the clinical tape (R_{et} -value for Hypafix™ $17.6 \text{ m}^2 \cdot \text{Pa} \cdot \text{W}^{-1}$, (Psikuta et al., 2013a)). However, the hot plate test is assumed to provide a 'profuse' perspiration state which is attained with human skin. Therefore, no such extreme differences have to be expected for human experiments when measuring skin temperature with attached contact sensors. Furthermore, the blood circulation in the human skin

might help to distribute the overheating underneath the entire skin surface leading to a lower temperature increase due to sensor attachment, whereas this effect is not present in case of the instrumented test.

However, any extrapolation of these results for equivalent measurements on human skin should be carefully addressed as assuming a constant temperature surface and completely wet skin is a simplification of the dynamics of the human thermophysiological response.

4.6 VALIDATION OF THE PHYSIOLOGICAL MODEL BY FIALA FOR PREDICTION OF GLOBAL AND LOCAL SKIN TEMPERATURES

4.6.1 Introduction

This section presents the validation of the mathematical model of the human physiology by Fiala (Fiala and Havenith, 2015; Fiala et al., 2012, 2001, 1999) in its most recent version released in 2015 (FPCm5.3. model, *Ergosim*, Germany). This model has been validated for prediction of global and local skin temperature by comparing simulations against the developed data base of human experiments described in section 4.3. Selected scenarios included relevant human and environmental factors, such as cold, moderate and warm environmental temperature, different levels of relative humidity, high wind speed, presence of solar radiation, moderate and high activity levels and protective clothing.

4.6.2 Methods

4.6.2.1 FPCm5.3. model

The FPCm5.3. model (*Ergosim*, Germany) is the most recent version released in 2015 of the mathematical model of the human physiology by Fiala (Fiala and Havenith, 2015; Fiala et al., 2012, 2001, 1999). It consists of two interacting systems: the controlled or passive system and the controlling or active system. The passive system includes the physical characteristics of the human tissue and the heat and mass transfer occurring within and between the body elements as well as between the body surface and environment. The modelling of the sensible and latent heat exchange between body surface and the environment considers the clothing locally represented by thermal and evaporative resistances, the clothing area factors, long-wave radiation surface emissivity and short-wave radiation surface absorptivity. The human anthropometry represents an average person (35-years old unisex) with 71.4 kg body weight, 169.7cm tall, 1.83m² skin surface area and 22.6% body fat content. The body is divided into 20 multi-layered body elements (head, face, neck, thorax, abdomen, hip, shoulders, upper arms, lower arms, hands, upper legs, lower legs and feet). The model includes description of conductive and convective heat transfer within tissues, blood circulation and respiratory heat exchange. The active system predicts the thermoregulatory actions driven by the central and peripheral nervous system including vasomotion, shivering and sweating. The FPCm5.3. model version allows adjustment of the fitness level, acclimatization days, body size and percentage of body fat of a simulated person (Fiala and Havenith, 2015; Havenith, 2001).

4.6.2.2 Validation procedure

The validation of the FPCm5.3. model was done by comparing experimental human data with a corresponding simulated virtual exposure. The exposures were built up based on description of the experimental test conditions described by experimenters. For each exposure, the experimental protocol, the environmental conditions, the clothing worn and the activity level were individually modelled. In some cases, description of the experiments was not detailed enough and some information about attaching method for skin temperature sensors, activity of the participants before the exposure and some particular issues about how the clothing was worn and how it was fitting was missing. Based on additional discussion with the experimenters and analysis of pictures from the trials, the most probable scenario for the pre-exposure and exposure was selected for simulation. However, it was not possible to quantify the effect of the sensor attaching method in any simulation case. The definition of the input parameters is a crucial step in the simulation process. The real scenarios have to be reflected as close as possible to ensure reliable simulations by the FPCm5.3. model (Jones, 2002).

4.6.2.3 Derivation of input parameters

Exposures were simulated by providing environmental conditions and activity levels as constant values for a given period of time. For outdoor experiments, environmental parameters were provided as time-dependent values changing every minute within the exposure period (exposures 18-20).

The clothing thermal resistance for the simulations were determined by using either direct measurement with thermal manikins or estimated according to ISO 9920 guidelines if information from direct measurements was not available. Due to

reduced information about evaporative clothing resistance in ISO 9920 and some controversy in its determination (Havenith et al., 2008; ISO9920, 2007), clothing evaporative resistance values has been taken from different manikin studies if not similar clothing ensemble data was available in the standard (Wang et al., 2014b, 2011).

Activity levels were estimated based on the available data provided for each exposure as the difference between metabolic rate and the rate of mechanical work accomplished as required by FPCm5.3 model. In cases of low activity levels such as reclining, sitting or standing, metabolic rate was estimated according ISO 8996 guidelines. For higher activity levels, metabolic rate was estimated from measured oxygen consumption if available (ISO8996, 2004) or workloads required by the cycling ergometer were transformed into oxygen consumption applying Hawley & Noakes conversion formula (Hawley and Noakes, 1992). In exposures taking place on a treadmill, the metabolic rate was estimated based on the treadmill slope and walking speed by applying the empirical equation by Givoni and Goldman (Givoni and Goldman, 1971). Mechanical efficiency was considered to be close to zero for level-walking, whereas a maximum value of 0.2 was applied for cycling independently of the intensity (Zatsiorsky and Prilutsky, 2012). Intermediate mechanical efficiency values were assumed for graded-walking as proposed by Margaria (Margaria, 1968).

In this validation study, body temperatures have been used for assessing the performance of the FPCm5.3. model for predicting human thermal responses. For assessing the prediction of the overall thermal responses, core temperatures and mean skin temperatures were investigated. Core temperatures were usually assessed based on rectal temperatures (only for exposures 21, 24 and 25, intestinal

Validation of a thermophysiological model against a dedicated database

measurements were provided for core temperature monitoring) and mean skin temperature data were available for 31 out of the 41 exposures. Mean skin temperatures were mostly provided according to ISO 9886 calculations (8-points for 13 exposures, 14-points for two exposures). For the remaining exposures, non-standard methods based on 15, 7, 6 and 4 points were applied (exposures 10-15, exposure 16, exposures 18-20 and exposures 26-31 respectively). The mean skin temperature predicted by the simulation was calculated using the same body locations and weighing coefficients as used on experimental data. All skin temperature measurements were obtained by contact thermometry sensors attached to skin with clinical tape.

For the assessment of the prediction of local skin temperatures, a single location was selected for representing head-site (forehead), three locations were selected on the trunk (chest, abdomen and scapula) and two locations were assigned on the limbs (thigh and calf). This selection of locations was based on the human data mostly available in the experiments included in the database. Skin temperatures measured at arms, hands and feet were discarded from validation as details regarding the exact position or local insulation values were not carefully controlled or even missing in the experiment description.

Most of the exposures were simulated considering a standard person according to FPCm5.3. This was not the case for exposures 4-9, 17 and 21-25. The simulated person's characteristics were adjusted to trained athletes according to experimenter's description. Table 4.3 describes simulated person's characteristics in these particular exposures.

Multi-sector thermophysiological head simulator

Table 4.3. Individual characteristics for trained athletes profile in exposures 4-9, 17 and 21-25.

Exposure	VO₂max [ml·kg⁻¹·min⁻¹]	Height [cm]	Weight [kg]	Age [years]	Gender [-]	Fat content [%]
4,6 & 8	60	177	75.0	35	male	14
5,7 & 9	52	170	59.0	32	female	23
17	57	181	72.5	27	male	14
21	60	180	75.1	25	male	11
22 & 23	58	180	74.3	23	male	11
24 & 25	55	176	72.8	29	male	15

4.6.2.4 Data analysis

The precision and the accuracy of the FPCm5.3. predictions were statistically assessed by root-mean square deviation (rmsd) and by bias similarly to the study by Psikuta et al. (Psikuta et al., 2013b). Both parameters were calculated for each of the aforementioned body temperatures and for each exposure. The fit of the FPCm5.3. model was considered acceptable when the rmsd was within the standard deviation of the experimental data, typically 0.2°C and 1°C for core and skin temperatures (Psikuta et al., 2012a). The bias should be ideally close to zero to ensure unbiased model prediction. For each measured temperatures, outliers exposures were detected and excluded for the average statistics to avoid bias of single exposures.

Statistical parameters for each exposure are summarized in Table 4.4. Core temperature values from exposures 21, 24 and 25 were not included in overall rmsd and bias calculations as measurements corresponded to telemetric pill registered at intestinal-site. Although this measurement method has become very popular in the last time for estimating core temperature due to good agreement with rectal probes measurements, a consistent bias ranging between 0.15 and 0.2°C has been

reported in some studies (Casa et al., 2007; Easton et al., 2007; Teunissen et al., 2012). When graphically represented, red diamonds with standard deviation bars represented human experimental temperature, blue diamonds corresponded to simulated temperature in the most probable simulated scenario included in

Table 4.4 whereas yellow dots corresponded to simulated temperature after some modification in the input parameters of the most probable scenario as described in the corresponding section. Similarly, when sweat rates were represented, blue line corresponded to the most probable simulated scenario included in Table 4.4 whereas yellow line corresponded to the modified scenario.

4.6.3 Results

The average rmsd and bias values with standard deviations for each of the target variables are depicted in Figure 4.8 for the total of 41 exposures studied in this work. Overall core temperature rmsd and bias values do exclude exposures 21, 24 and 25 as core temperature was exceptionally measured at intestine-site. Additionally, the average standard deviation observed for each body site in our experimental data is shown in Figure 4.8 as well.

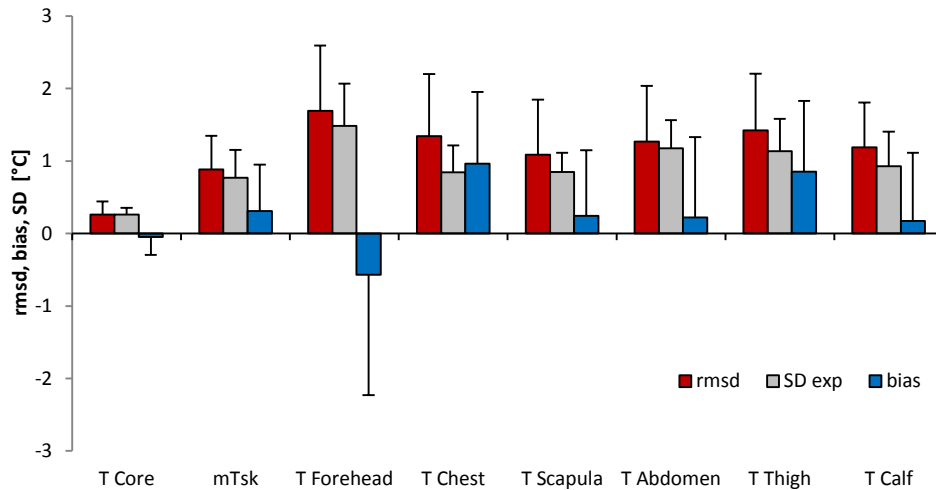


Figure 4.8. Overall values for precision (rmsd), accuracy (bias) and experimental inter-participant standard deviation (SD_{exp}) for a total of 41 simulations carried out with FPCm5.3.

Core and mean skin temperatures were predicted with average rmsd values of $0.26 \pm 0.18^{\circ}\text{C}$ and $0.89 \pm 0.46^{\circ}\text{C}$ respectively, which is comparable to typical standard deviation values observed in our database (0.26°C for core and 0.77°C for mean skin temperature) and typically assumed in human subjects trials (0.20°C for core and 1.00°C for mean skin temperature (Psikuta et al., 2012a)).

Local skin temperatures for all body sites included in this study were predicted on average with rmsd value of $1.33 \pm 0.78^{\circ}\text{C}$. This value was slightly above the average experimental standard deviation found for local skin temperature in the experiments (average $SD_{exp} = 1.07^{\circ}\text{C}$). Global rmsd did not show noticeable differences when averaged separately for trunk or for limbs ($1.22 \pm 0.8^{\circ}\text{C}$ and 1.29

Validation of a thermophysiological model against a dedicated database

$\pm 0.70^{\circ}\text{C}$). Maximum discrepancy in prediction was observed for skin temperatures at forehead and thigh (rmsd of $1.69 \pm 0.90^{\circ}\text{C}$ and $1.42 \pm 0.78^{\circ}\text{C}$, respectively) and minimum at scapula ($1.09 \pm 0.76^{\circ}\text{C}$). However, these average values improved when outliers were put aside. For example, rmsd improved from $1.34 \pm 0.86^{\circ}\text{C}$ to $1.20 \pm 0.67^{\circ}\text{C}$ at chest and from $1.42 \pm 0.78^{\circ}\text{C}$ to $1.19 \pm 0.47^{\circ}\text{C}$ at thigh. Table 4.4 shows corresponding statistical parameters for variables available in each exposure.

Multi-sector thermophysiological head simulator

Table 4.4. Statistical parameters for measured variables in each exposure. Cases marked with * provided core temperature at intestinal-site and are not included in statistical calculations.

Experiment	Exposure	Exposure description	Global		Head		Trunk				Legs				Reference				
			Tre (°C)		mTsk (°C)		T Head (°C)		T Chest (°C)		T Scapula (°C)		T Abdm (°C)			T Thigh (°C)		T Calf (°C)	
			bias	rmsd	bias	rmsd	bias	rmsd	bias	rmsd	bias	rmsd	bias	rmsd		bias	rmsd	bias	rmsd
1	1	Hot exposure with protective clothing	-0.12	0.14	-0.04	0.36	-0.31	0.47	0.15	0.42	-0.56	0.83	0.05	0.62	0.25	0.50	-0.12	0.57	Unpublished data from Anaheim, Empa
	2		-0.18	0.20	-0.01	0.37	-0.48	0.81	0.20	0.47	-0.34	0.60	0.22	0.63	0.38	0.57	-0.09	0.63	
	3		-0.25	0.28	0.05	0.38	-0.25	0.54	-0.23	0.75	-0.37	0.69	-0.57	0.66	0.47	0.79	0.34	0.67	
2	4	Cycling in moderate environments	-0.15	0.18	0.39	0.60	-2.07	2.14	2.16	2.40	0.45	0.65			1.48	1.54	0.55	1.02	Jack, 2010
	5		0.00	0.07	-0.44	0.53	-3.12	3.13	0.48	0.67	-0.55	0.95			0.79	1.03	0.53	0.75	
	6		-0.15	0.18	0.70	0.81	-1.93	2.03	3.06	3.29	1.06	1.13			1.52	1.61	0.53	0.91	
	7		0.06	0.07	-0.28	0.49	-4.16	4.16	0.75	0.85	-0.24	0.94			0.34	0.63	0.81	0.91	
	8		-0.17	0.20	0.72	0.85	-1.74	1.90	3.63	3.90	1.50	1.58			1.28	1.32	0.29	0.88	
3	9	Standing in the cold	-0.03	0.06	-0.07	0.34	-3.37	3.38	1.39	1.49	0.05	0.63			0.53	0.76	1.08	1.23	Makinen et al. 2000 and unpublished data from H. Rintamäki, Finnish Institute of Occupational Health, Oulu, Finland
	10		-0.29	0.30	0.12	0.48	0.47	0.69	-0.01	0.35	-0.04	0.18	0.09	1.07	0.06	0.60	-0.09	0.78	
	11		-0.18	0.19	0.26	0.49	0.99	1.42	0.27	0.35	-0.07	0.40	0.04	1.02	0.30	0.70	-0.17	0.69	
	12		-0.18	0.20	-0.27	0.66	-0.52	1.00	-0.74	1.19	0.19	0.43	-0.69	1.35	-0.79	1.92	-0.50	0.57	
	13		-0.10	0.12	0.50	0.72	2.70	2.95	0.97	1.11	-0.35	0.40	2.53	2.88	0.69	1.28	0.52	0.78	
4	14	Sedentary activity in cold	-0.09	0.10	0.58	0.76	3.01	3.29	1.06	1.17	-0.12	0.17	1.88	2.18	0.81	1.35	0.67	0.89	Wagner and Horvath, 1985
	15		-0.11	0.12	0.03	0.85	1.93	2.54	-0.01	1.51	-0.64	0.68	0.74	1.94	-0.27	1.97	0.29	0.61	
5	16	Cycling in warm environment	-0.27	0.32	0.53	0.74	1.26	1.44	0.44	0.96					1.97	2.04	-1.96	2.15	Bogerd et al. 2010
6	17	Guard duty in the cold	-0.13	0.14	2.11	2.45	1.44	1.67	2.36	2.62	2.54	2.67			2.77	3.13	0.95	1.83	Unpublished from I. Mekjavic, Josef Stefan Institute in Ljubljana, Slovenia
6	18		0.14	0.16	0.64	0.69			0.90	0.94	0.61	0.69			-0.69	0.85	0.72	0.90	

Validation of a thermophysiological model against a dedicated database

Table 4.4. Statistical parameters for measured variables in each exposure. Cases marked with * provided core temperature at intestinal-site and are not included in statistical calculations (continuation).

Experiment	Exposure	Exposure description	Global		Head		Trunk				Legs				Reference				
			Tre (°C)		mTsk (°C)		T Head (°C)		T Chest (°C)		T Scapula (°C)		T Abdm (°C)			T Thigh (°C)		T Calf (°C)	
			bias	rmsd	bias	rmsd	bias	rmsd	bias	rmsd	bias	rmsd	bias	rmsd		bias	rmsd	bias	rmsd
7	19	Hiking in warm conditions	-0.13	0.21	0.42	1.00			1.85	2.03	-1.56	1.82			-0.20	1.29	0.07	1.74	Unpublished from I. Mekjavic, Josef Stefan Institute in Ljubljana, Slovenia
	20		-0.26	0.48	0.44	1.23			1.96	2.55	-1.56	2.31			0.69	1.40	0.36	1.81	
8	21	Walking in the cold	0.08*	0.17*	-1.09	1.24	-2.20	2.28	-0.36	1.19	-1.84	2.31	-2.16	2.42	1.20	1.37	-1.93	2.03	Niedermann et al., 2014
9	22	Walking in hot conditions	-0.19	0.23	0.01	0.43	1.23	1.32	0.73	0.94	1.04	1.57	-0.14	0.57	0.90	1.10	0.59	0.76	Niedermann et al., 2014
	23		-0.01	0.17	1.30	1.42	0.64	0.89	1.37	1.61	0.99	1.63	0.50	0.88	1.52	1.58	0.73	1.00	
10	24	Cycling in moderate environment	0.42*	0.43*	1.04	1.11	-0.76	0.89	1.10	1.29	1.19	1.27	0.67	0.83	2.42	2.88	1.48	1.57	Priego Quesada et al., 2015 and unpublished data from Empa
	25		0.33*	0.34*	1.11	1.21	-0.87	1.11	1.94	2.33	1.44	1.56	-0.06	0.69	2.93	3.35	1.74	1.87	
11	26	Cycling in moderate and warm environment	-0.52	0.83	-0.67	1.13					-0.86	3.82					-2.39	3.36	Den Hartog, 2002
	27		0.46	0.47	0.77	1.17					1.46	2.00					-1.31	1.45	
	28		0.41	0.47	0.64	1.08					1.06	1.39					0.42	0.75	
	29		0.51	0.58	0.35	1.04					1.17	1.75					0.32	1.04	
	30		0.39	0.42	0.53	0.95					0.96	1.02					0.50	1.39	
	31		0.24	0.44	-0.76	1.87					0.14	1.28				0.42	1.29		

Multi-sector thermophysiological head simulator

Table 4.4. Statistical parameters for measured variables in each exposure. Cases marked with * provided core temperature at intestinal-site and are not included in statistical calculations (continuation).

Experiment	Exposure	Exposure description	Global		Head		Trunk				Legs				Reference				
			Tre (°C)		mTsk (°C)		T Head (°C)		T Chest (°C)		T Scapula (°C)		T Abdm (°C)			T Thigh (°C)		T Calf (°C)	
			bias	rmsd	bias	rmsd	bias	rmsd	bias	rmsd	bias	rmsd	bias	rmsd		bias	rmsd	bias	rmsd
12	32	Sedentary cold exposures					-1.52	1.63	0.27	0.52	-0.33	0.49							
	33				-1.74	1.91	-0.07	0.60	-0.28	0.54									
	34				-1.49	1.68	0.63	0.71	0.33	0.59									
	35				-1.09	1.33	-0.14	0.36	0.39	0.55									
	36				-1.05	1.32	1.06	1.13	0.27	0.49									
	37				-1.21	1.60	0.56	0.75	0.16	0.50									
	38				-0.80	1.23	1.02	1.12	0.27	0.56									
	39				-0.34	1.05	1.57	1.63	0.77	0.85									
	40				-0.53	1.24	2.03	2.15	0.84	0.90									
	41				-0.40	1.12	1.42	1.60	0.61	0.69									
		Average	-0.05	0.26	0.31	0.89	-0.57	1.69	0.96	1.34	0.24	1.09	0.22	1.27	0.85	1.42	0.17	1.19	
		SD	0.25	0.18	0.64	0.46	1.66	0.90	0.99	0.86	0.90	0.76	1.11	0.77	0.97	0.78	0.94	0.62	

From Kuklane, National Institute for Working Life, Sweden. Test conditions and limb cooling are described in Kuklane et al. 1998 and Geng et al. 1998.

4.6.4 Discussion

4.6.4.1 Prediction of core temperature

The average core temperature rmsd value of 0.26°C has been found to be comparable to standard deviation observed in our database ($SD_{exp} = 0.26^{\circ}C$). Bias was $-0.05^{\circ}C$, indicating that simulated results were on average just slightly above the experimental data. The lower precision was systematically observed for exposures 26-31 which included one male and one female participant in each test only (see Table 4.2). An over-prediction of the core temperature was particularly observed in exposures with participants exercising at moderate to high activity levels when simulating these exposures with the standard person defined in the FPCm5.3. model. Thus, poor agreement was found for exposure scenarios in which well-trained athletes participated. This effect was already observed by Psikuta et al. (Psikuta et al., 2012a) and related to a possible mismatch in the fitness level of the simulated person which has been recognized to determine the thermal response. Hence, these specific exposures included the adjustment of the individual characteristics of the simulated person according to experimental data, showing a noticeable improvement in the prediction of core temperature. Figure 4.9 shows exemplary prediction for exposure 1 and 4 (see description in

Table 4.2). Individual characteristics of participants in exposure 1 corresponded to a standard person whereas they corresponded to well-trained athletes in exposure 4. Graph for exposure 4 (Figure 4.9 (b)) includes simulation cases for both standard person and adjusted fit simulated person (see Table 4.3). In this case, rmsd improved from $0.39^{\circ}C$ calculated for a standard person to $0.18^{\circ}C$ if simulation considered a well-trained person.

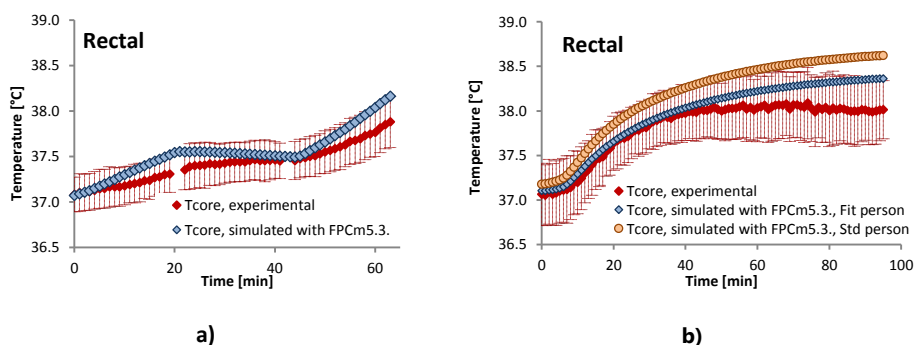


Figure 4.9. Core temperature measured in experiments and predicted using FPCm5.3 model. a) Exposure 1: Standard person walking on a treadmill at 3.3 and 4.4 met, $T_a = 40^\circ\text{C}$, $\text{RH} = 30\%$, protective clothing worn. Rest period between minutes 20 and 40, $T_a = 25^\circ\text{C}$, $\text{RH} = 30\%$. b) Exposure 4: Well-trained athletes cycling at 7.3 met, $T_a = 20^\circ\text{C}$, $\text{RH} = 50\%$, short cycling clothing.

4.6.4.2 Prediction of mean skin temperature

The average rmsd value was $0.89 \pm 0.46^\circ\text{C}$ and average bias value was 0.31°C for mean skin temperature, indicating an average slight under-estimation of mean skin temperature. The upcoming sections analyse in-depth skin temperature prediction at each body-site, giving an insight on results for mean skin temperature.

4.6.4.3 Prediction of forehead temperature

The average forehead rmsd value has been found to be $1.69 \pm 0.90^\circ\text{C}$, being comparable to the average standard deviation of our database ($\text{SD}_{\text{exp}} = 1.48^\circ\text{C}$). The bias was -0.57°C , indicating that on average, skin temperature at forehead is over predicted compared to experimentally measured data.

In cold exposures (i.e. exposures 13-15, see description in Table 4.2) the precision was lower than the average value. In these particular scenarios, participants usually wore any kind of winter headgear. Depending on the head anatomy, headgear

design and wearing style, the forehead area could have been partially dressed for some of the participants. The forehead surface covered by the headgear affected the thermal and evaporative resistances present at this body part and might have even covered the thermal sensor. Consequently, this had a strong influence on skin temperature recordings. Unfortunately, this aspect is not systematically reported by the experimenters and even some inconsistencies between participants wearing style could occur if it was not carefully controlled. This presumption is supported by the highest experimental standard deviation observed at the forehead among all local skin temperatures.

Figure 4.10 shows experimental data compared with simulations considering dressed and undressed forehead for exposure 13. In this exposure the participant wore cold protective clothing and they were standing still in an ambient temperature at 5°C for one hour followed by transition to the ambient temperature of -10°C for another 30 minutes. No detailed information was given about the location of the temperature sensor on the forehead site and if it was covered by clothing or not. Moreover, predicted skin temperature at forehead represented the average of the entire forehead surface area and thus, some inconsistencies with punctual temperature measurements could occur due to temperature heterogeneities if the sensor location is not representative enough. This lack of information of the scenario description might decrease the precision of the simulations. For the global statistical analysis in Table 4.4, the forehead was considered to be undressed in exposure 10-15.

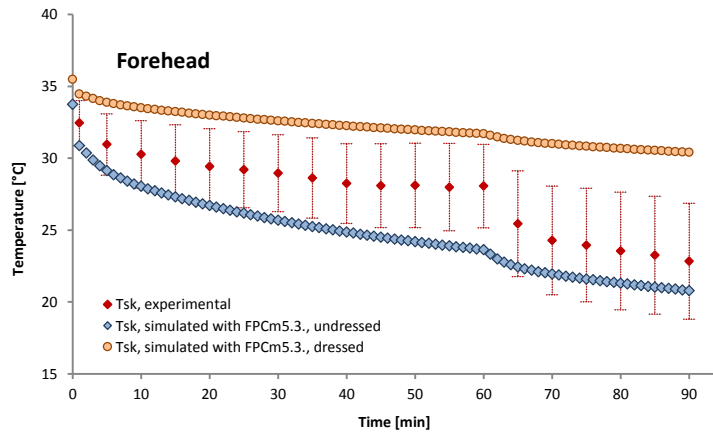


Figure 4.10. Forehead skin temperature in exposure 13: Standard person standing in a cold environment (one hour at 5°C, half an hour at $T_a = -10^\circ\text{C}$, still air), cold protective clothing. Experimental data are presented together with simulations that considered dressed and undressed forehead.

Looking more closely to forehead temperature in some specific exposures in exercising scenarios in which a resting period came just right after an exercise bout, it was observed that experimental skin temperature at forehead decreased during the resting period, whereas simulation predicted stabilization or increase during the subsequent resting period. Some illustrative cases from exposure 1 (resting period between minutes 23 and 43) and exposure 24 (resting period from minute 68 until the end) are presented in Figure 4.11. These exposures are described in Table 4.2. Once the person was resting after the exercise, the FPCm5.3 model assumed a rapid decrease in sweating and concomitant evaporative heat loss. The remaining moisture absorbed by clinical tape or clothing attaching the temperature sensor was possibly underestimated as was the continued evaporative cooling of the skin surface nearby. Nevertheless, the resting periods were usually short and the

aforementioned effects were not noticeably reflected in the rmsd calculated for the entire exposure duration that is shown in Table 4.4.

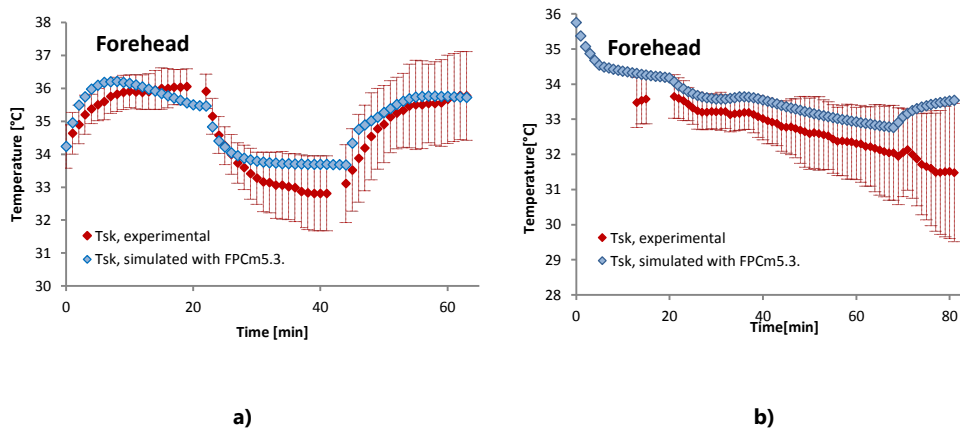


Figure 4.11. Forehead skin temperature in exposure 1 and 24. Exemplary results showing effect of possibly cumulated sweat on forehead surface due to previous exercising conditions. a) Exposure 1: Standard person walking on a treadmill at 3.3 and 4.4 met, $T_a = 40^\circ\text{C}$, $\text{RH} = 30\%$, protective clothing worn. Resting period between minutes 20 and 40, $T_a = 25^\circ\text{C}$, $\text{RH} = 30\%$. b) Exposure 24: Well-trained athletes cycling at 4 met, $T_a = 21.8^\circ\text{C}$, $\text{RH} = 39.4\%$, short cycling clothing. Resting period after 68 min.

4.6.4.4 Prediction of trunk temperatures (chest, abdomen and scapula)

The FPCm5.3. model predicted chest temperature with an average precision of $1.34 \pm 0.86^\circ\text{C}$ which is above the average standard deviation observed in our database ($\text{SD}_{\text{exp}} = 0.85^\circ\text{C}$). Similarly, the FPCm5.3. model predicted abdomen temperature in our database with an average precision of $1.27 \pm 0.77^\circ\text{C}$, whereas the highest precision among prediction of local skin temperatures was found at the scapula ($1.09 \pm 0.76^\circ\text{C}$). At the three body-sites, a bias of 0.96°C , 0.22°C and 0.24°C for chest, abdomen and scapula was observed, respectively. In general, local skin temperature was usually under-predicted at these body sites for the experiments in our database.

Multi-sector thermophysiological head simulator

The FPCm5.3. model predicted skin temperature at chest and abdomen with precision comparable to average standard deviation observed for corresponding temperature measurements when participants wore protective clothing in still air conditions, while walking on a treadmill in a hot scenario (exposures 1-3, see Table 4.2) and when sitting or standing in a calm air cold scenario ($v_{\text{air}} < 0.2 \text{ m}\cdot\text{s}^{-1}$) (exposures 10-11 and 32-37, see

Table 4.2). Figure 4.12 presents exposures 1 and 34 in which participants were wearing protective clothing in hot and cold conditions respectively.

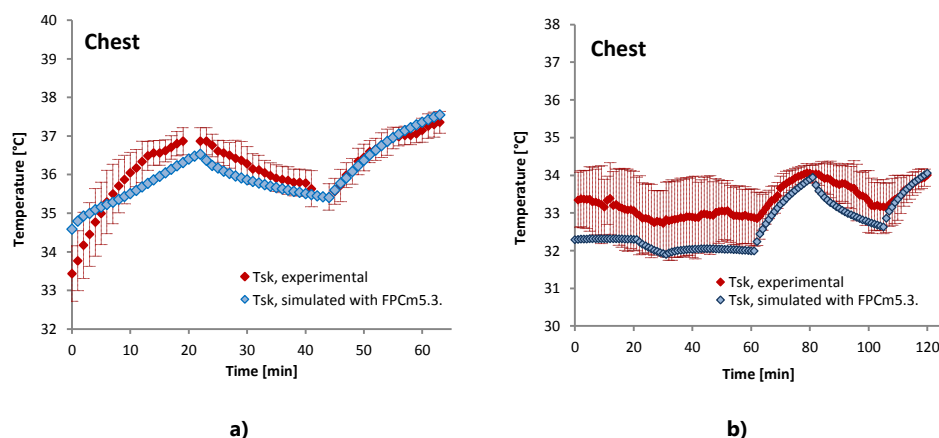


Figure 4.12. Experimental and predicted chest temperature in exposure 1 and 34. a) Exposure 1: Standard person walking on a treadmill at 3.3 and 4.4 met, $T_a = 40^\circ\text{C}$, $\text{RH} = 30\%$, protective clothing worn. Resting period between minutes 20 and 40, $T_a = 25^\circ\text{C}$, $\text{RH} = 30\%$. b) Exposure 34: Standard person exposed in a cold environment at $T_a = -12^\circ\text{C}$, sedentary, protective clothing.

However, when frontal wind was applied to participants in a cold scenario such as exposure 12 (see exposure description in Table 4.2), chest and abdomen temperature were noticeable over-predicted during the last phase in which wind was applied (i.e. partial bias -2.01 and -2.11°C at chest and abdomen for exposure

Validation of a thermophysiological model against a dedicated database

12, see whole-exposure bias in Table 4.4). The most probable reason is a reduction in clothing thermal insulation due to wind compression as previously discussed by as Psikuta et al. (Psikuta et al., 2012a). In this study, clothing thermal insulation for such exposures was measured on a thermal manikin (Psikuta, 2009; Richards and McCullough, 2005). Clothing insulation values were, therefore, provided spatially for trunk, upper and lower limbs. Because the correction for wind compression given in ISO 9920 (ISO9920, 2007) refers to global total insulation values, they could not be applied locally at the chest where the actual wind compression was observed. At the back, no wind induced compression was found. In the study by Psikuta et al. (Psikuta et al., 2012a) it was shown that not applying the wind compression correction at the back improved the correlation of the simulated and measured back skin temperature.

On the other hand, the high rmsd values observed on the chest pointed to some discrepancies when cycling at moderate-to-high metabolic rates in warm conditions (exposures 4, 6, 8, 17, 24 and 25, Table 4.2). It has been hypothesized that cycling posture can result in different heat transfer conditions than standing or sitting. Arms are usually separated from trunk side and slightly put forward and trunk is bent towards thighs. This position can affect the local air speed, local air and radiant temperatures for anterior sectors in chest, abdomen and thighs due to possible stagnant air layer in the cavity of bent body. The reflected radiation from sectors facing the body may be different than in standing position as well. Both effects are complex to estimate and were not included in detail to our database. Based on some single trials in our laboratory we tried to approximate the size of these effects (air speed and air and radiant temperatures in the cavity of bent body) for conditions as in exposure 24 to rate model sensitivity to such phenomena. In this particular case, we reduced the local air speed to be the 50% of the front wind

Multi-sector thermophysiological head simulator

if applied and increased the local air and radiant temperatures by 1°C above ambient air temperature for front body sectors partially facing each other (chest, abdomen and thigh).

Figure 4.13 shows skin temperature and local evaporation rate at chest-site for exposures 17 and 25 simulated in two scenarios: considering similar local environmental conditions than in standing posture and considering the aforementioned modifications of local environmental conditions due to cycling posture. For both scenarios, the experimental skin temperatures were above predicted values. Interestingly, it can be observed in Figure 4.13 that the opposition between trends of experimental and simulated skin temperatures became more evident as long as local skin moisture evaporation rate increased.

Validation of a thermophysiological model against a dedicated database

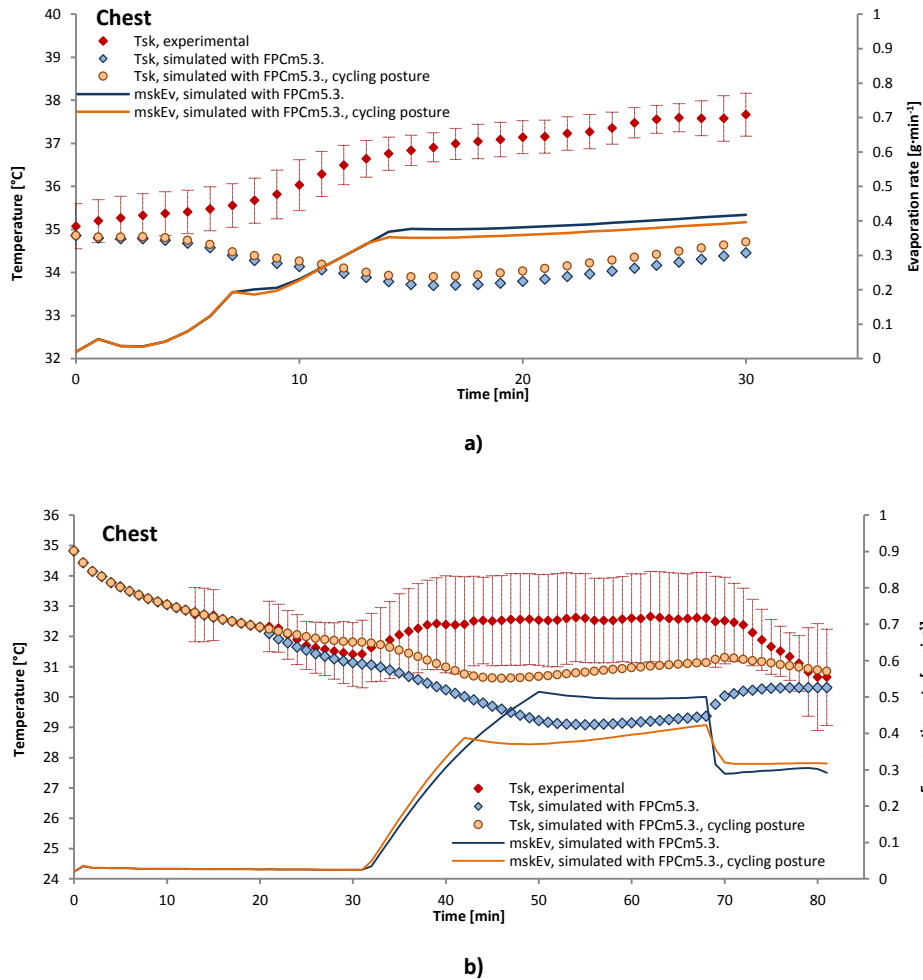


Figure 4.13. Chest temperature and evaporation rate measured in the experiment and predicted by FPCm5.3 in exposure 17 and 25 representing cycling scenario in warm environment. a) Exposure 17: Well-trained athletes cycling at 7.12 met, $T_a = 29^\circ\text{C}$, $\text{RH} = 80\%$. b) Exposure 25: Well-trained athletes cycling at 5.3 met, $T_a = 21.2^\circ\text{C}$, $\text{RH} = 39\% \text{RH}$ (exercise period between minutes 21 and 68).

This general modification increased precision of the FPCm5.3. by mainly reducing local convective and radiative heat exchange at these body sectors as well as evaporation rate. For exposure 17, rmsd at chest improved from 2.62 to 2.44°C and

Multi-sector thermophysiological head simulator

for exposure 25, the improvement was from 2.33 to 1.24°C. The simulations including adjusted air speed, air and radiant temperatures were not considered for statistical analysis, since our experiment provided only a rough estimate of the local environmental condition. No information for a precise adjustment has been reported in the cycling experiments of our database.

Other issues related to cycling posture could occur if moisture accumulates in the stagnant air in the cavity of the bent body. This leads to a reduction in evaporation potential of sweat. Additionally, if the trunk is bent forward, it could facilitate the sweat dripping off and further reduce the effective evaporation rates. In these cases, the exact position of the sensor on the chest surface could be decisive as locations much closer to the arm can have even more reduced cooling conditions than the middle part. Moreover, the attaching method used for skin temperature sensors, particularly different kinds of clinical tapes, can generally impair heat exchange and sweat evaporation at the sensor location, leading to a measured skin temperature value not representative for the body region (Buono and Ulrich, 1998; Psikuta et al., 2013a). Although less experimental data for abdomen part was available in our experiments database, the aforementioned temperature under-prediction in case of scenarios in which participants were cycling at moderate intensities in warm conditions was also observed at this body part (i.e. exposure 24 showed a bias value of 0.67°C).

In cold scenarios and low activity level, the FPCm5.3. model prediction of scapula temperature fitted to the experimental data better than the average obtained for the total 41 exposures (i.e. exposures 10-15 and 32-41, see Table 4.2). For exposures 17 and 22-23 (

Validation of a thermophysiological model against a dedicated database

Table 4.2) presenting the lowest precision when predicting skin temperature of the scapula, it was found an initial mismatch in the starting temperature value being predicted between 1 and 2°C below experimental data. This fact produced an artificially lower precision during the initial phases of the exposures most probably due to an initial increased local vasodilation state of the participants in the experiments. Although thermal initial conditions were adjusted according to the most probable scenario, some poorly described factors can locally alter some skin temperatures i.e. leaning against a seatback right before the exposure.

Precision values for scapula below the average were observed in outdoor scenarios as well, most probably due to changing body orientation along the exposure (exposures 19-20, see description in Table 4.2). Therefore, as exact information on which body region was exposed to the solar radiation or wind applied at each moment were missing, the precision in local skin temperature prediction was reduced. Nevertheless, the agreement in core temperature showed rmsd values within and close to the upper limit of the average precision of core temperature (0.21 and 0.48°C for exposures 19 and 20 respectively).

4.6.4.5 Prediction of leg temperatures (thigh and calf)

Prediction of skin temperature at thigh showed on average the highest deviation (rmsd = $1.42 \pm 0.78^\circ\text{C}$) among local skin temperatures. Average standard deviation in experiments of our database for this variable was found to be 1.13°C . The observed bias was 0.85°C , indicating that thigh skin temperature was on average under-estimated. Skin temperature at calf was predicted with rmsd = $1.19 \pm 0.62^\circ\text{C}$, whereas average standard deviation of experiments was 0.93°C . Similar to thigh, the bias for prediction of temperature at calf was 0.17°C demonstrating a good predicting power of the FPCm5.3 model for this location.

Multi-sector thermophysiological head simulator

Similarly, the over-prediction observed at chest and abdomen in cold exposures in the period in which $5 \text{ m}\cdot\text{s}^{-1}$ frontal wind was applied on whole body (i.e. partial bias -2.01 and -2.11°C at chest and abdomen respectively for exposure 12, see exposure description in Table 4.2 and whole-exposure bias in Table 4.4) was detected for skin temperature at thigh as well (partial bias -3.19°C at thigh for exposure 12, see whole-exposure bias in Table 4.4). At the same time a precision higher than average was observed for prediction of calf temperature. From this finding it can be suggested that wind compression can provide a reduction in clothing insulation at the front parts of the body (i.e. exposures 12 and 15, see Table 4.2) while rear body regions remain unaffected (such as calf showing partial bias of -0.28°C for exposure 12, see whole-exposure bias in Table 4.4). Figure 4.14 shows skin temperature at thigh and calf sites for exposure 12 in which participants underwent one-hour of thermal adaptation in thermoneutral conditions (20°C) followed by half an hour cold exposure (-10°C) by standing and facing the $5 \text{ m}\cdot\text{s}^{-1}$ wind. The simulation is based on measured clothing values and not corrected for wind compression effect.

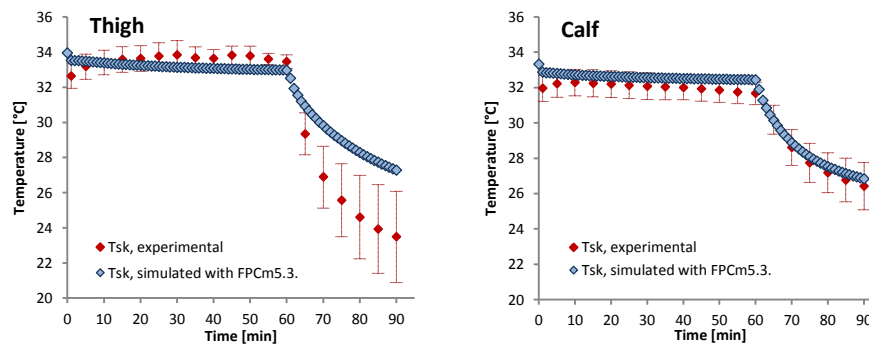
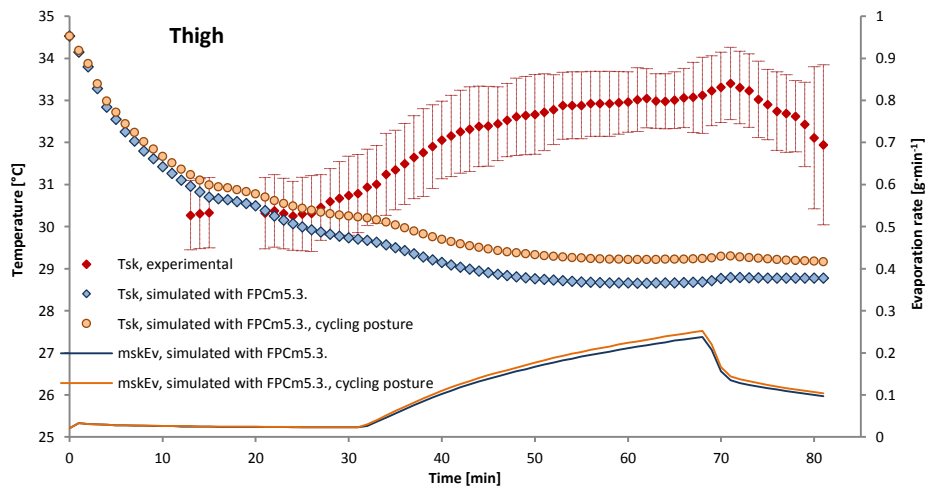


Figure 4.14. Prediction of thigh and calf temperature in exposure 12. Exposure 12: Standard person standing in the cold wearing cold protective clothing (pre-exposure: 60 minutes at $T_a = 20^\circ\text{C}$, still air / main exposure 30 minutes at $T_a = -10^\circ\text{C}$, $5 \text{ m}\cdot\text{s}^{-1}$ frontal wind applied).

Validation of a thermophysiological model against a dedicated database

Precision values below the average for thigh and calf were detected in moderate or warm environment for high activity level during cycling (ranging from 4 up to 7.3 mets). The predicted values for skin temperature showed different trends than measured in participants' skin temperature at the same both body-sites. Similarly to chest and abdomen, the effect of the local environment due to cycling posture on skin temperature of the thigh was explored. Figure 4.15 shows skin temperature and local evaporation rates for thigh and calf in exposure 25 (see Table 4.2). Scenarios with and without correcting the air speed and air and radiant temperatures in the cavity of the bent body due to cycling posture are represented for thigh but no local effect of cycling posture was assumed for calf. Figure 4.15 shows that both simulations, without or with consideration of local environmental effects due to cycling posture, predicted opposite skin temperature evolution if compared with experimental data in for thigh and calf.



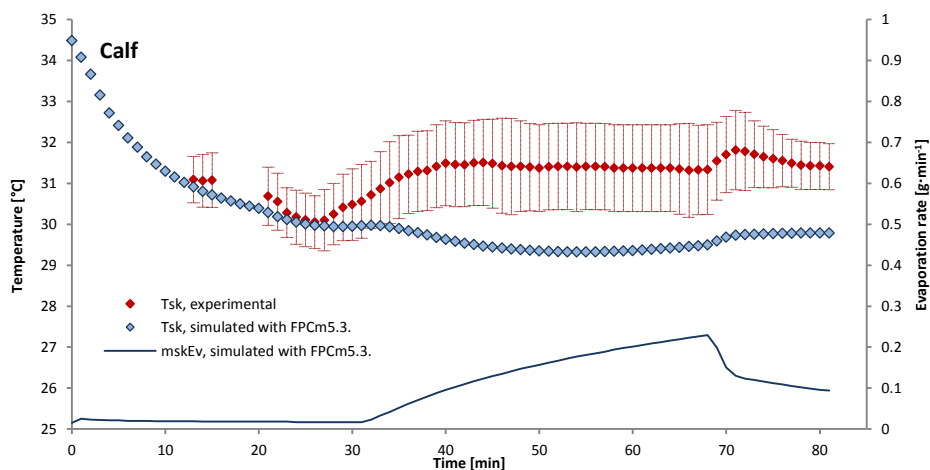


Figure 4.15. Prediction of thigh and calf temperatures in exposure 25. Exposure 25: Well-trained athletes cycling at 5.3 met, $T_a = 21.2^{\circ}\text{C}$, $\text{RH} = 39\%\text{RH}$ (exercise period between minutes 21 and 68).

Interestingly, the observed differences between experimental and predicted values became more apparent at the onset of sweating, and thus, a possible source of this discrepancy could be that either sweat secretion or sweat evaporation efficiency in the experiments might be not as high as assumed by FPCm5.3. No information about sweat secretion rates was available in this experiment for verification. However, when comparing the local sweat rate predictions for the experimental data provided by Smith and Havenith, the model predicted values considerably agreed for body parts of interest (Smith and Havenith, 2011). The sweat evaporation efficiency from the human skin defined as the ratio of the actual evaporative heat loss to evaporative heat loss calculated based on the mass lost can approximate 100% only in ideal cases (all secreted sweat evaporates taking the entire latent energy for evaporation from the body). At this respect, studies on evaporative cooling efficiency of clothing have highlighted a possible over-

Validation of a thermophysiological model against a dedicated database

estimation of the evaporative heat loss for both hot and cold environments if 100% evaporation efficiency is assumed (Havenith et al., 2013; Wang et al., 2013). Wang et al. (Wang et al., 2013) showed in their study on thermal manikins that in warm environments, about 17-49% of the heat needed for evaporation could have been taken from the surrounding air at 35°C instead from the manikin surface for thin tight sport garments (thickness less than 1.2mm). It resulted in reduced evaporation efficiency due to sweat absorbed by clothing and evaporating at a certain distance from skin surface. Therefore, a similar situation could be expected on human skin. The complexity of different exposures might bring the evaporation efficiency below 100%. In reality, some sweat drip-off can eventually occur even for skin wettedness below 1 due to vigorous body movement during exercise. As discussed for chest region, the sensor attachment method could prevent the local evaporative cooling as showed for convective and radiative heat exchange (Buono and Ulrich, 1998; Psikuta et al., 2013a; Tyler, 2011) leading to an unrealistic higher measured temperature. On the other hand, the local skin temperature results from the heat balance at skin level. During exercise, metabolic heat produced in the active muscles is brought to the skin by the blood stream and tissues conduction. The type of activity determines which muscles are active at each body part and hence, skin blood at lower limbs might increase when cycling more than during others activities such as walking or running. However, although the mechanisms responsible for differences in the efficiency of the exercising legs due to the eccentric-concentric contractions ratio have been analyzed (Bijker et al., 2002; Millet et al., 2009), there is still lack of quantitative information for specific modelling of the blood flow in different types of activities.

4.7 CONCLUSION

The major limitation of thermophysiological models is the lack of validation and tools for assessing their performance. In this work, a database containing global and local human physiological data in 41 different exposures has been developed to assist the validation process. Two out of the 41 exposures corresponded to data collected in collaboration with the University of Valencia for investigating the evolution of core and local skin temperatures at different body parts with special focus on the head-site during cycling in moderate environments.

The influence of the thermal contact attaching method used for collecting local skin temperature in those experiments was studied in dry and wet conditions on a hot plate. In dry conditions, the covered sensors provided slightly but significantly higher temperature (+ 0.5°C) compared to non-covered ones and IRT measurements. In wet conditions, absolute differences between sensors and IRT rose up to 3°C and 3.7°C for non-covered and covered sensors, respectively. These differences were presumably due to the thermal insulation and the evaporative resistance induced by the attaching clinical tape. These observations support the assumption that thermal contact sensors attached to the skin can locally interfere in the dry and wet heat exchange process as previously discussed in the literature (Fernandes et al., 2014; Psikuta et al., 2013a; van den Heuvel et al., 2003). However, any extrapolation of these results for equivalent measurements on human skin should be carefully addressed due to the assumed simplifications of the human thermal regulation mechanisms.

Based on the developed database, this work provides an estimation of the precision that can be expected for global and local skin temperature prediction when using

Validation of a thermophysiological model against a dedicated database

the human thermoregulation model FPCm5.3. Furthermore, it gives relevant insights for a more careful interpretation of the model predictions and about experimental procedures limitations. The FPCm5.3. model has shown in general a good precision when predicting core and mean skin temperatures (rmsd of 0.26 and 0.89°C, respectively) in different exposures. This was also the case for exposures including well-trained participants exercising at high activity levels due to the possibility of adjusting the individual factors of the simulated person. It has also mostly shown good precision when predicting local skin temperatures for most body sites in well-controlled exposures (average rmsd for local skin temperatures 1.33°C). Nevertheless, the predictions showed a reduced precision when predicting the forehead skin temperature (rmsd of 1.69°C) most probably due to the lack of input parameter description and at the thigh during exercising exposures (rmsd of 1.42°C). In these exposures, the sweat evaporation represents one of principal heat exchange mechanisms. Therefore, a miscalculation on the local evaporative heat exchange might occur in case the evaporation does not occur with 100% efficiency in reality as it is assumed by the FPCm5.3. model. This results in an under-estimation of the measured skin temperature. As this work focused mainly on the validation of prediction of local skin temperatures, it highlights the need of providing additional local environmental and clothing parameters for an accurate description of heat exchange conditions at the different body parts. This should include a detailed description of how the clothing was exactly worn and how and where the sensors were attached to skin in the simulations.

To get maximum benefit from physiological data obtained from human experiments, the experiments have to be carefully planned and controlled and a representative number of participants has to be recruited. However, not all

Multi-sector thermophysiological head simulator

scenarios can be addressed due to ethical reasons. Scientists and ergonomists can definitely benefit from predictions obtained from physiological models for a more efficient experimental planning or to assist early-stage product development processes. Therefore, this validation study on FPCm5.3. provides highly useful information for a careful and critical interpretation of prediction of local skin temperatures, increasing the applicability of the model, and hence, accelerating the investigation in the field of ergonomics.

Additionally, the FPCm5.3. model was selected to be partially coupled with the head manikin to build up the thermophysiological human head simulator. The next chapter 5 aims at describing the coupled system based on the physiological model by Fiala and the head manikin. This system predicts both global and local body temperatures with special attention to head-site, and therefore, the precision of the model when running alone obtained in this validation study serves as a reference for the upcoming validation of the coupled system, or so-called, thermophysiological human head simulator.

5 DEVELOPMENT AND VALIDATION OF THE COUPLED SYSTEM

5.1 INTRODUCTION

Physiological models include in general a simplified model for clothing that considers only a few static parameters, such as thermal and evaporative resistances and clothing area factor. Nevertheless, the dynamic nature of the thermal exchange occurring within the clothing might significantly affect complex heat and mass transfer phenomena such as moisture absorption-desorption cycles, condensation-evaporation cycles or moisture migration across clothing layers that can contribute to a substantial heat loss depending on fabric properties and location (Fan and Cheng, 2005a; Havenith et al., 2013, 2008; Wissler and Havenith, 2009; Wu and Fan, 2008). Clothing models describing the transient processes in the human skin-clothing-environment system have been introduced in the scientific literature but

Multi-sector thermophysiological head simulator

they have still some simplification in the modelling of decisive aspects such as air gaps or contact area over the body surface (Fan and Cheng, 2005b; Li et al., 2004; Lotens and Havenith, 1994; Lotens et al., 1995). Additionally, they are scarcely combined with advance physiological models (Fiala et al., 1999; Tanabe et al., 2002; Wissler, 1985) or if combined, their performance has not been validated (Lotens, 1993; Stolwijk, 1971).

Thermal devices enable to experimentally quantify the real heat and mass exchange accounting for the given actual gear and surrounding environment. Therefore, the possibility of incorporating the exact heat loss at skin into the physiological model calculations is a highly reliable alternative to the virtual modelling of the transient response and can potentially lead to a more precise prediction of human thermal response (Jones, 2002). For this reason, several attempts to couple thermal manikins (full-body manikins and cylinders) with thermophysiological models have been successfully undertaken and have proved to accurately evaluate the effect of clothing and environmental factors on human thermal response. The first such a tool reported in the literature was developed for the automotive industry at the National Renewable Energy Laboratory (Colorado, USA) (Farrington et al., 2004; Rugh et al., 2004). They developed a new thermal comfort tool by coupling the ADAM manikin with a physiological finite-element model and the Berkeley comfort model (Smith, 1991; Zhang, 2003). The manikin measured heat loss from each body segment and the model calculated the surface temperatures and sweat rates for each segment accordingly. This thermal comfort tool has been applied for several purposes (i.e. evaluation of transient automotive environments, ventilated seats or cooling garments), however some validation against physiological data highlighted some important issues to be further improved such as deviation in core and skin

Development and validation of the coupled system

temperature prediction of 0.6 and 4.2°C, respectively (Farrington et al., 2005; Rugh and Bharathan, 2005; Rugh and Lustbader, 2006).

Using a similar coupling principle, Psikuta et al. introduced the coupling between the physiological model by Fiala with a single-sector manikin representing the whole human body (Fiala et al., 2001, 1999; Psikuta et al., 2008). The iterative feedback loop included set points for mean skin (surface) temperature and mean sweat rate provided by the physiological model and respective heat exchange for this condition measured by the thermal manikin. This feedback signal provided the basis for the calculation of the new set points by the physiological model. They validated the system in a wide range of environmental temperatures (15-37.5°C) obtaining in general good prediction for core and mean skin temperature. Although it was still within the experimental standard deviation of the skin temperature measurements that was used as acceptability criteria, a slightly higher mean skin temperature for the coupled system or so-called thermophysiological human simulator than in the human experiments was observed in warm and hot environments. Additionally, the advantages of the coupled system over the physiological model alone for accounting with the effect of the dynamic heat and mass process through protective clothing were shown (Psikuta, 2009; Psikuta et al., 2013b). The same coupling principle was extended to a multi-sector manikin for representing a more realistic heterogeneous physiological response (Sweating Agile Manikin, SAM, *Empa*, Switzerland). This system provided a good agreement for cold, cool and neutral conditions when operating with homogeneous temperature and heat flux (Bogerd et al., 2010b; Psikuta, 2009), however, some higher discrepancies and erroneous predictions were observed when a heterogeneous temperature distribution was set (Psikuta, 2009).

Multi-sector thermophysiological head simulator

Redortier and Voelcker also applied this coupling principle for coupling the Xu's six segment physiological model with a 38-zone Newton sweating manikin (*Thermetrics*, USA) (Redortier and Voelcker, 2010; Xu and Werner, 1997). However, the heat exchanged measured by the thermal manikin at each zone did not match directly with the heating power in transient conditions. Thus, they calculated the actual skin heat flux based on the heat capacity of the manikin shell. In this way, they observed a good agreement with human experimental data for a transient environmental exposure but at the same time some significant discrepancy in exercising scenarios. They suggested further efforts to increase the accuracy and realism of the sweating, such as including diffusive sweating (Redortier and Voelcker, 2011, 2010).

More recently, Foda and Sirén combined the operation of the multi-segmental Pierce model with the thermal manikin "Therminator" to find an alternative method for calculating the segmental equivalent temperature t_{eq} or so-called equivalent homogeneous temperature (Foda and Sirén, 2011; Nilsson, 2004; Wyon et al., 1989). They showed that operating in this thermoregulatory control mode allowed a better prediction of the subjective mean votes than other traditional control modes, such as constant temperature mode (Foda and Sirén, 2012).

A different coupling approach was applied for Newton sweating manikin (*Thermetrics*, USA) (Burke et al., 2009), where the surface temperatures from the thermal manikin were used as input parameters to the physiological model. Based on this information, the physiological model calculated the metabolic heat flux in the human body and adapted upon the manikin's thermal properties to set the corresponding skin heat loss. The skin heat loss and sweat rates were given as a feedback to be set at the manikin (Curran et al., 2014). This adaptive manikin is

commercially available and some research work on clothing have been already published (Coca et al., 2015; Wang et al., 2014a). Validation studies showed in general good agreement when predicting core and mean skin temperature, whereas discrepancies up to 7°C in some cases were observed for local skin temperatures (Blood and Burke, 2010; Psikuta et al., 2015b).

Specialized body parts thermal manikins, such as thermal foot, hand or head, are an increasing trend as an alternative to full-body manikins for investigating heat transfer properties of human wear goods. Their finer segmentation allows investigating local thermal properties of garments or protective equipment with great detail. However, despite all the advances reported in the literature, the partial coupling of a body part manikin with a mathematical model of the thermal physiology has not been addressed so far. When a multi-segmented body part manikin, such the head manikin is coupled, the main benefit of coupling a physiological model with a thermal manikin, namely the availability of more precise quantification of the heat exchanged when clothing is worn, would be further increased. The protective headgear, such as bicycle helmets, combine different materials and singular elements designs such as vents, visors, soft pads for wearer's comfort and inner liner shape. This results in heterogeneous thermal insulation and evaporative resistance that produce a complex thermal effect on the head especially if wind is present. Full-body manikins usually represent head divided into cranial and face parts and neck is mostly integrated into one them. Therefore, the nine-zone manikin coupled with a physiological model would assess the local effect that the characteristics of the headgear produce on the heat exchanged more specifically, and thus, it would allow a more precise prediction of the head thermal response. In this work, this challenge has been taken and a preliminary validation study has been conducted to better understand how the heat and mass transfer

processes occur at the manikin surface and how the head manikin characterization described in chapter 3 allows the representation of the human head thermal response. This step is of high importance for correctly interpreting the results when the coupled system is applied for clothing evaluation.

5.2 AIM AND OBJECTIVES

The aim of this chapter was twofold. First part of the chapter aimed at describing the coupled system composed of the nine-zone thermal head manikin and the physiological model by Fiala (Fiala and Havenith, 2015; Fiala et al., 2012, 2001, 1999). Second part of the chapter aimed at analysing the effect of the physical presence of the head in the physiological model and at validating the physiological response predicted by the coupled system against human experimental data. For this purpose, four main objectives have been undertaken and described in this chapter:

- Development of an algorithm implemented in Matlab R2013a to allow the communication between the thermal head manikin and the physiological model in a real-time feedback loop.
- Analysis of the consistency of pure virtual simulations calculated by the physiological model under different types of boundary conditions.
- Analysis of the convergence of the coupled simulations towards the pure virtual simulations.
- Validation of the coupled system by comparing predicted global and local thermal responses against human data in ten different exposures representing different environmental temperatures and activity levels as preliminary study before its application for clothing evaluation.

5.3 COUPLING METHOD

5.3.1 Coupling principle

The nine-zone thermal head manikin was coupled with the mathematical model of the human physiology by Fiala (Fiala and Havenith, 2015; Fiala et al., 2012, 2001, 1999) in its most recent version FPCm5.3 (*Ergosim*, Germany). The coupling procedure was based on a real-time feedback loop for controlling the head manikin by the physiological model. In each iteration, the physiological model provided local surface temperature and sweat rates in real-time according to heat loss from the manikin surface measured for each head part (see Figure 5.1). This coupling principle was successfully applied for a single-sector thermal simulator (Psikuta et al., 2008). High accuracy and reliability in heat loss measurements with respect to the magnitude and spatial distribution is necessary to correctly quantify complex effects on heat transfer at skin surface level. In case of a body-part manikin coupled with a thermophysiological model, the possibility of measuring the real heat exchange exists only partially. Because only the head is actually dressed and exposed to the environment, the rest of the body needs to be simulated virtually. Accordingly, the model is challenged to simultaneously accept different types of boundary conditions, such as measured surface heat losses at head-site and virtual environmental conditions for the rest of the body (see description in section 5.4.1). The head manikin is required to closely reproduce the skin temperatures and sweat rates imposed by the physiology model in real-time including its dynamic changes.

In the physiological model by Fiala (Fiala et al., 2001, 1999), the head is divided into seven sectors if left/right symmetry is considered with independent own skin

Multi-sector thermophysiological head simulator

temperature, sweat rate and skin heat flux values. The physiological model considers the basal skin wettedness as a basic property of the skin all over the body surface. Thus, a permanent insensible perspiration rate produces an evaporative heat loss at skin in all conditions. As the head manikin provides dry surface if it is not sweating, the insensible perspiration had to be artificially added to the dry heat loss measured. The combination of segmentations in both the manikin and the model resulted in four independently controlled head parts as described in chapter 3 (section 3.3). The skin temperature and sweat rate of the head sectors as defined in the model are area-weighted averaged to provide surface temperature and water flow set points for each corresponding head manikin zone. Similarly, the heat flux measured at each head manikin zone is area-weighted averaged and corrected by the evaporation of the insensible perspiration rate to provide the skin heat loss for the corresponding head sectors as boundary conditions for each time step included in the simulation.

As in a pure virtual simulation carried out with the physiological model, the boundary conditions for the rest of the body were provided in advance for the complete exposure in terms of environmental parameters, activity level and clothing properties as no instrument was available to directly measure heat loss from the rest of the body. This information is later on timely distributed for each time step.

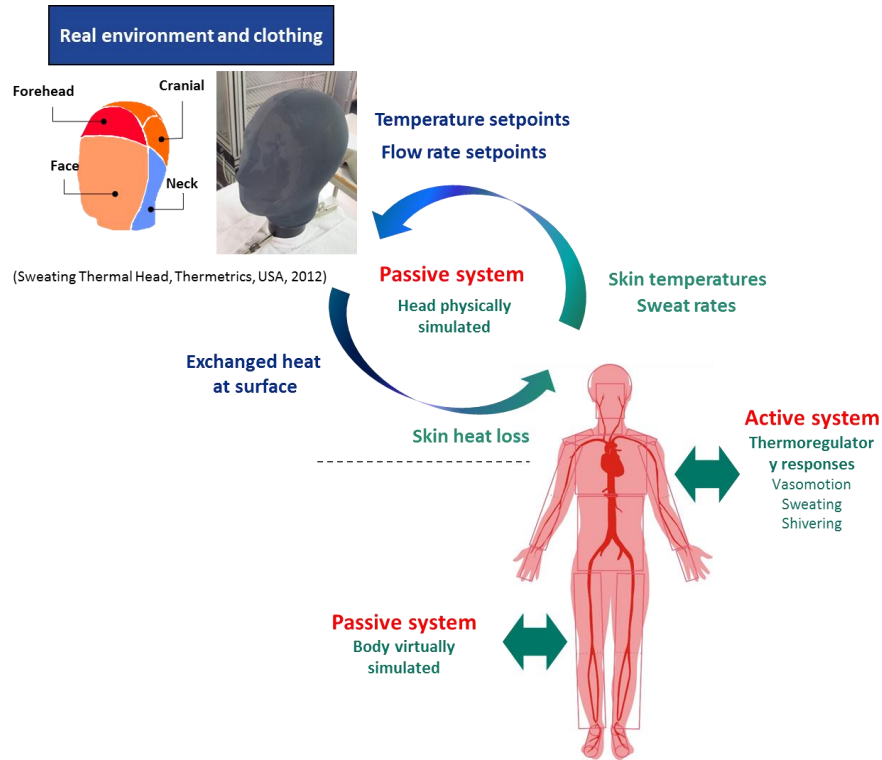


Figure 5.1. Principle of the partial coupling between the head manikin and the physiological model

5.3.2 Operation of the coupled system

For running a coupled simulation, three independent pieces of software operated in the same time such as:

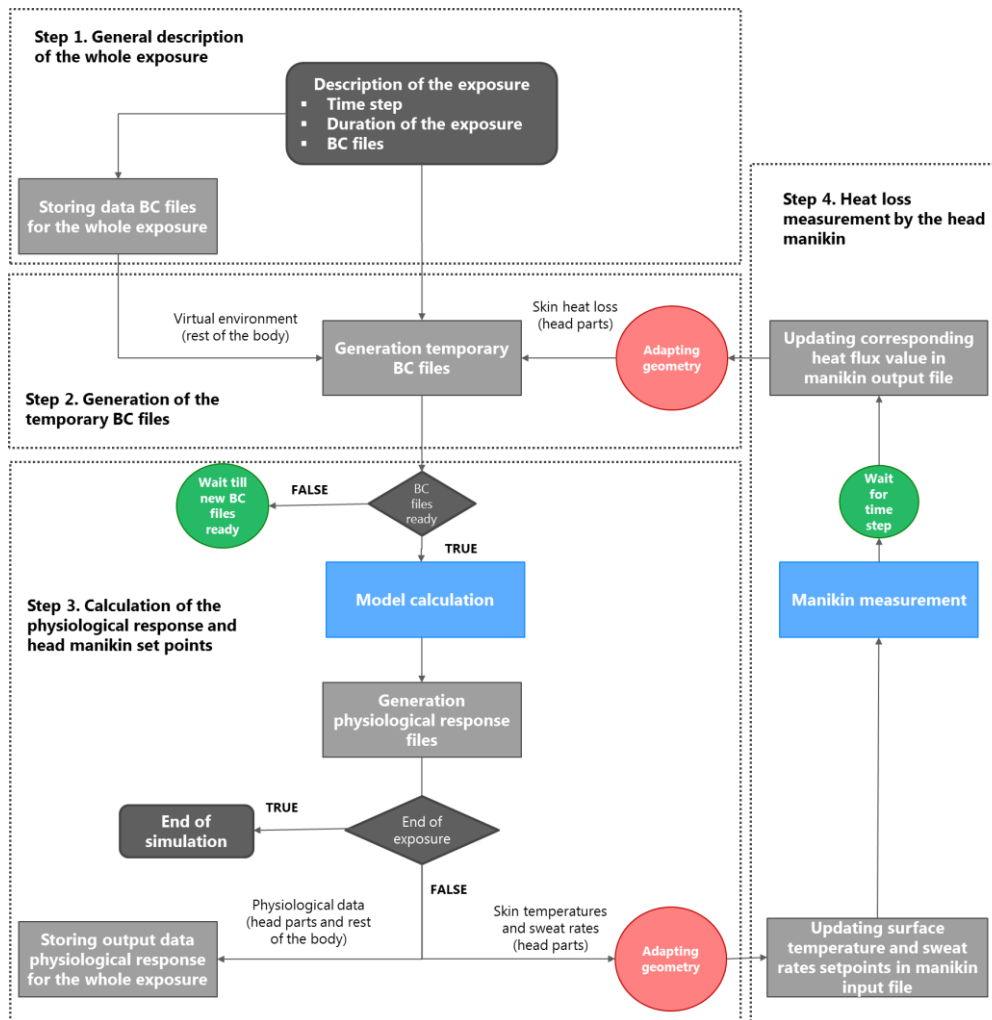
- **ThermaDac8 (Thermetrics, USA)**. It is the head manikin software provided by the manufacturer. This software controls the head manikin operation. In a coupled simulation, the surface temperature and water flow rate set points were read from a dedicated input file and the corresponding

heating power set accordingly in each time step was written in a dedicated output file.

- **FPCm5.3. model (*Ergosim*, Germany).** This software is the most recent version released in 2015 of the physiological model by Fiala (Fiala and Havenith, 2015; Fiala et al., 2012, 2001, 1999). In a coupled simulation, the physiological model calculated the physiological response for each time step based on the skin heat loss measured by the head manikin and the virtual environment set for the rest of the body.
- **Coupling interface.** In a coupled simulation, this interface ensured the correct data exchange between the head manikin and the physiological model by adapting the head segmentation and by time-controlling the simulation. It was implemented in Matlab R2013a.

5.3.3 Description of the coupling interface

To ensure the correct data exchange, an additional communication interface was required. The interface was programmed in Matlab R2013a. It aimed at managing the communication between the thermal head manikin and the physiological model. A coupled simulation consisted of the steps represented in Figure 5.2 and described below. The total time needed for one iteration accounted for the time step defined by the simulation and three additional seconds corresponding to FPCm5.3. calculations.



BC: boundary condition

Figure 5.2. Flow chart for a coupled simulation

- **Step 1. General description of the whole exposure.** The user had to select the files describing the entire exposure, namely every local boundary

conditions files (BC files) demanded by the physiological model. The time step and duration of the exposure were used for time-controlling and termination of the coupled simulation, respectively. The local boundary condition file represented a virtual environment description for the rest of the body for the entire duration of the exposure. It was stored and used for the creation of the temporary boundary conditions files for each individual time step of the exposure.

- **Step 2. Generation of the temporary boundary conditions files.** For each time step, the coupling interface generated one-line temporary boundary conditions files. Two types of files were created: the first type describing a virtual environment for the rest of the body upon the information included in the files initially introduced by the user and second type describing the skin heat loss measured by the head manikin corresponding to forehead, cranial, face and neck parts. For this second type of files, the interface read the individual heat fluxes measured at each zone of the head manikin from the manikin output file, then applied the area-weighted average calculation according to the head segmentation (see chapter 33, section 3.3), added the insensible perspiration heat loss and finally wrote them in individual boundary conditions files for head parts. The different types of boundary condition files are described in detail in the upcoming section 5.4.1.
- **Step 3. Calculation of the physiological response and head manikin set points.** Once the temporary boundary condition files for each body part were ready, the physiological model received the order to calculate the human physiological response corresponding to that time step. The calculated human physiological response at the current time step was

stored in the corresponding output files. If the simulation did not reach the end of the exposure duration according to the duration value pre-defined by the user, the skin temperatures and the sweat rates at head parts were used to calculate the set points for the head manikin. Therefore, the coupling interface used the local skin temperatures and local sweat rates calculated by the physiological model for each head part, then calculated the area-weighted average of the local skin temperature and sweat rate according to head segmentation (see chapter 3, section 3.3) and finally, wrote them in the manikin input file containing the surface temperature and flow rate set points for each part of the head manikin at each time step.

- **Step 4. Heat loss measurement by the head manikin.** Once the corresponding surface temperature and flow rate set points for each head part were set on the manikin, it adjusted the heat fluxes accordingly to reach the new set points. After the time step duration elapsed, the coupling interface read the heat fluxes written in the manikin output file and subsequently generated the temporary boundary conditions files for the head parts for the next time step. Step 2, 3 and 4 were repeated till the end of the exposure was reached.

5.4 CONSISTENCY OF PREDICTIONS FOR DIFFERENT TYPES OF BOUNDARY CONDITIONS

5.4.1 Introduction

The software FPCm5.3. containing the physiological model by Fiala allowed two types of input boundary conditions for the calculation of the physiological response:

- **Boundary conditions type 1 (BC1) or virtual environment.** When introducing boundary conditions type 1 (BC1), the given parameters were air temperature, radiant temperature, relative humidity, air speed, solar radiation (diffuse, direct and sun elevation), activity level and clothing for each body part and time step. The physiological model calculated the heat exchanged by the different mechanisms between the skin and the environment and it accordingly calculated the physiological response.
- **Boundary conditions type 2 (BC2) or skin heat loss.** When introducing boundary conditions type 2 (BC2), the given parameter was the net skin heat loss for each body part and time step. This skin heat loss was used directly by the physiological model for calculating the physiological response. In this case, it was not possible to separate the different types of exchanged heat (sensible or latent). Additionally, the model required the air temperature and humidity to calculate respiratory heat loss.

In a pure virtual simulation with the physiological model, the input boundary conditions are most usually introduced as BC1 (virtual environment). This was the case of simulations presented in chapter 4 (section 4.6). However, when the

physiological model is coupled with a full-body manikin, the boundary condition for every body part had to be introduced as BC2 (skin heat loss) and thus, maximal differences could occur if compared with the case in which boundary conditions were set as BC1 for the entire body. Additionally, when a thermal head manikin is partially coupled with the physiological model, the input boundary conditions at head-site were introduced as BC2, whereas they had to be introduced as BC1 for the rest of the body as in a pure virtual simulation. As the validation of the physiological model presented in chapter 4 was carried out applying BC1 for the entire body and the coupled system presented in this dissertation needed to use BC2 for head parts and BC1 for the rest of the body, it was necessary to compare predictions of the physiological model under different types of boundary conditions to quantify differences due to technical issues in the model.

This section aimed at checking the consistency of the three different possibilities of application of boundary condition of our interest, namely, BC1 for the entire body, BC2 for the entire body and combined BC1/BC2 as foreseen in the coupled head manikin system in a cold-sedentary and in a warm-exercising scenario to elicit the different thermal regulation mechanisms. Comparison between BC1 and BC2 for the entire body provided maximum differences expected between predictions in the most critical case of coupling a full-body manikin. Additionally, comparison between BC1 and combined BC1/BC2 as foreseen the coupled head manikin system provided the reference case for analysing the effect of the physical presence of the head in the prediction of the thermophysiological response.

5.4.2 Method

Two scenarios have been selected for checking the consistency between predictions using the different settings, such as cold-sedentary and warm-exercising exposure conditions (referred to as cold and warm hereafter) (see Table 5.1). For each scenario, a first simulation introducing the virtual environment described in Table 5.1 for the entire body, namely, boundary conditions type 1 was carried out (case BC1). The local skin heat loss obtained as an output for each body part from this first simulation was used as boundary conditions type 2 for a second simulation (case BC2). Finally, a third simulation was done combining the application of BC2 for head parts and BC1 for the rest of the body (case BC1/BC2). Predictions of the three model applications were graphically compared. Additionally, the discrepancy between the cases BC1, BC2 and BC1/BC2, respectively, was statistically assessed by root-mean square deviation (rmsd) and by bias similarly to the study by Psikuta et al. (Psikuta et al., 2013b). The consistency between the different modes of applying the physiology model was considered complete when the rmsd and the bias approached to zero.

Table 5.1. Description of the boundary conditions type 1 (BC1) or virtual environment for the cold and the warm scenario.

Virtual exposure	Air temperature [°C]	Radiant temperature [°C]	Relative humidity [%]	Air speed [m·s ⁻¹]	Activity [met]	Duration [min]	Type of clothing
Cold	15	15	40	0.06	0.8	120	nude
Warm	30	30		0.1	6		

5.4.3 Results

5.4.3.1 Cold scenario

The thermoregulation actions in the cold conditions, namely, regulation of skin blood flow and shivering, were predicted identically in the three types of the model applications. In this cold scenario where the simulated person stayed sedentary, no sweating occurred. However, the physiological model defined the basal skin wettedness as a basic property of the human skin. Therefore, some evaporative heat loss occurred with BC1 (48.3 g of sweat evaporated in the two hours). This was not the case with BC2. For the combined case BC1/BC2, a total of 43.8 g evaporated from the total skin surface except from the head. Nevertheless, the total skin heat loss remained the same for the three application cases as it was pre-defined.

Figure 5.3 shows the prediction of the overall thermal response represented by the rectal and mean skin temperature in the cold scenario and Figure 5.4 shows the local skin temperature at forehead as an illustrative case. For predicted rectal temperature almost no differences were observed. However, slightly lower mean skin and local skin temperature at forehead for BC1 simulations were found compared to simulation with BC2 (differences below 0.1°C).

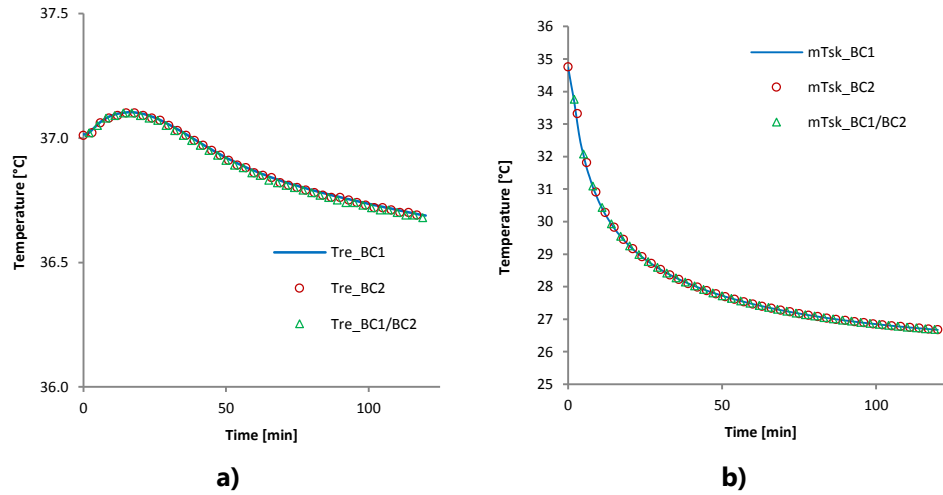


Figure 5.3. Comparison of prediction of overall thermal response between the three model applications in the cold scenario, a) rectal temperature and b) mean skin temperature. BC1 (boundary conditions type 1 entire body), BC2 (boundary conditions type 2 entire body) and BC1/BC2 (combined boundary conditions as in the coupled head system).

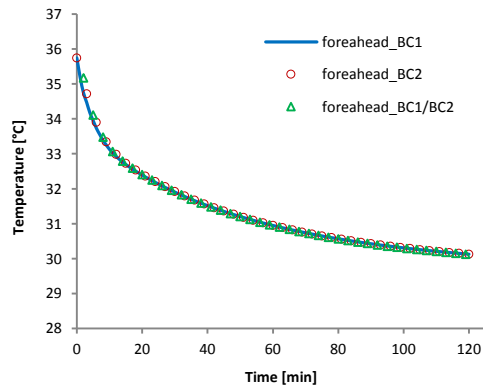


Figure 5.4. Comparison of local skin temperature at forehead between the three model applications in the cold scenario. BC1 (boundary conditions type 1 entire body), BC2 (boundary conditions type 2 entire body) and BC1/BC2 (combined boundary conditions as in the coupled head system).

Development and validation of the coupled system

Table 5.2 shows bias and rmsd values for rectal and mean skin temperatures and local skin temperatures at head-site calculated between the case BC1 and the case with maximum discrepancy expected BC2. Same statistical values were found for comparison between the case BC1 and BC1/BC2 except for the mean skin temperature. The mean skin temperature rmsd was 0.08°C when the entire body applied BC2 and just 0.01°C when BC2 where applied just on the head parts.

Table 5.2. Bias and rmsd for the comparison of physiological model predictions in the cold scenario calculated between cases BC1 (boundary conditions type 1 entire body) and BC2 (boundary conditions type 2 entire body).

	Temperature	
	bias [°C]	rmsd [°C]
Rectal	0.01	0.01
Mean skin	-0.02	0.08
Forehead	-0.03	0.08
Cranial	-0.03	0.07
Face	0.00	0.07
Neck	-0.01	0.07

5.4.3.2 Warm scenario

As pre-defined, the total skin heat loss from body surface was the same for the three simulation cases, however, in case BC1, 13% was sensible and 87% was latent heat loss, whereas in case BC2, 100% of the heat loss was assumed to be sensible. In the case combining boundary conditions types (BC1/BC2) the distribution was in-between both previous cases, 20% was sensible and 80% was latent heat loss.

Multi-sector thermophysiological head simulator

Figure 5.5 shows the prediction of the overall thermal response represented by the rectal and mean skin temperatures and total sweat rate in the warm scenario. Some slight but consistent differences seemed to appear between the simulations carried out for predicted overall body temperatures, especially when comparing between cases BC1 and BC2. The differences became more apparent in case of the thermoregulation actions. The total amount of secreted sweat cumulated for two hours was 274 g more and the regulation of the skin blood flow with regards to the basal state was 26 percentage points higher at the end of the exposure in case BC2 compared to case BC1 (see Table 5.3). Differences observed in the same variables were much lower between BC1 and BC1/BC2 (see Table 5.4).

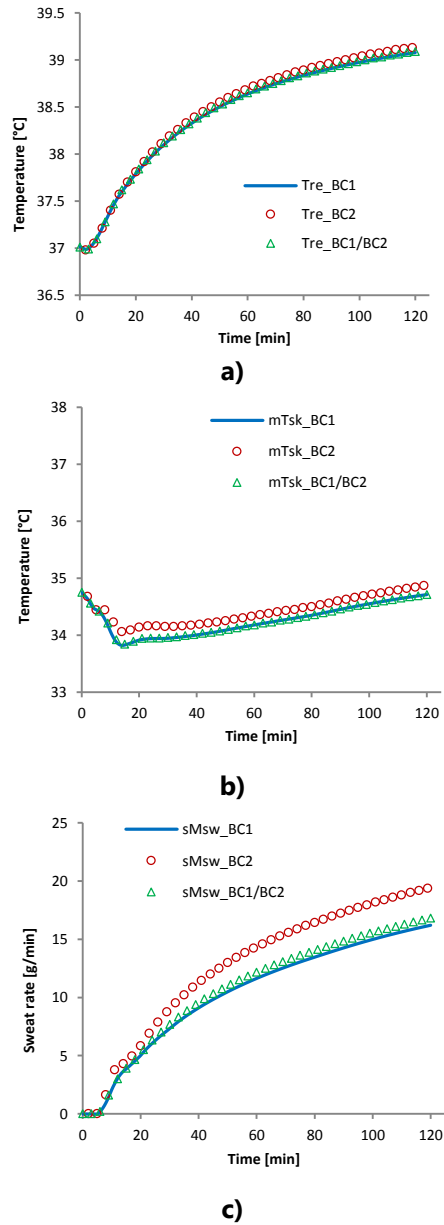


Figure 5.5. Comparison of prediction of overall thermal response between the three model applications in a warm scenario, a) rectal temperature, b) mean skin temperature and c) total sweat rate. BC1 (boundary conditions type 1 entire body), BC2 (boundary conditions type 2 entire body) and BC1/BC2 (combined boundary conditions as in the coupled head system).

Slightly higher local skin temperature was observed when body parts had BC2 compared to BC1. Figure 5.6 presents this effect for the local skin temperature at forehead as an illustrative case. In this case, the local skin temperature was on average 0.1°C lower and the secreted sweat cumulated for the entire two hours exposure duration in the forehead was 2.64 g more in case BC2 than for case BC1 (see Table 5.3). Smaller differences were observed for the local skin temperatures at head-site in case of comparing cases BC1 and BC1/BC2 (see Table 5.4).

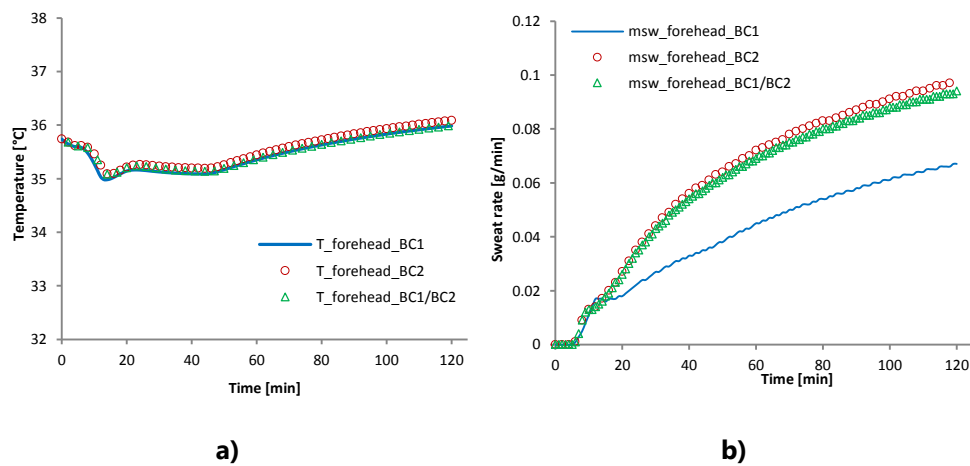


Figure 5.6. Comparison of prediction of local thermal response at forehead between the three model applications in a warm scenario, a) local skin temperature at forehead and b) local sweat rate at forehead. BC1 (boundary conditions type 1 entire body), BC2 (boundary conditions type 2 entire body) and BC1/BC2 (combined boundary conditions as in the coupled head system).

Development and validation of the coupled system

Table 5.3. Bias and rmsd for the comparison of physiological model predictions for the warm scenario calculated between cases BC1 (boundary conditions type 1 entire body) and BC2 (boundary conditions type 2 entire body).

	Temperature		Sweat rate	
	bias [°C]	rmsd [°C]	bias [g·min ⁻¹]	rmsd [g·min ⁻¹]
Rectal	-0.04	0.05	--	--
Mean skin	-0.16	0.17	-2.26	2.46
Forehead	-0.09	0.10	-0.02	0.02
Cranial	-0.09	0.10	-0.22	0.25
Face	-0.09	0.10	-0.05	0.05
Neck	-0.1	0.11	-0.05	0.06

Table 5.4. Bias and rmsd for the comparison of physiological model predictions for the warm scenario calculated between cases BC1 (boundary conditions type 1 entire body) and BC1/BC2 (combined boundary conditions as in the coupled head system).

	Temperature		Sweat rate	
	bias [°C]	rmsd [°C]	bias [g·min ⁻¹]	rmsd [g·min ⁻¹]
Rectal	-0.01	0.01	--	--
Mean skin	-0.01	0.01	-0.42	0.47
Forehead	-0.03	0.05	-0.02	0.02
Cranial	-0.03	0.05	-0.20	0.22
Face	-0.03	0.05	-0.04	0.05
Neck	-0.03	0.05	-0.05	0.05

5.4.4 Discussion

The prediction of the main thermoregulation actions in a cold scenario was the same for simulation cases with BC1 and BC2. However, the calculation of the evaporative heat loss due to basal skin wettedness defined in the model was not allowed in BC2. Almost no differences were observed in the prediction of rectal

temperature but some slight differences below 0.1°C appeared in the mean skin and local skin temperatures when comparing the case BC1 with the case BC2, for which the maximum differences were expected (rmsd of mean skin temperatures was 0.08°C). In the case combining different types of boundary conditions, the aforementioned evaporative heat loss was allowed for the parts of the body with BC1 (entire body except head). The differences between BC1 and BC1/BC2 were reduced for the mean skin temperature (rmsd = 0.01°C) but similarly to BC2, difference remained with rmsd = 0.08°C for local skin temperatures at forehead. These small differences could be, however, merely attributed to the precision of the calculation.

Simulation applying BC1 or BC2 revealed differences in the prediction of the main thermoregulation actions in the warm scenario. In this warm scenario, higher discrepancies occurred in the prediction of the overall and local amount of secreted sweat that was considerably higher in case of BC2 than in case of BC1 (274 and 2.64 g more sweat cumulated in BC2 after two-hour exposure for whole body skin and forehead skin surface, respectively). The skin heat loss used to represent BC2 was attributed fully to the dry heat loss while 87% of the total skin heat loss resulted from the sweat evaporation in simulation with BC1. The physiological model calculated the sweat rate based on the response of the central nervous system, which was then corrected locally for the hidromeiosis effect related to the skin wettedness. When the BC2 were applied in the model, the information on the skin wettedness was not available for the algorithm correcting the local sweat rates since the entire information on the boundary conditions was lumped to a single value of the resultant heat flux at the skin. The measurement of the total liquid water accumulation on the manikin surface could be theoretically possible using the change of manikin weight as an indicator. Nonetheless, such measurement

would give only overall value for all body parts and would not be possible as soon as any clothing or protective equipment was worn. In such a case, the location of the moisture accumulation would be not known and the correction for skin wettedness turns out to be impossible. Therefore, generally, discrepancies due to using the physiological model with different type of boundary conditions can be expected for exposures with sweating (in warm or exercising conditions). In case of coupling the physiological model with a thermal manikin, the coupled simulations of a full-body manikin would apply BC2 to all body parts and the highest discrepancy with regards to the reference case BC1 would be expected.

In our coupled system, the physiological model was used partially coupled and thus, BC2 were applied just for body parts at head-site, whereas BC1 were used for the rest of the body, meaning that BC2 were imposed just in 7% of the body skin surface. The comparison of predictions between BC1 and BC1/BC2 showed reduced differences in the overall thermal response (rectal, mean skin temperature and total sweat rate). Head parts for which BC2 was applied, showed the same differences in local skin temperature as in BC2 in the cold scenario (rmsd values below 0.1°C). However, in the warm scenario, discrepancy for local skin temperatures at head-site in case BC1/BC2 was lower compared to case BC2 most probably due to the contribution of a better agreement of the rest of the body set with BC1, whereas the discrepancy remained similar for the local sweat rate at head-site.

5.5 ANALYSIS OF THE CONVERGENCE OF THE COUPLED SYSTEM TOWARDS PURE SIMULATIONS

5.5.1 Introduction

The previous section 5.4 has pointed to some differences already due to using the physiological model with different types of boundary conditions. Apart from that, when the physiological model is used coupled with the head manikin, the real heat and mass transfer processes could occur differently compared to the virtually described processes in the model. The first step of the validation of the coupled system consisted of testing the convergence of the coupled system towards the pure simulations to better understand the heat and mass transfer processes at the head manikin surface. The aim of this work was to compare the prediction of the coupled system with the prediction corresponding to pure virtual simulations for global and local physiological variables at head-site in different scenarios covering cold, thermoneutral and warm exposures that elicited different thermoregulation mechanisms.

5.5.2 Methods

The predictions of the physiological model running alone and the prediction of the coupled system have been compared in three exposures that represent different physiological states such as cold-sedentary, thermoneutral and warm-exercising (cold, thermoneutral and warm hereafter)(Table 5.5). Thermoneutral exposure was selected according to description in the physiological model by Fiala (Fiala et al., 1999).

Table 5.5. Description of boundary conditions in the exposures selected for the virtual and coupled simulations.

Virtual exposure	Air temperature [°C]	Radiant temperature [°C]	Relative humidity [%]	Air speed [m·s ⁻¹]	Activity [met]	Duration [min]	Type of clothing
Cold	15	15		0.06	0.8		
Thermoneutral	30	30	40	0.1	0.8	120	nude
Warm	30	30		0.1	6		

First, each exposure was simulated with the FPCm5.3. model by entering boundary conditions BC1 as environmental parameters, clothing and activity for all body parts. This simulation was regarded as a reference case (Table 5.5). Secondly, each exposure was simulated by the coupled system. In this case, the environmental conditions described in Table 5.5 were set in the climatic chamber and the coupled system was run for the given activity level. The boundary conditions for the forehead, cranial, face and neck parts corresponded to the heat fluxes measured by the head manikin and were introduced to the model as skin heat loss for each head part (BC2), whereas the rest of the body was virtually exposed to BC1 as described in Table 5.5. The head manikin was placed in the middle of the climatic chamber and dressed with the pre-equipped tight-fitting elastic fabric. The environmental conditions were also externally monitored with a thermal conditions monitoring system (ThermCondSys 5500, *Sensors Electronic*, Gliwice, Poland) that was placed 80 cm in front of the head manikin. Actual thermal conditions were assumed to represent the virtual environment if air temperature was within $\pm 0.5^{\circ}\text{C}$, relative humidity within $\pm 5\%$ and air speed within $\pm 0.05 \text{ m}\cdot\text{s}^{-1}$. Before the simulation of each exposure, the head manikin was conditioned by intense sweating till water

flew profusely and removed the air held in sweating system and the corresponding initial surface temperature of the manikin was set for 30 minutes.

The study of the convergence of the coupled simulations towards to the pure virtual simulations was based on the comparison of global and local predicted variables, namely, body temperatures, skin heat loss and sweat rates for each exposure. The discrepancy between the pure virtual and coupled system simulations was statistically assessed by root-mean square deviation (rmsd) and by bias, similarly to the study by Psikuta et al. (Psikuta et al., 2013b). For assessing the differences between the pure virtual and the coupled simulations, the rmsd value for body temperatures was compared to the absolute reference value of 0.2°C proposed as the accuracy for measurement of the surface temperature in manikin standards (ISO15831, 2004). No absolute reference value was assumed for skin heat loss and sweat rate, however, relative assessment was done based on the corresponding difference observed in the surface temperature. The effect of the physical presence of the head in the predictions of the physiological model should be negligible if rmsd and bias are close to values obtained in the comparison of cases BC1 and BC1/BC2 presented in section 5.4.

5.5.3 Results

5.5.3.1 Cold exposure

The actual values of the environmental parameters measured in the climatic chamber were $15.00 \pm 0.02^\circ\text{C}$, $41.90 \pm 0.28\%$ and $0.06 \pm 0.02 \text{ m}\cdot\text{s}^{-1}$.

Table 5.6 shows the bias and rmsd values out of the comparison of the predictions of the pure virtual model and the coupled system in the cold exposure with

sedentary activity. It depicts these values for body temperatures (rectal, mean skin temperatures and local skin temperature at head parts) and skin heat loss (mean skin and local skin heat loss at head parts).

Table 5.6. Bias and rmsd for the comparison of predictions of pure virtual model and the coupled system simulations for body temperatures and skin heat loss in the cold exposure.

	Temperature		Skin heat loss	
	bias [°C]	rmsd [°C]	bias [W·m ⁻²]	rmsd [W·m ⁻²]
Rectal	0.01	0.01	--	--
Mean skin	0.00	0.05	-0.21	1.33
Forehead	-0.01	0.27	-1.24	17.84
Cranial	0.17	0.31	-6.01	16.26
Face	-0.29	0.43	2.84	18.78
Neck	0.08	0.39	-2.29	18.92

5.5.3.2 Thermoneutral exposure

The actual values of the environmental parameters measured in the climatic chamber were $30.10 \pm 0.02^{\circ}\text{C}$, $42.51 \pm 0.25\%$ and $0.12 \pm 0.02 \text{ m}\cdot\text{s}^{-1}$.

Table 5.7 shows the bias and rmsd values for the comparison of the predictions of the pure virtual model and the coupled system in a thermoneutral exposure, such as body temperatures (rectal, mean skin temperatures and local skin temperature at head parts) and skin heat loss (mean skin and local skin heat loss at head parts).

Multi-sector thermophysiological head simulator

Table 5.7. Bias and rmsd for the comparison of predictions of the pure virtual model and the coupled system simulations for body temperatures and skin heat loss in the thermoneutral exposure.

	Temperature		Skin heat loss	
	bias [°C]	rmsd [°C]	bias [W·m ⁻²]	rmsd [W·m ⁻²]
Rectal	0.01	0.01	--	--
Mean skin	0.02	0.02	-0.24	0.28
Forehead	0.06	0.06	-2.81	3.91
Cranial	0.03	0.03	-1.47	2.12
Face	0.14	0.15	-8.35	8.81
Neck	0.10	0.10	-3.96	4.46

5.5.3.3 Warm exposure

The actual values of the environmental parameters measured in the climatic chamber were $29.90 \pm 0.02^{\circ}\text{C}$, $42.68 \pm 0.37\%$ and $0.14 \pm 0.02 \text{ m}\cdot\text{s}^{-1}$.

Table 5.8 shows the bias and rmsd values for the comparison of the predictions of the pure virtual model and the coupled system in a warm scenario with high activity level. It depicts these values for body temperatures (rectal, mean skin temperatures and local skin temperature at head parts), skin heat loss (mean skin and local skin heat loss at head parts) and sweat rates (total skin and local sweat rates at head parts).

Development and validation of the coupled system

Table 5.8. Bias and rmsd for the comparison of predictions of the pure virtual model and the coupled system simulations for body temperatures, skin heat loss and sweat rates in the warm exposure.

	Temperature		Skin heat loss		Sweat rate	
	bias [°C]	rmsd [°C]	bias [W·m ⁻²]	rmsd [W·m ⁻²]	bias [g·min ⁻¹]	rmsd [g·min ⁻¹]
Rectal	-0.02	0.02	--	--	--	--
Mean skin	-0.05	0.08	-0.26	1.69	-0.51	0.55
Forehead	-0.15	0.35	4.97	29.55	-0.02	0.02
Cranial	-0.55	0.59	45.46	48.01	-0.23	0.25
Face	0.03	0.43	-14.03	51.41	-0.04	0.05
Neck	0.07	0.49	-20.39	49.26	-0.05	0.05

5.5.4 Discussion

This section has highlighted the differences in the performance of the physiological model when parts of the passive system, namely forehead, cranial, face and neck parts were physically represented by the head manikin in different simulated exposures. As shown in section 5.4, the convergence between coupled simulations and pure virtual simulations is constrained by the agreement observed between cases BC1 and BC1/BC2.

In the cold scenario, the observed discrepancy between the coupled simulation and the pure virtual simulation was higher than the discrepancy observed due to the application of different types of boundary conditions described in section 5.4 for local skin temperatures at head-site (i.e. rmsd for forehead increased from 0.08°C up to 0.27°C). However, it was still within the acceptability range of $\pm 1^\circ\text{C}$ corresponding to the observed standard deviation in human experiments (Psikuta et al., 2012a). The observed discrepancy in skin temperature prediction at head-site due to coupling the physiological model with the head manikin was more apparent

at the beginning of the exposure and most probably due to discrepancy in the initial skin heat loss as illustrated for forehead in Figure 5.7. It should be noticed that all simulations discussed in section 5.4 have been included in the figure for a better estimation of the size of the discrepancy due to having head physically represented. The simulated exposure assumed the person to start from thermoneutral conditions (sedentary nude person in air temperature of 30°C and relative humidity of 40% (Fiala et al., 1999)). Although the manikin surface temperature was conditioned at the skin temperature in thermoneutral conditions, the heat flux had to be higher during the conditioning time to compensate for an actual colder environment at 15°C for every head part (i.e. 190 instead of 54.3 W·m⁻² for forehead), and thus, high discrepancy was observed during the initial phase of the exposure. With this respect, the same coupled simulation was carried out after adjusting the PI control settings for a faster response as proposed in chapter 3 (section 3.8). However, the variation in the heat flux measurement observed in this particular case prevented from having a better agreement between the pure virtual and the coupled simulation. A possible explanation could be a definition of the PI control different than the one assumed for the manual tuning in section 3.8. As the adjustment was done for a fix temperature step change of 3°C, the actual PI control with the proposed values might provide an increased variation due to the temperature set point being constantly updated every minute along the exposure.

After the skin heat loss became closer, part of the discrepancy observed in the heat flux and consequently in skin temperature at the different head parts could be due to slight uncontrolled lateral heat loss drifting from forehead and cranial parts towards face and neck parts as their temperature was below the forehead and cranial skin temperatures by 3°C on average along this cold exposure. In general, in a cold and sedentary scenario if the face is not insulated, forehead is usually

warmer than face part and due to some uncontrolled lateral heat loss, the coupled system might slightly underpredict the skin temperature at forehead due to temperature gradients with face as shown in chapter 3 (section 3.5).

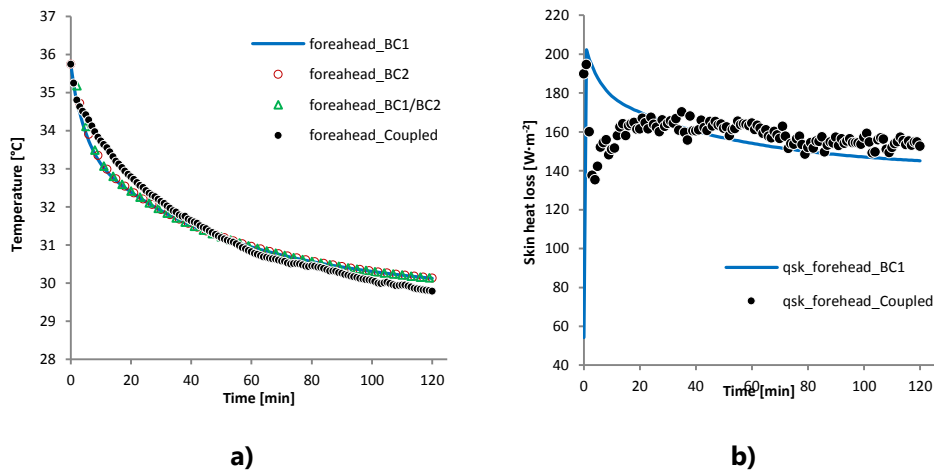


Figure 5.7. Evolution of the forehead skin temperature and skin heat loss in the cold exposure for pure virtual and coupled simulations. Pure virtual simulation is presented calculated for different types of boundary conditions for a better estimation of the size of the discrepancy just due to having head physically represented. BC1 (boundary conditions type 1 entire body), BC2 (boundary conditions type 2 entire body) and BC1/BC2 (combined boundary conditions as in the coupled head system).

In general, less discrepancy was observed for the thermoneutral scenario as the pre-conditioning in thermoneutral state occurred at 30°C as defined in the physiological model (Fiala et al., 1999). Thus, no initial mismatch in skin heat loss at head parts and minor temperature gradients between head parts occurred. In thermoneutral scenario, the rmsd values observed for the face and neck were slightly higher than those observed for the forehead and cranial parts (Table 5.6 and Table 5.7). Since the combined heat transfer coefficients observed at the

Multi-sector thermophysiological head simulator

manikin surface revealed slightly higher values by 10.7 and 17.2% at the manikin than assumed by the physiological model for the face and neck, respectively, this could be the reason for the coupled simulations having slightly higher heat loss than the pure virtual one (see chapter 3, section 3.4).

A higher discrepancy was observed in the warm exposure simulation than in the cold and thermoneutral scenario. Figure 5.8 shows surface temperature, skin heat loss and sweat rate for the cranial and neck parts to illustrate the convergence along the whole warm exposure. Pure virtual simulations were calculated by applying different types of boundary conditions discussed in section 5.4 to illustrate the size of the discrepancy due to coupling the head manikin compared to the consistency due to using either BC1 or BC2. In general, differences increased with regards to differences observed due to applying different types of boundary conditions. Increase in the discrepancy was more apparent for the head parts than for overall thermal response due to the rest of the body being just virtually simulated with BC1 (see Table 5.2 and Table 5.8).

Development and validation of the coupled system

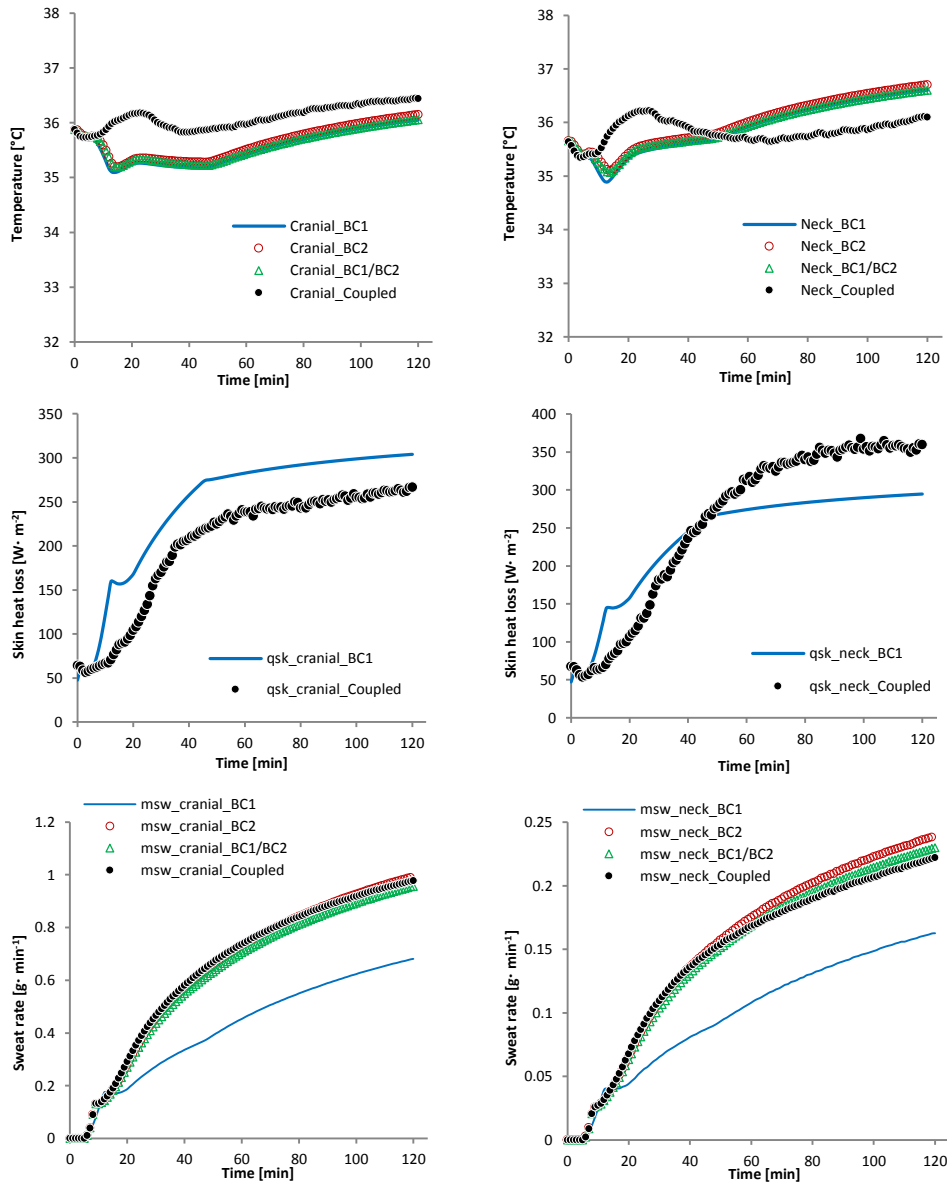


Figure 5.8. Evolution of the skin temperature, skin heat loss and local sweat rate for cranial and neck parts in the warm exposure for pure virtual and coupled simulations. Pure virtual simulation is presented calculated for different types of boundary conditions for a better estimation of the size of the discrepancy just due to having head physically represented. BC1 (boundary conditions type 1 entire body), BC2 (boundary conditions type 2 entire body) and BC1/BC2 (combined boundary conditions as in the coupled head system).

Multi-sector thermophysiological head simulator

The surface temperature curves for the cranial and neck parts showed that after the initial five minutes of a consistent prediction, the coupled system and pure virtual simulations started to diverge coinciding with the point at which the predicted sweat rate in BC1 and BC2 diverged. As discussed in section 5.4, when simulations applied BC2, the total skin heat loss was lumped into one single value and the physiological model could not calculate the actual skin wettedness value and the sweat predicted by the central regulation system could not be reduced due to this factor.

In spite of a higher sweat rate in the coupled simulation, the observed local skin temperature was still higher than it was observed when BC2 were virtually applied on the head, especially in the first stages of the simulation. Additionally, the skin heat loss measured by the manikin was generally lower than predicted in all the pure virtual simulations for which skin heat loss was enforced to be exactly the same. These results pointed out to some differences in the sweating system responsiveness or the evaporation efficiency considered in the physiological model for calculation as compared to the actual evaporation at the head manikin surface. The physiological model assumes that while the skin wettedness is below 100%, all secreted sweat should evaporate taking the complete latent heat of the water lost. However, when a thermal manikin is simulating the evaporative heat exchange at human skin, there are some factors that might potentially decrease the theoretical evaporation rate assumed by the physiological model. The most advanced thermal manikins are equipped with a limited number of water-releasing outlets to simulate sweating. However, the distribution of these outlets does not correspond to the one of the human sweat glands on skin and they usually include a tight-fitting elastic fabric that aims at evenly spreading the water on the thermal manikin surface and increasing the evaporation surface. In this case, the characterization of

the evaporation efficiency showed values below 100% and time delays for the entire head approximating 10 minutes till at least 75% of the expected evaporative cooling in steady-state for a given sweat rate was reached (chapter 3, section 3.9). In case of neck, this trend in skin temperature and heat loss was reverted after 50 minutes of the exposure. A similar change in trend was observed for forehead and face as well. The most probable reason for that trend is the water migration from top to bottom parts of the head as hinted in section 3.9.3.1. The need of improving the accuracy and realism of the sweating function was already suggested by Redortier and Voelcker (Redortier and Voelcker, 2010). Consequently, for exposures in which the evaporative cooling is the main responsible for reducing skin temperature, namely, warm and exercising scenarios, the coupled system could slightly overpredict skin temperatures at the different head parts specially at the beginning of the exposure. However, after some time the opposite could be expected for forehead, face and neck parts due to some water migration over the tight-fitting fabric.

Consequently, it seemed that a more efficient evaporation of the sweat offered by a different type of skin fabric could help to approach the skin temperature prediction of the coupled system to values obtained in the pure virtual simulations at the head-site. Alternatively, a correction of the sweat rate for faster or greater delivery of the sweat corresponding to the evaporative properties of the used skin fabric could also contribute to increase the system accuracy, especially at the beginning of the sweating periods.

5.6 VALIDATION AGAINST HUMAN DATA

5.6.1 Introduction

Physiological models represent a simplification of the human physiology and the heat and mass exchange that occurs between the human skin and the thermal environment. They usually predict thermal response for a standard person while the thermophysiological reactions are modelled based on statistical regression models rather than physiological principles. Moreover, physiological models include in general a simplified model for clothing considering few static parameters, mainly thermal and evaporative resistances and clothing area factor that could not account for the dynamic heat and mass exchange phenomena such moisture absorption-desorption cycles, condensation or perspiration migration across clothing layers. Although the physiological model by Fiala included in the coupled system has been extensively validated for prediction of the overall body temperatures by Psikuta et al. (Psikuta et al., 2012a), the validation of the physiological model for local skin temperatures presented in chapter 4 (section 4.6) indicated some possibilities for improving the local skin temperature prediction of the forehead. Main suggestions for improving the prediction of the skin temperature of the forehead were related to uncertainties about how the clothing was worn and how it fitted the head. The headgear could be placed on the head manikin and provide a realistic wearing. This would facilitate the heat and mass transfer processes occurring realistically on the head manikin surface within the clothing and their exact quantification for a more precise prediction of the head thermal response. This first validation study focused on understanding the heat and mass transfer exchange at the head manikin surface, and thus, complex headgear exposures remained out of the scope of this validation. This preliminary study was essential for adequately interpreting the

results in scenarios including complex headgear for which the coupled system is expected to precisely quantify the net heat exchange between skin and environment overcoming the physiological models limitations when simulating the dynamic thermal phenomena within the clothing.

The aim of this work was to validate the predictions of the coupled system against physiological data obtained in ten human experiments excluding complex headgear. Furthermore, the differences in the predicted thermal response between the pure virtual simulations carried out by the physiological model (BC1) and the coupled simulations were analysed to better understand the origin of the differences and allowing for the thermal head manikin characterization for physiological simulations referenced in chapter 3.

5.6.2 Methods

Ten human exposures have been used to validate the predictions of the coupled system (Table 5.9). These exposures were selected among exposures available in the human database referenced in chapter 4 (Table 4.2) and representing combinations of cold, moderate and warm environments with and without activity. For exposures including headgear or neck dressed, the thermal and evaporative resistance values previously measured on the thermal head manikin at head-site included in the clothing files initially used in the pure virtual simulations were removed as in the coupled simulation the thermal head manikin was dressed with the real clothing or headgear.

Multi-sector thermophysiological head simulator

Table 5.9. Description of the human exposures included in the validation study of the coupled system.

Experiment [in Table 4.2.]	Exposure [in Table 4.2]	Exposure description	Duration [min]	Air temperature [°C]	Radiant temperature [°C]	Relative humidity [%]	Air speed [m·s ⁻¹]	Activity [met]	Mean clothing thermal resistance [m ² K·W ⁻¹]	Mean clothing evaporative resistance [m ² Pa·W ⁻¹]	Headgear	Number of participants [male/female]	Reference
1	16	Sedentary activity in cold	120	10	10	40	0.05	0.8	0.12	5.38	No	10/0	(Wagner and Horvath, 1985)
8	21	Walking in the cold	120	10	10	50	0.5	1.4/5.9	0.32	27.85	Winter cap and turtle-neck shirt	10/0	(Niedermann et al., 2014)
3	10	Standing in the cold*	60	20	20	50	0.2	1	0.29	51.55	Turtle-neck jacket	8/0	(Mäkinen et al., 2000) and unpublished data from H. Rintamäki, FIOH, Oulu, Finland
2	4	Cycling in moderate environment	95	20	20	50	3	3.4/7.3	0.06	3.67	Bicycle helmet	9/0	(Jack, 2010)
	2.8/4.7							0.06	3.99	0/5			
10	24	Cycling in moderate environment	81	21.8	21.8	39	0.15/0.44	2.5/4	0.05	2.47	Thin bandage	14/0	(Priego Quesada et al., 2015)
	21.2			21.2	2.5/5.3								
13	42	Sedentary activity in moderate and warm environments	40	19.4	19.4	54.4	0.11	1	0.03	0.92	No	15/0	(Munir et al., 2009)
	29.3			29.3									
9	22	Walking in hot conditions*	43	30	30	40	0.3	4.9	0.21	20.95	No	10/0	(Niedermann et al., 2014)

*Just first phase simulated

Figure 5.9 provides an overview on the air temperature and activity level of the ten exposures presented in Table 5.9.

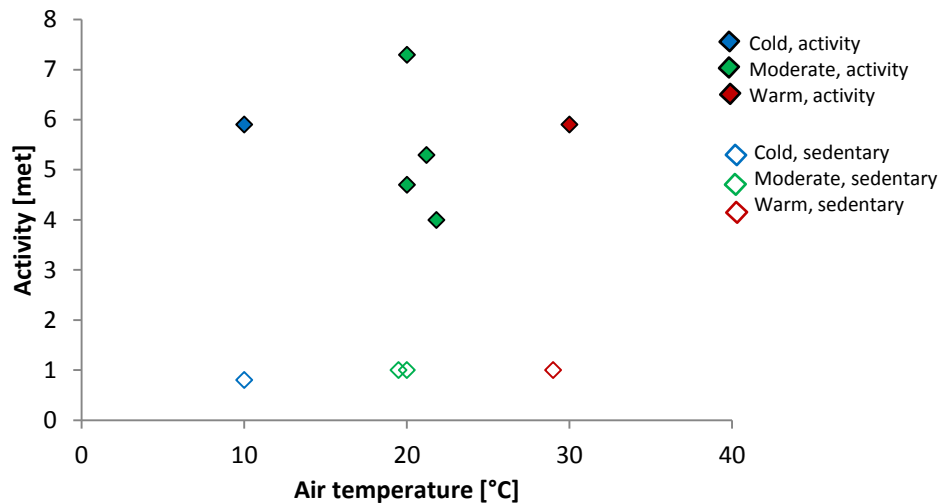


Figure 5.9. Overview of the air temperature and activity level of ten exposures selected for the validation.

As described in chapter 4, the precision and the accuracy of the coupled system predictions were statistically assessed by the root-mean square deviation (rmsd) and by the bias similarly to the study by Psikuta et al. (Psikuta et al., 2013b). Both parameters were calculated for the core and mean skin temperatures and the local skin temperature at forehead in each exposure as it was the local temperature available in most of the exposures. The fit of the coupled simulations was considered acceptable when the rmsd was within the standard deviation of the experimental data. The bias should be ideally close to zero to ensure unbiased model prediction. Additionally, the rmsd and bias values have been compared to the rmsd and bias values obtained when simulating the same exposures with the

model running alone. Some exemplary results have been graphically discussed to illustrate some of the main challenges faced by the coupled system.

5.6.3 Results

Figure 5.10 shows the overall bias and rmsd values calculated separately for the pure virtual simulations and the coupled simulations for ten validation exposures. Overall core temperature rmsd and bias values were calculated for rectal temperature. Therefore, exposures 21, 24 and 25 were not included as core temperature was measured at intestine-site. Although ingestible telemetric pills located at the intestine have become very popular in the last time for estimating core temperature due to good agreement with rectal probes measurements, a consistent bias ranging between 0.15 and 0.2°C has been reported in some studies (Casa et al., 2007; Easton et al., 2007; Teunissen et al., 2012). Bias and rmsd values for core and mean skin temperature stayed close to the average standard deviation observed in the experiments that was $0.26 \pm 0.05^{\circ}\text{C}$ and $0.77 \pm 0.34^{\circ}\text{C}$, respectively, similarly to pure virtual simulations. However, higher variability was observed in the predictability of the forehead temperature in both systems as average rmsd was $1.40 \pm 0.89^{\circ}\text{C}$ for the model alone and $1.91 \pm 1.75^{\circ}\text{C}$ for the coupled system compared to an average experimental standard deviation of $1.31 \pm 0.48^{\circ}\text{C}$. The higher standard deviation in the rmsd value calculated for the coupled system hinted that the precision of the coupled simulations could depend on the specific exposure simulated.

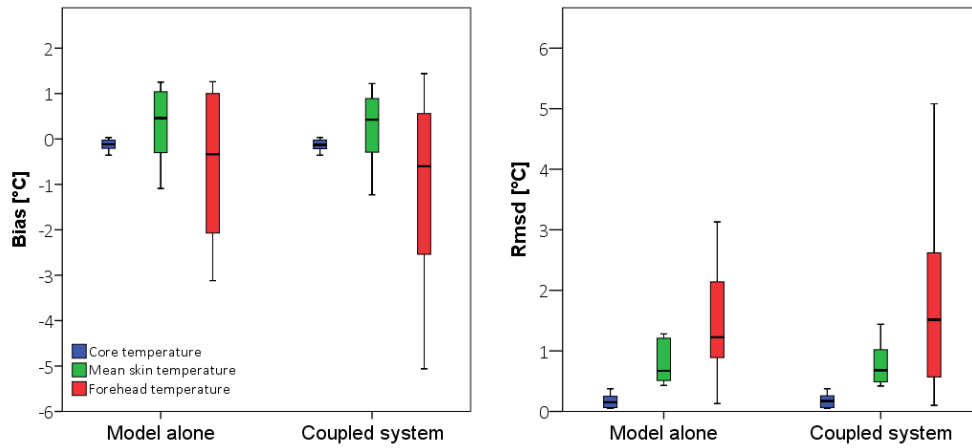


Figure 5.10. Box-plot diagram of the overall bias and rmsd values calculated for ten validation exposures for the pure virtual simulations (model alone) and the coupled system simulations. Box divisions corresponds to data quartiles, upper whisker to the upper quartile plus 1.5 times the interquartile range and lower whisker to the lower quartile minus 1.5 times the interquartile range.

Table 5.10 shows corresponding bias and rmsd for the variables studied in each exposure obtained by the model alone and by the coupled system.

Multi-sector thermophysiological head simulator

Table 5.10. Statistical parameters for measured variables in each exposure when simulated by the model alone and when simulated by the coupled system with human subject experimental data as a reference.

Exposure	Core [°C]				Mean skin [°C]				Forehead [°C]				Reference
	bias-model	rmsd-model	bias-coupled	rmsd-coupled	bias-model	rmsd-model	bias-coupled	rmsd-coupled	bias-model	rmsd-model	bias-coupled	rmsd-coupled	
16	-0.27	0.32	-0.28	0.33	0.53	0.74	0.52	0.73	1.26	1.44	1.44	1.67	(Wagner and Horvath, 1985)
21	0.08	0.17	0.06	0.17	-1.09	1.24	-1.12	1.27	-2.20	2.28	-1.97	2.08	(Niedermann et al., 2014)
10	-0.36	0.37	-0.36	0.37	-0.30	0.43	-0.29	0.43	0.09	0.13	0.02	0.10	(Mäkinen et al., 2000)
4	-0.15	0.18	-0.15	0.19	0.39	0.60	0.19	0.49	-2.07	2.14	-4.90	4.94	(Jack, 2010)
5	0.00	0.07	0.01	0.07	-0.44	0.53	-0.56	0.63	-3.12	3.13	-5.06	5.08	
24	0.33	0.34	0.32	0.33	1.11	1.21	0.89	0.99	-0.87	1.11	-1.59	1.80	(Priego Quesada et al., 2015)
25	0.42	0.43	0.42	0.42	1.04	1.11	0.95	1.02	-0.76	0.89	-1.17	1.36	
42	-0.05	0.06	-0.05	0.06	1.25	1.28	1.22	1.25	1.26	1.34	0.97	1.08	(Munir et al., 2009)
43	0.03	0.05	0.03	0.05	0.50	0.51	0.50	0.50	0.51	0.51	0.56	0.57	
22	-0.12	0.15	-0.13	0.17	0.42	0.50	0.35	0.42	1.00	1.03	0.36	0.41	(Niedermann et al., 2014)

When comparing the average precision (rmsd-value) obtained by the model alone to the one obtained by the coupled system, the differences were $0.01 \pm 0.01^{\circ}\text{C}$ for the core and $0.07 \pm 0.07^{\circ}\text{C}$ for the mean skin temperature. This difference increased up to $0.73 \pm 0.91^{\circ}\text{C}$ for the forehead. Interestingly, if clustering the exposures according to the activity level (Table 5.9), the difference in the average precision between pure virtual and coupled simulations was much lower in the sedentary cluster (exposures 16, 10, 42 and 43 with activity $\leq 1\text{met}$) than in the activity cluster (exposures 21, 4, 5, 24, 25 and 22 with activity $> 1\text{met}$) for the mean skin and forehead temperatures as shown in Figure 5.11.

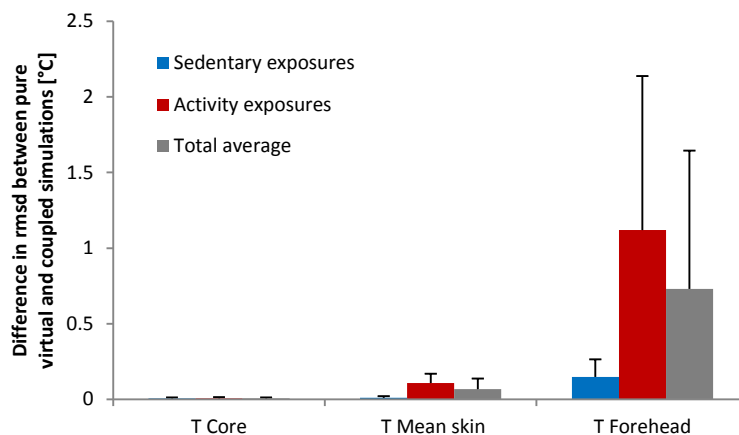


Figure 5.11. Differences in rmsd values [$^{\circ}\text{C}$] between pure virtual and coupled simulations for core, mean skin and forehead temperature predictions. Average results are presented separately for sedentary, activity and all exposures.

5.6.4 Discussion

This section has shown the precision of the coupled simulations by comparing predictions with human experimental data obtained in exposures ranging from 10

Multi-sector thermophysiological head simulator

to 30°C and for activity levels between 0.8 and 7.3 met when no complex headgear was worn.

In general, the coupled system precisely predicted core temperature and mean skin temperature meaning that the average rmsd values stayed close to the average standard deviation observed in the human experiments database that was in agreement with accepted values in the literature of 0.2°C and below 1°C, respectively (Haslam and Parsons, 1994; Psikuta et al., 2012a). However, the coupled system showed higher discrepancy for skin temperature at the forehead (average rmsd of $1.91 \pm 1.75^\circ\text{C}$) when compared with the average standard deviation observed in the experiments. This discrepancy was, however, much more apparent for the exposures including activity than for the sedentary exposures. Comparing the precision of the coupled system for the forehead temperature prediction with the precision of the model alone, the difference in the average rmsd value was $0.15 \pm 0.12^\circ\text{C}$ for sedentary exposures, whereas it rose up to $1.12 \pm 1.02^\circ\text{C}$ for activity exposures.

In activity exposures, the cooling of the skin had to be achieved mainly by the evaporation of the sweat. Figure 5.12 and Figure 5.13 show the prediction of forehead temperature and the corresponding sweat rate obtained in a moderate and a warm scenario, respectively (exposures 25 and 22 respectively in Table 5.9). The temperature predicted by the coupled system was slightly above the temperature predicted by the model alone from the moment the sweating started. The total amount of sweat excreted at the forehead was not very different in the moderate exposure 25 (0.89 and 0.86 g for the whole activity phase till minute 68 in the virtual and coupled simulation, respectively) but higher predicted by the coupled system than by the model alone in the warm environment presented in

exposure 22 (0.95 and 1.42 g for the whole activity phase till minute 43 in the virtual and coupled simulation, respectively). As shown in section 5.4 of this chapter, when the model applied boundary conditions type 2 (BC2), the predicted sweat rates were higher than those predicted if boundary conditions type 1 would have been applied (see Table 5.3 and Table 5.4). Additionally, in case of exposure 25 (Table 5.9), some temperature gradients of up to 1.8°C were observed between the forehead and face parts that could potentially produce some deviation in the measured heat loss due to uncontrolled lateral heat exchange, and consequently, in the local skin temperature as shown in chapter 3 (section 3.5).

Although the coupled simulation showed a higher forehead temperature than the pure virtual simulation in both cases, the coupled simulation showed a better agreement than the pure virtual simulation when compared with the human experimental data in exposure 22 but the opposite was observed in exposure 25. As previously pointed in chapter 4, the attachment method for skin temperature sensors might have affected the temperature measurement as the heat and moisture transfer would be locally modified at the measurement-site (Buono and Ulrich, 1998; Priego Quesada et al., 2015; Psikuta et al., 2013a).

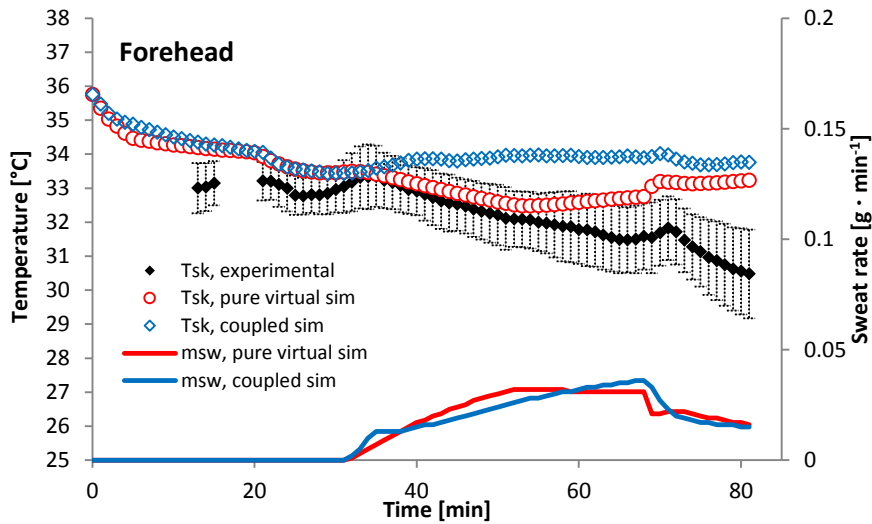


Figure 5.12. Prediction of skin temperature (Tsk) and sweat rate (msw) at forehead for exposure 25. Well-trained athletes cycling at 5.3 met in a moderate environment at $T_a = 21.2^\circ\text{C}$.

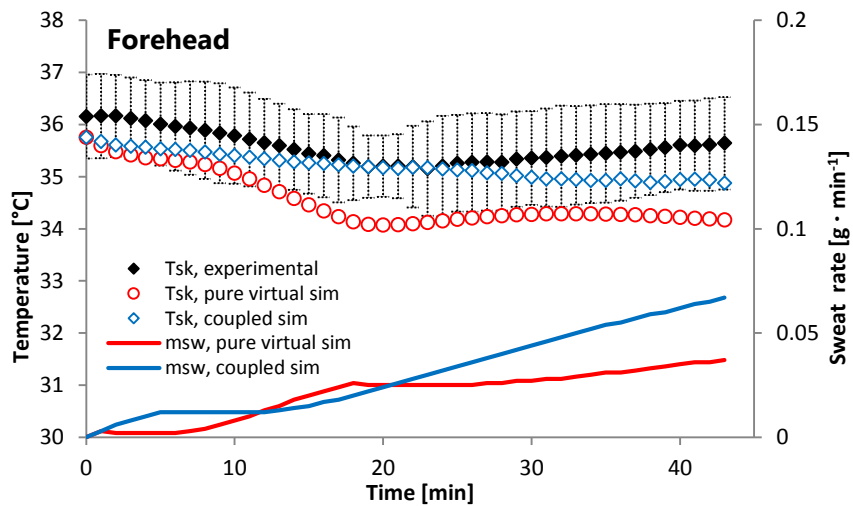


Figure 5.13. Prediction of skin temperature (Tsk) and sweat rate (msw) at forehead for exposure 22. Well-trained athletes walking at 4.9 met in a warm environment at $T_a = 30^\circ\text{C}$.

In case of exercising in the cold environment presented in exposure 21 (Table 5.9), Figure 5.14 shows similar skin temperature prediction at forehead in the pure virtual and in the coupled simulations, although the sweat rates ratio between simulations was similar as in the equivalent exposure in warm environment (exposure 22) (1.01 and 1.5 g cumulated in the activity phase till minute 60 in the virtual and coupled simulation, respectively). In this exposure 21, participants were walking in a cold environment at 10°C wearing a winter cap. In the pure virtual simulation, the thermal insulation value was measured first using head manikin at steady-state, and subsequently, the same winter cap was placed on the head manikin during the coupled simulation. In this case, skin temperature of other head parts either dressed or not showed the common case observed for exposures involving the sweating function, in which coupled simulation prediction for skin temperature was above the pure virtual simulation prediction. As it showed an exceptional behaviour, it might occur that the evaporative resistance of the winter cap in the pure virtual simulation was overestimated and produced higher skin temperatures at forehead during the pure virtual simulation. However, in cold environments, other coupled heat and moisture transfer phenomena increasing the net heat loss could occur within the winter cap in the coupled simulations that did not occur in the pure virtual simulation due to the use of a simplified clothing model (i.e. condensation (Havenith et al., 2008)). The gap between both simulations and the experimental data could be related to the different ways of providing the skin temperature at forehead. The coupled simulations provided the average skin temperature for the entire forehead that was partially dressed. However, in the human experiments, skin temperature at forehead was collected with a thermal contact sensor at one single point that if allocated below the cap, the measurement would correspond to the much colder skin temperature outside the winter cap.

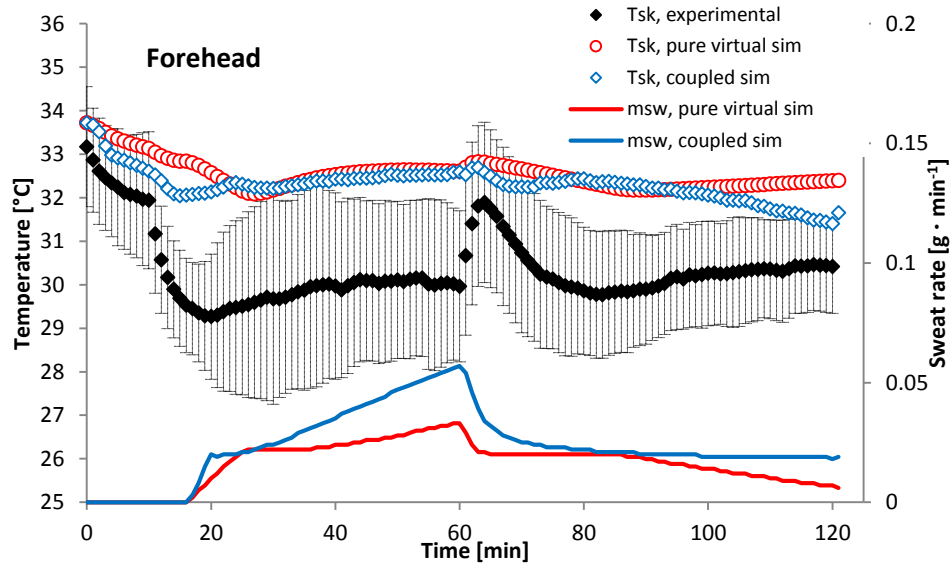


Figure 5.14. Prediction of skin temperature (Tsk) and sweat rate (msw) at forehead for exposure 21. Well-trained athletes walking at 5.9 met in a cold environment at $T_a = 10^\circ\text{C}$.

As discussed in section 5.4, the physiological model considers the mean skin and core temperature to calculate the overall sweating response of the central nervous system. However, the local sweat rates are calculated by modulating this overall signal with the effect of the local skin temperature and the skin wettedness. When the physiological model was coupled with the head manikin, it did not update the skin wettedness values along the exposure and the sweat suppression effect due to an increase in the skin wettedness could be dismissed. As previously mentioned in this chapter, the calculation of the secreted sweat and the evaporated skin moisture could be impaired when the boundary conditions were put in as a lumped single value corresponding to total skin heat loss (boundary conditions type 2) as it is in the coupled simulation.

5.7 CONCLUSIONS

This chapter has described the partial coupling principle applied for controlling the head manikin with the physiological model and the validation of the coupled system at this stage. The applied coupling principle consisted of a real-time feedback loop in which the physiological model provided skin temperatures and sweat rates for the different head parts of the head manikin and received the heat fluxes as an integral feedback from the environment. A coupling interface was developed in Matlab2013a to ensure the correct data exchange between the physiological model and the head manikin.

The pure virtual simulation of the same scenario but applying different types of boundary conditions, namely, BC1 (virtual environment) or BC2 (skin heat loss) produced similar prediction of the rectal and mean skin temperatures in the cold-sedentary and warm-exercising exposures. However, a higher prediction of the sweat rate was observed in the warm-exercising scenario when the simulation applied boundary conditions type 2. This mismatch has been attributed to the impairment in the calculation of the skin wettedness in case of boundary condition type 2 that is responsible for an inhibitory effect of the sweating function. Accounting for actual skin wettedness on the manikin is challenging at the moment, and thus, no possible correction can be applied. Consequently, differences already due to using the physiological model with different type of boundary conditions were expected to appear mainly in warm and exercising exposures.

When predictions of pure virtual and coupled simulations were compared, both simulation systems obtained similar predictions for global temperatures, namely

rectal and mean skin temperatures, in cold, thermoneutral and warm conditions. However, higher discrepancy was observed in warm scenario for local temperatures at head-site when the sweating function was active and main cooling mechanism was sweat evaporation. In this case, part of the discrepancy came from the different predictions provided by the physiological model when calculating human thermal response based on the boundary conditions type 1 and 2. Although the predicted sweat rate was higher using boundary conditions type 2, the local skin temperature resulted in higher values for the coupled simulations. The previous characterization of the evaporation efficiency of the head manikin sweating system described in chapter 3 (section 3.9) pointed to a reduced evaporation efficiency when compared with the 100% efficiency assumed by the physiological model. Additionally, time delays for the entire head approximating 10 minutes till at least 75% of the expected evaporative cooling in steady-state for a given sweat rate was reached were observed. Therefore, in the coupled simulation, slightly higher skin temperature prediction at head-site could be expected especially in the first phase of the exposure. Some improvements in the ability of the tight-fitting fabric to absorb and spread the moisture or in applying a greater sweat rate correcting for evaporation efficiency might contribute to increase the evaporative cooling of the head manikin surface, and thus, to better approximate predictions obtained by the model alone. Additionally, faster responsiveness of the sweating system could approach the skin temperature predictions to those obtained by the model alone at the first stages of the simulation.

Similarly, some time elapsed between the stop of the sweat function and the corresponding reduction in the evaporative heat loss until the dry heat loss value was reached. The absorbed water remaining in the tight-fitting skin fabric and some further evaporative cooling occurred for a certain time afterwards. During a

coupled simulation, this effect could physically represent the accumulation of liquid sweat on the human skin differently than considered in the pure virtual simulations by the physiological model.

The preliminary validation of the coupled system against human physiological data in several scenarios combining different environmental temperatures and activity levels showed a good agreement in predictions of rectal and mean skin temperatures close to the acceptability criteria of 0.2°C and 1°C proposed in the literature for core and mean skin temperature, respectively. In case of local skin temperature at forehead, the discrepancy between human experimental data and the coupled simulation was larger for exposures in which participants were exercising. As in these exposures main cooling mechanism was the sweat evaporation and the skin temperature was always higher in the coupled simulations than in the pure virtual simulations, the most probable reason was the reduced evaporation efficiency observed on the head manikin (section 3.9). The agreement with the experimental data depended on the particular exposure and it has been highlighted that a more complete description of the experimental setup would contribute to address the validation of any physiological model more consistently.

It is hypothesized that sweat might not evaporate from human skin with 100% efficiency as assumed by the physiological model. Several works have proposed expressions for the evaporation efficiency of the sweating (Alber and Holmér, 1994; Alber-Wallerström and Holmér, 1985; Vogt et al., 1982). One of these expressions based on the skin wettedness is applied in the calculation of the required sweat rate in the standardized Predicted Heat Strain model (PHS) (ISO7933, 2004; Malchaire et al., 2001). Similarly, the evaporation efficiency has been demonstrated to be lower than 100% on a thermal manikin surface (Havenith et al., 2013, 2008;

Multi-sector thermophysiological head simulator

Wang et al., 2013). Ideally, the sweating system in the head manikin made up by the water delivery system and the tight-fitting fabric should be able to closely represent the evaporation phenomena as it is in the human skin in the entire range of conditions, namely, similar sweat delivery responsiveness, similar evaporation rates in the same environment and similar capacity of holding water on its surface.

The literature search for gathering experimental physiological data has evidenced some lack of data for other head parts apart from forehead. Forehead is mentioned in standard methods for calculating mean skin temperature based on eight and 14 skin locations, whereas the neck is suggested for calculating mean skin temperature based on four and 14 locations, however, these methods are less commonly applied (ISO9886, 2004). Some difficulties such as the presence of hair or high dynamic vasomotor response that increase variability of the temperature measurement might be the reasons for head parts not being preferable sites for temperature measurements. Therefore, the validation studies for the coupled system against human experimental data might be restricted so far just to the forehead part.

To conclude, the coupled system consisting of a multi-sector thermal head manikin coupled with the physiological model by Fiala is able to quantify the heat and mass exchange at the human head skin when wearing complex headgear or in complex environments, and hence, it can contribute to a more precise prediction of the physiological response. However, further investigation would be needed to adjust the evaporative cooling of the head manikin for a realistic simulation of the sweat evaporation at the human skin the different situations.

6 CONCLUSIONS AND FUTURE WORK

6.1 CONCLUSIONS

This PhD work has presented a thermophysiological human head simulator as an advanced methodology for headgear testing based on the prediction of the thermophysiological response of the wearer. This thermophysiological human head simulator consisted of coupling a nine-zone thermal head manikin with a thermophysiological model. In this coupled system, the thermal head manikin is controlled by a physiological model in a real-time feedback loop. As just the head is actually dressed and exposed to the environment, the rest of the body is virtually simulated as in a pure virtual simulation. This methodology will allow the determination of the physiological and thermal comfort impact of headgear including casual, functional or protective applications. The industry will benefit from this knowledge, which will lead to the development of helmet designs with

Multi-sector thermophysiological head simulator

enhanced thermal comfort, and therefore, with higher acceptance by users. Next, the main conclusions after each chapter are summarized:

The evaluation of the nine-zone thermal head manikin (chapter 2)

The nine-zone thermal head manikin provided high spatial resolution when investigating heat transfer at head-site. Local heat transfer through headgear could be accurately quantified in several realistic situations accounting for different environmental conditions and air speeds in occupational, traffic or sport headgear applications.

The initial in-depth analysis of the stability of heat fluxes at the head manikin revealed some electrical cross-interaction between the zone heating and temperature sensing circuits resulting in lack of reliability in heat flux measurement and excessive high inter-test variability. After repair, the average intra-test variation of the absolute heat fluxes reduced from 4% down to 1.4% and the inter-test variation for more precise calculated variables such as radiant heat gain (described in section 2.4.2.3) reduced from 23 to 13% for facial section and from 17 to 5% for cranial section. The calibration of the surface temperature sensors led to maximum temperature differences up to 0.21°C in the extreme case of the left temple with regards to external reference sensors. No adjustment was applied on the head zones as these differences were within the variation observed among sensors used for the calibration of individual manikin zones.

The analysis of the headgear performance carried out for cycling scenarios showed the additional benefits of a more detailed investigation of headgear properties. The results of the reliability analysis for convection and radiation tests showed that the nine-zone manikin provided heat loss measurements with high consistency

compared to data from literature for a less finely segmented manikin (two-zone manikin) under the described test conditions. The variation of the measured heat fluxes was within the values reported in the literature. The results of the convection tests indicated a comparable overall thermal behaviour of the nine-zone manikin compared to the former two-zone manikin. In case of the radiation tests, some limitations were detected when tests were performed according to the previously described setup. For radiant heat gain measurements, the finer segmentation of the headform limited the amount of local radiation that the manikin could accept while maintaining a reliable measurement of the heat fluxes. The extra benefit of the existence of nine independent zones was the opportunity to detect local differences in heat transfer, whereas it was not possible to exactly allocate them with a less segmented headform. Therefore, the nine-zone manikin provided a precise quantification of local heat losses in steady-state, and thus, a reliable assessment of the contribution of design characteristics to the overall heat exchange that could support the conception of new helmet designs for optimized heat exchange and comfort.

The analysis of the specific requirements for the head manikin under physiological control mode (chapter 3)

The potential constraints of the head manikin to precisely represent the human head physiology as described by the physiological model foreseen for the coupled system were highlighted. By comparing the head segmentation in the physiological model and the head manikin, it was possible to consistently define four head parts that could be independently controlled in the coupled system, namely, forehead, cranial, face and neck parts. The total surface area of each head part agreed well when merging the head manikin zones and the head sectors in the physiological

Multi-sector thermophysiological head simulator

model, except for the forehead. When the combined heat transfer coefficients accounting for convective and radiative heat exchange were compared in still air conditions for these four head parts, differences were below 2% were observed for forehead and cranial part, whereas they were greater for the face and the neck. These discrepancies could be due to the fact that the head manikin did not account exactly for the same influence of the thermal plume resulting from lower body parts as assumed in the physiological model based on the full-body manikin measurements.

When heterogeneous surface temperature distribution was simulated in the head manikin, the gradients between head parts resulted in some uncontrolled lateral heat exchange. The analysis of the effect of these deviations in the heat flux at each head part for an extreme heterogeneous distribution revealed, however, an acceptable local skin temperature deviation at cranial and neck parts below 1°C. The skin temperature at the forehead and face differed by up to 2°C. Thus, no noticeable deviation in physiological response of cranial and neck parts was expected for any skin temperatures distribution accounting with differences below those in this extreme scenario. However, the precision of the coupled system for skin temperature prediction at forehead and face was prone to be compromised in case of large temperature gradients. Moreover, local extreme deviations at these two head parts could have a physiological impact on other body parts and affect the overall thermal response.

The passive heating and cooling responsiveness of the head manikin did not present any limitation for simulation of sudden temperature step changes observed in the human physiology. Nevertheless, when the manikin heating and cooling processes were modulated by the PI control with default settings, the time needed

to reach the temperature set point was larger than the time required by the human physiology for both extreme and moderate one-minute transients. To achieve a faster response, the PI control settings K_p and K_i were manually tuned. The time needed to achieve a temperature increase or decrease was reduced after adjusting the PI settings for a faster response for all heating step changes. For cooling step changes, the time needed to reach the temperature set point was within one minute unless the thermal response of the head manikin was limited by the maximum passive cooling capacity. The trade-off for that increased speed of temperature reaction was the increase in the variation in the steady-state heat flux from 1% up to 5 and 3% at 25 and 5°C respectively.

The evaporation efficiency and responsiveness of the sweating at the head manikin was studied. The evaporation efficiency in the head manikin could be reduced due to the evaporation taking place at the fabric surface and not directly on the head manikin surface and with some latent heat being taken from the environment, especially in warm conditions. The average evaporation efficiency for the entire head studied at different sweat rates ranged between 44 and 78% and no further increase was achieved with a higher sweat rate due to exceeding the maximum evaporation rate and a consequent water drip-off. The analysis of the dynamics of the sweating system at the head manikin showed that a time delay of up to 10 minutes elapsed between the onset of the sweat rate and the development of the 75% of the corresponding evaporative heat loss for each sweat rate. Similarly, the time elapsed between the termination of sweating and the reduction of the evaporative heat loss to the corresponding dry heat loss was proportionally increasing with the preceded sweat rate setting with the slope of 0.04 minutes per $1 \text{ ml}\cdot\text{m}^{-2}\cdot\text{h}^{-1}$ and approaching its maximum of more than 20 minutes for $500 \text{ ml}\cdot\text{m}^{-2}\cdot\text{h}^{-1}$ for the entire head. This drying time was due to some water retention in the

Multi-sector thermophysiological head simulator

tight-fitting fabric. This effect could physically represent the accumulation of liquid sweat on the human skin that was also considered in the pure virtual simulations by the physiological model.

The validation of a thermophysiological model against a dedicated database of human experiments (chapter 4)

As the major limitation of thermophysiological models is lack of validation and tools for assessing their performance, a database containing global and local human physiological data in 41 different exposures has been developed to assist the validation process. Two out of the 41 exposures corresponded to data collected in collaboration with the University of Valencia for investigating the evolution of core and local skin temperatures at different body parts with special focus on the head-site during cycling in moderate environments.

The influence of the thermal contact sensors attachment method used for collecting local skin temperature in those experiments was studied in dry and wet conditions on a hot plate. In dry conditions, the sensors covered with clinical tape provided slight but significant higher temperature by 0.5°C than the non-covered ones and infrared camera measurements, whereas in wet conditions, absolute differences with regards to infrared camera measurements rose up to 3.7°C and 3°C for covered and non-covered sensors, respectively. These differences were presumably due to the thermal insulation and the evaporative resistance offered by the clinical tape used in this experimental setup. This supports the idea that thermal contact sensors attached to the skin can locally interfere with the dry and wet heat exchange process as previously reported in the literature. However, any extrapolation of these results for equivalent measurements on human skin should be carefully addressed as assuming a constant temperature surface and completely

wet skin surface is a simplification of the dynamics of the human thermophysiological response.

The physiological model by Fiala showed a good precision in general when predicting core and mean skin temperature (rmsd 0.26 and 0.89°C, respectively) in different exposures including the exposures with well-trained participants exercising at high activity level since the model allowed the adjustment of the individual factors of the simulated person. A good precision was also observed when predicting local skin temperatures for most body sites in well-controlled exposures (average rmsd for local skin temperatures 1.33°C). A reduced precision of the predictions was obtained for the forehead skin temperature (rmsd of 1.69°C) most probably due to lack of information on measurement circumstances (hair, head coverage interference) and for the thigh during exercising exposures (rmsd of 1.42°C). In exercising exposures, the sweat evaporation represented one of the principal heat exchange mechanisms. An inadequate estimation of the local evaporative heat exchange could occur if the evaporative cooling at thigh skin occurred with lower efficiency than that of 100% assumed by the physiological model by Fiala. In such a case the measured skin temperature would be underestimated by the model predictions. Since this work focused mainly on the validation of prediction for local skin temperatures, the need for collection of detailed local environmental and clothing parameters for an accurate description of heat exchange conditions at the different body parts was highlighted. This should include a detailed description of how the clothing was exactly worn and how and where the sensors were attached to skin for achieving more precise results in the simulations.

Multi-sector thermophysiological head simulator

The most complete physiological data are derived from direct measurements during human experiments, however, to get reliable physiological data, human experiments should be carefully planned and controlled and involve a representative number of participants. Limitations of such tests are ethical concern, time and cost burden. Scientists and ergonomists could potentially benefit from predictions obtained from physiological models for a more efficient experimental planning or to assist product development processes in their early-stage. Therefore, this validation study on the thermoregulation model provided highly useful information not only for the coupling work but also for a careful and critical interpretation of prediction of local skin temperatures increasing the applicability of the model in general, and hence, accelerating the investigation in the field of ergonomics.

The development and validation of the coupled system (chapter 5)

The nine-zone thermal head manikin was coupled with the physiological model by Fiala. The first attempt to validate this coupled system showed the precision of the prediction in several scenarios at different ambient temperatures and activity levels and highlighted the upcoming challenges for the new methodology.

The coupling principle consisted of a real-time feedback loop in which the physiological model provided the skin temperatures and sweat rates for the different head parts of the head manikin and received the feedback on environmental and clothing conditions in form of the corresponding heat fluxes. A coupling interface was developed in Matlab2013a to ensure the correct data exchange between the physiological model and the head manikin.

The analysis of the consistency between predictions obtained by applying different types of boundary conditions showed that, in spite of considering the same total skin heat loss, there was some inconsistency between predictions calculated based on boundary conditions type 1 (virtual environment) and 2 (skin heat loss). In particular, the thermoregulation actions in warm and exercise conditions, namely, skin blood flow and sweat secretion, were overpredicted in case of using boundary conditions type 2 (skin heat loss). When the boundary condition type 2 was applied to the model, the information on the skin wettedness necessary to calculate the local sweat secretion inhibition was not provided, resulting in overprediction of the sweating. This seemed to produce small differences in the predicted rectal, mean skin and local skin temperatures but larger differences in the thermoregulatory actions such as sweating. Accounting for the actual skin wettedness is challenging so far and therefore, differences already due to using the physiological model with different type of boundary condition were expected to appear in warm and exercising exposures.

The initial analysis of the convergence of the coupled system towards pure virtual simulations carried out with the physiological model alone showed that both simulation systems obtained similar predictions for global temperatures, namely rectal and mean skin temperatures, in cold-sedentary, thermoneutral and warm-exercising conditions. In case of the local forehead temperature, higher discrepancy was observed when the sweating function was active and main cooling mechanism was sweat evaporation. One probable reason was the different predictions provided by the physiological model using boundary conditions type 2 and predicting greater sweat rates as the inhibitory effect due to an increase in skin wettedness could not be simulated for a warm and exercising scenarios. In addition, due to the characteristics of the head manikin sweating system, the water

Multi-sector thermophysiological head simulator

evaporated not directly from the head manikin surface but from a tight-fitting fabric placed on top for aiding the water to be evenly distributed. The evaporation efficiency of the sweating at the head manikin was studied for steady-state and transient periods and showed values below 100%. Consequently, it seemed that a more efficient evaporation of the sweat achieved by different types of skin fabrics could approach the skin temperature predictions of the coupled simulations to the pure virtual simulations at head-site. Additionally, a well-controlled faster or greater delivery of the sweat if accounting with the real evaporation efficiency of the head manikin could also contribute to the higher prediction accuracy of the coupled system as compared to the pure virtual simulations.

The comparison of the prediction of the coupled system with human physiological data in several scenarios combining different environmental temperatures and activity levels showed a good agreement in predictions of rectal and mean skin temperatures close to the acceptability criteria of 0.2°C and 1°C for core and mean skin temperature respectively. Nevertheless, the coupled system showed some higher discrepancy for forehead temperature predictions between the pure virtual simulation and the coupled simulations for exposures in which participants were exercising in moderate and warm environments. In these activity exposures, the cooling of the skin had to be achieved mainly by evaporation of the sweat. The skin temperature in the coupled simulations was always above the skin temperature predicted in the pure virtual simulations in moderate and warm exposures, however, the agreement with the experimental data depended on the particular exposure.

It is hypothesized that sweat does not evaporate from human skin with 100% efficiency as assumed by the physiological model. Ideally, the sweating system in

the head manikin made up by the water delivery system and the tight-fitting fabric should be able to closely represent the evaporation phenomena as it is in the human skin at head-site in the entire range of conditions, namely similar sweat delivery responsiveness, similar evaporation rates in the same environment and similar capacity of holding water on its surface for each head part.

6.2 FUTURE WORK

This research provided insights into the development of a thermophysiological human head simulator, which involves many aspects and considerations. Based on the findings, some recommendations for future work are proposed next, namely:

Regarding the evaluation of the thermal head manikin for headgear testing

- The higher inter-test variation for more precise calculated variables such as radiant heat gain was still above the variability accepted in thermal manikin standards for heat flux measurements for facial section (13%). As in cranial section it decreased to 5% after repair, a further tuning of the manikin heating power is suggested for increasing discrimination power when measuring radiant heat gain in the facial section.

Regarding the specific requirements of the thermal head manikin under the physiological control

- When heterogeneous surface temperature distribution occurred in the head manikin, the gradients between head parts resulted in uncontrolled lateral heat exchange. As a consequence, the precision of the coupled system for skin temperature prediction at forehead and face was

compromised in case of large temperature gradients. Furthermore, these local extreme deviations could have a physiological impact on other body parts leading to the offset of the overall physiological response. Therefore, a more complete characterization of the lateral heat exchange should be considered when interpreting results of the coupled system and eventually corrected. Alternatively, an appropriate structural change should be applied to prevent lateral heat exchange in the future manikins.

- The passive heating and cooling responsiveness of the head manikin did not present any limitation for simulation of sudden temperature step changes observed in the human physiology. Nevertheless, when the manikin heating and cooling processes were modulated by the PI control with default settings, the time needed to reach the temperature set point was larger than the time required by the human physiology for both extreme and moderate one-minute transients. To achieve a faster response, the PI control settings K_p and K_i were manually tuned. However, although the thermal manikin responded faster, the variation in the steady-state heat flux increased from 1% up to 5 and 3% at 25 and 5°C respectively for a fix temperature step change. This increase in the variation of the heat flux due to the adjusted PI settings was observed to be even higher during the coupled simulations (results not presented). Therefore, a further investigation on the optimal balance of the PI settings would contribute to a better performance of the coupled system needed in extreme transient simulations.

Regarding the validation of physiological models and development of a database of human experiments

- The major limitation of thermophysiological models is lack of validation and tools for assessing their performance. Human databases are necessary for assisting in the validation process. For prediction of local skin temperatures, it has been highlighted the need of locally collecting detailed local environmental and clothing parameters for an accurate description of heat exchange conditions at the different body parts. This should include a detailed description of the pre-exposure conditions, how the clothing was exactly worn and where the sensors were attached to skin for achieving more precise results in the simulations. The need for collection of detailed local environmental and clothing parameters for an accurate description of heat exchange conditions at the different body parts was highlighted. This should include a detailed description of how the clothing was exactly worn and how and where the sensors were attached to skin for achieving more precise results in the simulations.
- As previously reported in the scientific literature and shown in this dissertation, the sensors themselves and especially the attachment method to the skin (usually based on different types of clinical tapes) can potentially affect the local heat transfer, and hence, reduce the reliability of the measurement if this effect is not considered. Therefore, a precise description of the method applied to collect skin temperature and the quantification of its influence in the temperature readings would improve the reliability of the measurements.
- The literature search for gathering experimental physiological data has evidenced the lack of data for other head parts apart from forehead. Some

difficulties such as the presence of hair or high dynamic vasomotor response that increase variability of the temperature measurement might be the potential reasons for head parts not being preferable sites for temperature measurements. Therefore, the validation studies on thermophysiological models for head are restricted so far just to forehead part, and thus, increasing the number of data collected at head-site would be necessary.

Regarding the development and validation of the coupled system

- The comparison of the coupled system against the pure virtual simulations and ten human databases has highlighted a reduced precision in scenarios, in which the sweating function was active and main cooling mechanism was sweat evaporation. Therefore, further investigation of sweat delivery responsiveness and the water absorption properties of different tight-fitting fabric are needed. Ideally, in a coupled simulation the head manikin should closely represent the evaporation phenomena as it is in the human skin at head-site in the entire range of conditions, namely similar sweat delivery responsiveness, similar evaporation rates in the same environment and similar capacity of holding water on its surface. Additionally, a complete characterization of the evaporative efficiency in nude conditions in a wide range of conditions for a given manikin could provide the information needed for developing correction factors to adjust the amount of water released by the manikin to reach the expected evaporative heat loss at each sweat rate.

7 REFERENCES

- Abeysekera, J.D.A., Holmér, I., Dupuis, C., 1991. Heat transfer characteristics of industrial safety helmets, in: Kumashiro, M., Megaw, E.D. (Eds.), *Towards Human Work - Solutions to Problems in Occupational Health and Safety*. Taylor & Francis, London, pp. 297–303.
- Abeysekera, J.D.A., Shahnava, H., 1988. Ergonomics evaluation of modified industrial helmets for use in tropical environments. *Ergonomics* 31, 1317–1329.
- Alam, F., Chowdhury, H., Elmir, Z., Sayogo, A., Love, J., Subic, A., 2010. An experimental study of thermal comfort and aerodynamic efficiency of recreational and racing bicycle helmets. *Procedia Eng.* 2, 2413–2418. doi:10.1016/j.proeng.2010.04.008
- Alber, B., Holmer, I., 1994. Sweating efficiency of unacclimatised women and men working in hot, humid environments, in: Frim, J., Ducharme, M.B., Tikuisis, P. (Eds.), *Sixth Int. Conf. on Environ. Ergon.* Sept. 25-30, 1994, Montebello (Canada). Montebello, Canada, pp. 24–25.
- Alber-Wallerström, B., Holmér, I., 1985. Efficiency of sweat evaporation in unacclimatized man working in a hot humid environment. *Eur. J. Appl. Physiol.*

Occup. Physiol. 54, 480–487. doi:10.1007/BF00422956

Amoros, E., Chiron, M., Martin, J.-L., Thélot, B., Laumon, B., 2012. Bicycle helmet wearing and the risk of head, face, and neck injury: a French case-control study based on a road trauma registry. *Inj. Prev.* 18, 27–32. doi:10.1136/ip.2011.031815

Anttonen, H., Niskanen, J., Meinander, H., Bartels, V., Kuklane, K., Reinertsen, R.E., Varietas, S., Sołtyński, K., 2004. Thermal manikin measurements - exact or not? *Int. J. Occup. Saf. Ergon.* 10, 291–300.

Arens, E.A., Zhang, H., Huizenga, C., 2006a. Partial- and whole-body thermal sensation and comfort—Part II: Non-uniform environmental conditions. *J. Therm. Biol.* 31, 60–66.

Arens, E.A., Zhang, H., Huizenga, C., 2006b. Partial- and whole-body thermal sensation and comfort, Part I: Uniform environmental conditions. *J. Therm. Biol.*

ASTM F2370-10, 2010. Standard Test Method for Measuring the Evaporative Resistance of Clothing Using a Sweating Manikin. ASTM International, West Conshohocken, PA, 2010.

Bijker, K.E., de Groot, G., Hollander, a. P., 2002. Differences in leg muscle activity during running and cycling in humans. *Eur. J. Appl. Physiol.* 87, 556–561. doi:10.1007/s00421-002-0663-8

Blood, K., Burke, R., 2010. Further Validation of the Model-Controlled Newton Thermal Manikin Against Historical Human Studies, in: 8th International Meeting for Thermal Manikin and Modeling (8I3M), Victoria, 22-26 August 2010, Canada. pp. 1–5.

Bogdan, A., Zwolinska, M., 2012. Future trends in the development of thermal manikins applied for the design of clothing thermal insulation. *FIBRES & TEXTILES East. Eur.* 20, 89–95.

References

- Bogerd, C.P., Brühwiler, P.A., 2008. The role of head tilt, hair and wind speed on forced convective heat loss through full-face motorcycle helmets: A thermal manikin study. *Int. J. Ind. Ergon.* 38, 346–353. doi:10.1016/j.ergon.2008.01.003
- Bogerd, C.P., Brühwiler, P.A., Heus, R., 2008. The effect of rowing headgear on forced convective heat loss and radiant heat gain on a thermal manikin headform. *J. Sports Sci.* 26, 733–41. doi:10.1080/02640410701787783
- Bogerd, C.P., Rossi, R.M., Brühwiler, P.A., 2010. Thermal perception of ventilation changes in full-face motorcycle helmets: subject and manikin study. *Ann. Occup. Hyg.* 55, 192–201. doi:10.1093/annhyg/meq074
- Bogerd, N., Perret, C., Bogerd, C.P., Rossi, R.M., Daanen, H.A.M., 2010a. The effect of pre-cooling intensity on cooling efficiency and exercise performance. *J. Sports Sci.* 28, 771–779. doi:10.1080/02640411003716942
- Bogerd, N., Psikuta, A., Daanen, H.A.M., Rossi, R.M., 2010b. How to measure thermal effects of personal cooling systems: human, thermal manikin and human simulator study. *Physiol. Meas.* 31, 1161–1168. doi:10.1088/0967-3334/31/9/007
- Boutcher, S., Maw, G., Taylor, N., 1995. Forehead skin temperature and thermal sensation during exercise in cool and thermoneutral environments. *Aviat. Space. Environ. Med.* 66, 1058–1062.
- Brühwiler, P.A., 2009. Role of the visor in forced convective heat loss with bicycle helmets. *Int. J. Ind. Ergon.* 39, 255–259. doi:10.1016/j.ergon.2008.08.001
- Brühwiler, P.A., 2008. Radiant heat transfer of bicycle helmets and visors. *J. Sports Sci.* 26, 1025–31. doi:10.1080/02640410801930143
- Brühwiler, P.A., 2003. Heated, perspiring manikin headform for the measurement of headgear ventilation. *Meas. Sci. Technol.* 14, 217–227.
- Brühwiler, P.A., Buyan, M., Huber, R., Bogerd, C.P., Sznitman, J., Graf, S.F., Rösgen, T.,

Multi-sector thermophysiological head simulator

2006. Heat transfer variations of bicycle helmets. *J. Sports Sci.* 24, 999–1011.
doi:10.1080/02640410500457877
- Brühwiler, P.A., Ducas, C., Huber, R., Bishop, P.A., 2004. Bicycle helmet ventilation and comfort angle dependence. *Eur. J. Appl. Physiol.* 92, 698–701.
doi:10.1007/s00421-004-1114-5
- Buono, M.J., Ulrich, R.L., 1998. Comparison of mean skin temperature using “covered” versus “uncovered” contact thermistors. *Physiol. Meas.* 19, 297–300.
- Burke, R., Curran, A., Hepokoski, M., 2009. Integrating an active physiological and comfort model to the Newton sweating thermal manikin, in: 13th International Conference on Environmental Ergonomics. Boston, Massachusetts, USA.
- Burton, A.C., 1944. An analysis of the physiological effects of clothing in hot environments , Report No. 186, Associate Comitee on Aviation Medical Research.
- Buyan, M., Brühwiler, P.A., Azens, A., Gustavsson, G., Karmhag, R., Granqvist, C.G., 2006. Facial warming and tinted helmet visors. *Int. J. Ind. Ergon.* 36, 11–16.
- Cabanac, M., 1993. Selective brain cooling in humans: “fancy” or fact? *FASEB J.* 7, 1143–1146; discussion 1146–1147.
- Carr, W.W., Sarma, D.S., Johnson, M.R., Do, B.T., Williamson, V.A., Perkins, W.A., 1997. Infrared Absorption Studies of Fabrics. *Text. Res. J.* 67, 725–738.
doi:10.1177/004051759706701005
- Casa, D.J., Becker, S.M., Ganio, M.S., Brown, C.M., Yeargin, S.W., Roti, M.W., Siegler, J., Blowers, J. a, Glaviano, N.R., Huggins, R. a, Armstrong, L.E., Maresh, C.M., 2007. Validity of devices that assess body temperature during outdoor exercise in the heat. *J. Athl. Train.* 42, 333–42.
- Cheung, S.S., 2007. Neuropsychological determinants of exercise tolerance in the

- heat. *Prog. Brain Res.* 162, 45–60. doi:10.1016/S0079-6123(06)62004-9
- Chou, C., Tochihara, Y., Kim, T., 2008. Physiological and subjective responses to cooling devices on firefighting protective clothing. *Eur. J. Appl. Physiol.* 104, 369–374. doi:10.1007/s00421-007-0665-7
- Coca, A., Dileo, T., Kim, J.-H., Roberge, R., Shaffer, R., 2015. Physiological and subjective evaluation of PPE using a sweating thermal manikin, in: House, J.R., Tipton, M.J. (Eds.), 16th International Conference on Environmental Ergonomics, 29 June-3 July, 2015, Portsmouth, UK.
- Cotter, J.D., Taylor, N.A.S., 2005. The distribution of cutaneous sudomotor and alliesthesial thermosensitivity in mildly heat-stressed humans: an open-loop approach. *J. Physiol.* 565, 335–345. doi:10.1113/jphysiol.2004.081562
- Croitoru, C., Nastase, I., Bode, F., Meslem, A., Dogeanu, A., 2015. Thermal comfort models for indoor spaces and vehicles—Current capabilities and future perspectives. *Renew. Sustain. Energy Rev.* 44, 304–318. doi:10.1016/j.rser.2014.10.105
- Curran, A.R., Peck, S.D., Hepokoski, M.A., Burke, R.A., 2014. Physiological model control of a sweating thermal manikin, in: *Ambience`14&10i3m*, 7-9 Sept 2014 Tampere, Finland. pp. 7–9.
- Davis, G.A., Edmisten, E.D., Thomas, R.E., Rummer, R.B., Pascoe, D.D., 2001. Effects of ventilated safety helmets in a hot environment. *Int. J. Ind. Ergon.* 27, 321–329. doi:10.1016/S0169-8141(00)00059-7
- De Bruyne, G., Aerts, J.M., Sloten, J. Vander, Goffin, J., Verpoest, I., Berckmans, D., 2012. Quantification of local ventilation efficiency under bicycle helmets. *Int. J. Ind. Ergon.* 42, 278–286.
- De Bruyne, G., Aerts, J.M., Sloten, J. Vander, Goffin, J., Verpoest, I., Berckmans, D., 2010. Transient sweat response of the human head during cycling. *Int. J. Ind. Ergon.* 40, 406–413. doi:10.1016/j.ergon.2010.02.005

- De Bruyne, G., Aerts, J.M., Van der Perre, G., Goffin, J., Verpoest, I., Berckmans, D., 2008. Spatial differences in sensible and latent heat losses under a bicycle helmet. *Eur. J. Appl. Physiol.* 104, 719–26. doi:10.1007/s00421-008-0828-1
- de Dear, R.J., Arens, E.A., Hui, Z., Oguro, M., 1997. Convective and radiative heat transfer coefficients for individual human body segments. *Int. J. Biometeorol.* 40, 141–56.
- den Hartog, E., 2002. Evaluation of the THDYN model during student practical tests, in: 10th International Conference on Environmental Ergonomics, 23-27 September, 2002. Fukuoka, Japan, pp. 475–478.
- Desruelle, A.V., Candas, V., 2000. Thermoregulatory effects of three different types of head cooling in humans during a mild hyperthermia. *Eur. J. Appl. Physiol.* 81, 33–39. doi:10.1007/PL00013794
- Dullah, A.R., Guan, Z.W., Crompton, R.H., 2011. A pilot study on thermal and moisture mapping of the head-helmet system using micro-sensor technology. *J. Test. Eval.* 39.
- Easton, C., Fudge, B.W., Pitsiladis, Y.P., 2007. Rectal, telemetry pill and tympanic membrane thermometry during exercise heat stress. *J. Therm. Biol.* 32, 78–86. doi:10.1016/j.jtherbio.2006.10.004
- Essick, G., Guest, S., Martinez, E., Chen, C., McGlone, F., 2004. Site-dependent and subject-related variations in perioral thermal sensitivity. *Somatosens. Mot. Res.* 21, 159–175.
- Fan, J., Cheng, X.-J., 2005a. Heat and Moisture Transfer with Sorption and Phase Change Through Clothing Assemblies: Part I: Experimental Investigation. *Text. Res. J.* 75, 900–105. doi:10.1177/004051750507500301
- Fan, J., Cheng, X.-J., 2005b. Heat and Moisture Transfer with Sorption and Phase Change Through Clothing Assemblies: Part II: Theoretical Modeling, Simulation, and Comparison with Experimental Results. *Text. Res. J.* 75, 187–

196. doi:10.1177/004051750507500301

Fan, J., Qian, X., 2004. New functions and applications of walter, the sweating fabric manikin. *Eur. J. Appl. Physiol.* 92, 641–4. doi:10.1007/s00421-004-1134-1

Fanger, P.O., 1970. *Thermal Comfort*. Copenhagen: Danish Technical Press.

Farrington, R.B., Rugh, J.P., Bharathan, D., Burke, R., 2004. Use of a Thermal Manikin to Evaluate Human Thermoregulatory Responses in Transient, Non-Uniform, Thermal Environments, in: *Society of Automotive Engineers Technical Paper*. pp. 2004–01–2345.

Farrington, R.B., Rugh, J.P., Bharathan, D., Paul, H., Bue, G., Trevino, L., 2005. Using a Sweating Manikin , Controlled by a Human Physiological Model , to Evaluate Liquid Cooling Garments, in: *Society of Automotive Engineers Technical Paper*. doi:10.4271/2005-01-2971

Fernandes, A.D.A., Amorim, P.R.D.S., Brito, C.J., de Moura, A.G., Moreira, D.G., Costa, C.M.A., Sillero-Quintana, M., Marins, J.C.B., 2014. Measuring skin temperature before, during and after exercise: a comparison of thermocouples and infrared thermography. *Physiol. Meas.* 35, 189–203. doi:10.1088/0967-3334/35/2/189

Fiala, D., Havenith, G., 2015. Modelling human heat transfer and temperature regulation, in: *Springer-Verlag Berlin Heidelberg (Ed.), Studies in Mechanobiology, Tissue Engineering and Biomaterials*. pp. 1–38. doi:10.1007/8415

Fiala, D., Havenith, G., Bröde, P., Kampmann, B., Jendritzky, G., 2012. UTCI-Fiala multi-node model of human heat transfer and temperature regulation. *Int. J. Biometeorol.* 56, 429–41. doi:10.1007/s00484-011-0424-7

Fiala, D., Lomas, K.J., Stohrer, M., 2001. Computer prediction of human thermoregulatory and temperature responses to a wide range of environmental conditions. *Int. J. Biometeorol.* 45, 143–159. doi:10.1007/s004840100099

Multi-sector thermophysiological head simulator

- Fiala, D., Lomas, K.J., Stohrer, M., 1999. A computer model of human thermoregulation for a wide range of environmental conditions: the passive system. *J. Appl. Physiol.* 87, 1957–1972.
- Finnoff, J.T., Laskowski, E.R., Altman, K.L., Diehl, N.N., 2001. Barriers to bicycle helmet use. *Pediatrics* 108, e4. doi:10.1542/peds.108.1.e4
- Foda, E., Almesri, I., Awbi, H.B., Sirén, K., 2011. Models of human thermoregulation and the prediction of local and overall thermal sensations. *Build. Environ.* 46, 2023–2032. doi:10.1016/j.buildenv.2011.04.010
- Foda, E., Sirén, K., 2012. A thermal manikin with human thermoregulatory control: Implementation and validation. *Int. J. Biometeorol.* 56, 959–971.
- Foda, E., Sirén, K., 2011. A new approach using the Pierce two-node model for different body parts. *Int. J. Biometeorol.* 55, 519–532. doi:10.1007/s00484-010-0375-4
- Fonseca, G.F., 1976. Physiological factors in protective helmets design. US Army Research Institute of Environmental Medicine Natick, Massachusetts, Report M1/77/14/USARIEM.
- Fonseca, G.F., 1974. Heat transfer properties of military protective headgear. US Army Natick Laboratories, Massachusetts, Report No.74-29-CE.
- Formenti, D., Ludwig, N., Gargano, M., Gondola, M., Dellerma, N., Caumo, A., Alberti, G., 2013. Thermal Imaging of Exercise-Associated Skin Temperature Changes in Trained and Untrained Female Subjects. *Ann. Biomed. Eng.* 1–9.
- Fox, B.Y.R.H., Goldsmith, R., Kidd, D.J., 1962. Cutaneous vasomotor control in the human head, neck and upper chest. *J. Physiol.* 161, 298–312.
- Frackiewicz-Kaczmarek, J., Psikuta, A., Bueno, M.A., Rossi, R.M., 2015. Air gap thickness and contact area in undershirts with various moisture contents: influence of garment fit, fabric structure and fiber composition. *Text. Res. J.*

doi:10.1177/0040517514551458

- Froese, G., Burton, A.C., 1957. Heat Losses From the Human Head. *J. Appl. Physiol.* 10, 235–241.
- Gagge, A.P., 1971. An Effective Temperature Scale Based on a Simple Model of Human Physiological Regulatory Response. *ASHRAE Trans.* 77, 247–262.
- Gagge, A.P., Nishi, Y., 2011. Heat Exchange Between Human Skin Surface and Thermal Environment, in: *Comprehensive Physiology*. John Wiley & Sons, Ltd., pp. 69–92.
- Geng, Q., Kuklane, K., Holmer, I., 1998. Tactile Sensitivity of Gloved Hands in the Cold Operation. *Appl. Hum. Sci. - J. Physiol. Anthropol.* 16, 229–236.
- Gerrett, N., Ouzzahra, Y., Coleby, S., Hobbs, S., Redortier, B., Voelcker, T., Havenith, G., 2014. Thermal sensitivity to warmth during rest and exercise: a sex comparison. *Eur. J. Appl. Physiol.* 114, 1451–62. doi:10.1007/s00421-014-2875-0
- Gisolfi, C. V., Mora, F., 2000. *The hot brain: survival, temperature, and the human body*. Cambridge, Mass.: MIT Press.
- Givoni, B., Goldman, R., 1971. Predicted metabolic energy cost. *J. Appl. Physiol.* 30, 429–433.
- Guan, Z.W., Dullah, A.R., Zhou, H.L., 2007. Experimental thermal/moisture mapping of industrial safety helmets, in: D.Harris (Ed.), *Engineering Psychology and Cognitive Ergonomics (Lectures Notes in Computer Science - Volume 4562)*. Springer-Verlag Berlin Heidelberg, pp. 678–686.
- Gunga, H.-C., Sandsund, M., Reinertsen, R.E., Sattler, F., Koch, J., 2008. A non-invasive device to continuously determine heat strain in humans. *J. Therm. Biol.* 33, 297–307. doi:10.1016/j.jtherbio.2008.03.004

- Hardy, J.D., DuBois, E.F., 1938. The technic of measuring radiation and convection. *J. Nutr.* 15, 461–475.
- Haslam, R.A., Parsons, K.C., 1994. Using computer-based models for predicting human thermal responses to hot and cold environments. *Ergonomics* 37, 399–416. doi:10.1080/00140139408963659
- Havenith, G., 2001. Individualized model of human thermoregulation for the simulation of heat stress response Individualized model of human thermoregulation for the simulation of heat stress response. *J. Appl. Physiol.* 90, 1943–1954.
- Havenith, G., Bröde, P., den Hartog, E., Kuklane, K., Holmer, I., Rossi, R.M., Richards, M., Farnworth, B., Wang, X., 2013. Evaporative cooling: effective latent heat of evaporation in relation to evaporation distance from the skin. *J. Appl. Physiol.* 114, 778–85. doi:10.1152/jappphysiol.01271.2012
- Havenith, G., Coenen, J.M., Kistemaker, L., Kenney, W.L., 1998. Relevance of individual characteristics for human heat stress response is dependent on exercise intensity and climate type. *Eur. J. Appl. Physiol. Occup. Physiol.* 77, 231–241. doi:10.1007/s004210050327
- Havenith, G., Middendorp, H. van, 1990. The relative influence of physical fitness, acclimatization state, anthropometric measures and gender on individual reactions to heat stress. *Eur. J. Appl. Physiol. Occup. Physiol.* 61, 419–427.
- Havenith, G., Richards, M.G., Wang, X., Bröde, P., Candas, V., Den Hartog, E., Holmér, I., Kuklane, K., Meinander, H., Nocker, W., 2008. Apparent latent heat of evaporation from clothing: attenuation and heat pipe effects. *J. Appl. Physiol.* 104, 142–149. doi:10.1152/jappphysiol.00612.2007
- Hawley, J.A., Noakes, T.D., 1992. Applied Physiology and performance time in trained cyclists. *Eur. J. Appl. Physiol.* 79–83.
- Holland, E.J., Laing, R.M., Lemmon, T.L., Niven, B.E., 2002. Helmet design to facilitate

References

- thermoneutrality during forest harvesting. *Ergonomics* 45, 699–716. doi:10.1080/00140130210159959
- Holmér, I., Nilsson, H., 1995. Heated manikins as a tool for evaluating clothing. *Ann. occup. Hyg* 39, 809–818.
- Houghton, F.C., Yaglou, C.P., 1923. Determining Lines of Equal Comfort. *ASH&VE Trans.* 28, 163–176 and 361–384.
- Hsu, Y.-L., Tai, C.-Y., Chen, T.-C., 2000. Improving thermal properties of industrial safety helmets. *Int. J. Ind. Ergon.* 26, 109–117.
- Huizenga, C., Hui, Z., Arens, E.A., 2001. A model of human physiology and comfort for assessing complex thermal environments. *Build. Environ.* 36, 691–699.
- ISO11092, 2014. Textiles - Physiological effects - Measurement of thermal and water-vapour resistance under steady-state conditions (sweating guarded-hotplate test). International Organisation for Standardisation, Geneva (Switzerland).
- ISO15831, 2004. Clothing - Physiological effects - Measurement of thermal insulation by means of a thermal manikin. International Organisation for Standardisation, Geneva (Switzerland).
- ISO18434-1, 2008. Condition monitoring and diagnostics of machines -- Thermography -- Part 1: General procedures. International Organisation for Standardisation, Geneva (Switzerland).
- ISO7933, 2004. Analytical determination and interpretation of heat stress using calculation of the predicted heat strain. International Organisation for Standardisation, Geneva (Switzerland).
- ISO8996, 2004. Ergonomics of the thermal environment - Determination of metabolic rate. International Organisation for Standardisation, Geneva (Switzerland).

Multi-sector thermophysiological head simulator

- ISO9886, 2004. Ergonomics - Evaluation of thermal strain by physiological measurements. International Organisation for Standardisation, Geneva (Switzerland).
- ISO9920, 2007. Ergonomics of the thermal environment - Estimation of thermal insulation and water vapour resistance of a clothing ensemble. International Organisation for Standardisation, Geneva (Switzerland).
- Jack, A., 2010. Einfluss hoch funktioneller Sporttextilien auf die Thermoregulation von Ausdauerathleten bei unterschiedlichen Umgebungstemperaturen. Kulturwissenschaftlichen Fakultät der Universität Bayreuth.
- James, C.A., Richardson, A.J., Watt, P.W., Maxwell, N.S., 2014. Reliability and validity of skin temperature measurement by telemetry thermistors and a thermal camera during exercise in the heat. *J. Therm. Biol.* 45, 141–149. doi:10.1016/j.jtherbio.2014.08.010
- Jones, B.W., 2002. Capabilities and limitations of thermal models for use in thermal comfort standards. *Energy Build.* 34, 653–659. doi:10.1016/S0378-7788(02)00016-6
- Jones, B.W., Ogawa, Y., 1993. Transient response of the human clothing system. *J. Therm. Biol.* 18, 413–416.
- Jones, B.W., Ogawa, Y., 1992. Transient interaction between the human and the thermal environment. *ASHRAE Trans.* 98, 189–196.
- Kelly, G., 2006. Body temperature variability (Part 1): a review of the history of body temperature and its variability due to site selection, biological rhythms, fitness, and aging. *Altern. Med. Rev.* 11, 278–93.
- Kobayashi, Y., Tanabe, S., 2013. Development of JOS-2 human thermoregulation model with detailed vascular system. *Build. Environ.* 66, 1–10. doi:10.1016/j.buildenv.2013.04.013

References

- Kolka, M.A., Levine, L., Stephenson, L.A., 1997. Use of an ingestible telemetry sensor to measure core temperature under chemical protective clothing. *J. Therm. Biol.* 22, 343–349.
- Kuklane, K., Geng, Q., Holmer, I., 1998. Effect of footwear insulation on thermal responses in the cold. *Int. J. Occup. Saf. Ergon.* 4, 137–152.
- Lahiri, B.B., Bagavathiappan, S., Jayakumar, T., Philip, J., 2012. Medical applications of infrared thermography: a review. *Infrared Phys. Technol.* 55, 221–235.
- Lee, S.M.C., Williams, W.J., Schneider, S.M., 2000. Core Temperature Measurement During Submaximal Exercise: Esophageal , Rectal , and Intestinal Temperatures.
- Li, Y., Li, F., Liu, Y., Luo, Z., 2004. An integrated model for simulating interactive thermal processes in human-clothing system. *J. Therm. Biol.* 29, 567–575. doi:10.1016/j.jtherbio.2004.08.071
- Liu, X., Holmér, I., 1997. Evaluation of evaporative heat transfer characteristics of helmets. *Appl. Hum. Sci. J. Physiol. Anthropol.* 16, 107–113.
- Liu, X., Holmér, I., 1995. Evaporative heat transfer characteristics of industrial safety helmets. *Appl. Ergon.* 26, 135–140.
- Lotens, W.A., 1993. Heat transfer from human wearing clothing. Technical University Delft, Delft, The Netherlands.
- Lotens, W.A., Havenith, G., 1994. Effects of moisture absorption in clothing on the human heat balance. *Ergonomics* 38, 1092–1113.
- Lotens, W.A., van de Linde, F.J.G., Havenith, G., 1995. Effect of condensation in clothing on heat transfer. *Ergonomics* 38, 1114–1131.
- Lucia, A., Hoyos, J., Perez, M., Santalla, A., Chicharro, J.L., 2002. Inverse relationship between [latin capital V with dot above] O₂max and economy/efficiency in

world-class cyclists. *Med. Sci. Sport. Exerc.* 34, 2079–2084.

Machado-Moreira, C.A., Smith, F.M., van dem Heuvel, A.M.J., Mekjavic, I.B., Taylor, N.A.S., 2008a. Sweat secretion from the torso during passively-induced and exercise-related hyperthermia. *Eur. J. Appl. Physiol.* 104, 265–270. doi:10.1007/s00421-007-0646-x

Machado-Moreira, C.A., Wilming, F., Meijer, A., Mekjavic, I.B., Taylor, N.A.S., 2008b. Local differences in sweat secretion from the head during rest and exercise in the heat. *Eur. J. Appl. Physiol.* 104, 257–64. doi:10.1007/s00421-007-0645-y

Mäkinen, T., Gavhed, D., Holmér, I., Rintamäki, H., 2000. Thermal responses to cold wind of thermoneutral and cooled subjects. *Eur. J. Appl. Physiol.* 81, 397–402. doi:10.1007/s004210050060

Malchaire, J., Piette, A., Kampmann, B., Mehnert, P., Gebhardt, H., Havenith, G., Den Hartog, E., Holmér, I., Parsons, K., Alfano, G., Griefahn, B., 2001. Development and validation of the predicted heat strain model. *Ann. Occup. Hyg.* 45, 123–135. doi:10.1093/annhyg/45.2.123

Margaria, R., 1968. Positive and negative work performances and their efficiencies in human locomotion. *Int. Zeitschrift für Angew. Physiol. Einschl. Arbeitsphysiologie* 25, 339–351. doi:10.1007/BF00699624

McCullough, E.A., 2005. The use of thermal manikins to evaluate clothing and environmental factors, in: Elsevier Ergonomics Book Series. pp. 403–407.

McCullough, E.A., 1991. Transient thermal response of different types of clothing due to humidity step changes, in: Proceedings of International Symposium on Clothing Comfort Studies in Mount Fuji. pp. 1–22.

McCullough, E.A., Jones, B.W., Huck, J., 1985. A Comprehensive Data Base for Estimating Clothing Insulation. *ASHRAE Trans.* 92, 29–47.

Mehrabyan, A., Guest, S., Essick, G., McGlone, F., 2011. Tactile and thermal

References

- detection thresholds of the scalp skin. *Somatosens. Mot. Res.* 28, 31–47.
- Merla, A., Mattei, P. a, Di Donato, L., Romani, G.L., 2010. Thermal imaging of cutaneous temperature modifications in runners during graded exercise. *Ann. Biomed. Eng.* 38, 158–63. doi:10.1007/s10439-009-9809-8
- Millet, G.P., Vleck, V.E., Bentley, D.J., 2009. Physiological Differences Between Cycling and Running. *Sport. Med* 39, 179–206.
- Munir, A., Takada, S., Matsushita, T., 2009. Re-evaluation of Stolwijk's 25-node human thermal model under thermal-transient conditions: Prediction of skin temperature in low-activity conditions. *Build. Environ.* 44, 1777–1787. doi:10.1016/j.buildenv.2008.11.016
- Nadel, E.R., Mitchell, J.W., Stolwijk, J.A., 1973. Differential thermal sensitivity in the human skin. *Pflügers Arch.* 340, 71–6.
- Nakamura, M., Yoda, T., Crawshaw, L.I., Yasuhara, S., Saito, Y., Kasuga, M., Nagashima, K., Kanosue, K., 2008. Regional differences in temperature sensation and thermal comfort in humans. *J. Appl. Physiol.* 105, 1897–1906.
- Netter, F.H., 2014. *Atlas of human anatomy*, 6th ed. Saunders / Elsevier, Philadelphia/PA.
- Niedermann, R., Wyss, E., Annaheim, S., Psikuta, A., Davey, S., Rossi, R.M., 2014. Prediction of human core body temperature using non-invasive measurement methods. *Int. J. Biometeorol.* 58, 7–15. doi:10.1007/s00484-013-0687-2
- Nilsson, H., 2004. Comfort climate evaluation with thermal manikin methods and computer simulation models. doi:ISBN 91-7045-703-4
- Nunneley, S.A., Troutman, Jr., S.J., Webb, P., 1971. Head cooling in work and Heat Stress. *Aerosp. Med.* 42, 64–68.
- Osczevski, R.J., 1996. Design and evaluation of a three-zone thermal manikin head.

Multi-sector thermophysiological head simulator

Defence and Civil Institute of Environmental Medicine (DCIEM), Report No. 96-R-60.

Pang, T.Y., Subic, A., Takla, M., 2013. A comparative experimental study of the thermal properties of cricket helmets. *Int. J. Ind. Ergon.* 43, 161–169.

Pang, T.Y., Subic, A., Takla, M., 2011. Thermal comfort of cricket helmets: An experimental study of heat distribution. *Procedia Eng.* 13, 252–257. doi:10.1016/j.proeng.2011.05.081

Priego Quesada, J.I., Martínez Guillamón, N., Cibrián Ortiz de Anda, R.M., Psikuta, A., Annaheim, S., Rossi, R.M., Corberán Salvador, J.M., Pérez-Soriano, P., Salvador Palmer, R., 2015. Effect of perspiration on skin temperature measurements by infrared thermography and contact thermometry during aerobic cycling. *Infrared Phys. Technol.* 72, 68–76. doi:10.1016/j.infrared.2015.07.008

Psikuta, A., 2009. Development of an “artificial human” for clothing research. De Monfort University, Leicester, Leicester.

Psikuta, A., Fiala, D., Laschewski, G., Jendritzky, G., Richards, M., Blazejczyk, K., Mekjavič, I., Rintamäki, H., de Dear, R., Havenith, G., 2012a. Validation of the Fiala multi-node thermophysiological model for UTCI application. *Int. J. Biometeorol.* 56, 443–460.

Psikuta, A., Frackiewicz-Kaczmarek, J., Frydrych, I., Rossi, R., 2012b. Quantitative evaluation of air gap thickness and contact area between body and garment. *Text. Res. J.* 82, 1405–1413. doi:10.1177/0040517512436823

Psikuta, A., Kuklane, K., Bogdan, A., Havenith, G., Annaheim, S., Rossi, R.M., 2015a. Opportunities and constraints of presently used thermal manikins for thermophysiological simulation of the human body. *Int. J. Biometeorol.* Accepted.

Psikuta, A., Niedermann, R., Rossi, R.M., 2013a. Effect of ambient temperature and attachment method on surface temperature measurements. *Int. J.*

Biometeorol. doi:10.1007/s00484-013-0669-4

Psikuta, A., Richards, M., Fiala, D., 2008. Single-sector thermophysiological human simulator. *Physiol. Meas.* 29, 181–192.

Psikuta, A., Wang, L.-C., Rossi, R.M., 2013b. Prediction of the physiological response of humans wearing protective clothing using a thermophysiological human simulator. *J. Occup. Environ. Hyg.* 10, 222–32. doi:10.1080/15459624.2013.766562

Psikuta, A., Weibel, M., Burke, R., Hepokoski, M., Schwenn, T., Annaheim, S., Rossi, R.M., 2015b. A systematic approach to the development and validation of adaptive manikins, in: House, J.R., Tipton, M.J. (Eds.), 16th International Conference on Environmental Ergonomics, 29 June-3 July, 2015, Portsmouth, UK.

Rasch, W., Cabanac, M., 1993. Selective brain cooling is affected by wearing headgear during exercise. *J. Appl. Physiol.* 74, 1229–1233.

Rasch, W., Samson, P., Cote, J., Cabanac, M., 1991. Heat loss from the human head during exercise. *J. Appl. Physiol.* 71, 590–595.

Redortier, B., Voelcker, T., 2011. A 38-zone thermal manikin with physiological control: validation for simulating thermal response of the body for sports exercise in cold and hot environment, in: 14th International Conference on Environmental Ergonomics. Napflio, Greece.

Redortier, B., Voelcker, T., 2010. Implementation of thermo-physiological control on a multi-zone manikin, in: 8th International Meeting for Thermal Manikin and Modeling (8I3M), Victoria, 22-26 August 2010, Canada.

Reid, J., Wang, E.L., 2000. A system for quantifying the cooling effectiveness of bicycle helmets. *J. Biomech. Eng.* 122, 457–60.

Reischl, U., 1986. Fire Fighter helmet ventilation analysis. *Am. Ind. Hyg. Assoc. J.* 47,

546–551.

Rezendes, J.L., 2006. Bicycle helmets: overcoming barriers to use and increasing effectiveness. *J. Pediatr. Nurs.* 21, 35–44. doi:10.1016/j.pedn.2005.06.005

Richards, M.G.M., McCullough, E.A., 2005. Revised Interlaboratory Study of Sweating Thermal Manikins Including Results from the Sweating Agile Thermal Manikin. *J. ASTM Int.* 2, Paper ID JAI12109. doi:10.1520/JAI12109

Rugh, J.P., Bharathan, D., 2005. Predicting Human Thermal Comfort in Automobiles, in: *Society of Automotive Engineers Technical Paper*. pp. 2005–01–2008. doi:10.4271/2005-01-2008

Rugh, J.P., Farrington, R.B., Bharathan, D., Vlahinos, A., Burke, R., Huizenga, C., Zhang, H., 2004. Predicting human thermal comfort in a transient nonuniform thermal environment. *Eur. J. Appl. Physiol.* 92, 721–727.

Rugh, J.P., Lustbader, J., 2006. Application of a Sweating Manikin Controlled by a Human Physiological Model and Lessons Learned. 6th Int. Therm. Manikin Model. Meet.

Salloum, M., Ghaddar, N., Ghali, K., 2007. A new transient bioheat model of the human body and its integration to clothing models. *Int. J. Therm. Sci.* 46, 371–384. doi:10.1016/j.ijthermalsci.2006.06.017

Smith, C.E., 1991. A transient three-dimensional model of the thermal system. Kansas State University.

Smith, C.J., Havenith, G., 2011. Body mapping of sweating patterns in male athletes in mild exercise-induced hyperthermia. *Eur. J. Appl. Physiol.* 111, 1391–404. doi:10.1007/s00421-010-1744-8

Stolwijk, J.A., 1971. A mathematical model of physiological temperature regulation in man.

References

- Takada, S., Sakiyama, T., Matsushita, T., 2011. Validity of the two-node model for predicting steady-state skin temperature. *Build. Environ.* 46, 597–604. doi:10.1016/j.buildenv.2010.09.008
- Tanabe, S., Arens, E.A., Bauman, F., Zhang, H., Madsen, T., 1994. Evaluating thermal environments by using a thermal manikin with controlled skin surface temperature. *ASHRAE Trans.* 100.
- Tanabe, S., Kobayashi, K., Nakano, J., Ozeki, Y., 2002. Evaluation of thermal comfort using combined multi-node thermoregulation (65MN) and radiation models and computational fluid dynamics (CFD). *Energy Build.* 34, 637–646.
- Tanaka, H., Kitada, M., Taniguchi, Y., Ohno, Y., Shinagawa, T., Aoki, H., 1992. Study on Car Air Conditioning System Controlled by Car Occupants' Skin Temperatures - Part 2: Development of a New Air Conditioning System. doi:10.4271/920170
- Teunissen, L.P.J., de Haan, A., de Koning, J.J., Daanen, H.A.M., 2012. Telemetry pill versus rectal and esophageal temperature during extreme rates of exercise-induced core temperature change. *Physiol. Meas.* 33, 915–24. doi:10.1088/0967-3334/33/6/915
- Tyler, C.J., 2011. The effect of skin thermistor fixation method on weighted mean skin temperature. *Physiol. Meas.* 32, 1541–7. doi:10.1088/0967-3334/32/10/003
- Uibel, S., Müller, D., Klingelhofer, D., Groneberg, D.A., 2012. Bicycle helmet use and non-use - recently published research. *J. Occup. Med. Toxicol.* 7, 9. doi:10.1186/1745-6673-7-9
- Van Brecht, A., Nuyttens, D., Aerts, J.M., Quanten, S., De Bruyne, G., Berckmans, D., 2008. Quantification of ventilation characteristics of a helmet. *Appl. Ergon.* 39, 332–41. doi:10.1016/j.apergo.2007.08.003
- van den Heuvel, C.J., Ferguson, S. a, Dawson, D., Gilbert, S.S., 2003. Comparison of

digital infrared thermal imaging (DITI) with contact thermometry: pilot data from a sleep research laboratory. *Physiol. Meas.* 24, 717–725. doi:10.1088/0967-3334/24/3/308

van Marken Lichtenbelt, W.D., Frijns, A.J.H., Fiala, D., Janssen, F.E.M., van Ooijen, A.M.J., van Steenhoven, A.A., 2004. Effect of individual characteristics on a mathematical model of human thermoregulation. *J. Therm. Biol.* 29, 577–581. doi:10.1016/j.jtherbio.2004.08.081

Vogt, J.J., Candas, V., Libert, J.P., 1982. Graphical determination of heat tolerance limits. *Ergonomics* 25, 285–294.

Wagner, J.A., Horvath, S.M., 1985. Influences of age and gender on human thermoregulatory responses to cold exposures. *J. Appl. Physiol.* 58, 180–186.

Wang, F., Annaheim, S., Morrissey, M., Rossi, R.M., 2013. Real evaporative cooling efficiency of one-layer tight-fitting sportswear in a hot environment. *Scand. J. Med. Sci. Sport.* 24, 1–11. doi:10.1111/sms.12117

Wang, F., Del Ferraro, S., Molinaro, V., Morrissey, M., Rossi, R., 2014a. Assessment of body mapping sportswear using a manikin operated in constant temperature mode and thermoregulatory model control mode. *Int. J. Biometeorol.* 58, 1–10. doi:10.1007/s00484-013-0774-4

Wang, F., Gao, C., Kuklane, K., Holmér, I., 2011. Determination of clothing evaporative resistance on a sweating thermal manikin in an isothermal condition: Heat loss method or mass loss method? *Ann. Occup. Hyg.* 55, 775–783. doi:10.1093/annhyg/mer034

Wang, F., Havenith, G., Mayor, T.S., Kuklane, K., Zwolinska, M., Hodder, S., Wong, C., Kishino, J.U.N., 2014b. Clothing real evaporative resistance determined by means of a sweating thermal manikin: a new round-robin study, in: *Ambience`14&10i3m*, 7-9 Sept 2014 Tampere, Finland.

Wang, X.-L., 1990a. Free convective heat transfer coefficients of a heated full-scale

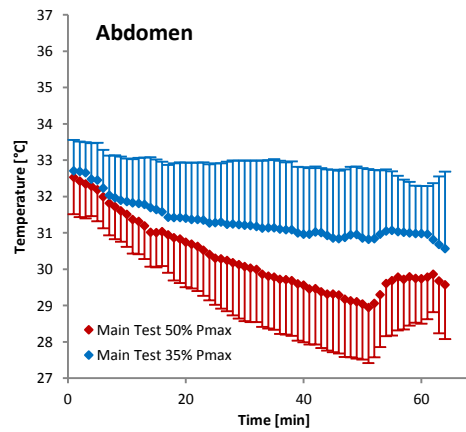
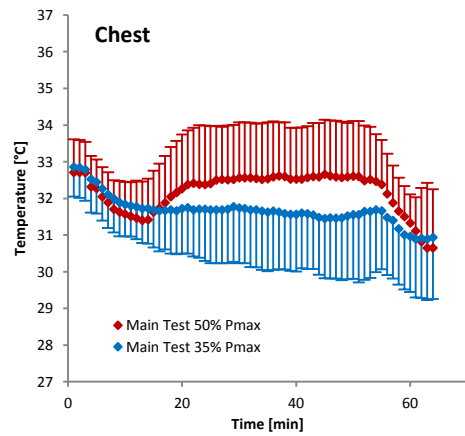
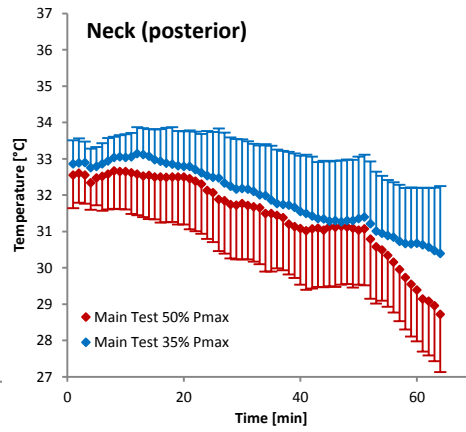
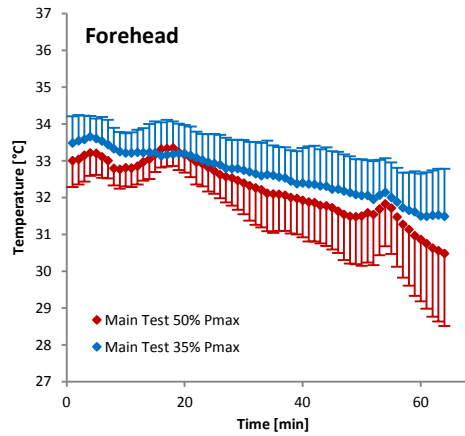
- manikin. *Clim. Build.* 1, 17–31.
- Wang, X.-L., 1990b. Convective heat transfer coefficients from head and arms. *Clim. Build.* 2, 3–7.
- Wang, X.-L., 1990c. Convective heat losses from segments of the human body. *Clim. Build.* 3, 8–14.
- Wardle, S., Iqbal, Z., 1998. Cycle helmet ownership and wearing; results of a survey in South Staffordshire. *J. Public Health Med.* 20, 70–7.
- Werner, J., Webb, P., 1993. A six-cylinder model of human thermoregulation for general use on personal computers. *Ann. Physiol. Anthropol.* 12, 123–134. doi:10.2114/ahs1983.12.123
- Wissler, E.H., 1985. Mathematical simulation of human thermal behaviour using whole body models., in: In: Shitzer A., E.R.C. 1198. (Ed.), *Heat Transfer in Medicine and Biology—Analysis and Applications*. PlenumNew York, pp. chapt. 13, p.325–373.
- Wissler, E.H., Havenith, G., 2009. A simple theoretical model of heat and moisture transport in multi-layer garments in cool ambient air. *Eur. J. Appl. Physiol.* 105, 797–808. doi:10.1007/s00421-008-0966-5
- Wu, H., Fan, J., 2008. Study of heat and moisture transfer within multi-layer clothing assemblies consisting of different types of battings. *Int. J. Therm. Sci.* 47, 641–647. doi:10.1016/j.ijthermalsci.2007.04.008
- Wyon, D., Larsson, S., Forsgren, B., Lundgren, I., 1989. Standard Procedures for Assessing Vehicle Climate with a Thermal Manikin, in: *Society of Automotive Engineers Technical Paper*. p. 890049. doi:10.4271/890049
- Xu, X., Werner, J., 1997. A dynamic model of the human/clothing/environment-system. *Appl. Human Sci.* 16, 61–75.

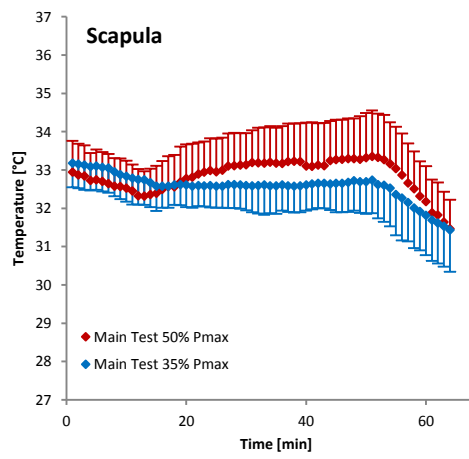
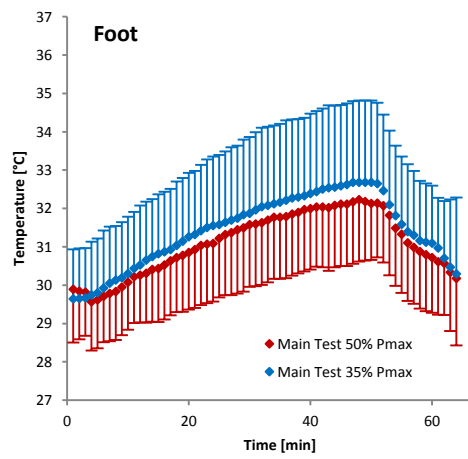
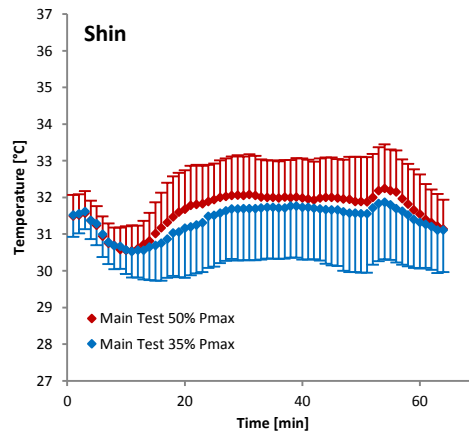
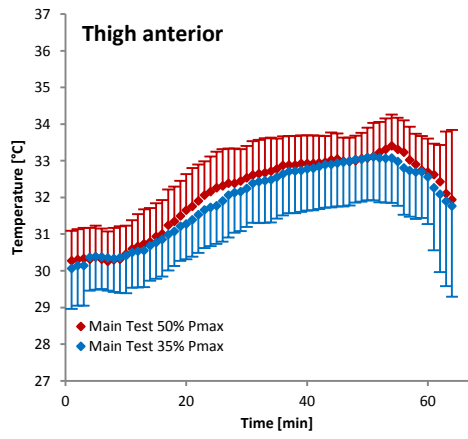
Multi-sector thermophysiological head simulator

- Yokoyama, S., Maeda, T., Kuramae, M., Kakuta, N., 2007. Human Thermal Model Expressing Local Characteristics of Each Segment. *J. Human-Environment Syst.* 10, 51–61. doi:10.1618/jhes.10.51
- Zaproudina, N., Varmavuo, V., Airaksinen, O., Närhi, M., 2008. Reproducibility of infrared thermography measurements in healthy individuals. *Physiol. Meas.* 29, 515. doi:10.1088/0967-3334/29/4/007
- Zatsiorsky, V., Prilutsky, B., 2012. Chapter 7. Eccentric muscle action in human motion, in: *Biomechanics of Skeletal Muscles. Human Kinetics*, p. 536.
- Zhang, H., 2003. Human thermal sensation and comfort in transient and non-uniform thermal environments. University of California, Berkeley.
- Zhang, H., Arens, E.A., Huizenga, C., Han, T., 2010a. Thermal sensation and comfort models for non-uniform and transient environments: Part I: Local sensation of individual body parts. *Build. Environ.* 45, 380–388. doi:10.1016/j.buildenv.2009.06.018
- Zhang, H., Arens, E.A., Huizenga, C., Han, T., 2010b. Thermal sensation and comfort models for non-uniform and transient environments, part III: Whole-body sensation and comfort. *Build. Environ.* 45, 399–410.

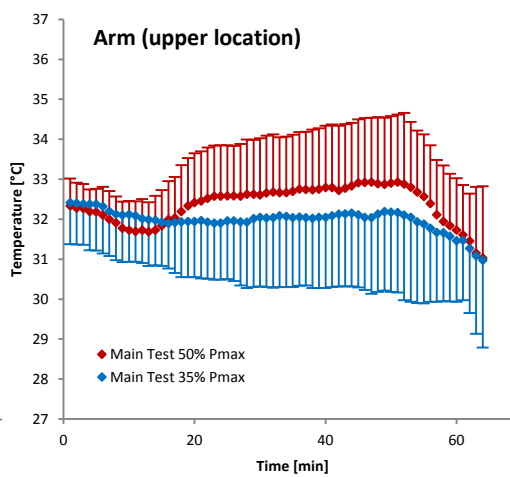
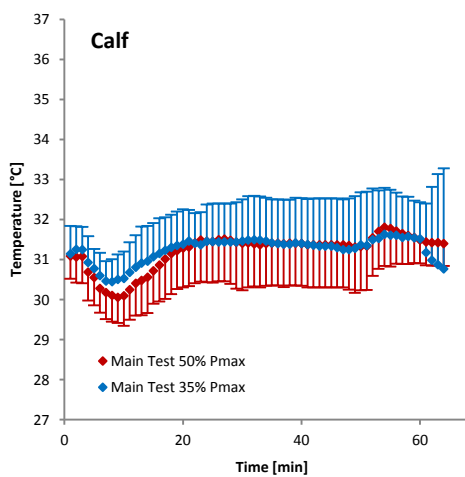
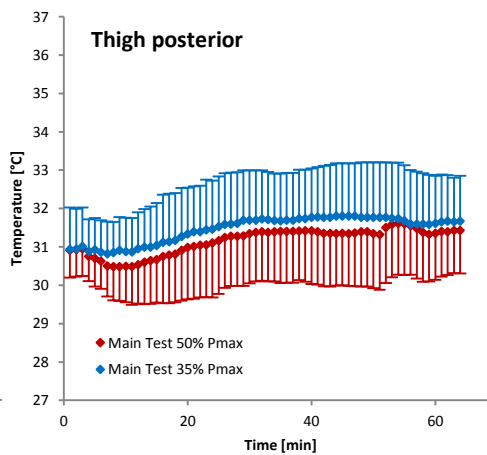
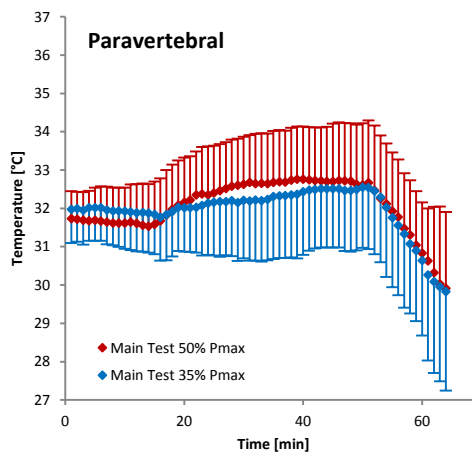
8 APPENDIX

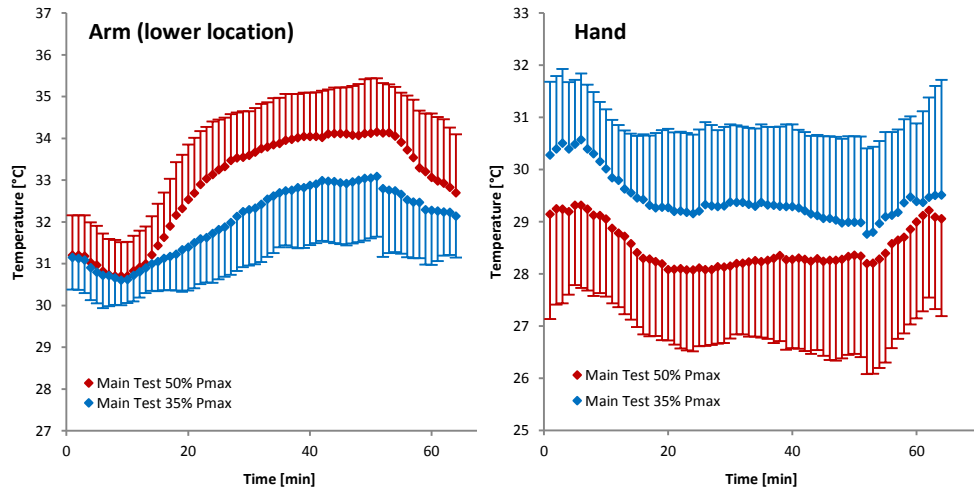
8.1 APPENDIX 1: LOCAL SKIN TEMPERATURES UPON THE 14 BODY-SITES (ISO 9886)





Multi-sector thermophysiological head simulator





8.2. APPENDIX 2: LOCAL SKIN TEMPERATURES AT HEAD-SITE

